

**Functional analysis of Chikungunya
virus non-structural protein 3
alphavirus unique domain**

Yanni Gao

Submitted in accordance with the requirements for the degree of

Doctor of Philosophy

University of Leeds

Faculty of Biological Sciences

School of Molecular and Cellular Biology

December 2018

The candidate confirms that the work submitted is her own, except where work which has formed part of jointly-authored publications has been included. The contribution of the candidate and the other authors to this work has been explicitly indicated below. The candidate confirms that appropriate credit has been given within the thesis where reference has been made to the work of others.

Chapter 3 to 5 within this thesis has been based on work from a jointly-authored publication:

Yanni Gao, Niluka Goonawardane, Joseph Ward, Andrew Tuplin and Mark Harris. Multiple roles of the non-structural protein 3 (nsP3) alphavirus unique domain (AUD) during Chikungunya virus genome replication and transcription. PLoS Pathog. 2019 Jan 22;15(1):e1007239. doi: 10.1371/journal.ppat.1007239. eCollection 2019 Jan.

- Yanni Gao performed experiments for figures 1, 2, 3, 4, 5, 6, 7, 8, 9, 10, 11, 12 and supporting figures 1, 2, 3, 4, and co-authored the paper.

- Dr. Niluka Goonawardane performed image processing and data analysis for figures 11 and 12, and co-authored the paper.

- Dr. Joseph Ward performed experiments for figure 8 and co-authored the paper.

- Dr. Andrew Tuplin provided supervision and co-authored the paper.

- Prof. Mark Harris provided supervision and co-authored the paper.

This copy has been supplied on the understanding that it is copyright material and that no quotation from the thesis may be published without proper acknowledgement.

© 2018 University of Leeds Yanni Gao

The right of Yanni Gao to be identified as Author of this work has been asserted by her in accordance with the Copyright, Designs and Patents Act 1988.

Acknowledgements

Greatest appreciation will be given to my supervisor Prof. Mark Harris for his invaluable supervision of this project. Many thanks for his tolerance and help in my improvable English, and his care throughout my three and a half years study. Without his advice and encouragement, this project would have never been able to be accomplished.

Thanks should also go to past and present members in Lab Garstang 8.61 and other colleagues from Virology group in University of Leeds, especially Dr. Niluka Goonawardane and Dr. Joseph Ward for their scientific input in this project, and Raymond Li for his kindness throughout my Ph.D study in Leeds.

A big thank you to my families, my mum, my dad and my little sister. They are always having my back in my life, and they are my forever spiritual handholds. My mum is my greatest heroine!

I finally would like to acknowledge the China Scholarship Council and University of Leeds Scholarship for funding this project and funding from FBS. I would also like to thank the Microbiology Society and Arbovirus Meetings for providing opportunities to present my work to the wider scientific community.

Abstract

Chikungunya virus (CHIKV) is a re-emerging alphavirus causing fever, joint pain, skin rash, arthralgia, and occasionally death. Antiviral therapies and/or effective vaccines are urgently required. CHIKV biology is poorly understood, in particular the functions of the non-structural protein 3 (nsP3). nsP3 consists of three domains, of these the macrodomain is reported to have ADP-ribose and RNA-binding activity, the hypervariable region is involved in various interaction with host proteins, however, the alphavirus unique domain (AUD), as a homologous sequence unique to alphaviruses, is essential for CHIKV replication with absolutely unknown functions.

To investigate the function of AUD, a mutagenic analysis was performed. Informed by the structure of the Sindbis virus AUD and an alignment of amino acid sequences of multiple alphaviruses, a series of mutations in the AUD were generated in a CHIKV sub-genomic replicon. This analysis revealed an essential role for the AUD in CHIKV RNA replication, with mutants exhibiting species- and cell-type specific phenotypes. To test if the AUD played a role in other stages of the virus lifecycle, the mutant panel was also analysed in the context of infectious CHIKV. Results indicated that, in addition to a role in RNA replication, the AUD was also required for virus assembly.

Further analysis revealed that one mutant (P247A/V248A) specifically blocked transcription of the subgenomic RNA leading to a dramatic reduction in synthesis of the structural proteins and concomitant reduction in virus production. This phenotype could be explained by both a reduction in the binding of the P247A/V248A mutant nsP3 to viral genomic RNA *in vivo*, and the reduced affinity of the mutant AUD for the subgenomic promoter RNA *in vitro*. A high-resolution confocal microscopy analysis on the track of nsP3, capsid protein and dsRNA confirmed the P247A/V248A replication defect.

In parallel, this project also set out to investigate a variety of biochemical characters of nsP3/AUD, for example, RNAi suppression activity, self-multimerization and interactions with cellular proteins by the approach of quantitative proteomic analysis. In conclusion, this study reveals that the AUD is a pleiotropic protein domain, with multiple functions during CHIKV RNA synthesis.

Table of Contents

Chapter 1: Introduction	1
1.1 Chikungunya virus	3
1.1.1 Identification of Chikungunya virus (CHIKV)	3
1.1.2 Classification of CHIKV	3
1.1.3 Pathology of CHIKV	6
1.1.4 Epidemiology of CHIKV.....	7
1.1.5 Diagnosis and therapies or vaccines against CHIKV	9
1.2 Molecular virology of CHIKV	10
1.2.1 Molecular structure and genome organisation of CHIKV	10
1.2.2 Non-coding regions of CHIKV genome	11
1.2.3 Structural proteins	14
1.2.4 Non-structural proteins.....	16
1.3 nsP3.....	18
1.3.1 Macrodomain.....	19
1.3.2 AUD	20
1.3.3 Hypervariable region.....	21
1.4 CHIKV life cycle.....	22
1.4.1 Entry of CHIKV.....	22
1.4.2 Intracellular replication of CHIKV	24
1.4.3 Assembly, budding and maturation of CHIKV	26
1.5 Systems for the study of CHIKV.....	29
1.5.1 Cell culture system	29
1.5.2 Animal models	29
1.6 Aims and objective.....	31
Chapter 2: Materials and Methods.....	33
2.1 General materials.....	35
2.1.1 Bacterial strains.....	35

2.1.2 Cell lines	35
2.1.3 Plasmids and virus constructs	35
2.1.4 Oligonucleotide primers.....	35
2.1.5 Antibodies	36
2.1.6 Chromatography columns and resins.....	36
2.2 Basic techniques of molecular biology.....	36
2.2.1 Manipulation of nucleic acid	36
2.2.2 Basic technology on Protein work.....	43
2.3 Basic techniques of tissue culture	44
2.3.1 Passaging of cells.....	44
2.3.2 Transfection of nucleic acids	45
2.3.3 Electroporation of RNAs into mammalian cells.....	45
2.3.4 Cell lysates collection	45
2.4 CHIKV-D-Luc-SGR work.....	46
2.4.1 Dual-luciferase assay	46
2.4.2 Sequencing of the subgenomic replicon RNA post transfection	46
2.5 ICRES-CHIKV full-length virus experiments	46
2.5.1 Infectious virus collection.....	46
2.5.2 Sequencing of infectious virus genome RNA.....	46
2.5.3 Virus titration by plaque assay	47
2.5.4 Infectious centre assay (ICA)	47
2.5.5 Quantification of CHIKV genome RNA by qRT-PCR	47
2.5.6 Virus infection	48
2.5.7 One step virus growth kinetics	48
2.5.8 Intracellular virus collection	48
2.5.9 Quantification of CHIKV genomic RNA and subgenomic RNA synthesis	48
2.5.10 Immunoprecipitation	49
2.5.11 Immunofluorescence analysis	49

2.5.12 Co-localisation analysis	50
2.6 In vitro protein experiments	50
2.6.1 Expression and purification of AUD	50
2.6.2 Protein identification by mass spectrometry	51
2.6.3 Circular Dichroism spectroscopy	53
2.6.4 Fluorescent Polarisation Anisotropy	53
2.6.5 RNA filter binding assay	53
2.6.6 GST-pull down assay	54
2.6.7 Tandem Mass Tag (TMT) comparative proteomic analysis.....	55
2.7 Statistical analysis of data	55
Chapter 3: The role of nsP3 AUD in virus genome replication.....	57
3.1 Introduction	59
3.2 Results.....	60
3.2.1 Generation of a panel of AUD alanine mutations in CHIKV-D-Luc-SGR	60
3.2.2 The role of AUD in CHIKV genome replication	63
3.2.3 Sequence analysis of the CHIKV-D-Luc-SGR-AUD (R243A/K245A) RNA following replication in different cell types	70
3.2.4 Lethal mutations do not interfere the expression and stability of nsP3/AUD	70
3.3 Discussion	71
Chapter 4: nsP3 AUD is required for production of subgenomic RNA and structural proteins during CHIKV infection.....	75
4.1 Introduction	77
4.2 Results.....	78
4.2.1 The effect of AUD mutations in infectious CHIKV production	78
4.2.2 One-step virus growth kinetics	81
4.2.3 Role of AUD in CHIKV assembly and release	82
4.2.4 The P247A/V247A mutation selectively impairs subgenomic RNA synthesis.....	84
4.2.5 nsP3 RNA binding activity to CHIKV genome RNA	87

4.2.6 Sub-cellular localisation of nsP3, capsid and dsRNA during CHIKV replication	89
4.3 Discussion.....	92
Chapter 5: Biochemical analysis of AUD	97
5.1 AUD RNA binding activity	99
5.1.1 Introduction.....	99
5.1.2 Results	101
5.1.3 Discussion.....	117
5.2 RNAi suppression activity.....	120
5.2.1 Introduction.....	120
5.2.2 Results	121
5.2.3 Discussion.....	127
5.3 nsP3/AUD formation/distribution in cells	128
5.3.1 Introduction.....	128
5.3.2 Results	129
5.3.3 Discussion.....	133
5.4 Proteomic analysis of nsP3 binding partner	134
5.4.1 Introduction.....	134
5.4.2 Results	135
5.4.3 Discussion.....	139
Chapter 6: Conclusion and future perspectives	141
References.....	147
Appendix	169

Table of Figures

Figure 1.1 A simplified phylogenetic tree of Alphaviruses assuming their New World origin...	4
Figure 1.2 CHIKV phylogenetic analysis based on 80 CHIKV isolates with different temporal, spatial and host coverage.	5
Figure 1.3 Dissemination of CHIKV in vertebrates.	7
Figure 1.4 Global transmission of CHIKV.....	9
Figure 1.5 Structure of CHIKV genome RNA.	11
Figure 1.6 A comparison between mRNA capping of cellular and alphavirus mRNAs.....	12
Figure 1.7 Evolutionary history and lineage-specific structures of the CHIKV 3'UTR.	13
Figure 1.8 Diagram of nsP3.	19
Figure 1.9 Structure of CHIKV macro domain.	20
Figure 1.10 ZBD of nsP3.	21
Figure 1.11 Model of the Alphavirus life cycle.....	28
Figure 1.12 Diagram of CHIKV-D-Luc-SGR.....	29
Figure 2.1 Diagram for AUD point mutants in CHIKV-D-Luc-SGR.....	39
Figure 2.2 Diagram for AUD truncations in CHIKV-D-Luc-SGR.	41
Figure 3.1 AUD residues selection for mutagenic strategy.....	62
Figure 3.2 Preliminary data of CHIKV AUD mutants replication in Huh7 and U4.4 cells.	65
Figure 3.3 CHIKV AUD mutant replication in human cells.	67
Figure 3.4 CHIKV AUD mutant replication in non-human mammalian cells.	68
Figure 3.5 CHIKV AUD mutant replication in Aedes. albopictus mosquito cells.	69
Figure 3.6 RT-PCR and sequencing analysis of CHIKV-D-luc-SGR-R243A/K245A.	70
Figure 3.7 Expression and stability of nsP3.....	71
Figure 4.1 Phenotype of AUD mutations in the production of infectious virus.	80

Figure 4.2 Multi-step growth kinetics of CHIKV.	82
Figure 4.3 Phenotype of AUD mutations on virus entry, release and assembly.	84
Figure 4.4 Effect of AUD mutations on CHIKV protein expression and RNA synthesis.	86
Figure 4.5 CHIKV genome RNA association with nsP3 during virus replication.	88
Figure 4.6 Fluorescence analysis of nsP3, capsid and dsRNA distribution during infection of C2C12 cells with wildtype CHIKV.	90
Figure 4.7 Fluorescence analysis of nsP3, capsid and dsRNA distribution during infection of C2C12 cells with P247A/V248A CHIKV.	91
Figure 5.1 Diagram of pET-28aSUMO-AUD.	101
Figure 5.2 Optimization of AUD expression in pET-28aSUMO-AUD.	102
Figure 5.3 Purification of AUD.	103
Figure 5.4 Identification of AUD protein.	104
Figure 5.5 Expression of wildtype AUD and its mutants.	105
Figure 5.6 Mass spectrometry analysis of AUD-R243A/K245A.	107
Figure 5.7 Circular Dichroism results of AUDs.	108
Figure 5.8 AUD binding activity to short RNAs.	109
Figure 5.9 AUD RNA-binding activity to CHIKV 3'UTR RNA.	111
Figure 5.10 AUD RNA-binding activity to HCV 3'UTR RNA.	113
Figure 5.11 RNA-filter binding assay with AUD and FMDV aptamer RNA.	114
Figure 5.12 AUD RNA binding activity to CHIKV 5' UTR(-) and sg-5' prom(-).	116
Figure 5.13 Diagram of pMKO.1-GFP and pMKO.1-GFP-siGFP.	122
Figure 5.14 GFP reversion assay of CHIKV nsP3/AUD in C2C12 cells.	123
Figure 5.15 Expression of GST-AUD.	124
Figure 5.16 GST tagged AUD failed to pull down Dicer protein.	126

Figure 5.17 GFP tagged nsP3 or AUD failed to pull down Dicer protein.	127
Figure 5.18 GFP tagged wildtype AUD and mutant distribution in C2C12 cells.....	130
Figure 5.19 Distribution of wildtype nsP3 and its AUD mutants with G3BP in C2C12 cells...	132
Figure 5.20 Purification of Twin-Strep-Tagged nsP3 (TST-nsP3).....	136
Figure 5.21 Flow chart of comparative analysis of nsP3-binding proteins involved in nsP3- P247A/V248A.....	137
Figure 5.22 nsP3 interacting protein network inhibited by P247A/V248A.....	138
Appendix Figure 9.1 Alignment of full AUD amino acid sequences among different alphaviruses.	171

Table of Tables

Table 1 AUD mutant replication phenotypes in different cell types.....	73
Table 2 RNAs used in the detection of protein-RNA interaction.....	117
Appendix Table 9.1 List of constructs generated and used throughout this study.	172
Appendix Table 9.2 List of oligonucleotide primers used in this project.	174
Appendix Table 9.3 Host proteins identified by proteomic analysis.....	185

Abbreviations

A	Ala, alanine
CYC1	Cytochrome c-1
2'-O me	2'-O-methyl modification
aa	Amino Acid
ActD	actinomycin D
ADP	Adenosine diphosphate
AGO	Argonaute protein
arbovirus	arthropod borne virus
ATP	Adenosine triphosphate
AUD	Alphavirus unique domain
BCA	Bicinchoninic acid
bp	Base Pairs
BSA	Bovine serum albumin
BSL3	Biosafety laboratory level 3
C	Cys, cysteine
CD	Circular Dichroism
CD4	Cluster of Differentiation 4
CDC	Centres for Disease Control and Prevention
cDNA	Complementary DNA
CHIKV	Chikungunya virus
CHIKV-D-Luc-SGR	Chikungunya virus dual luciferase subgenomic replicon
CP	Capsid protein
CPE	Cytopathic Effect
CSE	Conserved sequence element
CV	Column Volume
Cyp	Cyclophilin
Cys	Cysteine
D	Asp, aspartate
Da	Dalton
DAPI	4', 6'-diamidino-2-phenylindole dihydrochloride
DENV	Dengue Fever Virus
DEPC	Diethyl pyrocarbonate
DMEM	Dulbecco's modified eagles medium
DMSO	Dimethyl sulfoxide
DNA	Deoxyribonucleic acid
dNTP	Deoxynucleotide
DRs	Direct repeats
dsRNA	double stranded RNA
E	Glu, glutamate
E.coli	Escherichia Coli
E1	Envelope 1 protein
E2	Envelope 2 protein
EDTA	Ethylenediamine tetraacetic acid
eIF	eukaryotic initiation factor

ELISA	Enzyme-linked immunosorbent assays
EM	Electron Microscopy
ER	Endoplasmic Reticulum
FBS	foetal bovine serum
Fluc	Firefly luciferase
FMDV	Foot-and-Mouse Disease Virus
FXR	Fragile-X-related
g	Gravitational force
G	Gly, glycine
G3BP	Ras-GTPase-activating protein-binding protein
GA	Glutathione agarose
GAPDH	Glyceraldehyde-3-phosphate dehydrogenase
GFP	Green fluorescent protein
GLB	Glasgow lysis buffer
gRNA	genomic RNA
GST	Glutathione S-transferases
h.p.e.	hours post electroporation
h.p.i.	hours post infection
h.p.t.	hours post transfection
HCV	Hepatitis C Virus
Huh7	Human hepatocellular carcinoma cell line-7
Huh7.5	Human hepatocellular carcinoma cell line-7.5
I	Ile, isoleucine
ICA	Infectious centre assay
ICRES	ECSA strain
ID	Identity
IF	Immunofluorescence
IFIT1	Interferon Induced Protein with Tetratricopeptide Repeats 1
IFN	Interferon
IFN α	Interferon- α
Ig	Immunoglobulin
IP	Immunoprecipitation
IPTG	isopropyl β -D-1-thiogalactopyranoside
IRES	Internal Ribosome Entry Site
ISG	Interferon-stimulated gene
ISG15	Interferon-stimulated gene 15
IU	Infectious Unit
K	Lys, lysine
kb	Kilobase
kDa	Kilodalton
L	Leu, leucine
LarII	Luciferase reagent II
LB	Luria Bertani
LC-MS	Liquid chromatography-mass spectrometry
M	Met, methionine
M.Wt	Molecular weight
m/z	mass to charge

m7G	7-methylguanosine
MAR	Mono-ADP-ribose
MCS	Multiple Cloning Site
MeOH	Methanol
min	Minutes
miRNA	MicroRNA
MOI	Multiplicity of infection
mRNA	message RNA
MS	Mass Spectrometry
MTCH1	Mitochondrial Carrier 1
MT-like	Methyltransferase-like
N	Asn, asparagine
NC	Nucleocapsid
NDUFS1	NADH dehydrogenase (ubiquinone) Fe-S protein 1
NEAA	non-essential amino acids
NMR	Nuclear magnetic resonance
nsP	non-structural protein
nsP1	Non-structural protein 1
nsP2	Non-structural protein 2
nsP3	Non-structural protein 3
nsP4	Non-structural protein 4
nt	Nucleotide
NTPase	Nucleoside triphosphatase
o/n	Overnight
ORF	Open Reading Frame
P	Pro, proline
PAGE	Polyacrylamide gel electrophoresis
PARP	Poly(A)-poly(A) binding protein
PBS	Phosphate buffered saline
PCR	Polymerase chain reaction
PDB	Protein database
PEG	Pegylated
PFA	Paraformaldehyde
PFU	Plaque forming units
PLB	Passive lysis buffer
prom	Promoter
PVDF	Polyvinylidene fluoride
Q	Gln, glutamine
qRT-PCR	Quantative Reverse Transcription Real Time PCR
R	Arg, arginine
RCF	Relative Centrifugal Force
RdRp	RNA-dependent RNA-polymerase
RISC	RNA-induced silencing complex
Rluc	Renilla luciferase
RNA	Ribonucleic acid
RNAi	RNA interference
rpm	Revolutions Per Minute

RRV	Ross River Virus
RSE	Repeat sequence element
RT	Room Temperature
RTPase	RNA triphosphatase
RT-PCR	reverse transcriptase-polymerase chain reaction
S	Ser, serine
SAM	S-adenosyl methionine
SDS	Sodium dodecyl sulphate
SE	Standard Error
SEC	Size Exclusion Chromatography
SEC-MALLS	Size Exclusion Chromatography - Multi-Angle Laser Light Scattering
SEM	Standard error of the mean
SFV	Semliki Forest Virus
sg P	subgenomic promoter
SGR	Sub-Genomic Replicon
sgRNA	subgenomic RNA
SH3	Src homology
SINV	Sindbis virus
siRNA	Small interfering RNA
SLC25A20	Solute Carrier Family 25 (carnitine/acylcarnitine translocase), member 20
SLC25A4	Solute Carrier Family 25 (mitochondrial carrier; adenine nucleotide translocatoer), member 4
SLC25A5	Solute Carrier Family 25 (mitochondrial carrier; adenine nucleotide translocator), member 5
SOC	Standard of care
ssRNA	Single stranded RNA
SUCLG1	Succinate-CoA Ligase, alpha subunit
SUMO	Small Ubiquitin-like Modifier
T	Thr, threonine
TAE	Tris-Acetate-EDTA buffer
TBS	Tris-buffered saline
TC	Tissue culture
TEMED	Tetramethylrhodamine
TMT	Tandem Mass Tag
TST	Twin-strep-tag
U	Uracil
UTR	Untranslated Region
V	Val, valine
v/v	Volume by Volume
VEEV	Venezuelan Equine Encephalitis Virus
W	Trp, tryptophan
w/v	weight by volume
WEEV	West Equine Encephalitis Virus
WHO	World Health Organisation
WT	Wildtype
Y	Tyr, tyrosine

YBX1	Y-box-binding protein 1
YFV	Yellow Fever Virus
ZBD	Zinc-binding domain

Chapter 1: Introduction

1.1 Chikungunya virus

1.1.1 Identification of Chikungunya virus (CHIKV)

CHIKV is the pathogen causing Chikungunya fever, an acute febrile illness associated with severe arthralgia and rash (Deller and Russell, 1967, McGill, 1995, Adebajo, 1996, Ligon, 2006). Chikungunya is a Makonde word (Bantu language) meaning ‘the one that bends up’, referring to the stooped appearance of sufferers due to the excruciating pain in the joints (Robinson, 1955). CHIKV can cause acute, subacute or chronic disease. The disease shares some clinical signs with Dengue fever and Zika infection, and can be misdiagnosed in areas where they are common. For diagnosis, serological tests such as enzyme-linked immunosorbent assays (ELISA), and virological methods such as reverse transcriptase-polymerase chain reaction (RT-PCR) are available but are of variable sensitivity.

CHIKV was first isolated and recognized as a human pathogen in 1952 from the Makonde plateaus, along the borders between Tanzania and Mozambique (Lo Presti et al., 2014). During the last few decades, numerous re-emergences of CHIKV have been documented in over 60 countries in Asia, Africa, Europe and the Americas (Wahid et al., 2017, Burt et al., 2017). However, there is no specific antiviral drug treatment or safe and effective vaccines against CHIKV. The dramatic spread of CHIKV in recent years highlights the urgent need to take precautionary measures, as well as to investigate options for control.

1.1.2 Classification of CHIKV

CHIKV is a re-emerging mosquito-borne enveloped alphavirus in the *Togaviridae* family. The family *Togaviridae* consists of two genera: *Alphavirus* and *Rubivirus* (composed of a single member, *Rubella virus*). The *Alphavirus* genus contains a number of important human and animal pathogens (Strauss and Strauss, 1994). They are transmitted mainly by mosquito vectors where they cause systemic infection but no symptomatic disease. Therefore the *Alphavirus* are also referred to as arthropod borne virus (arbovirus), although it is uncertain whether salmonid alphaviruses are transmitted through lice or directly transmitted from fish to fish. The genus *Alphavirus* contains 31 members (Forrester et al., 2012) which can be classified antigenically into seven complexes: Barmah Forest (BF), Eastern equine encephalitis (EEE), Middelburg (MID), Ndumu (NDU), Semiliki Forest (SF), Venezuelan equine encephalitis (VEE), and Western equine encephalitis (WEE) (Solignat et al., 2009). Based on their geographic distribution, *Alphaviruses* can be divided into two categories: Old World and New World virus (Figure 1.1), and some transoceanic exchanges have possibly occurred mediated by birds (Powers et al., 2001). Old World viruses can be characterised by fever, rash and arthritic

symptoms, whereas some New World viruses may cause encephalitis. CHIKV, together with Ross River virus, O'nyong-nyong virus, Semliki Forest is part of the SF group of Old World viruses.

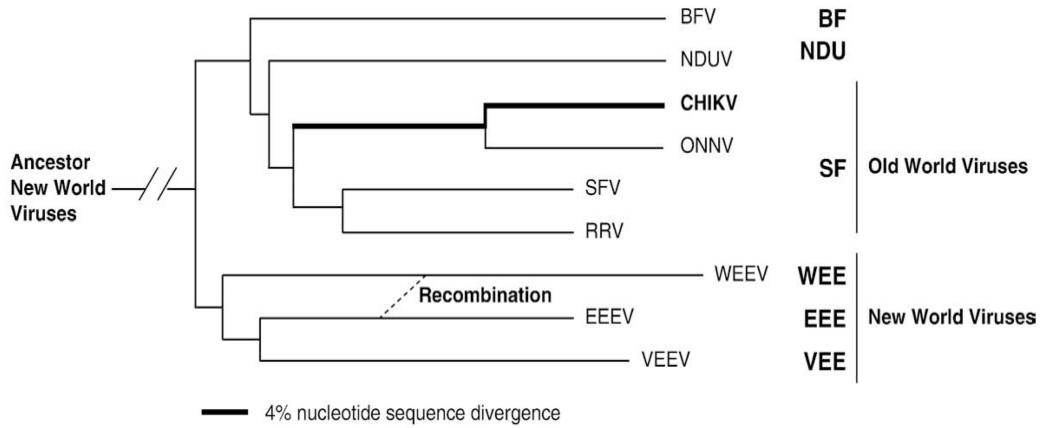


Figure 1.1 A simplified phylogenetic tree of Alphaviruses assuming their New World origin.

Picture is copied from (Powers et al., 2001).

CHIKV is divided into four geographically associated genotypes, ECSA, West Africa, Asian and Indian Ocean Outbreak, by an extensive and genome-scale phylogenetic analysis, using the whole open reading frame (ORF) sequences of a total of 80 isolates with broad temporal, spatial and host coverage (Figure 1.2). The divergence of each distinct lineage reflected the path of global transmission and occasional outbreaks (Volk et al., 2010).

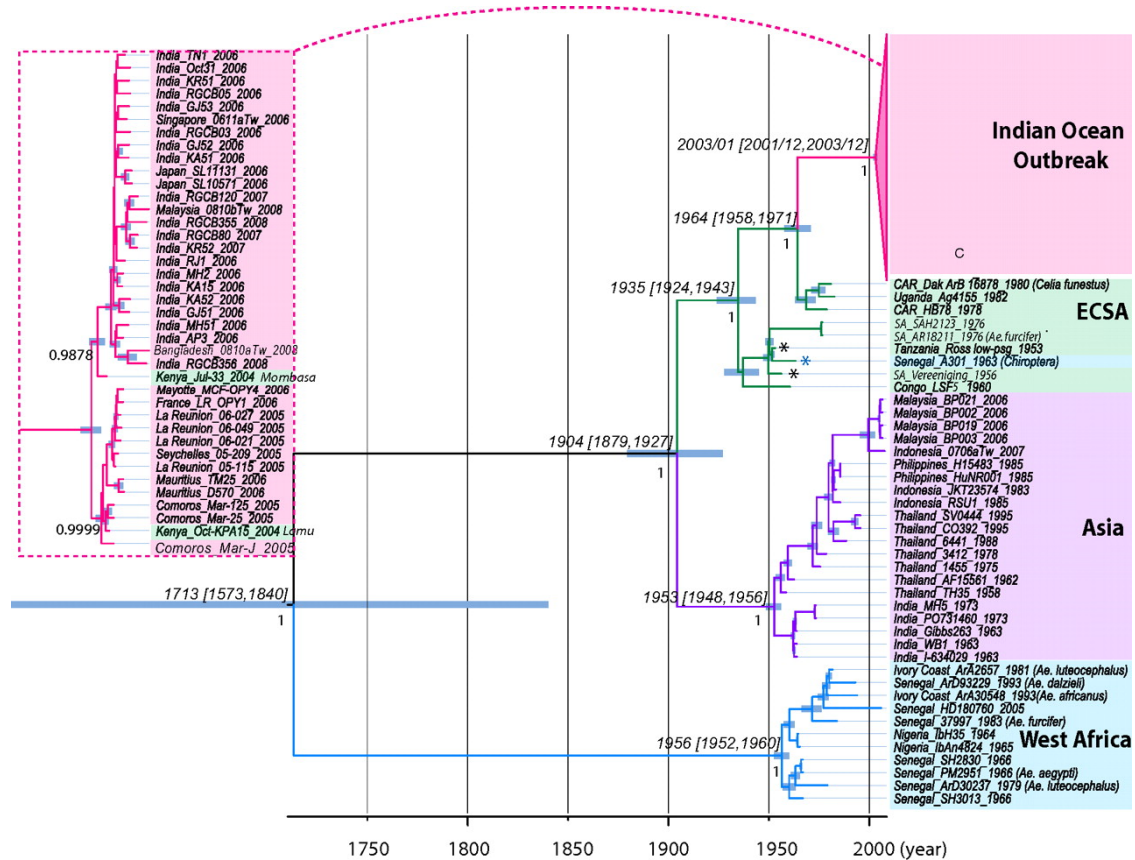


Figure 1.2 CHIKV phylogenetic analysis based on 80 CHIKV isolates with different temporal, spatial and host coverage.

Picture is copied from (Volk et al., 2010).

1.1.3 Pathology of CHIKV

Chikungunya disease does not often result in death, but the symptoms can be severe and disabling. In the early stages when the illness appeared, it was diagnosed as 'dengue-like' disease until CHIKV was confirmed as the pathogen of the illness by laboratory evaluation. It is characterized by an abrupt onset of fever frequently accompanied by joint pain, and also causes muscle pain, headache, nausea, fatigue and rash. The abrupt fever (usually >38.9 °C) always lasts from a few days to 2 weeks and can be biphasic in nature (Deller and Russell, 1968, Halstead et al., 1969b). The onset of fever is always followed by severe and debilitating polyarthrititis. The symmetric joint pains commonly occur in wrists, knees, ankles, elbow and fingers, but may also be involved in more-proximal joints (Simon et al., 2007). The joint pain usually lasts for a few days or may be prolonged to weeks (Sissoko et al., 2009, Manimunda et al., 2010). Rash is also a common symptom after CHIKV infection (Taubitz et al., 2007, Queyriaux et al., 2008, De Ranitz et al., 1965). It often appears following fever as maculopapular across trunk, extremities as well as palm, soles and even face (Borgherini et al., 2007, Inamadar et al., 2008). Symptoms caused by CHIKV infection usually begin 3-7 days (in range of 2-12 days) after being bitten by an infected mosquito and most patients feel better within one week. Not all infected individuals develop symptoms. Serosurveys show that 3-25% of the infected people with antibodies to CHIKV have no symptoms (Queyriaux et al., 2008, Sissoko et al., 2008). New-borns infected around the time of birth, older adults, and people with medical conditions such as high blood pressure, diabetes, or heart disease may at risk for more severe diseases (Lo Presti et al., 2014). Rare death is caused by chikungunya infections, however, it has been reported to increase during the 2004-2008 epidemics (Mavalankar et al., 2008, Beesoon et al., 2008, Higgs, 2006, Renault et al., 2007).

CHIKV replicates in the skin, and disseminates to the liver, muscle, joints, lymphoid tissue (lymph nodes and spleen) and brain, presumably through the blood (Figure 1.3) (Talarmin et al., 2007, Robin et al., 2010, Schwartz and Albert, 2010, Lo Presti et al., 2014). Therefore, some subclinical pathological changes will also occur in tissues post infection, mostly in liver (hepatocyte apoptosis) and lymphoid organs (adenopathy); and those in muscles and joints are associated with strong pain, with some of the patients presenting arthritis (Robin et al., 2010, Dupuis-Maguiraga et al., 2012).

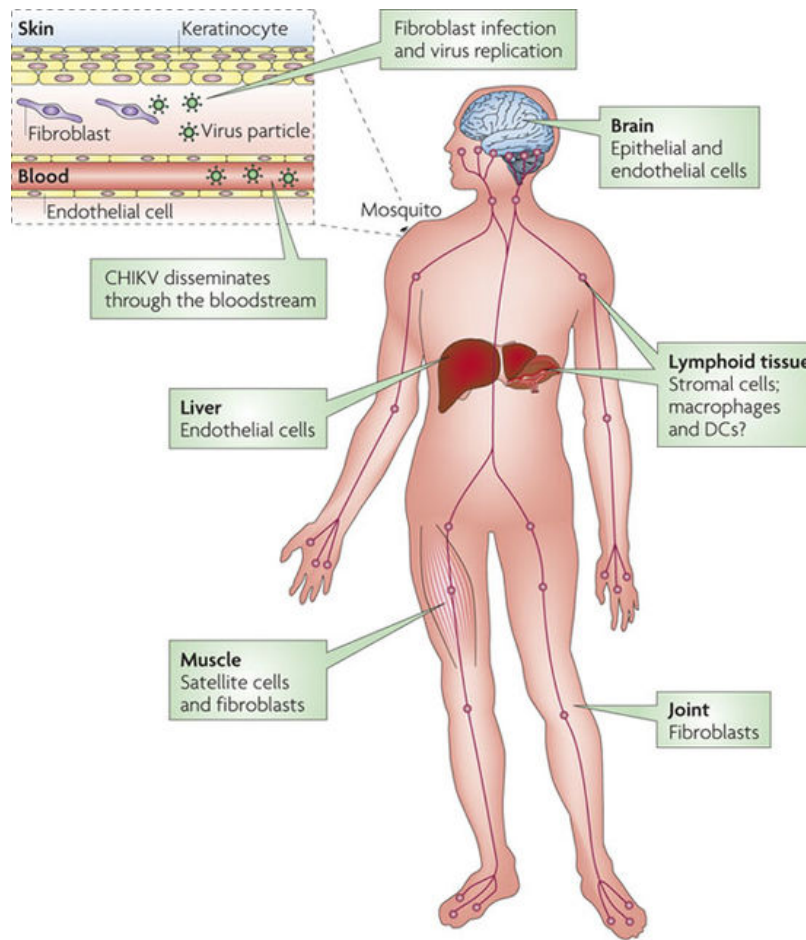


Figure 1.3 Dissemination of CHIKV in vertebrates.

Picture is copied from (Schwartz and Albert, 2010).

1.1.4 Epidemiology of CHIKV

Alphaviruses are maintained in natural cycles by transmission between susceptible vectors and vertebrate hosts (Strauss and Strauss, 1994). Arthropods (typically the mosquitoes) are usually the vectors for most alphaviruses, where viruses would cause a persistent, lifelong infection with minimal effect on biological functions. CHIKV transmission to humans is mainly through *Aedes* species mosquitoes, including *Aedes aegypti*, *Aedes albopictus* and *Aedes polynesiensis*, while *Culex* has also been reported for transmission in some cases (Schuffenecker et al., 2006, Diallo et al., 1999, Vanlandingham et al., 2005).

CHIKV is becoming a global threat nowadays (Figure 1.4). It was first isolated in 1952 in Tanzania. After that, several other epidemics have been reported in Central African Republic, Burundi, Uganda, Nigeria, Angola, Democratic Republic of the Congo and some other countries (Wahid et al., 2017). The first severe chikungunya fever outbreak documented in urban area was in the early 1960s in Bangkok (Nimmannitya et al., 1969), and from 1963 to 1973 in India

(Shah et al., 1964). The seroprevalence rate increased abruptly from 70% to 75% (Renault et al., 2012), followed by spreading to surrounding regions including Mauritius, Comoros, Seychelles, and La Reunion Island until April 2005 (Renault et al., 2012). CHIKV was found to infect another species of mosquito, i.e. *Aedes albopictus* due to a single point mutation in the genome during the epidemic from 2004 to 2009 (Schuffenecker et al., 2006). A CHIKV variant which presented a substitution of the amino acid alanine with valine at position 226 of the E1 protein was selected during the epidemic. This variant made *A. albopictus*, which was largely represented compared to *Aedes aegypti* in the specific affected area, became a predominant transmission vector, especially in La Reunion and the Kerala districts in India (Lo Presti et al., 2012). Recently, CHIKV infections have also been reported in Indonesia, Malaysia, Singapore, Philippines and some European countries such as Italy and France (Maha et al., 2015, Delisle et al., 2015). In the Americas, CHIKV first occurred in Saint Martin in 2013. So far, CHIKV transmission has been identified in 45 countries in North America, Central America, South America and Caribbean (Yactayo et al., 2016).

CHIKV infection is now increasing its important threat to global health and welfare as the epidemiological findings give a hint that global distribution of *A. aegypti* and *A. albopictus*, as well as travellers, are involved in the ongoing CHIKV transmission in areas which were free of it before. The recognition of these infections is still difficult and remains underestimated because of its similar symptoms to other arboviruses (Pierro et al., 2014). The dramatic spread of CHIKV in recent decades highlights the urgent need to take precautionary measures and options for control. Hopefully, timely sharing of accurate information may help to control the spread and magnitude of more outbreaks in the future.

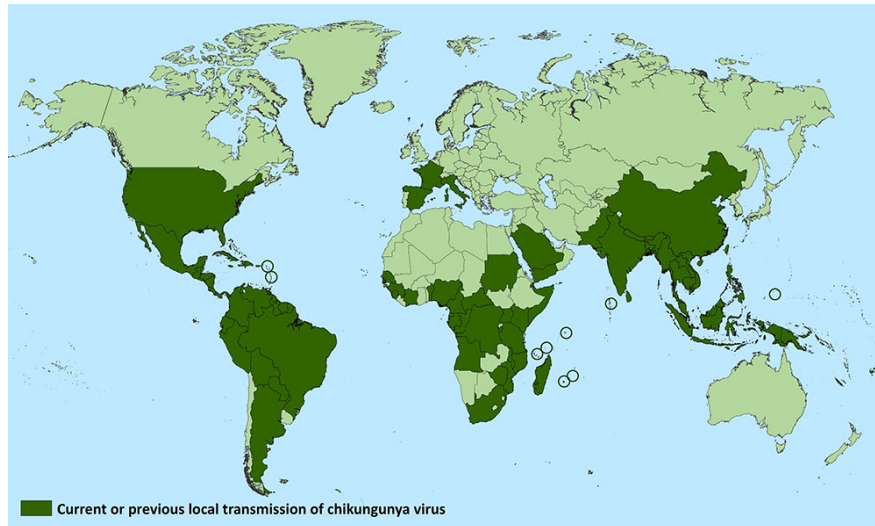


Figure 1.4 Global transmission of CHIKV.

(Copied from CDC, May 29th, 2018) * Does not include countries or territories where only imported cases have been documented.

1.1.5 Diagnosis and therapies or vaccines against CHIKV

Diagnosis of CHIKV infections may be confused with Dengue infections as they both lead to high temperatures and myalgias, and usually occur in tropical areas. And also, the two viruses are both transmitted by the *Aedes* species mosquitoes and possibly co-circulate and result in dual infections and epidemics (Nimmannitya et al., 1969, Myers and Carey, 1967, Halstead et al., 1969a, Ratsitorahina et al., 2008). However, the two diseases still have some differences in symptoms, CHIKV is more consistent in prominent and prolonged arthritis while dengue virus infection is more commonly associated with haemorrhage (Nimmannitya et al., 1969, Hochedez et al., 2008).

CHIKV fever is confirmed by laboratory diagnostic detection of virus, viral RNA or CHIKV-specific antibodies. RT-PCR or viral culture performed on an acute-phase specimen is a useful method for CHIKV diagnosis because of the high levels and long last of viremia caused by CHIKV infection (Lanciotti et al., 2007, Laurent et al., 2007). Virus can be isolated from the serum collected during the first week of the illness, then viral nucleic acid can be detected by real-time RT-PCR (Lanciotti et al., 2007, Panning et al., 2008). In 2008, a real-time PCR detection method developed at the Centres for Disease Control and Prevention (CDC) became commercially available (Focus Diagnostics), but the validity and sensitivity still need more confirmation (Staples et al., 2009). ELISAs is another quick and specific method for CHIKV detection. Both anti-CHIKV immunoglobulin (Ig) M and IgG antibodies can be used for test, IgM

antibodies develop fast and can persist for a few months (Lanciotti et al., 2007, Panning et al., 2008). Rapid dipstick is also in development for CHIKV diagnosis in the field (Panning et al., 2008), whereas the sensitivity and popularization still need more improvement. Immunofluorescence assays and plaque assays are also useful for CHIKV diagnosis but are limited in laboratories as they have high demand of equipment, training and biosafety level 3 laboratory containment laboratory environment (Litzba et al., 2008).

Treatment against CHIKV infection is now directed primarily at relieving the symptoms, including the joint pain using anti-pyretic, optimal analgesics and fluids. Although some in vitro studies and limited clinical data have suggested that some certain drugs, such as chloroquine, acyclovir, interferon- α (IFN- α), ribavirin and corticosteroids might be effective in treatment against CHIKV infection, the proof is still not sufficient to confirm the benefits and effectiveness of these interventions.

The exploitation of CHIKV vaccines develops step by step from formalin-inactivated vaccines to CHIKV live-attenuated vaccines, and nowadays virus-like particles (VLP) and viral-vectored vaccines (Reyes-Sandoval, 2019). So far, there is still no licensed vaccine against CHIKV, but various developments have entered phase I and II trials and are now viable options to fight this incapacitating disease. The VLP, known as VRC-CHKVLP059-00-VP, has been proved to be safe and efficient in an assessment of the VRC 311 phase I clinical trial in a dose-escalation, open label trial with 25 adults of 18-50 years of age, and now has entered phase II trials for further evaluation in 400 healthy adults between 18-60 years of age (Chang et al., 2014, Reyes-Sandoval, 2019). In 2013, Samantha Brandler et al. reported the development of a recombinant Measles viral-vectored (MVV) vaccine expressing the heterologous structural genes of CHIKV (Brandler et al., 2013). This MV-CHIKV vaccine has been assessed in both phase I clinical trial and a subsequent double-blind, randomised, placebo-controlled and active-controlled phase II trial, and showed excellent safety and tolerability (Ramsauer et al., 2015, Reisinger et al., 2019).

In conclusion, there is still no confirmed anti-viral treatment or safe and effective vaccines available but research in this area is developing vigorously.

1.2 Molecular virology of CHIKV

1.2.1 Molecular structure and genome organisation of CHIKV

As a member of the *Alphavirus* genus, CHIKV is a small (60-70 nm-diameter), spherical, enveloped virus with a positive-strand RNA genome (Powers et al., 2001, Strauss and Strauss,

1994). *Alphavirus* is one of the simplest enveloped virus, with one copy of genome RNA, 240 copies of capsid protein, formed as 120 copies of dimers (Perera et al., 2001), arranged in a $T=4$ lattice, and the surface glycoprotein spikes, consisting of E1 and E2, forming a $T=4$ structure as 80 trimers of heterodimers (Cheng et al., 1995, Zhang et al., 2002).

The genome structure of CHIKV is as follows: 5'cap-nsP1-nsP2-nsP3-nsP4-(junction)-C-E3-E2-6k-E1-poly(A)-3' (Figure 1.5). Similar to eukaryotic mRNAs, it possesses 5'cap structure and 3'poly(A) tail. It contains two open reading frames (ORF) encoding non-structural proteins (7425 nt) and structural proteins (3747 nt), respectively. The second ORF is expressed through a subgenomic RNA produced from an internal promoter in the negative strand RNA replication intermediate (Strauss et al., 1984).



Figure 1.5 Structure of CHIKV genome RNA.

1.2.2 Non-coding regions of CHIKV genome

1.2.2.1 5'-untranslated region (UTR) of CHIKV

The 5'UTR of CHIKV is highly conserved and composed of 76-77 nucleotides (Hyde et al., 2015). The 5' termini modification by the addition of a 7-methylguanosine (m7G) cap structure helps to promote RNA stability and translation of viral transcripts. The m7G capping for alphaviruses is performed in a distinct way from host mRNA capping (Ahola and Kaariainen, 1995) (Figure 1.6). As m7G cap is important for translation of alphavirus RNAs, 5'UTR regulates it by both its sequence and structure. Host translation initiation factors eIF4E and eIF4F recognise specific 5'UTR, forming distinct secondary structures to initiate viral protein translation (Hyde et al., 2015). However, it was shown recently that Sindbis virus produced non-capped viral genomic RNAs, especially in significant numbers during the early phase of infection (Sokoloski et al., 2015). The precise importance of these non-capped viral RNAs during infection was not clear, but these uncapped viral RNA containing 5'-triphosphate (5'-ppp) are the target of RIG-I/MDA5 mediated IFN innate immune response (Chiu et al., 2009, Barral et al., 2009, Akhrymuk et al., 2016). 5'UTR and its complementing sequence in the 3' end of the negative strand are also critical for alphavirus genome replication (both positive- and negative-strand RNA synthesis) based on its sequence and stable secondary structure (Kulasegaran-Shylini et al., 2009, Nickens and Hardy, 2008). Some previous studies have found that compensatory mutations within viral replicase proteins (nsPs) appeared to alter the host

factors that bind the UTR when mutations were introduced into 5'UTR. This indicates that the motifs within 5'UTR must be significant for the coordinated recruitment of viral and host factors required for replication, although the actual role of 5'UTR sequence and structure in RNA synthesis is not yet absolutely understood (Berben-Bloemheugel et al., 1992, Pardigon and Strauss, 1992, Pardigon et al., 1993, Shirako et al., 2003, Castello et al., 2006). Alphavirus 5'UTR is also involved in immune restriction and viral pathogenesis. A single mutation introduced into a VEEV attenuated strain compromised virulence in immunocompetent mice (White et al., 2001). Sequence deletions and point mutations within Sindbis or Semliki Forest Virus (SFV) 5'UTR also affect their pathogenicity and neurovirulence in rodents (Klimstra et al., 1999, Kobiler et al., 1999, Kuhn et al., 1992, Logue et al., 2008). In conclusion, the 5'UTRs of alphaviruses are multifunctional regions important in promoter function, initiation of translation, translational shutoff and cellular innate immune escape of the viruses.

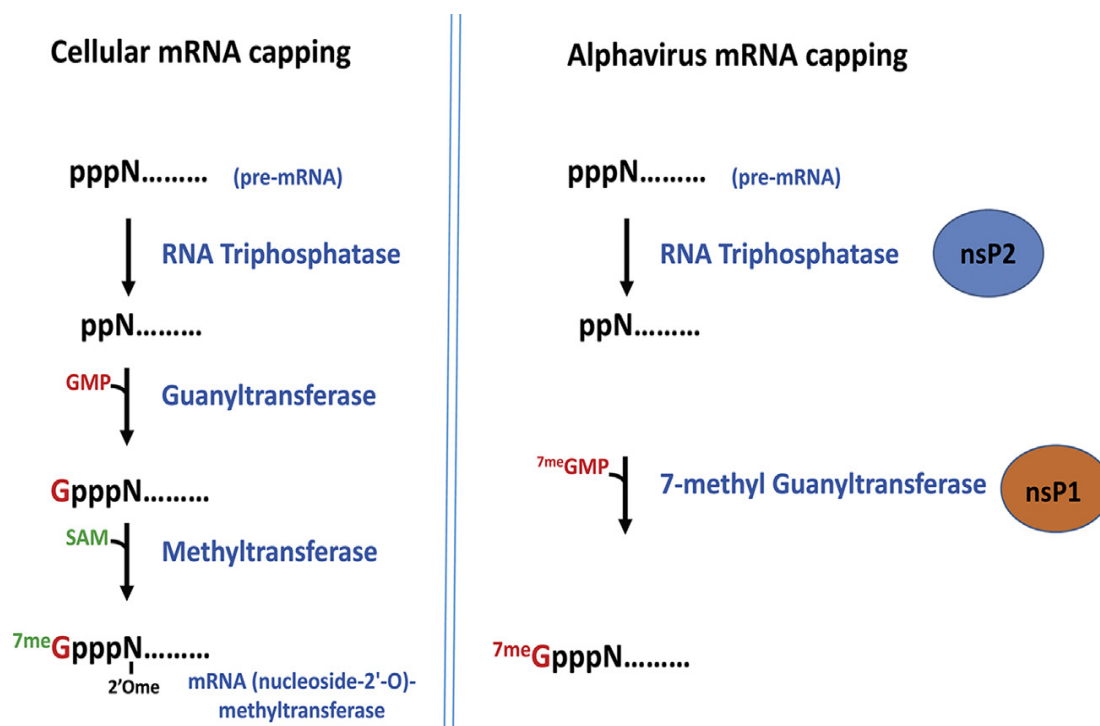


Figure 1.6 A comparison between mRNA capping of cellular and alphavirus mRNAs.

The methyl donor S-adenosyl methionine (SAM) is indicated in green. In alphavirus capping, the nsP1 protein methylates GMP prior to covalently attaching the modified GMP to the diphosphate at the 5' end of the pre-mRNA generated by triphosphatase activity associated with nsP2. Cellular mRNAs generally contain a 2'-O-methyl modification (2'-O me) of the first nucleotide downstream of the N-7^{me}Gppp cap that is not seen in alphavirus transcripts. Picture is copied from (Hyde et al., 2015).

1.2.2.2 3'UTR of CHIKV

The 3'UTR of CHIKV genome varies from 498 to 723 nt. As shown in Figure 1.7, it contains a number of direct repeats (DRs), which possibly result from historical duplication events, occurring in lineage-specific patterns (Chen et al., 2013). The 3'UTR plays an important role in virus genome replication. A 19-nt highly conserved sequence element (CSE) at the end of 3'UTR, followed by poly(A) tail, is the promoter for negative-strand intermediate RNA synthesis (Kuhn et al., 1990, Pfeffer et al., 1998). The poly(A) tail functions in both negative-strand RNA synthesis and efficient translation. It is predicted that the poly(A)-poly(A) binding protein (PABP) complex and 5'UTR-translation initiation factors complex could interact to form a mRNA circularization and initiate translation (Lemay et al., 2010, Hardy and Rice, 2005). There are also some repeat sequence elements (RSEs) within 3'UTR which may contribute to virus replication in mosquito cells by producing microRNA (miRNA) or interaction with host proteins (Trobaugh et al., 2014). It also serves as a target for host miRNAs to block virus replication (Trobaugh et al., 2014). The 3'UTR is also reported to interact with host factors such as HuR proteins to stabilize viral RNA in the cytoplasm in host cells by inhibiting deadenylation and viral RNA decay (Garneau et al., 2008, Sokoloski et al., 2010, Dickson et al., 2012).

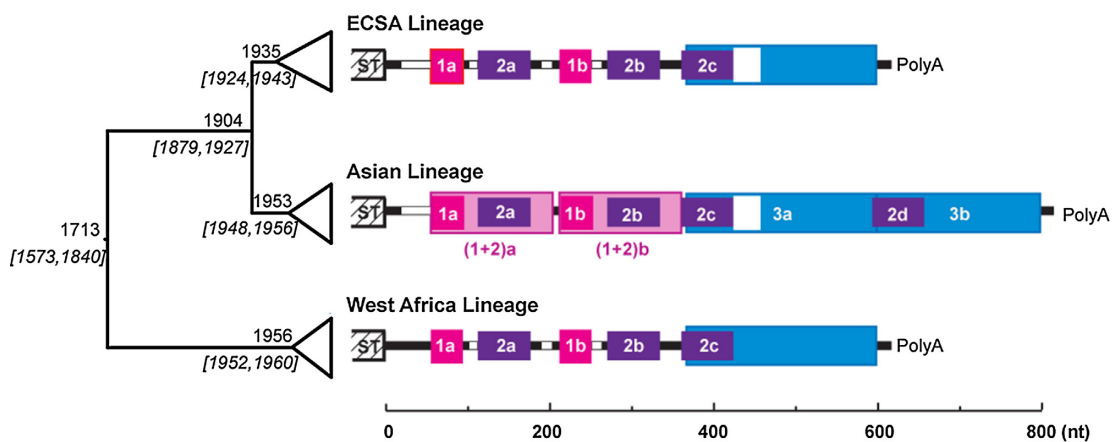


Figure 1.7 Evolutionary history and lineage-specific structures of the CHIKV 3'UTR.

On the left is the Maximum Clade Credibility tree based on the complete ORF sequences. The sequence alignment-based 3'UTR structures are shown next to each lineage. Direct repeats are illustrated by different coloured blocks, and each of the four colours represents a different homologous sequence region. White blocks indicate sequence gaps during alignment. Picture is copied from (Chen et al., 2013).

1.2.2.3 Subgenomic RNA promoter of CHIKV

Subgenomic RNA promoter, another sequence element, locates at the junction between the two ORFs. The core sequence starts from the last 19th nt of nsP4 to the 5th nt within junction area between non-structural proteins and structural proteins coding region. Additional enhancer elements and contextual effect were identified by studies using dual-promoter viruses (Raju and Huang, 1991, Wielgosz et al., 2001). The full, optimal promoter was mapped to -98 to +14 and the specific requirements within this region were identified (Wielgosz et al., 2001). The subgenomic RNA promoter capping modification and its interaction with host proteins are important for viral genome replication and structural protein production (Castello et al., 2006).

1.2.3 Structural proteins

CHIKV has 5 structural proteins: capsid protein (CP), E1, E2, E3 and 6k, that translated from a 4269 nt subgenomic RNAs. The five structural proteins are expressed as a polyprotein at first and then processed co-translationally and post-translationally into structural proteins CP, pE2 (precursor to the E3 and E2 proteins prior to furin cleavage), E1 and a small peptide 6k. The CP is firstly translated and released from the polyprotein with its own protease activity, exposing a translocation signal at the new N-terminal to transfer pE2 sequence across the ER membrane, resulting in pE2, 6k and E1 cleavage, and post-translational modifications such as addition of high-mannose chains, carbohydrate chains (Garoff et al., 1990, Hsieh and Robbins, 1984, Knight et al., 2009). During transport of the pE2-E1 complex, after the heterodimer reaches the trans-Golgi network but before it arrives at plasma membrane, pE2 is cleaved to form E3 and E2 before generation of infectious virus (Gaedigk-Nitschko and Schlesinger, 1990, Heidner et al., 1994, Salminen et al., 1992).

1.2.3.1 Capsid protein

The capsid protein consists of 261 amino acids (aa), with a poorly conserved N-terminus which may be important for nucleocapsid (NC) core assembly and a highly conserved C-terminal autoprotease domain. The first 100 aa of alphavirus CP are presumed to bind to the genomic RNA (Coombs and Brown, 1989); and the later domain helps to release itself from the nascent structural polyprotein with serine protease activity acting in cis (Solignat et al., 2009). 240 copies of CP, shown as 120 copies of dimer, complexed with one single copy of RNA will form one NC.

1.2.3.2 E1

The E1 protein is 440 aa long. It covers most of the lipid membrane by forming a continuous icosahedral protein shell on the virion. For SFV, the E1 ectodomain is composed of 3 β -barrel domains. Domain I lies between domain II and III, and contains the two amino terminus. The C-terminus locates within domain III and the fusion part is at the distal end of domain II. The E1 monomers lie at the bottom of the surface spikes in the formation of lattice on virus surface (Mukhopadhyay et al., 2006). The alphavirus E1 protein functions to convert the viral surface proteins into plasma membrane through the ion-permeable pores, and is responsible to fuse viral envelope with the host endosomal membrane during virus entry (Wengler et al., 2003).

1.2.3.3 E2

E2 is a long, thin molecule of a leaf-like structure, highly exposed at the top of the spike followed by a narrower stem twisting around E1 molecule (Zhang et al., 2002). E2 include three domains: the ectodomain consisting of the first 260 aa, the stem region consisting of about 100 aa, and a transmembrane helix of 30 aa. E2 is the link between envelope proteins and the NC. The 33 aa E2 C-terminal domain is responsible for interaction with NC core, and the leaf-like structure interacts with E1 domain II distal end while the stalk portion has contact with E1 domain I and III (Mukhopadhyay et al., 2006, Pletnev et al., 2001). E2 is also involved in receptor binding and subsequent receptor-mediated endocytosis (Jose et al., 2009).

1.2.3.4 E3

E3 protein is a small peptide cleaved from pE2 by fusion in the Golgi. On the surface of virus particles, E3 is predominantly located between the petals of the spike and forms a dual-lobed petal (Wu et al., 2008). E3 has a central role in pE2/E1 complex formation and viral structural components transportation to the site of budding. Also, it is required for efficient virus assembly with an enzymatic or functional role that not yet proved (Parrott et al., 2009), mediating both spike folding and spike activation for viral entry (Jose et al., 2009).

1.2.3.5 6k

6k is a small, 6 kDa polypeptide that serves as a very small part of virions. Although only a small amount (7-30 copies) of 6k are needed in each virus particle, it is expressed in a same molecular amount as other structural proteins (Gaedigk-Nitschko and Schlesinger, 1990, Lusa et al., 1991). Although 6k is not detected in any identified cryo-EM virion structures so far, it is believed to be an essential component of infectious virus particles. Some mutations or

deletion of the 6k coding sequences lead to severely reduced infectious virus production in some specific host cell species (Loewy et al., 1995). In 2008, a frameshifting event was discovered by a bioinformatics team at a conserved UUUUUUA motif within the sequence encoding 6k, resulting in the synthesis of an additional protein, termed TF (TransFrame protein), and the presence of TF was confirmed by mass spectrometry in the Semliki Forest virion (Firth et al., 2008). Following studies demonstrated that 6k was likely involved in virus release by its role inside the cell, including interactions with glycoprotein spikes; and TF protein was present in virions with unknown functions in virus spread in an animal host (Ramsey and Mukhopadhyay, 2017).

1.2.4 Non-structural proteins

The non-structural proteins (nsPs) are translated from the first 7425-nt ORF of the viral genome. They are firstly expressed as a polyprotein and then cleaved into four different proteins, nsP1, nsP2, nsP3 and nsP4, necessary for virus genome replication and viral protein expression. Translation of viral genomic RNA produced two kinds of non-structural protein precursors, nsP123 and nsP1234. nsP1234 is expressed when an opal termination codon at the end of nsP3 is read-through (Firth et al., 2011). The precursor polyprotein is then cleaved by nsP2 carboxy-terminal protease (de Groot et al., 1990). nsP4 is firstly cleaved from the polyprotein either in cis or trans followed by nsP1 cleavage in cis (Vasiljeva et al., 2003). Both nsP123+nsP4 and nsP1+nsP23+nsP4 are used to form early replication complex with host proteins to synthesize negative-strand viral RNA intermediate. After that, cleavage between nsP2/3 occurs to produce 4 mature nsPs and switch RNA synthesis from negative-strand RNA to positive-strand genomic and subgenomic RNA with poorly understood mechanism.

1.2.4.1 nsP1

The 60 kDa nsP1 mainly functions in two aspects during virus replication. The first one is the capping activity to add 5'cap to alphavirus genomic and subgenomic RNA, with the Rossman-like methyltransferase (MTase) motifs in the N-terminal domain of it (Martin and McMillan, 2002, Schluckebier et al., 1995, Rozanov et al., 1992). The other revealed function of nsP1 is its association to host membranes. An amphipathic helix and palmitoylation are the key factors to anchor nsP1 or nsP1-containing non-structural polyprotein to the host membrane (Ahola et al., 2000, Lampio et al., 2000, Spuul et al., 2007). nsP1 is also predicted to be involved in membrane and cytoskeletal rearrangement, cell filopodia formation and alphavirus cell-to-cell transmission (Karo-Astover et al., 2010, Martinez et al., 2014). Although the specific molecular

understanding is still unknown, nsP1 is believed to be important for negative-strand RNA synthesis (Hahn et al., 1989, Wang et al., 1991).

1.2.4.2 nsP2

nsP2 is about 90 kDa and is a multifunctional protein during virus infection. It was initially thought to contain 2 domains, an N-terminal helicase domain which also performs nucleoside triphosphatase (NTPase) activity, and a C-terminal protease domain. Then crystallographic analysis revealed that the C-terminal domain contains a third domain with an MTase-like fold which likely had no enzymatic activity due to a lack of active-site residues (Russo et al., 2006). During virus replication, nsP2 serves three different important functions as a helicase, a triphosphatase and a protease. Besides these, nsP2 is also involved in the shutoff of host macromolecular synthesis leading to the virus cytotoxicity. As a helicase, nsP2 functions to unwind RNA secondary structures during virus genome replication. This helicase activity is dependent on the NTPase activity of the N-terminal domain (Rikonen et al., 1994). nsP2 exhibits also a RNA triphosphatase (RTPase) activity within its N-terminal domain and this activity is required to enable nascent virus genomic RNA as a substrate for nsP1-mediated capping reaction (Vasiljeva et al., 2000). As a protease, nsP2 is responsible for the processing of the non-structural polyproteins into 4 individual mature non-structural proteins. The protease domain is essential for protease activity but the entire protease activity must also be modulated by other domains of nsP2 and nsP2-containing polyprotein (Vasiljeva et al., 2003). nsP2 has also been predicted to be involved in virus subgenomic RNA synthesis by binding to subgenomic promoter but evidence for this function is as yet lacking (Suopanki et al., 1998).

1.2.4.3 nsP3

nsP3 consists of 530 aa and is divided into 3 domains: the macrodomain, the alphavirus unique domain (AUD) and the hypervariable region. The importance of nsP3 in alphavirus replication is in no doubt as mutations have been shown to disrupt virus negative-strand or subgenomic RNA synthesis (LaStarza et al., 1994b, Wang et al., 1994, Rupp et al., 2011). nsP3 is also proved to specifically suppress different host antiviral pathways in alphavirus (Fros and Pijlman, 2016). However, the precise roles of nsP3 during virus replication is still unknown. More information about nsP3 will be described in 1.3.

1.2.4.4 nsP4

The ~70 kDa nsP4 is the most highly conserved protein in alphavirus, solely responsible for the RNA synthesis properties of the viral replicase complex. The expression on nsP4 is restricted

because of a leaky opal stop codon in the end of nsP3 coding sequence. The core RNA-dependent RNA polymerase (RdRp) domain is located at the C-terminal of nsP4. The RdRp plays a role in producing genomic RNA via the negative-strand intermediate and transcribing subgenomic RNA. The model of RdRp domain exhibits a classical structure of RdRp with well-defined finger, palm containing the GDD active site and thumb domains (O'Reilly and Kao, 1998, Tomar et al., 2006, Rubach et al., 2009). The N-terminal sequences of nsP4 are unique to alphavirus RdRp, and are targeted for degradation (de Groot et al., 1990).

1.3 nsP3

Alphavirus nsP3 is always involved in complexes together with other viral proteins or host factors. It was initially thought stable until a degradation signal was discovered at the C-terminal region of SFV and SINV nsP3 (Varjak et al., 2010). The rapid degradation of nsP3 only occurs when individually expressed in the early stage of virus replication, but not in the context of the polyprotein nsP123. However, the significance of the degradation signal is not yet characterised. The function of CHIKV nsP3 has not been clearly revealed but a lot of studies of nsP3 have been performed on other alphaviruses.

During alphavirus replication, nsP3 could be observed in different parts of the infected cells. Some of nsP3 are located on the cytoplasmic surface of virus replication complex that exists on the plasma membrane in the early stage of virus replication. Then for some alphaviruses replication in some specific cell lines, nsP3 could be found in the spherules anchored on CPVs in the perinuclear area (Froshauer et al., 1988, Cristea et al., 2006, Kujala et al., 2001). Besides the ones occupied in the replication complexes, there are also some replication complex separated nsP3 aggregates existing in cytoplasm, suggesting that nsP3 has other functions independent of virus genome replication.

nsP3 is predicted as a vector specificity determinant. Replacement of CHIKV nsP3 with ONNV nsP3 made chimeric CHIKV infectious to *Anopheles gambiae* mosquitoes which are naturally refractory to CHIKV WT infection (Saxton-Shaw et al., 2013), presumably by specific viral-host proteins interactions (Lastarza et al., 1994a). A study of RNAi suppressor activity also suggests that the function of nsP3 varies between mosquito and mammalian cells (Mathur et al., 2016).

Moreover, nsP3 has been demonstrated to be the major determinant of neurovirulence for Old World alphaviruses but not New World alphaviruses (Tuittila et al., 2000, Tuittila and Hinkkanen, 2003, Suthar et al., 2005, Atkins and Sheahan, 2016).

As described above, nsP3 is essential for alphavirus infection with multiple functions. It is divided into three domains (Figure 1.8) and each domain has different roles during virus infection.

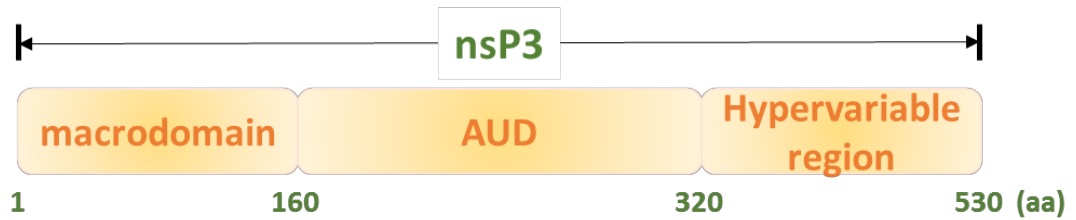


Figure 1.8 Diagram of nsP3.

1.3.1 Macrodomain

The N-terminal macrodomain of nsP3 is conserved among alphaviruses and its homologous domains can be found in the proteins of many other species such as other positive-strand RNA viruses, bacteria and eucaryotes (Koonin et al., 1992, Rack et al., 2016). Structural studies revealed that the macrodomain consists of a central twisted six-stranded β sheet surrounded by three helices on one side and one on the other (Figure 1.9), indicating its biochemical and structural basis of ADP-ribose binding and RNA binding (Lykouras et al., 2018, Malet et al., 2009). Studies have demonstrated the ADP-ribose binding activity of macrodomain, as well as its dephosphorylation function of ADP-ribose-1''-phosphate and de-ADP-ribosylating activity (Fehr et al., 2018). The activity of ADP-ribose-protein hydrolase for mono-ADP-ribose (MAR) chain removal (de-MARylation activity) is also demonstrated recently in different alphaviruses (Eckei et al., 2017). These enzymatic activities of macrodomain are significant for both virus replication and virulence. Besides these, macrodomain is also considered to have other functions. For example, it is shown to serve as a recognition site of nsP2 for cleavage of nsP2/3; and the ssRNA binding activity of macrodomain was predicted to affect nsP3 phosphorylation and virus negative-strand RNA synthesis (Lulla et al., 2012, De et al., 2003).

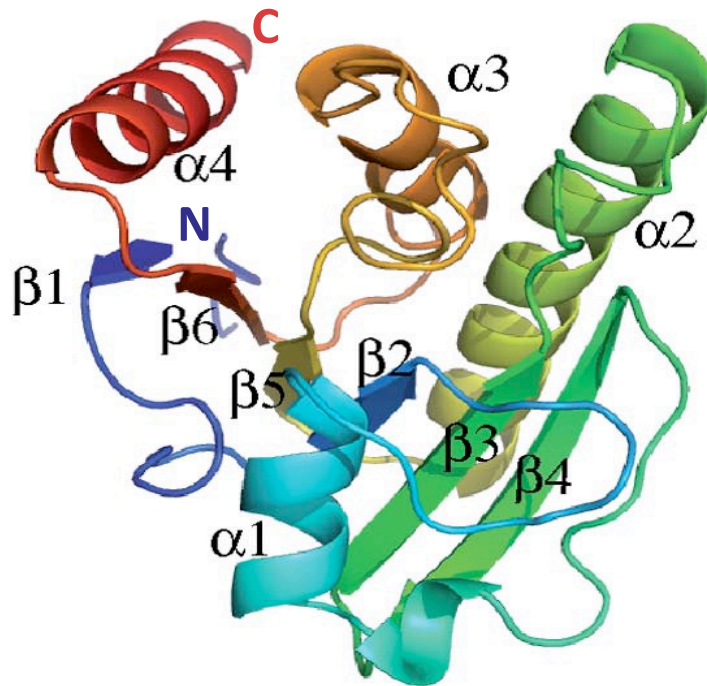


Figure 1.9 Structure of CHIKV macro domain.

Representation of CHIKV macrodomain in a purple-to-red gradient (from N terminus to C terminus). Secondary structure elements are labelled on the structure. Picture is copied from (Malet et al., 2009).

1.3.2 AUD

The AUD is located in the middle of nsP3 with essential but unknown functions for alphavirus replication. It exhibits a high degree of homology across all alphaviruses with a unique structure. Mutation in AUD has been shown to disrupt early events during virus genome replication with a defect in formation of early replication complex for negative-strand RNA synthesis (LaStarza et al., 1994b, Wang et al., 1994). In a study revealing the structure of an uncleaved SINV nsP2/3 precursor including the protease and methyltransferase-like (MT-like) domains of nsP2, as well as the macro domain and AUD of nsP3, the structure of AUD was analysed and a zinc-binding domain (ZBD) was found in it (Figure 1.10). Four absolutely conserved cysteine residues coordinate a zinc ion. Mutations of each cysteine residue could absolutely block CHIKV replication, indicating the four cysteine residues were individually essential for virus replication. In addition, a series of aa located around the ZBD were predicted to have RNA-binding activity. Besides, according to the revealed structure of nsP2/3, the nsP2/3 cleavage site was a narrow cleft between MT-like domain of nsP2 and nsP3 macrodomain. Macrodomain and AUD form a ring-like structure which shows an extensive

charged interface with nsP2 and encircles its MT-like domain. This interface between nsP2 and nsP3 were proved to be important for both virus cytopathic effect and virus RNA infectivity by mutations of the residues among this interface (Shin et al., 2012). The requirement of AUD for alphavirus replication is certain but the precise roles of this domain is not clear. A recent study also revealed that AUD might be involved in RNA interference (RNAi) suppression activity (Mathur et al., 2016).

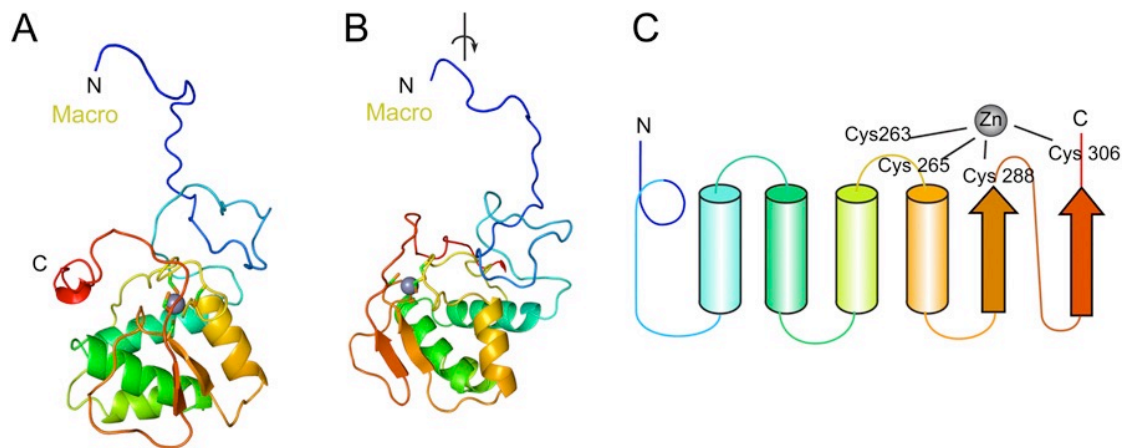


Figure 1.10 ZBD of nsP3.

(A and B) Ribbon diagrams of the middle region of nsP3, showing the linker and ZBD. The polypeptide chain is rainbow colored from the amino terminus (blue) to carboxyl terminus (red). The coordinated, zinc atom is represented by a gray sphere surrounded by the four coordinating cysteine residues in stick format. The view in B is rotated 90° along the vertical axis from A. (C) Topology model of the nsP3 linker and ZBD, highlighting the location of the cysteine-coordinating residues. The colouring follows the ribbons diagram in A and B. Picture is copied from (Shin et al., 2012).

1.3.3 Hypervariable region

Different from macrodomain and AUD, the C-terminal hypervariable region varies in both sequence and length among alphaviruses. Although it is not a conserved domain, it shares a lot of features existing in many members of the family, indicating it is involved in multiple virus-host protein interactions. For example, a hyperphosphorylated region and a proline rich region, as well as some repeated elements were found in this domain (Strauss et al., 1988, Vihinen et al., 2001, Lastarza et al., 1994a, Vihinen and Saarinen, 2000, Oberste et al., 1996, Meissner et al., 1999). The hypervariable region is essential for alphavirus replication but studies have shown that this domain is partially tolerant to some deletions or insertions (Lastarza et al., 1994a, Davis et al., 1989, Galbraith et al., 2006). Based on this, a series of signal proteins were fused into nsP3 to follow the subcellular distribution of nsP3 and explore novel interaction

factors with nsP3 during virus replication by immunofluorescence or immunoprecipitation (Remenyi et al., 2018, Spuul et al., 2010, Cristea et al., 2006, Remenyi et al., 2017). However, there are still some critical residues in hypervariable domain essential for virus replication efficiency (Panas et al., 2015, Schulte et al., 2016). Some host proteins have been identified to be recruited to the replication complex by interaction with the hypervariable domain, including PAR polymerase-1 (PARP-1), DEAD-box RNA helicase, Src homology 3 (SH3)-domain containing proteins, Ras-GTPase-activating protein (SH3-domain)-binding protein (G3BP) (Park and Griffin, 2009, Amaya et al., 2016, Neuvonen et al., 2011, Panas et al., 2015, Meshram et al., 2018). G3BP is essential for CHIKV replication as knockout of both G3BP1 and G3BP2 absolutely terminated CHIKV replication (Kim et al., 2016). The various interactions of the unstructured hypervariable region with host proteins implies its involvement in the adaptation to different hosts.

1.4 CHIKV life cycle

1.4.1 Entry of CHIKV

The process of entering a susceptible cell starts with the engagement of virus and a host receptor. Host receptors vary for different alphaviruses, and are thought to be proteins although non-protein factors may also in requirement during virus attachment and entry (Smith and Tignor, 1980). Alphaviruses envelope glycoproteins are responsible for the attachment of viruses to cells. The trimeric spikes on virus particles surface consist of E1 and E2 glycoproteins heterodimers. The crystal structures of the precursor p62-E1 heterodimer and of the mature E3-E2-E1 glycoprotein complexes have been reported in 2010, revealing the first step of CHIKV fusogenic transition was removal of the domain B cap covering the fusion loop without dissociation of the E2-E1 heterodimer, and the organization of the individual immunoglobulin-like domains of E2 which are responsible for receptor interactions, carrying important determinants of virulence and mosquito vector range (Voss et al., 2010). CHIKV is reported to persistently and productively infect a broad range of cell lines of its mammalian hosts, including human hepatocellular carcinoma cells (Huh7, HepG2), mouse muscle myoblast cells (C2C12), human brain astroglia cells (SVG-A), dermal fibroblast cells, human muscle rhabdomyosarcoma cells (RD), hamster kidney fibroblast cells (BHK-21), human lung epithelial carcinoma (A549), human cervical epithelial carcinoma cells (Hela) and African green monkey kidney epithelial cells (Vero E6) (Roberts et al., 2017). Together with some other research (Sourisseau et al., 2007), CHIKV was shown to be limited in its binding and activity to some specific cell lines and cellular subpopulations, indicating that similar to other enveloped viruses,

CHIKV has a tropism for some cells which may specifically express unknown receptors for CHIKV infection. The receptors of CHIKV in different cells have not been clearly demonstrated but Mxra8 has been proved to be a receptor for multiple arthritogenic alphaviruses including CHIKV in mammals, birds, and amphibians (Zhang et al., 2018), prohibitin was identified as a CHIKV receptor protein in microglial cells (Wintachai et al., 2012), and the heat shock cognate 70 protein was shown to facilitate its entry into mosquito cell line C6/36 (Ghosh et al., 2017). As CHIKV, as well as other alphaviruses, is able to infect various vertebrate and invertebrate hosts, there are two hypotheses to explain the mechanism of virus entry into different cells. One is as mentioned above, that the virus makes use of a conserved receptor expressed on the surface of cells of different host types. For example, the eukaryotic protein laminin is predicted to be a receptor for alphavirus entry as it exists on both mammalian and mosquito cells (Ludwig et al., 1996, Wang et al., 1992). The other hypothesis is that the viruses interact with different cellular receptors for entry into cells (Jose et al., 2009). This is supported by the facts that even a single change in E1 or E2 amino acid sequences can alter the receptors used for virus entry (Lustig et al., 1988, Tucker and Griffin, 1991).

Some alphaviruses, such as SFV and VEEV, have been shown to enter cells in a clathrin-dependent endocytosis manner (Helenius et al., 1980, Marsh et al., 1983, Kolokoltsov et al., 2006), and the experimentally introduced anti-clathrin antibodies inhibited SFV endocytosis into cells (Doxsey et al., 1987). Clathrin-coated pits are then uncoated to form endosomes. When the virus-containing endosome matures, the pH in the vesicle becomes mildly acidic, leading to the destabilization of E1-E2 heterodimer, and therefore exposing a fusion loop at the end of E1 protein (Lescar et al., 2001, Gibbons et al., 2003, Ahn et al., 1999, Hammar et al., 2003). The fusion loop inserts into the membrane of late endosomes and then trimerizes (Wahlberg et al., 1992, Gibbons et al., 2000). As a result of the fusion loop insertion, virus envelope and endosomal membranes fused and form a fusion pore for NC to be released into the host cell cytoplasm. CHIKV entry into mammalian cells has also been studied recently. It was found that a mutant of Eps15 protein which impeded clathrin-coated pits assembly but did not affect the clathrin-independent endocytic pathway dramatically reduced CHIKV infection (Solignat et al., 2009), indicating that CHIKV also utilizes the clathrin-dependent endocytic pathway for virus entry into cells. Interestingly, at the same time, they found that CHIKV infection of HEK293T mammalian cells was clathrin heavy chain-independent. The prevention of endosome acidification prior to virus infection also significantly reduced CHIKV infection (Bernard et al., 2010).

1.4.2 Intracellular replication of CHIKV

So far, the intracellular replication cycle of CHIKV has not been clearly demonstrated (Solignat et al., 2009). Therefore, to get a general understanding of CHIKV intracellular replication, deductions from the data obtained with other alphaviruses are made and strengthened by sequence comparison to make sure that the functional amino acids exist in the corresponding CHIKV proteins.

For alphaviruses, once delivered into cytoplasm, the NC disassembles in some way to expose the viral genome for viral protein translation. It has been shown by thin-section micrographs that the NC is originally intact once enters the cytoplasm and then disassembles within five minutes (Helenius, 1984). It is predicted that alphavirus NC disassembles through interaction between capsid protein and ribosomes (Singh and Helenius, 1992). The exposure of virions to low pH environment is also suggested to prime the NC disassembly in cytoplasm (Jose et al., 2009).

Replication of viral RNA occurs in cytoplasmic vacuoles derived from endosomal and lysosomal membranes (Froshauer et al., 1988). Alphavirus replication proceeds in several steps. At first, non-structural proteins are translated from virus genomic RNA as a polyprotein precursor. Nearly 90% of the translation products are nsP123 polyprotein, while 10% are nsP1234 polyprotein produced after the read-through of the opal stop codon located at the junction of nsP3 and nsP4 (Li and Rice, 1993, Strauss et al., 1983). After translation, nsP4 is promptly cleaved by nsP2 of its C-terminus protease activity (de Groot et al., 1990). The cleavage of nsP4 from the non-structural polyprotein is obligatory as nsP1234 polyprotein is not involved in any stages of virus genome replication (Kallio et al., 2016, Shirako and Strauss, 1994). After synthesis and maturation, nsP123 which presents only in high concentrations in early stage of infection, together with nsP4 as well as some cellular proteins, acts as early polymerase complex for negative-strand RNA synthesis using genomic RNA as a template (Strauss et al., 1992, Shirako and Strauss, 1994, Shirako and Strauss, 1990). The early polymerase complex is also capable but inefficiently to synthesize positive-strand RNA (Kallio et al., 2016, Lemm and Rice, 1993). Then nsP1 is cleaved from nsP123 and form the complex of nsP1, nsP23 and nsP4 which is able to synthesize both negative- and both positive-strand RNAs (Jose et al., 2009, van der Heijden and Bol, 2002). An *in trans* cleavage between nsP2 and nsP3 follows to fully process the four non-structural proteins into nsP1, nsP2, nsP3 and nsP4, and form the late replication complex. The late replication complex can only synthesize positive-strand RNA and subgenomic RNA using negative-strand RNA as template, and subgenomic RNA is produced in

higher quantities than genomic RNA (Keränen and Kaariainen, 1979). Subgenomic RNA is the template for structural proteins translation. The structural proteins are firstly translated as a polyprotein of CP-pE2-6k-E1 (Raju and Huang, 1991). During maturation, CP is the first to be released from the polyprotein through autoproteolysis. By the release of the CP, a translocation signal exposes in the new N-terminus of the polyprotein, translocating the pE2 and E1 proteins across the ER membrane (Garoff et al., 1990). The pE2 and E1 proteins translocated into the ER membrane are then processed by post translational modifications (Garoff et al., 1990, Sefton, 1977, Hsieh and Robbins, 1984, Knight et al., 2009). During the transport of the pE2-E1 complex from *trans*-Golgi network to plasma membrane, E3 and E2 is produced by cleavage of pE2 with furin (Gaedigk-Nitschko and Schlesinger, 1990).

The precise interactions between non-structural proteins and other non-structural proteins and/or cellular proteins to form early or late replication complex are poorly understood so far due to the lack of protein structural data. The N-terminal amino acid of nsP4 is critical for its function. Changing of the nsP4 N-terminal amino acid to a nonaromatic residue was lethal but an aromatic amino acid or histidine residue did not significantly affect virus replication (Shirako and Strauss, 1998). One suppressor mutation in nsP1 and two suppressor mutations in nsP4 allowed the nonaromatic amino acid N-terminal nsP4 to be functional (Shirako et al., 2000). This indicated that the N-terminus of nsP4 interacted with nsP1 and other parts of nsP4 to form a proper protein structure participated in interaction with other viral or host proteins to allow the virus replication. And the N-terminus of nsP4, due to its flexible nature, forms different contacts with other proteins at different stages of virus replication to allow the synthesis of various virus RNA species (Rupp et al., 2011, Fata et al., 2002, Pietila et al., 2017).

For negative-strand RNA synthesis, it is still not clear how it is initiated but the poly(A)-binding protein (PABP) is believed to be involved to perform a genome-circularization mechanism, which is a protein primer-dependent initiation on the 3' poly(A) tail, like what happens in poliovirus replication (Frolov et al., 2001, Rupp et al., 2011, Pietila et al., 2017). It is hypothesized that replication complex binds the 5' end of virus genome RNA together with other cellular proteins to form a translational machinery, and the translation factors interact with PARP which binds the poly(A) at the 3' end of genome RNA, finally brings 5' end and 3' end of virus genome RNA together. This hypothesis is supported by a competition assay which showed that the 5' competitor RNA significantly inhibited negative-strand RNA synthesis, indicating that the negative-strand RNA synthesis required the interaction between 5' end and viral or cellular proteins (Frolov et al., 2001).

The initiation site of the positive-strand RNA synthesis is highly conserved for alphavirus genomes. The genomic RNA promoter is located at the 3' end of the negative-strand RNA which is within the corresponding 5' UTR stem loop sequence of positive-strand RNA, and the complementary stem-loop structure is also predicted for the negative-strand RNA. Regulation of positive-strand RNAs synthesis, including both genomic RNA and subgenomic RNA, is dependent on nsP4 itself as the different fragments of nsP4 bind to distinct promoters (Li and Stollar, 2004, Li and Stollar, 2007). The template for positive-strand RNAs synthesis is the negative-strand RNA; however, there is evidence that the template remains double-stranded (Kaariainen and Ahola, 2002), from which three forms of RNAs were released after RNase treatment, the full-length genome, the non-structural protein ORF and the subgenomic RNA (Simmons and Strauss, 1972a, Simmons and Strauss, 1972b). But the non-structural protein ORF RNA is not functional once come out of the intermediate therefore is likely a semi-finished product of virus replication and may be reactivated and finished synthesis at some frequency (Wielgosz et al., 2001).

Although the proteolytic processing of the non-structural polyprotein has been revealed, the way how the processed non-structural proteins form distinct replication complexes for the synthesis of different species of viral RNAs remains poorly understood. Some research have been performed to elucidate the arrangement within the replicase complexes. Salonen et al attempted to uncover the interactions among the 4 individual non-structural proteins by yeast two-hybrid screening but did not obtain conclusive results (Salonen et al., 2003). Interactions between nsP1 and nsP3, and between nsP1 and nsP4 have been confirmed by co-immunoprecipitation but their significance during virus replication was not demonstrated (Salonen et al., 2003, Zusinaite et al., 2007, Lulla et al., 2008). In conclusion, although some information have been obtained on the function and structure of each non-structural proteins, a model of replicase complexes is in urgent need for the study of virus genome replication regulation by alphavirus non-structural proteins.

1.4.3 Assembly, budding and maturation of CHIKV

The assembly, budding and maturation steps of CHIKV are almost unknown so far, and very little is known for other alphaviruses.

Alphavirus virion assembly begins with NC assembly in the cytoplasm. The alphavirus NC consists of one copy of genome RNA and 240 copies of CP. The assembly of NC occur in multiple steps. The nucleic acid binds a dimer of CP at the beginning of the assembly process (Tellinghuisen and Kuhn, 2000). The process of alphavirus NC assembly is not yet clearly

identified but it was predicted to occur on the cytopathic vacuoles formed post virus infection (Froshauer et al., 1988). Most alphaviruses including Sindbis, eastern, western, and Venezuelan equine encephalitis have packaging signals (PSs) which can be recognized by the capsid proteins of heterologous alphaviruses. However, CHIKV and other SFV clade alphaviruses are exception to the general rule. They contains PSs in the nsP2 gene but their capsid protein retains the ability to use the nsP1-specific PS of other alphaviruses (Kim et al., 2011).

Alphaviruses bud through the cell plasma membrane in both mammalian and mosquito cells (Lu and Kielian, 2000, Brown et al., 2018). Virus envelope proteins move to cell surface after being transported to trans Golgi, and nascent NC are transported to cell membrane with virus envelope proteins to start virion assembly. During budding, NC goes through a maturation process by binding with E2 to target cell membrane (Suomalainen et al., 1992). Previous research revealed that the 33 amino acids of E2 were involved in capsid-E2 interactions for RRV, and a similar sequence was found in CHIKV (Lopez et al., 1994, Solignat et al., 2009). Phosphorylation of NC, E1 and E2 glycoproteins are also believed to be important for virus assembly and budding (Liu et al., 1996, Waite et al., 1974, Liu and Brown, 1993).

The whole life cycle of alphavirus is depicted in Figure 1.11.

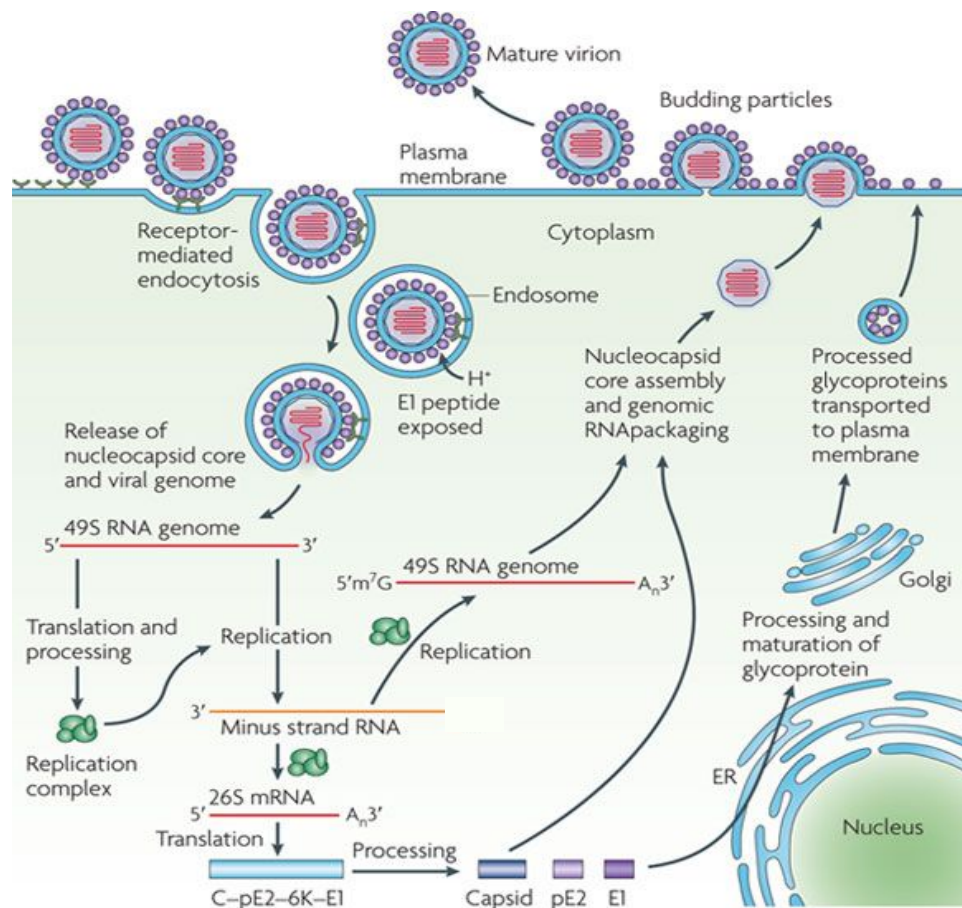


Figure 1.11 Model of the Alphavirus life cycle.

Alphaviruses enter target cells by endocytosis. A few receptors (for example, dendritic cell-specific ICAM3-grabbing non-integrin 1 (DC-SIGN; also known as CD209), liver and lymph node-SIGN (L-SIGN; also known as CLEC4M), heparan sulphate, laminin and integrins) have been implicated in this process, but their precise roles have not been firmly established. Following endocytosis, the acidic environment of the endosome triggers conformational changes in the viral envelope that expose the E1 peptide, which mediates virus-host cell membrane fusion. This allows cytoplasmic delivery of the core and release of the viral genome. Two precursors of non-structural proteins (nsPs) are translated from the viral mRNA, and cleavage of these precursors generates nsP1–nsP4. nsP1 is involved in the synthesis of the negative strand of viral RNA and has RNA capping properties, nsP2 displays RNA helicase, RNA triphosphatase and proteinase activities and is involved in the shut-off of host cell transcription, nsP3 is part of the replicase unit and nsP4 is the viral RNA polymerase. These proteins assemble to form the viral replication complex, which synthesizes a full-length negative-strand RNA intermediate. This serves as the template for the synthesis of both subgenomic (26S) and genomic (49S) RNAs. The subgenomic RNA drives the expression of the C–pE2–6K–E1 polyprotein precursor, which is processed by an autoproteolytic serine protease. The capsid (C) is released, and the pE2 and E1 glycoproteins are generated by further processing. pE2 and E1 associate in the Golgi and are exported to the plasma membrane, where pE2 is cleaved into E2 (which is involved in receptor binding) and E3 (which mediates proper folding of pE2 and its subsequent association with E1). Viral assembly is promoted by binding of the viral nucleocapsid to the viral RNA and the recruitment of the membrane-associated envelope glycoproteins. The assembled alphavirus particle, with an icosahedral core, buds at the cell membrane. Picture is adapted from (Schwartz and Albert, 2010).

1.5 Systems for the study of CHIKV

1.5.1 Cell culture system

A variety of CHIKV replicon or subgenomic replicon are used to explore the function of AUD in this project. There are a number of subgenomic replicon constructs available which were constructed by deletion of the structural genes from the cDNA of full length CHIKV (Fros et al., 2012). As these replicons lack any of the structural protein encoding sequences they are unable to produce virus and can be studied under standard BSL2 conditions.

A dual luciferase reporter system, using a CHIKV subgenomic replicon (CHIKV-D-Luc-SGR) (Figure 1.12), was used to study the significance of AUD in CHIKV genome replication in this project. CHIKV-D-Luc-SGR was derived from the ECSA strain (ICRES), containing two luciferase reporter genes, a renilla luciferase fused in frame in the C-terminus of nsP3 and a firefly luciferase replacing the structural protein encoding region of ORF2. Renilla luciferase is expressed as an internal fusion with nsP3 and thus is produced following translation of the input RNA and the nascent genome RNA; firefly luciferase is expressed from the subgenomic promoter and thus is only produced after RNA replication has occurred. Therefore CHIKV-D-Luc-SGR allows simultaneous assessment of both input translation and genome replication.

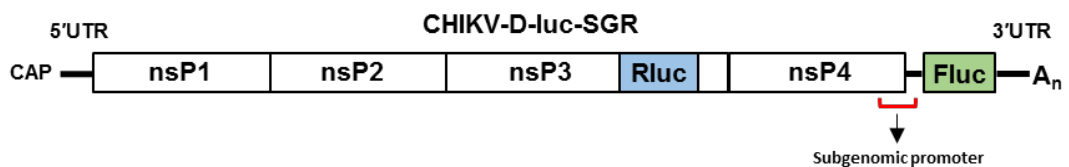


Figure 1.12 Diagram of CHIKV-D-Luc-SGR.

Renilla luciferase (Rluc) is inserted into the 5' end of nsP3 hypervariable region. Firefly luciferase (Fluc) is expressed in place of structural proteins, initiated with subgenomic promoter.

1.5.2 Animal models

CHIKV infection in humans is characterised by debilitating arthralgia which leads to intense pain and swelling to peripheral joints, high fever and rash (Dupuis-Maguiraga et al., 2012). Acute chikungunya symptoms in humans may resolve within 3-12 days after a bite by an infected mosquito (Suhrbier et al., 2012), but joint or muscle pain may remain for weeks to years (Schilte et al., 2013, Hoarau et al., 2010, Sissoko et al., 2009). The acute CHIKV infection-induced chronic joint pain is associated with the increased age of infected patients and the

disease severity during the acute stage (Hoarau et al., 2010, Sissoko et al., 2009, Chow et al., 2011). It is still in debate whether CHIKV is able to replicate and persist in the joints or muscles over the whole chronic pathologic stage. Despite the increasing importance of CHIKV all over the world, many details of its pathogenesis are not clearly demonstrated, especially the mechanisms of chronic CHIKV-induced joint and muscle pain. Therefore, animal models are raising increasing significance and interest for the study of CHIKV infection.

Mice and nonhuman primates are most commonly used as experimental animal models for CHIKV infection. Mouse models are advantageous in studying CHIKV pathogenesis and evaluation of CHIKV vaccines and therapeutics because of their low cost, ease of housing, high availability of various mouse-specific reagents, different inbred lines, as well as the possibility of genetically modification on individual animals (Haese et al., 2016). Mouse models include both acute infection models and chronic/persistent models. The acute models are divided into three categories: lethal neonatal challenge models, CHIKV arthritis/myositis models and immunocompromised models. The neonatal mice are useful as pathogenesis models to study severe disease in neonates as they develop lethal encephalitis (Couderc et al., 2008, Werneke et al., 2011). In addition, because of their high susceptibility to CHIKV infection, neonatal mice are also sensitive models to test the efficacy of CHIKV-specific antibodies or the safety of live attenuated vaccines (Levitt et al., 1986). Adult mouse arthritis/myositis models are valuable systems for the study of CHIKV-induced arthritis pathogenesis and for evaluation of CHIKV vaccines and therapies against CHIKV-induced arthritis and myositis (Muthumani et al., 2008, Hallengard et al., 2014). Subcutaneous CHIKV infection in the footpad of C57BL/6 mice leads to a biphasic swelling response, as well as severe arthritis, tendonitis and fasciitis in the infected foot while the contralateral foot exhibits no swelling symptoms and milder inflammatory changes (Morrison et al., 2011, Gardner et al., 2010). With gene-specific knockout mice, IFN-stimulated genes such as interferon-stimulated gene 15 (ISG15) and interferon induced protein with tetratricopeptide repeats 1 (IFIT1), as well as cluster of differentiation (CD4⁺) T cells, have been proved to be associated with CHIKV-induced pathology (Werneke et al., 2011, Mahauad-Fernandez et al., 2014, Hawman et al., 2013, Poo et al., 2014). The type I interferon (IFN) system is essential in the innate immune response against CHIKV infection. Therefore, the IFN system-defective mice models are highly susceptible to CHIKV infection (Rudd et al., 2012, Schilte et al., 2012, Gardner et al., 2012) and are useful for testing anti-CHIKV antibodies efficacy and CHIKV vaccines safety and efficacy (Plante et al., 2011, Pal et al., 2013). Chronic/persistent mouse models are used to investigate the persistence of CHIKV infection and its association with chronic disease. With the persistent mouse models, studies have

proved that the persistence of CHIKV in specific tissues are associated with the chronic symptoms (Hawman et al., 2013, Poo et al., 2014). While mouse models are powerful resources for study of CHIKV, they also have limitations as CHIKV infection in mouse is not absolutely relative to that in humans, for example, in maternal/neonatal transmission or CHIKV disease enhancement in elderly people. To cover the disadvantage of mouse models, nonhuman primate (NHP) models are developed. NHP CHIKV infection models are usually used for study of CHIKV pathogenesis and evaluation of the efficacy of vaccines and immunotherapeutic as preclinical models. Nowadays, NHP models for CHIKV infection mainly include cynomolgus macaque models, rhesus macaque models and the relative developed aged and pregnant populations (Labadie et al., 2010, Chen et al., 2010, Messaoudi et al., 2013).

1.6 Aims and objective

Alphaviruses are a group of globally distributed arthropod-borne RNA viruses with a broad host range. Although they are most commonly maintained between mosquito vectors and avian hosts, outbreaks of human and livestock infections frequently occur, and are thus of economic and public health concern. The recent numerous outbreaks of CHIKV epidemic have led to the re-emergence of CHIKV with wider epidemic ranges and more serious danger to public health. As there are still no antiviral therapies or safe, effective vaccines are available, the identification of targets for antiviral intervention and means of rational attenuation for vaccine development are in urgent need, which will ask for a deep understanding of the mechanisms of virus replication in both the vertebrate host and the vector. Consequently, this project aims to explore the function of CHIKV nsP3 in virus replication and contribute to the development of effective vaccines.

The first step was to identify critical residues for virus RNA replication in the AUD by a mutagenic strategy based on analysis of sequence alignment and three-dimensional structures, and the subsequent Dual-luciferase reporter system. The critical residues were then further explored in different virus infection stages in context of infectious virus.

Secondly, to explore the mechanism of the AUD function. In this stage, different kinds of viral RNAs synthesis, as well as non-structural and structural proteins expression were studied. Moreover, wild type and the mutant AUDs were expressed in *Escherichia coli* (E.coli) or cells, and then protein-RNA interaction and proteomics analysis were applied to identify the binding partners of the AUD.

The results obtained in this study shed light on the complex functionality of nsP3, and the AUD in particular. As well as making a major contribution to our understanding of the role of this 'enigmatic' protein, I believe that the data validate the AUD as a novel target for antiviral agents and provide opportunities for rational design of an attenuated virus vaccine.

Chapter 2: Materials and Methods

2.1 General materials

2.1.1 Bacterial strains

Escherichia coli (*E. coli*) DH5 α : Genotype F- Φ 80lacZ Δ M15 Δ (lacZYA-argF) U169 recA1 endA1 hsdR17 (rk-, mk-) phoA supE44 λ - thi-1 gyrA96 relA1 were used for molecular cloning.

Rosetta2 (DE3) Competent Cells: Genotype F- ompT hsdSB(rB- mB-) gal dcm (DE3) pRARE2 (CamR) was used for protein expression.

2.1.2 Cell lines

Five mammalian cell lines: Huh7 (human hepatoma cells), Huh7.5 (human hepatoma cells, a HCV cured cell line defective in retinoic acid-inducible gene-I (RIG-I)-induced IFN antiviral defense), RD (human muscle rhabdomyosarcoma cells), C2C12 (mouse muscle myoblast cells), BHK-21 (baby hamster kidney cells); and two mosquito cells: U4.4 (*Ae. albopictus* mosquito cells) and C6/36 (*Ae. albopictus* mosquito cells, RNAi defective due to a mutation in Dcr2 gene), were used in this study.

2.1.3 Plasmids and virus constructs

All the plasmids and CHIKV constructs are listed in Appendix Tables 9.1. DNA constructs of either sub-genomic replicon with dual-luciferase reporter (CHIKV-D-Luc-SGR, kind gift from Andres Merits, University of Tartu) or full length virus ECSA strain (ICRES-CHIKV, kind gift from Andres Merits, University of Tartu) with or without tags in nsP3 were used. *pcDNA 3.1 (+)* was used as the vector to subclone the CHIKV nsP3 fragment for site-directed mutagenesis. pEGFP-N1 vector was used to express GFP-tagged nsP3 or AUD. Lentivirus vectors were used to make GFP and GFP/GFP siRNA stable expressed cell lines.

pET28a-SUMO plasmid, a kind gift from John Barr, and pGEX6P-2 were used as the vectors for the construction of nsP3 AUD expression plasmids. DNA fragments flanked with BamHI and HindIII/XhoI restriction sites encompassing AUD wildtype or mutants were amplified by PCR using wildtype or mutant ICRES-CHIKV as templates. PCR products were cleaved with corresponding restriction enzymes and cloned into either pET28a-SUMO or pGEX6P-2 vectors to allow expression of AUD N-terminally fused to either a His-SUMO or GST affinity tag.

2.1.4 Oligonucleotide primers

DNA oligonucleotides were ordered from Integrated DNA Technologies and resuspended with deionised water to 100 μ M and stored at -20°C. All primers used are listed in Appendix Tables 9.2.

2.1.5 Antibodies

The following primary antibodies were used: rabbit anti-nsP3 (kind gift from Andres Merits, University of Tartu), rabbit anti-capsid protein (kind gift from Andres Merits, University of Tartu), J2 mouse anti-dsRNA antibody (Scicons), mouse anti- β -Actin antibody (Sigma Aldrich), mouse anti-myc antibody (Generon), mouse anti-dicer antibody (Santa Cruz Biotechnology), mouse anti-G3BP2 antibody (Source BioScience LifeSciences).

Secondary antibodies were as listed below: donkey anti-mouse (700nm) (Li-Cor), donkey anti-rabbit (800nm) (Li-Cor) were used in western blot; Alexa Fluor labelled donkey anti-rabbit (488 or 594 or 633 or 647nm) and donkey anti-mouse (488nm or 594nm) (life technologies) at dilution 1:750.

DAPI nucleic acid staining (Sigma), Concanavalin A conjugates (Alexa Fluor 647) (Invitrogen).

2.1.6 Chromatography columns and resins

HisTrap™ HP 1ml columns were purchased from GE Healthcare, Strep-Tactin® Sepharose® was purchased from IBA, and GFP-Trap® was from ChromoTek.

2.2 Basic techniques of molecular biology

2.2.1 Manipulation of nucleic acid

2.2.1.1 Preparation of plasmid DNA from bacteria

1 μ g Plasmid DNA or 10 μ l ligation products were added into 100 μ l chemically competent bacteria DH5 α and kept on ice for 30 min followed by addition of 900 μ l Luria broth (LB) into the mixture. After one hour of incubation at 37 °C, the transformed bacteria were coated on agar plates supplemented with appropriate antibiotics and left for incubation at 37 °C overnight (Inoue et al., 1990). After incubation, single colonies were picked from the agar plates and added in to 5 ml LB medium with corresponding antibiotics for bacteria growth at 37 °C in a rotary incubator at 180 rpm overnight. Bacterial cultures were centrifuged at 4000 \times g (RCF) for 20 min at 4 °C, and pellets were collected for purification of DNA plasmids using commercial Miniprep or Midiprep Kit following the manufacturer's instructions (Qiagen). DNAs were kept at -20 °C for storage and long-term storage of DNA was performed as glycerol stocks of 70% bacterial cultures and 30% of glycerol and kept in -80 °C.

2.2.1.2 Polymerase chain reaction (PCR)

PCR was used to amplify DNA fragments from plasmid DNA or reverse transcribed cDNA for PCR cloning and site-directed mutagenesis experiments. Each PCR reaction was performed in a 50 µl mixture composed of 100 ng template DNA, 10 µM forward primer, 10 µM reverse primer, 1 mM dNTP, 5 µl 10 × Thermopol[®] reaction buffer and 1 µl vent[®] DNA polymerase (NEB) and nuclease free water. Reactions were started with a denaturation step of 94 °C for 2 min followed by 35 cycles of a second denaturation step at 94 °C for 30 sec, annealing step at T_m for 60 sec and extension step at 72°C for 1 min/Kb. Final step was an additional extension process performed at 72 °C for 5-7 min.

2.2.1.3 DNA agarose gel electrophoresis

DNA agarose gels were made of 1% (w/v) agarose and 1 × TAE buffer (40 mM Tris, 20 mM Acetate and 1 mM EDTA), then the mixture was microwaved to dissolve agarose followed by the addition of SYBR[®] safe DNA gel Stain (Invitrogen) at 1:10,000. When electrophoresing the DNA samples together with molecular weight ladders, gels were electrophoresed in 1 × TAE buffer at a constant voltage of 80 V for 40-60 min. DNA samples were visualised by ultraviolet illumination with Gene Genius bio-imaging system (Syngene).

2.2.1.4 Endonuclease digestion with restriction enzymes

Digestion of DNA products with restriction enzymes were performed in a 50 µl mixture composed of 5 µg DNA products, 1 µl of each restriction enzymes, 5 µl 10 × corresponding buffer (NEB or Thermo fisher), and nuclease free water, followed by incubation at 37 °C for 3 hours to overnight.

2.2.1.5 DNA purification from DNA agarose gel

DNA bands in agarose gels were visualised in a darkroom with blue-light excitation. These bands were then cut out with minimal agarose and placed into 1.5ml microtubes. DNA purification was then performed using the commercial QIAquick Gel Extraction Kit (QIAGEN) following manufacturer's instructions.

2.2.1.6 Ligation reaction

After digestion with restriction enzymes, genes of interest and vectors with the same cohesive ends were ligated with T4 DNA ligase following the manufacturer's instructions (NEB). Subsequently, the ligation products were used for transformation into competent DH5α.

2.2.1.7 DNA sequencing and analysis

DNA was sent to a commercial company for sequencing using Sanger sequencing techniques with primers designed for the relevant sequence. Sequencing results were analysed via DNA Dynamo Sequence Analysis Software.

2.2.1.8 Site-directed mutagenesis

In order to introduce single amino acid mutations into CHIKV nsP3 protein, a DNA fragment encoding nsP3 AUD was firstly amplified as described in section 2.2.1.2, digested with HindIII and XbaI restriction enzymes, then ligated with HindIII and XbaI digested pcDNA3.1 (+) vector to finally obtain a 'pcDNA3.1-AUD for mutation' plasmid used as the template for Quickchange site-directed mutagenesis. Primers used for Quickchange site-directed mutagenesis were complementary based on the CHIKV nsP3 sequence, 30-45 nucleotides in length with required mutations centrally (all the primers used are listed in Appendix Table 9.2). Mutagenesis PCR were performed with an initial denaturation at 95 °C for 30 sec, then 15 cycles of denaturation at 95 °C for 30 sec, annealing at 53 °C for 1 min and extension at 68 °C for 7 min following the manufacturer instruction of pfuTurbo Polymerase (Agilent), followed by an addition of 1 µl DpnI and incubation at 37°C for 1h to remove Parental DNA and then transformed into component DH5α described in section 2.2.1.1. The schematic diagram for CHIKV-D-Luc-SGR-AUD point mutants made by Quickchange site-directed mutagenesis is shown in Figure 2.1.

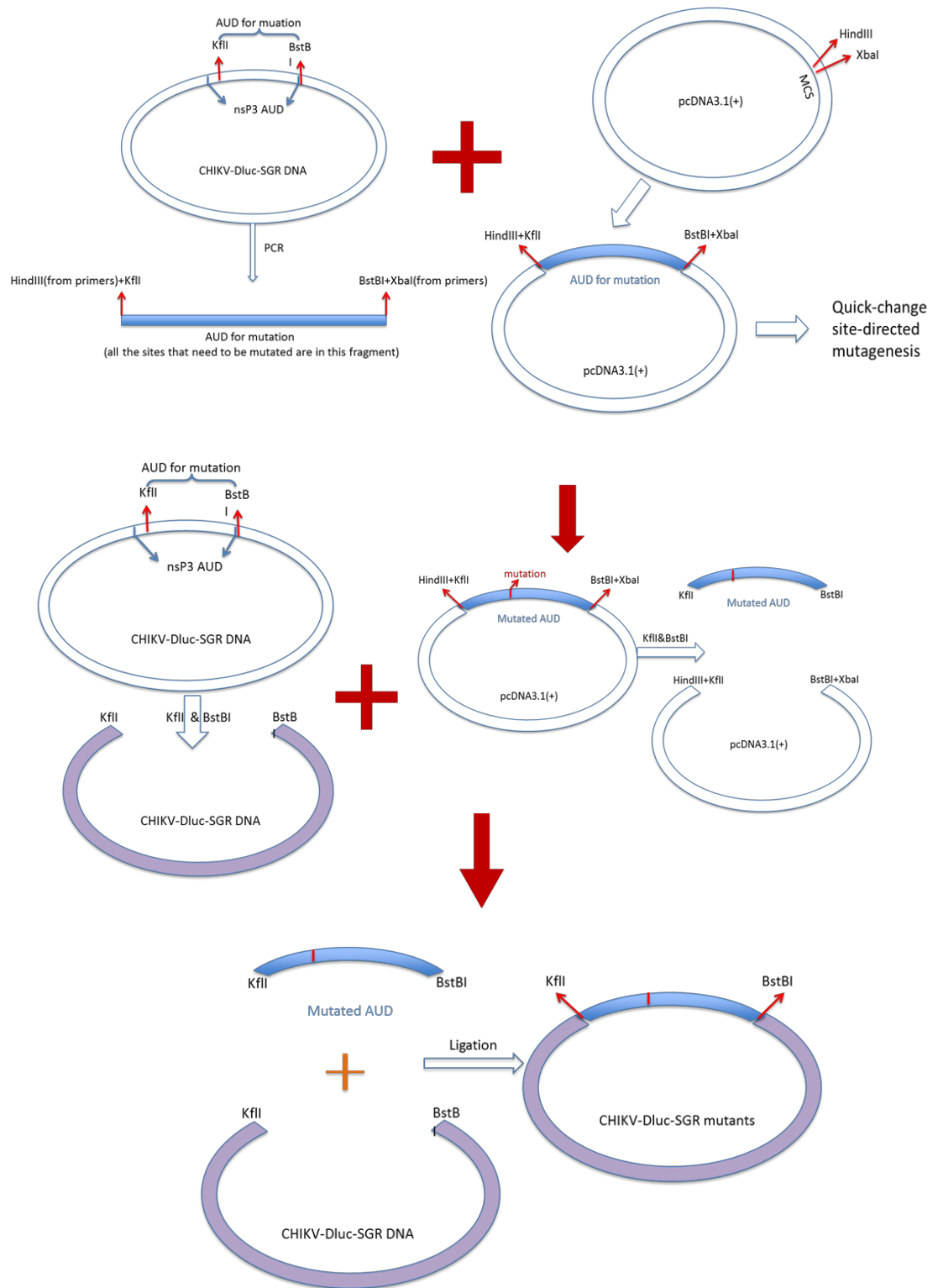


Figure 2.1 Diagram for AUD point mutants in CHIKV-D-Luc-SGR.

Briefly, fragment containing the mutation residues were cloned into pcDNA3.1 for site-directed mutagenesis and then the same fragment with AUD mutations were put back into CHIKV-D-Luc-SGR.

2.2.1.9 CHIKV-D-Luc-SGR-AUD truncation mutants construction

CHIKV-D-Luc-SGR mutants with AUD truncations were constructed in different ways. For Atru-1 to Atru-6, a DNA fragment of CHIKV-D-Luc-SGR was obtained by digestion of CHIKV-D-Luc-SGR with BstXI and BstBI. Then the BstXI & BstBI fragment was used as template for PCR with specific forward primers (PF) and reverse primers (sPR-1) to amplify the truncated AUD part of interest. Subsequently, PCR products of the last step were used as templates for a secondary PCR with same PF and new sPR-2. Finally, the secondary PCR products were digested with BstXI and BstBI and inserted into CHIKV-D-Luc-SGR vector (digested with BstXI and BstBI) for construction of CHIKV-D-Luc-SGR-Atru1-6 (schematic diagram shown in Figure 2.2).

For CHIKV-D-Luc-SGR-Atru7-12, a same DNA fragment of CHIKV-D-Luc-SGR was obtained by digestion of CHIKV-D-Luc-SGR with BstXI and BstBI. Then the fragment was divided into two parts by PCR with PF-fusion & PR-fusion or sPF & PR to get PCR-fusion fragment and Atru7-12 fragment, respectively. For the next step, the PCR-fusion fragment and Atru7-12 fragment were merged into one DNA fragment by a fusion PCR reaction as follows. 1st step: Mix 24.5 µl nuclease free water, 4 µl of Atru7-12, 2 µl PCR-fusion, 2 µl 25 mM dNTP, 10 µl 5 × Q5 reaction buffer and 1 µl Q5 polymerase (NEB) together, denaturation at 94 °C for 2 min followed by 10 cycles of a second denaturation step at 94 °C for 30 sec, annealing step at 50 for 60 sec and extension step at 72°C for 1 min/Kb, then add additional 2 µl PF-fusion, 2 µl PR, 1 µl 25 mM dNTP and 0.5 µl Q5 polymerase (NEB) into the product mixture, and repeat the cycle reaction described above for another 25 cycles. Finally, the fusion PCR products were digested with BstXI and BstBI and inserted into CHIKV-D-Luc-SGR vector (digested with BstXI and BstBI) for construction of CHIKV-D-Luc-SGR-Atru7-12 (schematic diagram shown in Figure 2.2).

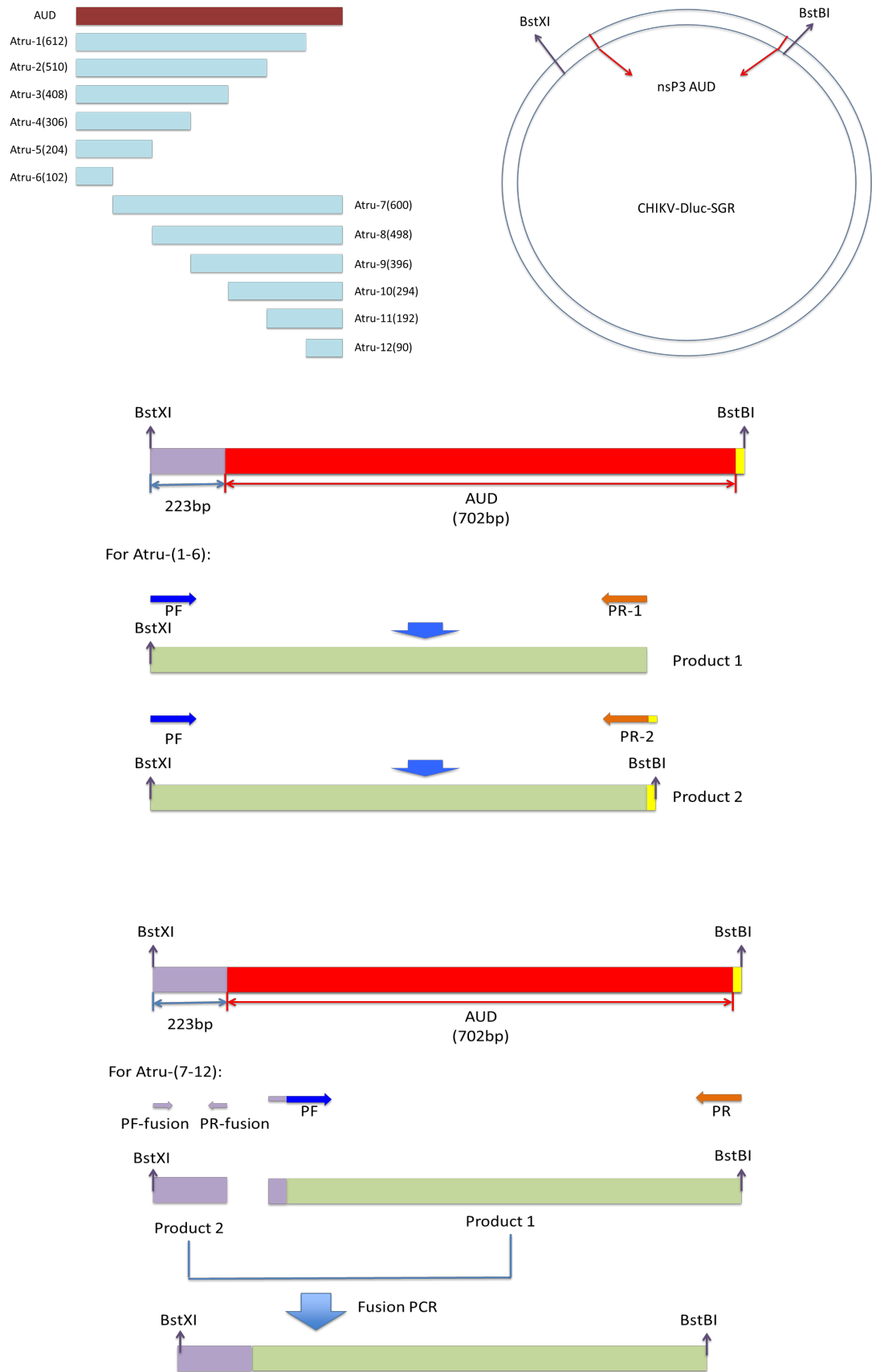


Figure 2.2 Diagram for AUD truncations in CHIKV-D-Luc-SGR.

2.2.1.10 Phenol: Chloroform purification of DNA

Linearized DNA needed to be purified before being used as template for in vitro transcription of RNA. For the first step, equal volumes of phenol: chloroform: isoamyl alcohol (25:24:1) were added in to linearized DNA mixture, vortexed thoroughly for 1 min and centrifuged at 13,000 rpm for 5 min. Upper aqueous phase layer was then carefully transferred into a fresh Eppendorf tube, followed by an addition of an equal volume of chloroform, thoroughly vortexed for 1 min, and centrifuged at 13,000 rpm for 5 min. Then DNA in the second aqueous phase of the centrifuged product from last step was transferred into a fresh Eppendorf tube and precipitated with 2 volumes of 100% ethanol and 0.1 volume of 3 M ammonium acetate (pH=5.2). Then the mixture was incubated in -20 °C for 3 hours, after which DNA was collected by centrifuge at 13,000 rpm for 20 min at 4 °C. Then the recovered DNA pellet was washed with 70% ethanol, air dried and finally resuspended with 20 µl DEPC-treated water.

2.2.1.11 Nucleic acid quantification

Quantification and purity of nucleic acids were detected using Nanodrop spectrophotometer (Thermo Scientific) by measurement of the samples' absorbance at 260 nm and 280 nm. Ratio of absorbance at 260 nm to that at 280 nm was used to detect the purity of nucleic acids.

2.2.1.12 In vitro transcription of RNA

DNA plasmids used as templates for in vitro transcription were linearized with NotI enzyme and purified as described in section 2.2.1.4 and 2.2.1.10. In vitro transcription and the following RNA purification experiments were performed with 1 µg linearized specific DNA as template using mMESAGE mMACHINE SP6 Transcription Kit (Thermo Fisher) following the manufacturer's instructions.

2.2.1.13 RNA agarose gel electrophoresis

RNA agarose gel was prepared with 1% (w/v) agarose and 30 ml MOPS (3-(N-morpholino) propanesulphonic acid) buffer (40 mM MOPS, 10 mM sodium acetate, 1 mM EDTA), microwaved till agarose dissolved followed by an addition of 6.5% (v/v) of formaldehyde and SYBR® safe DNA gel Stain (Invitrogen) (1:10,000) before leaving it in gel cast for moulding. RNA samples were heated at 65 °C for 10 min before loading in the gel and the gel electrophoresis was performed at a constant voltage of 80 V for 1 hour. RNAs in the gel were visualised by ultraviolet illumination with Gene Genius bio-imaging system (Syngene).

2.2.2 Basic technology on Protein work

2.2.2.1 Quantification of proteins

E.coli expressed and purified proteins were quantified with Nanodrop spectrophotometer (Thermo Scientific) by measurement of absorbance at 280 nm.

Concentration of proteins samples of cell lysates were measured using Pierce BCA protein assay kit (Thermo Scientific), and bovine serum albumin (BSA) gradient dilution were used to build a standard curve. To prepare BSA standard samples, 1 mg BSA was firstly dissolved in 1 ml dH₂O, and the 1 mg/ml BSA buffer was then serially diluted by 2-fold to totally get 8 gradient dilution samples. At the same time, cell lysates protein samples were diluted in dH₂O (1:10). BSA standard samples, as well as the cell lysates samples, together with 50 µl BCA solution buffer (prepared following the manufacturer's instructions), were then added into transparent 96-well plate and incubated at 37 °C for 30 min before absorbance at 570 nm was measured with Infinite F50 plate reader and Magellan for F50 software (Tecan). Protein concentrations were then calculated manually using linear regression equation.

2.2.2.2 SDS-PAGE gel preparation and protein separation

SDS-PAGE gel consists of two parts: the separation gel and the stacking gel. The separation gel, made up of 7.5% - 15% (v/v) (depending on the experiments) acrylamide (30:1), 376 mM Tris-HCl (pH=8.8), 0.1% (w/v) ammonium persulphate (APS), 0.1% (w/v) SDS and 0.01% (v/v) tetramethylethylenediamine (TEMED) and H₂O, was firstly made and added to the bottom of the gel cast. After solidification of the separation gel, the stacking gel, made up of 6% acrylamide, 376 mM Tris-HCl (pH=6.8), 0.1% APS, 0.1% SDS, 0.01% TEMED and H₂O, was then prepared and added onto separation gel with a gel comb inserted on the top of it. Gels were ready to be used after the stacking gel was solidified. Protein samples, mixed with SDS-PAGE gel loading buffer (62.5 mM Tris-HCl, pH 6.8, 10% (v/v) Glycerol, 2% (w/v) SDS, 0.01 % (w/v) Bromophenol blue, 5% (v/v) β-mercaptoethanol), were heated at 95 °C for 10 min and gradually cooled down before loaded into the gels along with Color Prestained Protein Standard, Broad Range (11–245 kDa). Gels were then run in 1x SDS-PAGE running buffer (25 mM Tris, 192 mM Glycine, 0.01(w/v) SDS) at a constant voltage of 180 V for 1 hour.

2.2.2.3 Coomassie Brilliant Blue staining of SDS-PAGE gels

Coomassie Brilliant Blue staining buffer consists of 10% (v/v) acetic acid, 50% (v/v) methanol, 40% (v/v) H₂O and 0.25% (w/v) Coomassie Brilliant Blue R250. SDS-PAGE gels were incubated

in the Coomassie Brilliant Blue staining buffer for 1 hour at room temperature (RT) followed by a destaining of the gels with destain buffer (10% (v/v) acetic acid, 50% (v/v) methanol, 40% (v/v) H₂O) for at least 3 hours with renewal of destain buffer until the gel background became clear enough.

2.2.2.4 Silver staining of SDS-PAGE gels

Silver staining of SDS-PAGE gels was performed using ProteoSilver Silver Stain Kit (Sigma) following the manufacturer's instructions.

2.2.2.5 Western Blot

After separation in SDS-PAGE gels, proteins were transferred onto a polyvinylidene fluoride (PVDF), Immobilon-FL Transfer Membrane pre-soaked with transfer buffer (25 mM Tris, 192 mM Glycine, 20% (v/v) methanol) as follows: filter paper, transfer membrane, SDS-PAGE gel and filter paper were put in the transfer machine in this order from bottom to top, protein transfer was then performed in a constant voltage of 15 V for 1 hour. After protein transfer, the PVDF membranes were blocked with 50% (v/v) Odyssey blocking buffer (Li-Cor) diluted in TBS (25 mM Tris-HCl, pH7.4, 137 mM NaCl) for 1 hour at RT. Then the membranes were incubated with primary antibodies diluted in TBS with 25% (v/v) of Odyssey blocking buffer at 4 °C overnight. After that, membranes were washed with TBST (TBS supplemented with 0.1% (v/v) Tween-20) for 3-5 times of 5 min each wash followed by secondary antibody incubation at 37 °C for 1 hour and another 3-5 times of wash as described above. After the final wash, membranes were dried with clean filter paper before imaging by Li-Cor Odyssey Sa Imager (Li-Cor).

2.3 Basic techniques of tissue culture

2.3.1 Passaging of cells

Five mammalian cells were used in this study. Huh7 and Huh7.5 cells were cultured in Dulbecco's Modified Eagles Medium (DMEM, Sigma) supplemented with 10 % (v/v) fetal bovine serum (FBS), 100 µg/ml streptomycin, 100 IU penicillin/ml, and 1 % non-essential amino acids (NEAA) (Lonza) (complete medium) typically in T75 or T175 flasks incubated in a humidified incubator at 37 °C with 5 % CO₂. Other mammalian cells including RD cells and BHK-21 cells were cultured in the similar complete medium as described above without NEAA and C2C12 cells were cultured with 20 % (v/v) fetal bovine serum (FBS) of complete medium. When cells got confluency, medium was removed and cells were washed with phosphate buffered saline (PBS). Then cells were trypsinized with trypsin-EDTA solution by incubation at 37 °C for 5

min followed by addition of complete medium to inactivate trypsin and resuspend the detached cells for next passage or certain experiments.

Two mosquito cells were used in this study. U4.4 and C6/36 cells were cultured in Leibovitz's L-15 supplemented with 10% FBS and 10% tryptose phosphate broth in T75 flasks incubated in a humidified incubator at 28 °C. When cells were confluency, medium was removed and cells were washed with PBS. Then 5 ml of medium was added into each flask and cells were scraped off by cell scraper for next passage or certain experiments.

2.3.2 Transfection of nucleic acids

Lipofectamine 2000 (Invitrogen) was used for transfection of nucleic acids into cells according to the manufacturer's instructions. In brief, cells were seeded into specific plate the night before transfection. For example, for 6-well plate, 4×10^5 cells were seeded in each well. After 12 hours, 2 µg nucleic acids and 4 µl lipofectamine 2000 were separately diluted into each 200 µl Opti-MEM (Life Technology) for incubation of 5 min. Then nucleic acids and lipofectamine were mixed thoroughly and gently and incubated for another 20 min before added onto the seeded cells which were washed with PBS and incubated in Opti-MEM during reagent incubation. Cells medium was removed and replaced with complete media at 6 hours post transfection (h.p.t).

2.3.3 Electroporation of RNAs into mammalian cells

Cells were washed twice in cold PBS, counted and resuspended into a density of 3×10^6 cells/ml with cold Opti-MEM. Then 400 µl resuspended cells was mixed with defined amount of RNAs in a chilled 4mm electroporation cuvette (Geneflow) for electroporation at 950 µF and 270 V. Then cells were resuspended in 10 ml complete medium and seeded into specific plates for certain experiments.

2.3.4 Cell lysates collection

At defined time points post electroporation or transfection, cells were washed with PBS for three times and scraped by cell scraper in PBS followed by centrifugation at 1200 x g for 5 min. Cell pellets were resuspended and lysed in Glasgow lysis buffer (GLB, 10 mM PIPES, pH 7.2, 120 mM KCl, 30 mM NaCl, 5 mM MgCl₂, 1% Triton X-100, 10% Glycerol) supplemented with protease and phosphatase inhibitors by incubation on ice for 45 min. Cell lysates were then centrifuged at 15,000 rpm for 10 min at 4 °C and supernatant was collected for certain experiments.

2.4 CHIKV-D-Luc-SGR work

2.4.1 Dual-luciferase assay

At 4, 12, 24 or 48 h.p.t, cells transfected with CHIKV-D-Luc-SGR RNAs in 24-well plates were washed with PBS for 3 times and lysed with 100 μ l passive lysis buffer (PLB, Promega) by incubation on ice for 30 min. Then 50 μ l of each lysates samples were transferred into white 96-well plate and luciferase activities were measured using BMG plate reader which automatically added LARII and Stop & Glo reagents (Promega) into each well and read the corresponding luciferase signals at each step.

2.4.2 Sequencing of the subgenomic replicon RNA post transfection

After transfection of the CHIKV-D-Luc-SGR RNA into cells, total cell RNAs were TRIzol extracted at 24, 48 and 72 h.p.t. cDNA was then made using SuperScript IV (Invitrogen) according to manufacturer's instructions with random primers. Amplification of whole nsP3 nucleotides was then performed with nsP3 forward and reverse primers and the last-step obtained cDNAs as template. PCR products were run in a DNA agarose gel before sent out for sequencing to confirm their identity. Finally, PCR products were sequenced with a short sequence among nsP3 macrodomain as sequencing primer (shown in Appendix Table 9.2).

2.5 ICRES-CHIKV full-length virus experiments

2.5.1 Infectious virus collection

400 μ l of cell suspension (3×10^6 cells/ml) mixed with 1 μ g ICRES-CHIKV RNA in 4mm electroporation cuvette were used for electroporation at 950 μ F and 270 V. After suspension of cells in 10 ml complete medium, cells were seeded in T75 flasks and incubated in humidified incubators at 37 °C with 5 % CO₂ for 48 hours. Then cell supernatant was collected and centrifuged at 1200 x g for 5 min to discard cells debris, and supernatant was aliquoted and stored in -80 °C.

2.5.2 Sequencing of infectious virus genome RNA.

Viral RNAs were TRIzol extracted from the collected virus stock. cDNA was then made using SuperScript IV (Invitrogen) according to manufacturer's instructions with random primers. Amplification of whole nsP3-encoding region was then performed with nsP3 forward and reverse primers and the last-step obtained cDNAs as template. PCR products were run in a DNA agarose gel before sent out for sequencing to confirm the right size of them. Finally, PCR products were sequenced with a short sequence among nsP3 macrodomain as sequencing primer (shown in Appendix Table 9.2).

2.5.3 Virus titration by plaque assay

The collected viruses were 10-fold serially diluted in complete medium from 10^0 to 10^{-8} . 200 μ l diluted viruses were added onto BHK-21 cells seeded in 6-well plate night before. After one hour incubation in humidified incubators at 37 °C with 5 % CO₂, viruses were removed and cells were washed with PBS for 3 times followed by addition of 2 ml 0.8% MC (1:1 in complete medium) and incubated for another 72 hours. After 72-hour incubation, MC was removed and cells were fixed by 4% paraformaldehyde (PFA) for 30 min before staining with crystal violet dye (0.25% (w/v) crystal violet, 10% ethanol, 35 mM Tris, 0.5% (w/v) CaCl₂ and 90% dH₂O) for 15 min. Finally, plaques were counted and virus titre was calculated by $\text{PFU ml}^{-1} = \text{number of plaques observed} \times (\text{dilution factor } (10^{-x}) \times \text{volumes of virus added (ml)})^{-1}$. Plaques were visualised by photography with a Canon EOS 80D.

2.5.4 Infectious centre assay (ICA)

Electroporated cells (as described in section 2.3.3) were 10-fold serially diluted from 10^{-1} to 10^{-6} . Diluted cells were added onto BHK-21 cells which were seeded in 6-well plate night before and incubated in humidified incubators at 37 °C with 5 % CO₂ for 2 hours. Then the electroporated cells were removed by wash with PBS for 3 times and 2 ml 0.8% MC (1:1 in complete medium) were added for incubation for another 72 hours. After that, MC was removed and cells were fixed by 4% paraformaldehyde (PFA) for 30 min before staining with crystal violet dye for 15 min. Finally, plaques were counted and virus titre was calculated by $\text{PFU ml}^{-1} = \text{number of plaques observed} \times (\text{dilution factor } (10^{-x}) \times \text{volumes of virus added (ml)})^{-1}$.

2.5.5 Quantification of CHIKV genome RNA by qRT-PCR

Virus or total RNA was extracted using TRIzol following the manufacturer's instructions (Invitrogen). qRT-PCR reactions were performed with One step MESA GREEN qRT-PCR MasterMix Plus for SYBR assay No Rox kit (EUROGENTEC). Briefly, each 25 μ l reaction was composed of 12.5 μ l 2 x reaction buffer, 2 μ l forward primer, 2 μ l reverse primer, 0.25 μ l EuroScript RT & RNase Inhibitor, 2 μ l RNA template and 6.25 μ l RNase free water. Program used for the reaction was as follows: 48 °C for 30 min as reverse transcription step; 95 °C for 5 min as meteor Taq activation and EuroScript inactivation step, 40 cycles of 95 °C for 15s and 56 °C for 1 min, and the last step was a meltcurve analysis. 8 dilutions of 10-fold diluted pcDNA3.1-AUD plasmid were used as standard samples to create standard curve and actin was quantified for normalization as reference. All primers used were shown in Appendix Table 9.2.

2.5.6 Virus infection

Cells used for virus infection were seeded in specific plate night before. On the day of infection, cell medium was firstly removed and cells were washed with PBS once before addition of 1/5 of normally used amount of cell medium into each well. Then a defined amount of virus was added into cell medium for incubation in humidified incubators at 37 °C with 5 % CO₂ for 1 hour. Then cell medium with virus was removed and cells were wash with PBS for 3 times followed by addition of complete medium and incubation of the infected cells as requested by each experiments.

2.5.7 Multi-step virus growth kinetics

1x10⁵ C2C12 cells were seeded in 12-well plate for 12 hours. Then C2C12 cells were infected with wildtype or mutant CHIKV at an MOI of 0.1 for 1 hour. Then virus was removed and cells were washed with PBS for 3 times followed by addition of 1 ml complete medium and incubation for 48 hours. Cell supernatant was aliquot collected from each independent parallel samples at different times post infection and the collected samples were used for virus titration by plaque assay (as described in section 2.4.2) or CHIKV genome quantification by qRT-PCR (as described in section 2.4.4) after TRIzol extraction of viral RNA.

2.5.8 Intracellular virus collection

Cells were washed with PBS for 3 times at defined times post virus infection followed by an addition of 1 ml complete medium into each well. Then cells were frozen at -80 °C for 1 hour before taken out in RT until thawed. This freeze/thaw process was repeated for at least 3 times and finally the thawed samples were centrifuged at 12,000 x g for 10 min to discard cell debris and supernatant were collected and stored at -80 °C.

2.5.9 Quantification of CHIKV genomic RNA and subgenomic RNA synthesis

C2C12 cells were electroporated with ICRES RNAs and seeded in 6-well plate for incubation of 10 hours. Actinomycin D (1 µg/ml) was added and the cells were incubated for 2 hours. [³H]-uridine (20 µCi/ml) was then added and the cells were incubated for 3 hours, at which time the monolayers were washed 3 times with ice-cold PBS, lysed and RNA extracted with TRIzol reagent.

For measurement of viral RNA synthesis, the harvested RNAs were separated on a MOPS-Formaldehyde gel. The gel was fixed (15% methanol, 10% acetic acid and 75% dH₂O) for 30 min followed by fluorography (Fluorographic reagent amplify, GE HEALTHCARE) for another 30 min. Gels were dried for 2 hours before exposure to autoradiographic film at -80 °C for 4 days.

For gradient analysis, equal volumes of harvested RNAs were loaded onto 14 ml 5-25% sucrose gradients in 100mM sodium acetate and 0.1% SDS followed by centrifugation at $150,000 \times g$ for 5 hours at room temperature. Gradients were fractionated into 350 μ l fractions, and radioactivity of each fractions was determined by liquid scintillation counting.

2.5.10 Immunoprecipitation

For precipitation of nsP3 and viral RNA, co-precipitation experiments were performed in C2C12 cells electroporated with ICRES Twin-Strep-tag (TST) RNAs using Streptactin-agarose (Thermo Fisher Scientific), following the manufacturer's protocol. Precipitated proteins were subjected to immunoblotting and co-precipitated RNAs were extracted by TRIzol and quantified by qRT-PCR.

For nsP3 and cellular proteins co-precipitation, GFP-trap was performed using GFP-Trap kit (ChromoTek) following the manufacturer's instructions. pEGFP-N1-nsP3/AUD and were co-transfected into cells seeded in 10 cm plate using lipofectamine 2000 as described in section 2.3.2 for 48 hours. Then cell lysates were collected with 500 μ l GLB and used for GFP-Trap assay, both cell lysates and GFP-Trap samples were used for WB to detect the existence of nsP3, AUD and dicer.

2.5.11 Immunofluorescence analysis

DNA transfected, virus RNA electroporated or virus infected cells were seeded onto 19 mm glass coverslips in 12-well plate. Cells were fixed at defined time points with 4% PFA for 30 min and cell membranes were permeabilised with ice-cold methanol for 10 min at -20°C . Permeabilised cells were washed with PBS for 3 times and blocked with 2% BSA in DEPC-PBS for 1 hour at RT. Then primary antibody was applied in 2% BSA in PBS at a requested dilution and incubated at 4°C overnight. To remove any unbound primary antibodies, cells were washed in DEPC-PBS for 4 times of 5 min each wash. Alexa Fluor-488, 594 or 647 conjugated secondary antibodies diluted in 2% BSA DEPC-PBS (1: 1000) were then applied to the cells for 2 hours at RT in dark. Unbound secondary antibodies were washed off the same as described above. The endoplasmic reticulum (ER) were stained using Alexa Fluor 647 conjugated concanavalin A (1:50 dilution in 2% BSA of DEPC-PBS) for 30 min at RT in dark. Nucleus was stained by 4', 6'-diamidino-2-phenylindole dihydrochloride (DAPI) diluted 1:10 000 in 2% BSA DEPC-PBS for 5 min at RT in dark. Coverslips were washed for 4 times as described above before mounted on a glass microscope slide in Prolong Gold antifade reagent (Invitrogen, Molecular Probes) and sealed with nail varnish. Slides were stored in dark for at least 24 hours before examined in confocal microscope. Confocal microscopy images were acquired with a

Zeiss LSM880 microscope, post-acquisition analysis of the images was performed on Zen software (Zen version 2015 black edition 2.3, Zeiss) or Fiji (v1.49) software.

2.5.12 Co-localisation analysis

For co-localisation analysis, Manders' overlap coefficient was calculated using Fiji ImageJ software with Just Another Co-localisation Plugin (JACoP) (National Institutes of Health). Coefficient M1 indicated here reports the fraction of the nsP3 signal that overlaps either the anti-dsRNA or anti-capsid signal. Coefficient values range from 0 to 1, corresponding to non-overlapping images and 100% co-localization images, respectively. Co-localisation calculations were performed on >5 cells from at least two independent experiments.

2.6 In vitro protein experiments

2.6.1 Expression and purification of AUD

For expression of His-SUMO tagged AUD, whole AUD DNA fragments flanked with BamHI and HindIII were amplified by PCR using wildtype or mutant CHIKV-D-Luc-SGR DNA as templates (primers sequences are shown in Appendix Table 9.2). PCR products were digested with BamHI and HindIII restriction enzymes before inserted into pET28a-His-SUMO vector to allow the expression of AUD fused to a His-SUMO affinity tag. *Escherichia coli* Rosetta 2 pLysS were transformed with pET28a-His-SUMO-AUD plasmids, which were grown to $OD_{600}=0.6-0.8$ at 37 °C before induction with 500 μ M isopropyl β -D-1-thiogalactopyranoside (IPTG) at 18°C for 5 hrs. Cells were pelleted by centrifugation at 4000 x g for 20 min and each 1 L original cell cultures were resuspended in 20 ml His-SUMO-AUD lysis buffer (binding buffer (100 mM Tris pH7; 200 mM NaCl, 20 mM Imidazole) supplemented with 40 μ l DNase, 40 μ l RNaseA, 2 mg/ml Lysozyme and protease inhibitors (Roche)) and incubated on ice for 30 min before sonication on ice at amplitude of 10 microns for 20 pulses of 10 seconds separated by 10 seconds. The extracts were clarified by centrifugation at 15,000 rpm for 1 hour at 4 °C and the supernatant was then filtered through a 0.22 μ m syringe filter. Filtered protein samples were applied to wash buffer equilibrated HisTrap columns (GE Healthcare). Then columns were washed 3 times with 5 column volumes of binding buffer each time and the combined proteins were eluted with 5 column volumes of elution buffer (50 mM Tris pH7, 300 mM NaCl, 500 mM Imidazol). Elution fractions of His-SUMO-AUD proteins were then dialyzed into dialysis buffer (50 mM Tris pH7, 300 mM NaCl) prior to addition of SUMO protease. After SUMO protease cleavage, the His-SUMO tag and SUMO protease were removed from the cleaved samples by going through the HisTrap column for a second time, after what the flowthrough samples were collected as purified AUD proteins and stored in -80 °C in different aliquots.

For expression and purification of GST tagged AUD, DNA fragments flanked with BamHI and XhoI restriction sites were cloned into pGEX6P-2 vector to express GST fused AUD. pGEX6P-2-AUD plasmids were transformed into cultures of Escherichia coli Rosetta 2 pLysS, which were grown to OD₆₀₀=0.6-0.8 at 37 °C before induction with 100 µM IPTG at 18°C for 5 hrs. Cells were pelleted by centrifugation at 4000 x g for 20 min and each 1 L original cell cultures were resuspended in 20 ml GST-AUD lysis buffer (binding buffer (PBS, 1% (v/v) Triton X-100) supplemented with 40 µl DNase, 40 µl RNaseA, 2 mg/ml Lysozyme and protease inhibitors (Roche)) and incubated on ice for 30 min before sonication on ice at amplitude of 10 microns for 20 pulses of 10 seconds separated by 10 seconds. The extracts were clarified by centrifugation at 15,000 rpm for 1 hour at 4 °C and the supernatant was then filtered through a 0.22 µm syringe filter. The clarified lysate was added to freshly made glutathione agarose (GA) beads (70 mg of GA powder (Sigma) added into 15 ml of PBS and rotating for 1 hour at RT. The slurry was centrifuged at 2000 x g for 2 min and the excess PBS removed. The beads were washed three times with PBS and finally 20% slurry was produced by adding 4 ml of PBS plus 1% (v/v) Triton X-100 to the beads) and allowed to bind at 4 °C for 3 hours with rotation. The GA beads and supernatant were centrifuged at 1500 x g for 2 min and the supernatant removed. The beads were washed twice in GST-AUD binding buffer and twice in 50 mM Tris-HCl pH=7. GST-AUD proteins were eluted from GA beads with 50 mM Tris-HCl pH=7 containing 20 mM reduced glutathione (Sigma). Fractions containing purified proteins were determined by Coomassie stained SDS-PAGE and dialysed overnight against 50 mM Tris-HCl pH=8.0 using dialysis tubing with a 10,000 MW cut off (Pierce) before stored in -80 °C.

2.6.2 Protein identification by mass spectrometry

2.6.2.1 Gel processing and tryptic digestion

Gel bands were excised and chopped into small pieces (about 1 mm³), covered with 30 % ethanol in a 1.5 ml Eppendorf tube and heated at 70 °C for 30 min with shaking. Then supernatant was removed and replaced with fresh ethanol solution and repeat the heating step with shaking. The heating step was repeated until all the Coomassie stain was removed from the gel. The gel slices were then covered with 25 mM ammonium bicarbonate/50% acetonitrile and incubated for 10 min with shaking. After that, 100% acetonitrile was added to cover and incubate the gel slices for five minutes before the being replaced with a fresh aliquot of acetonitrile. The sample was incubated at 57 °C for 1 hr with shaking 100 µL with an addition of 20 mM DTT solution, followed by the discard of the supernatant. Once the gel pieces were cooled down to room temperature, 100 µL 55 mM iodoacetic acid was added into

the samples for incubation for 30 min at room temperature with shaking in dark. After discard of the supernatant, the gel slices were covered with 100% acetonitrile and incubated for 5 min. The acetonitrile was then removed and the gel pieces were dried in a laminar flow hood for 1 hour. Once dried, the gel slices were cooled on ice before being covered with ice-cold trypsin solution (20 ng μL^{-1} in 25 mM ammonium bicarbonate) for 10 min incubation on ice for rehydration. Then trypsin solution was removed and a minimal amount of 25 mM ammonium bicarbonate was added to the gel slices for incubation at 37 °C for 18 hrs with shaking after briefly vortexing and spinning. The mixture from last step was vortexed and centrifuged and supernatant was collected into an Eppendorf tube containing 5 μL acetonitrile/ water/ formic acid (60/35/5; v/v) while the gel slices were vortexed with 50 μL acetonitrile/ water/ formic acid (60/35/5; v/v) for an additional 10 min. Then the supernatant was collected and pooled with the previous wash. Wash of the gel slices was performed once more and the pool of the three washes was dried through vacuum centrifugation. Finally the peptides were reconstituted with 20 μL 0.1% aqueous trifluoroacetic acid.

2.6.2.2 Protein molecular mass analysis

Purified AUD proteins were sent to the mass spectrometry analysis office in University of Leeds. LC-MS was used for molecular mass analysis.

LC separation of the peptide mixtures was performed on an ACQUITY M-Class UPLC (Waters UK, Manchester). 1 μL of each sample was loaded onto a Symmetry C18 trap column (180 μM i.d. * 20 mm) and washed with 1% acetonitrile/0.1% formic acid for 5 min at 5 μL /min. After valve switching, the peptides were then separated on a HSS T3 C18, 75 μm i.d. x 150 mm analytical column (Waters UK, Manchester) by gradient elution of 1-60% solvent B in A over 30 min at 0.3 μL /min. Solvent A was 0.1% formic acid in water, solvent B was 0.1% formic acid in acetonitrile.

The column eluant was directly interfaced to a quadrupole-ion mobility-orthogonal time of flight mass spectrometer (Synapt G2Si, Waters UK, Manchester) via a Z-spray nanoflow electrospray source. The MS was operated in positive TOF mode using a capillary voltage of 3.0 kV, cone voltage of 40 V, source offset of 80 V, backing pressure of 3.58 mbar and a trap bias of 2 V. The source temperature was 80°C. Argon was used as the buffer gas at a pressure of 8.6×10^{-3} mbar in the trap and transfer regions. Mass calibration was performed using Glu-fibrinopeptide (GFP) at a concentration of 250 fmol / μL . GFP was also used as a lock mass calibrant with a one second lock spray scan taken every 30 s during acquisition. Ten scans were

averaged to determine the lock mass correction factor. Data acquisition was using data dependent analysis with a 0.2 sec scan MS over m/z 350-2000 being followed by five 0.5 sec MS/MS taken of the five most intense ions in the MS spectrum. CE applied was dependent upon charge state and mass of the ion selected. Dynamic exclusion of 60 sec was used. Data processing was performed using the MassLynx v4.1 suite of software supplied with the mass spectrometer. Peptide MS/MS data were processed with PEAKS Studio (Bioinformatic Solutions Inc, Waterloo, Ontario, Canada) and compared with NS5A domain I sequence. Carbamidomethylation was selected as a fixed modification, variable modifications were set for oxidation of methionine and deamidation of glutamine and asparagine. MS mass tolerance was 20 ppm, and fragment ion mass tolerance was 0.05 Da. The false discovery rate was set to 1%.

2.6.3 Circular Dichroism spectroscopy

Far-UV CD spectroscopy was performed on an APP Chirascan CD spectropolarimeter to obtain the secondary structure of AUDs. Spectra (190-260) were recorded using 200 µl protein solution (at a concentration of 0.2 mg/ml) in a 1 mm path-length cuvette. Proteins applied for CD spectroscopy were dialysed in dialysis buffer (10 mM Tris-HCl pH=7, 100 mM NaCl) for reduction of NaCl and removal of chloride. Protein CD spectra deconvolution was analysed by DichroWeb.

2.6.4 Fluorescent Polarisation Anisotropy

15 µl RNA binding buffer (50 mM Tris pH=7, 300 mM NaCl) was added into each well of the 384-well black optiplate (Perkin Elmer). 30 µl protein solution was added into the first well of the row followed by dilution of the proteins along the row, taking 40 µl from the previous well to the next one. 20 µl of 20 mM RNA was then added into each well, mixed and incubated for 30 min at RT. Polarisation was measured using an EnVision multilabel Plate Reader (Perkin Elmer) that contains an excitation filter at 480 nm and S and P channel emission filters at 530 nm.

2.6.5 RNA filter binding assay

2.6.5.1 In vitro transcription and labelling of RNA probe

CHIKV 3'UTR (11314-11835) and its truncations (1-261, 262-522), 5'RNA (1-200, reverse complementary sequence), subgenomic promoter (7420-7566, reverse complementary sequence), HCV 3'UTR (genotype 2a, 9443-9678) and foot-and-mouth disease virus (FMDV) aptamer

RNA

(5'-

GGGAAAGGAUCCACAUCUACGAAUUCGGCUCAAAAUAGUCCGCACCAUACAUUCACUGCAGACU UGACGAAGCUU-3') were cloned into pcDNA3.1 vector. The resulting plasmids were then linearized with BglII and the linearized DNAs were used as templates for RNA *in vitro* transcription.

Each *In vitro* transcription reaction consisted of 500 µM each of ATP, CTP, and GTP; 20 µM UTP; 50 µCi (α -³²P) UTP; 1 µg linearized DNA template; 2 µl 10 x T7 transcription buffer (Roche); 40 U of T7 RNA polymerase (Roche) and 40 U of RNaseOUT (Invitrogen). Reactions were performed by incubation at 37°C for 2 hours before addition of 1U of RQ1 DNase (Promega) to remove template DNA. RNA transcripts were then purified using PureLink RNA Mini Kit (Thermo Fisher Scientific). Purified RNA transcripts were determined in 1 % RNA MOPS gels. Concentrations of the ³²P-labelled RNAs were measured by absorbance at 260 nm.

2.6.5.2 RNA-filter binding assay

Radiolabelled RNA transcripts and AUD proteins were diluted in binding buffer (40 mM Tris-HCl [pH 7.5], 5 mM MgCl₂, 10 mM DTT, 50 µg/ml bovine serum albumin, 10 µg/ml yeast tRNA [Ambion]) and pre-incubated separately for 10 min at 4 °C. The binding reaction was initiated by mixing 1 nM radio-labelled RNA and AUD proteins (0 to 500 nM) in a 200 µl final volume at 4°C for 30 min. Membranes were pre-soaked in binding buffer supplemented with 5% (v/v) glycerol and assembled from bottom to top as follows in a slot-blot apparatus (Bio-Rad): filter paper, Hybond-N nylon (Amersham Biosciences) to bind free RNA molecules, and nitrocellulose (Schleicher & Schuell) to trap soluble protein-RNA complexes. After assembly, 200 µl of each binding reaction mixture was applied to each slot and filtered through the membranes. Each slot was washed with 0.5 ml of binding buffer and air dried, and quantification of radioactivity was performed using an image plate, BAS 1000 Bioimager (Fuji), and Aida Image Analyser v4.22 software. Fitting was performed using GraphPad Prism 5 software (GraphPad Software). In each case, the data were fitted to the hyperbolic equation $R=R_{max} \times R/(K_d + [P])$, where R is the percentage of bound RNA, R_{max} is the maximal percentage of RNA competent for binding, [P] is the concentration of AUD, and K_d is the apparent dissociation constant.

2.6.6 GST-pull down assay

20 µg of GA beads per assay were equilibrated in 50 mM Tris-HCl pH=8.0. 40 µg of GST or GST-AUD domain protein was added and incubated overnight at 4 °C with rotation. The GA beads were centrifuged at 2000 x g for 2 min and the supernatant aspirated using a 19 gauge needle

with syringe. The beads were washed with 50 mM Tris-HCl pH=7 and then twice with GLB. 50 µg of total cell lysates (in GLB) containing Dicer protein was applied to the beads and mixed at 4 °C, rotating for 5 hours. The beads were washed twice with GLB containing 0.5 M KCl and three times in GLB only. Bound proteins were eluted from the GA beads by competition with 20 µl of reduced 20 mM glutathione (Sigma) in GLB. The samples were analysed by silver stained SDS-PAGE and western blot.

2.6.7 Tandem Mass Tag (TMT) comparative proteomic analysis

TMT mass spectrometry was carried out by Kate Heesom (University of Bristol Proteomics Facility) and analysed against both positive and negative control samples.

In brief, for multiplexed comparative proteomics 100 µg of each cell lysate was digested with trypsin and labelled with TMT reagents according to the manufacturer's protocol (Thermo Fisher Scientific, Waltham, Massachusetts, USA). The labelled samples were then pooled, evaporated to dryness and resuspended prior to fractionation by high pH reversed-phase chromatography using an Ultimate 3000 liquid chromatography system (Thermo Fisher Scientific). After high pH reversed-phase chromatography, fractions were further subjected to the Nano-LC Mass Spectrometry. The raw data files were processed and quantified using Proteome Discoverer software v1.4 (Thermo Scientific) and searched against the Uniporter Human database (134169 sequences) plus HCV protein sequences using the SEQUEST algorithm. All peptide data was filtered to satisfy false discovery rate (FDR) of 5%.

2.7 Statistical analysis of data

Statistical analysis of data was carried out using a Students *t-test* assuming a two-tailed distribution with an unequal variance. Error bars presented on all graphs illustrate the Standard Error (SE) of the Mean.

Chapter 3: The role of nsP3 AUD in virus genome replication

3.1 Introduction

AUD is the central domain of nsP3, unique to alphaviruses. It is reported to be essential for alphavirus replication, however, the role of it during virus replication is absolutely unknown. The high identity of AUD sequence among different alphaviruses suggests that it plays a fundamental role through virus replication. Therefore, in order to explore the function of it during CHIKV replication, a mutagenic strategy was initially applied. Using as a guide the structure of the SINV AUD (Shin et al., 2012) and an alignment of the AUD amino acid sequences of different alphaviruses, conserved solvent-accessible residues were identified and mutated in the context of CHIKV-D-Luc-SGR (as described in session 1.5). The effect of AUD mutations on both input translation and genome RNA replication of the replicon were reflected by dual-luciferase reporter assay. Firefly luciferase is a 61 kDa monomeric protein that does not require post-translational processing for enzymatic activity (Wood et al., 1984, de Wet et al., 1985). Thus, it functions as a genetic reporter immediately upon translation. With ATP, Mg²⁺ and O₂ in the reaction, photon emission of the firefly luciferase is achieved through oxidation of beetle luciferin. *Renilla* luciferase is a 36 kDa monomeric protein purified from *Renilla reniformis*. Similar to firefly luciferase, post-translational modification is not required for its activity, and the enzyme functions as a genetic reporter immediately following translation. The luminescent reaction is catalysed by *Renilla* luciferase using O₂ and coelenterate-luciferin. Firefly and *Renilla* luciferase, because of their distinct evolutionary origins, have dissimilar structures and substrate requirements, making it possible to selectively discriminate between their respective bioluminescent reactions. Therefore, in this project, the dual luciferase assay was able to reflect the effect of the AUD mutations within CHIKV-D-Luc-SGR to both input translation and genome replication level, respectively.

CHIKV is able to infect both mammalian and mosquito cells but pathogenic to only mammals while using mosquitoes as transmission vectors. CHIKV infection leads to apparent cytopathic effect (CPE) to a wide range of vertebrate cells and cell lines (Solignat et al., 2009, Her et al., 2010), but just light CPE in mosquito cells (Li et al., 2013), indicating different virus-host interactions for mammalian cells or mosquitoes. Therefore, in this chapter the effect of AUD mutations on CHIKV replication was detected in both mammalian cells and mosquito cells. Five mammalian cells were chosen for dual-luciferase assay, including Huh7, Huh7.5, RD, C2C12 and BHK-21 cells, to test AUD function in human and non-human cells, and cells isolated from different tissues. Huh7.5 cells are defective in host RIG-I-induced IFN antiviral response, therefore was used to detect if AUD was associated with host IFN antiviral response. Two cells derived from *Aedes albopictus* (U4.4 and C6/36 cells) were used to detect AUD function in

mosquito cells. As C6/36 cell is defective in Dcr2-induced RNAi response because of a mutation in its Dcr2 gene, the replication of CHIKV subgenomic replicons with AUD mutations in it reflected AUD association with Dcr2-induced RNAi antiviral response.

As a result of the high error rate of RNA-dependent RNA polymerase, RNA virus is known of its inherent instability (Holland et al., 1982). In general, the mutation rates of RNA viruses range from 10^{-3} to 10^{-5} substitutions per nucleotide copied (Domingo and Holland, 1997, Drake and Holland, 1999, Drake, 1993). This allows rapid adaptation and evolution when RNA viruses are subjected to selective pressures. Therefore, when studying CHIKV, a single positive strand RNA virus, with mutagenic strategy, virus genome sequencing to confirm the existence of mutations post virus replication is necessary.

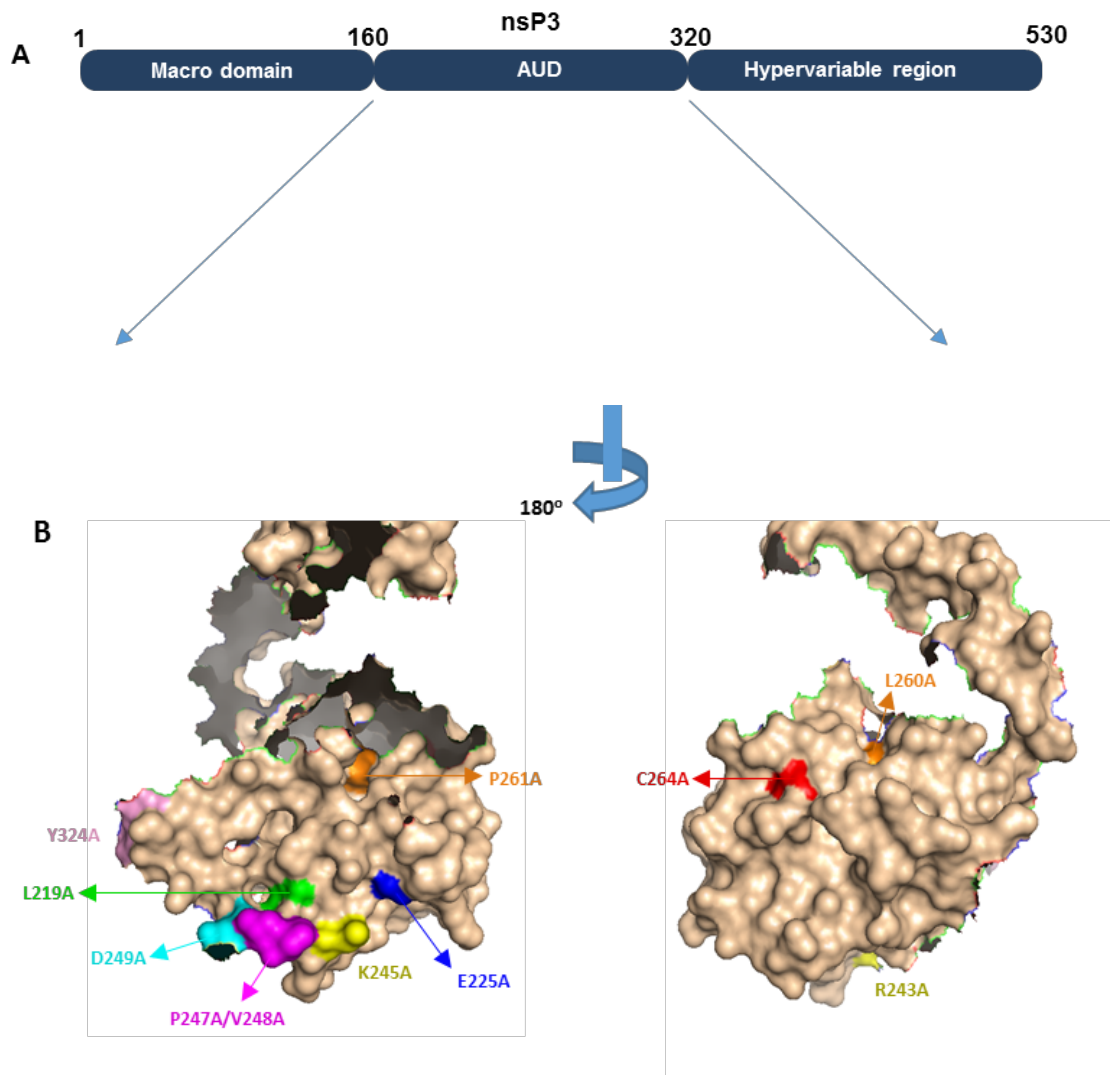
During virus replication, nsP3 was considered to be a stable protein as it was usually found in complex with other nsPs or host factors. However, Varjak et al found that nsP3 degraded rapidly when individually expressed due to a degradation signal at the C-terminal region of SFV and SINV nsP3, while significantly stable in the form of polyprotein nsP123. And this rapid degradation only occurred at the early stage of virus replication, probably when nsP3 is released from nonstructural polyproteins. Moreover, the degradation of nsP3 was shown to contribute in the regulation of nsP4 expression in SFV 41. As the mechanisms of how the degradation signal worked is not clear, therefore, in this chapter, the stability of nsP3 was also detected to determine if AUD, especially the mutations chosen in this study, was associated with nsP3 degradation.

3.2 Results

3.2.1 Generation of a panel of AUD alanine mutations in CHIKV-D-Luc-SGR

CHIKV nsP3 consists of three domains, macrodomain, AUD and hypervariable domain (Figure 3.1). AUD is a homologous sequence across alphaviruses, sharing an identity of over 80% with other alphaviruses. To identify residues within the AUD that are conserved across the Alphavirus genus we first aligned the AUD amino acid sequences of a range of both Old World and New World alphaviruses (Figure 3.1C). As the AUD sequences between SINV and CHIKV are highly conserved (118 of 243 residues are identical – (Figure 3.1C), the nsP2/nsP3 protein structure of SINV (Shin et al., 2012) was referenced to identify the putative location of each of the conserved residues. Following from the above analysis, 12 residues were chosen for further study as they were located on the surface of the protein and were either absolutely conserved throughout the alphaviruses, or in other cases were substituted by residues with

similar physical characteristics (specifically the corresponding residue for both Met219 and Val260 in CHIKV is leucine in SINV) (Figure 3.1 B, C and Appendix Table 9.3). M219, P247, V248 and D249 are located closely in a limited surface area of AUD and are presumed to perform related functions. R243 and K245 are the only positive-charged residues among where they are located and are speculated to be involved in RNA-binding activity. Y324 was chosen because it is located at the junction between AUD and macro domain. C262 and C264 are chosen as negative controls because they are important components of the zinc coordination site within AUD which are essential for alphavirus replication (Shin et al., 2012); and two other residues located next to C262 and C264 (V260 and P261) were chosen for further study of the zinc coordination site.



As shown in Figure 2.1, a fragment of the CHIKV cDNA containing the AUD coding sequence and those residues targeted for mutagenesis was amplified from the CHIKV-D-Luc-SGR and inserted into pcDNA3.1 vector. Then the resulting plasmid (pcDNA3.1-AUDforMutation) was used as template for Quick-change site-directed mutagenesis to produce mutant AUDs in pcDNA3.1, followed by subcloning the mutant AUD fragment back into CHIKV-D-Luc-SGR. In this way, AUD mutants M219A, E225A, R243A, K245A, R243A/K245A, P247A, V248A, P247A/V248A, D249A, V260A/P261A, C262A/C264A and Y324A were introduced into CHIKV-D-Luc-SGR.

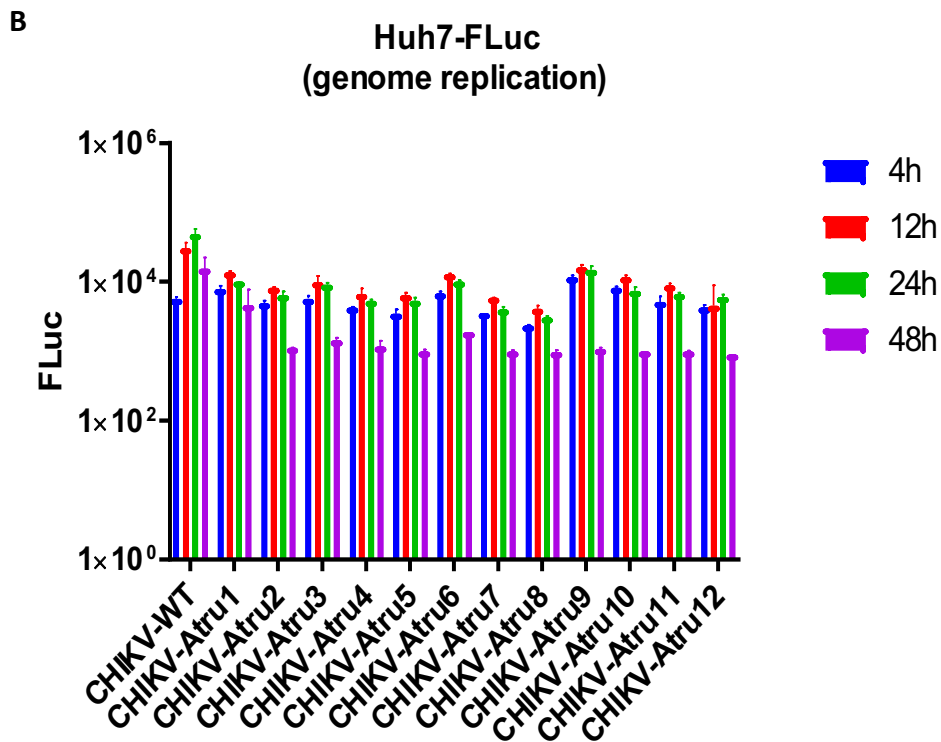
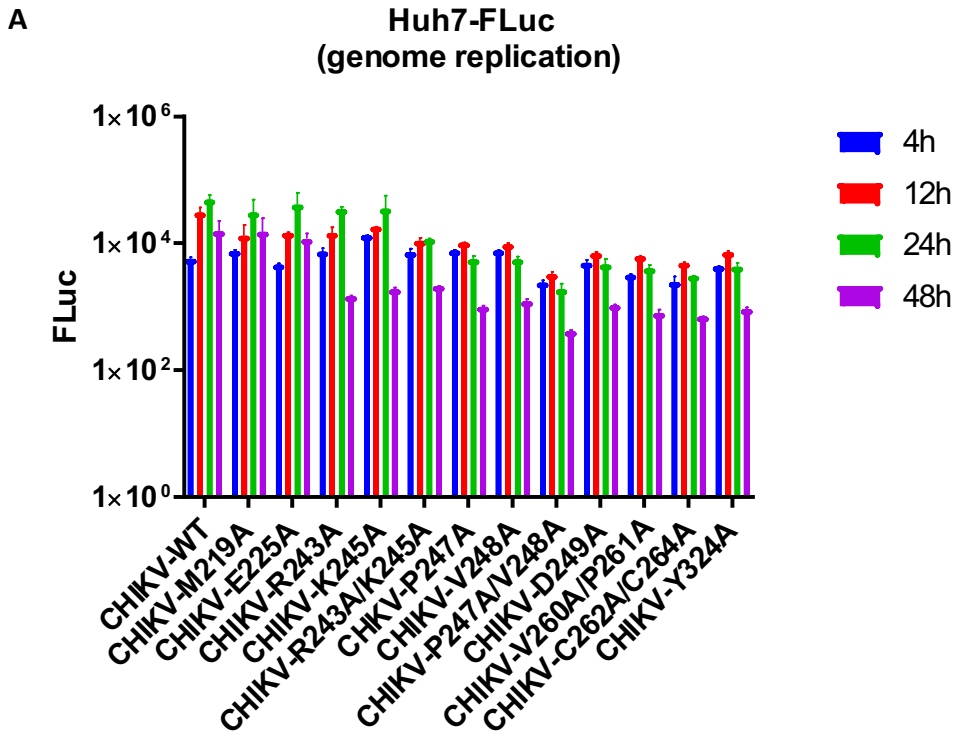
As AUD is highly conserved among alphaviruses and the 12 residues chosen for mutation were just a small fraction of the conserved residues, in order to determine which part of AUD was critical for CHIKV replication, an alternative strategy was performed to construct 12 truncations of AUD into CHIKV-D-Luc-SGR (Figure 2.2).

3.2.2 The role of AUD in CHIKV genome replication

CHIKV subgenomic replicon replication was measured by dual-luciferase assay. The nsP3-fused renilla showed an input translation and replication level of the replicon, while the firefly signal which was expressed in place of virus structural proteins showed only replication level. Preliminary experiments were firstly performed with the 12 AUD point mutants and 12 AUD truncations of CHIKV-D-Luc-SGR in Huh7 cells, which is a well characterised human hepatoma cell line and have been previously shown to efficiently support CHIKV replication (Roberts et al., 2017), and U4.4 cells which are derived from the *Ae. albopictus* mosquito. In Huh7 cells, wildtype CHIKV-D-Luc-SGR exhibited robust replication with Fluc levels increasing from 6×10^3 to 5×10^4 between 4 h and 24 h post-transfection. Of the mutants, E225A replicated as wildtype, R243A and K245A exhibited a slight reduction in replication, while the other point mutants, as well as the AUD truncations, failed to replicate. Rluc levels of wildtype and all the mutants were at a similar level at 4 h post transfection, indicating that all replicon RNAs were well translated in Huh7 cells.

A different picture emerged for U4.4 cells although all the AUD truncations still showed no replication. Firstly, M219A failed to replicate in U4.4 cells although it showed impaired replication in Huh7 cells; Secondly, all the other point mutants except V260A/P261A and C262A/C264A showed replication in U4.4 cells although P247A/V248A replicated at a lower level than wildtype. In conclusion, based on the preliminary experiments, 6 point mutants were chosen for further study, including M219A, E225A, R243A/K245A, P247A/V248A,

V260A/P261A and C262A/C264A; and the nsP4 mutant GAA which withdrew nsP4 RNA polymerase activity was used as negative control.



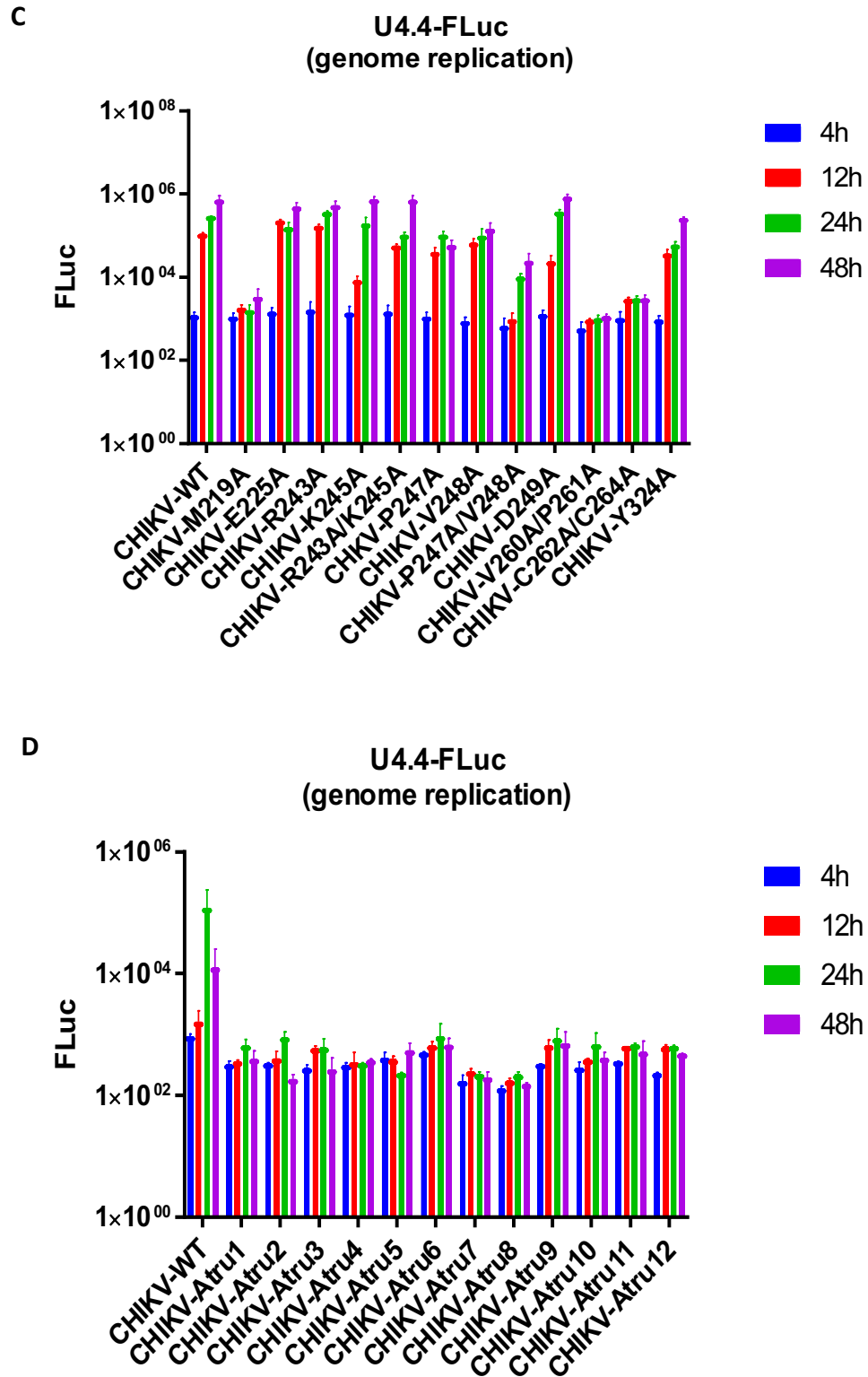


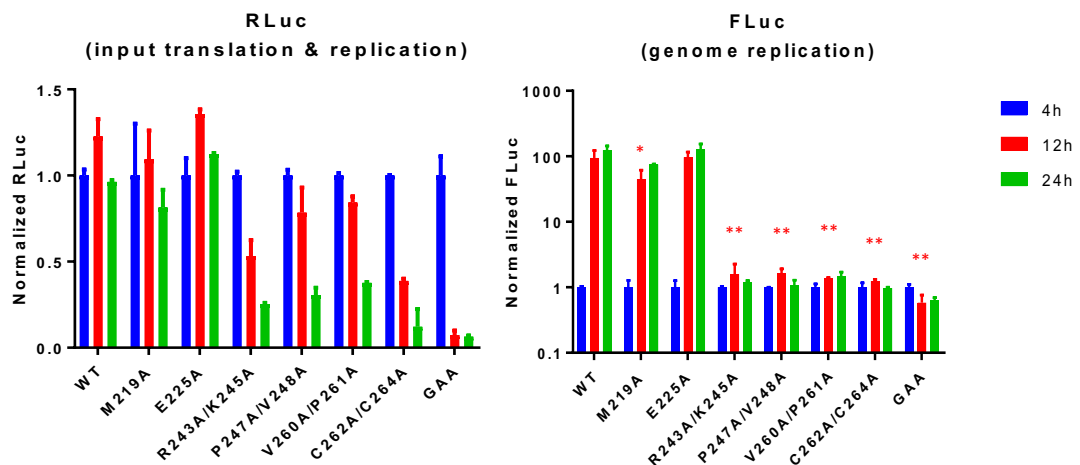
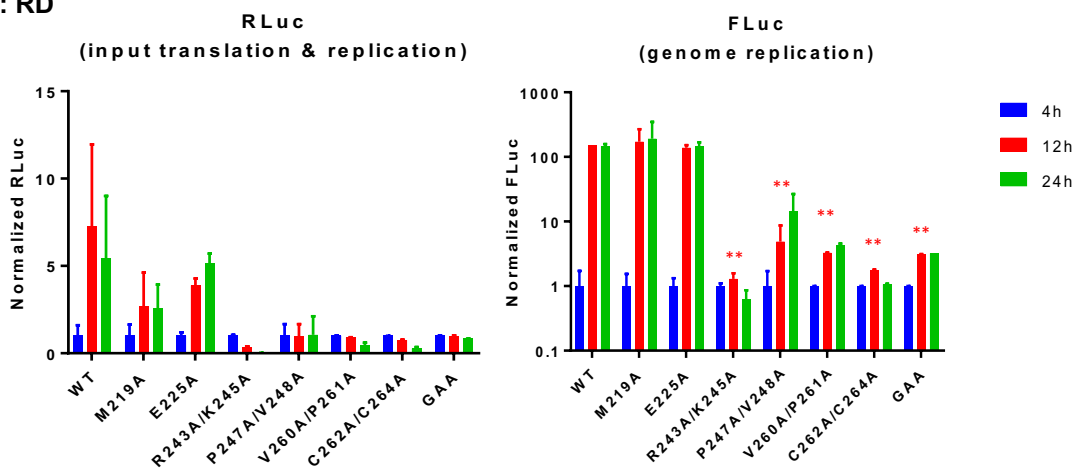
Figure 3.2 Preliminary data of CHIKV AUD mutants replication in Huh7 and U4.4 cells.

The indicated cells were seeded in 24-well plates 12 hours before transfection. Cells were then transfected with 0.5 μg CHIKV-D-luc-SGR wildtype and mutant RNAs and harvested at 4, 12, 24 and 48 h.p.t. for firefly luciferase assays. AB. Wildtype CHIKV and its mutants replication capability in Huh7 cells. CD. Wildtype CHIKV and its mutants replication capability in U4.4 cells.

To analyse the effects of the AUD mutations on CHIKV genome replication, the panel of mutant CHIKV-D-Luc-SGR RNAs chosen for further study were transfected into a range of cell lines. As both liver and muscle are target organs for CHIKV infection three human cell lines were used. Besides Huh7 cells, to test any potential role of the AUD in protecting CHIKV from innate immune sensing we also used the Huh7 derivative cell line Huh7.5, which have a defect in innate immunity due to a mutation in one allele of the retinoic acid-inducible gene I (RIG-I) (Sumpter et al., 2005). To investigate the role of the AUD in infection of muscle cells a human rhabdomyosarcoma cell line, RD, was applied. Additionally, two other mammalian (non-human) cell lines were used: C2C12 (a murine myoblast cell line) and BHK-21 (baby hamster kidney cells) based on their ability to support high levels of CHIKV replication (Roberts et al., 2017). Lastly, we used two mosquito (*Ae. albopictus*) derived cell lines: U4.4 and C6/36. Of note C6/36 have a defect in RNA interference (RNAi) due to a frameshift mutation in the Dcr2 gene, leading to production of a truncated and inactive Dcr2 protein (Morazzani et al., 2012). Again, use of these cells was intended to allow us to assess any role of the AUD in counteracting mosquito innate immunity.

3.2.2.1 The role of AUD during CHIKV replication in human cells

Besides Huh7 cells (Figure 3.2), the replication of wildtype CHIKV and its mutants were also analysed in another 2 human cell lines, Huh7.5 and RD cells. Replication of the mutants screened in Huh7.5 cells showed a similar picture to that in Huh7 cells (Figure 3.3A). Replication of wildtype, M219A and E225A was higher in Huh7.5 cells compared to Huh7, probably because of its defect in cytosolic RNA sensing, however, this did not allow replication of the inactive mutants. For RD human rhabdomyosarcoma cells, a slightly different picture emerged (Figure 3.3B): firstly both M219A and E225A replicated to a similar level as wildtype. Secondly, the P247A/V248A mutant, which was unable to replicate in Huh7 or Huh7.5 cells, was able to replicate to a low level in RD cells. The other 3 mutants and nsP4 GAA again failed to replicate.

A: Huh7.5**B: RD****Figure 3.3 CHIKV AUD mutant replication in human cells.**

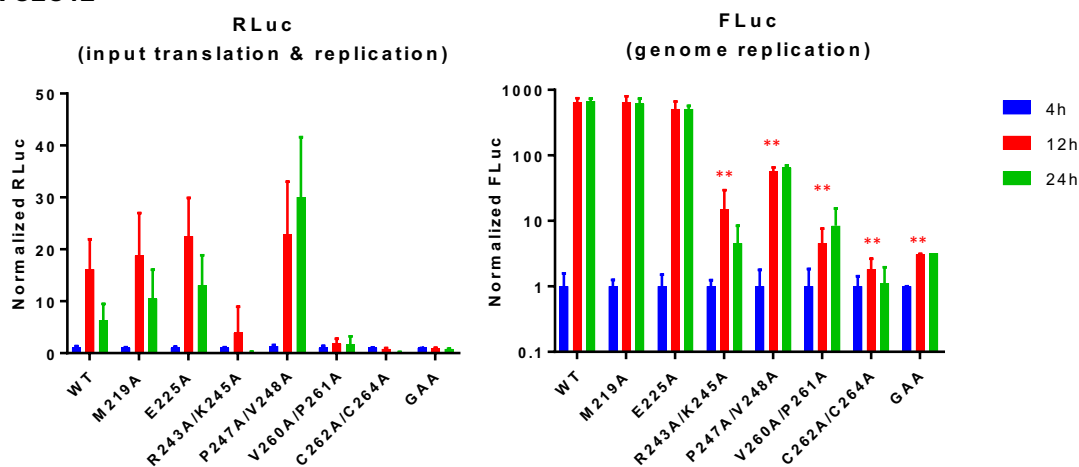
The indicated cells were transfected with CHIKV-D-luc-SGR wildtype and mutant RNAs and harvested for both renilla and firefly luciferase assays at the indicated time points. Luciferase values of wildtype and each mutant were normalized to 4 h values. (GAA: inactive mutant of nsP4 polymerase). Significant differences denoted by * ($P < 0.05$), and ** ($P < 0.01$), compared to wildtype.

3.2.2.2 The role of AUD during CHIKV replication in non-human mammalian cells

We then evaluated the mutant panel in another two mammalian cell lines: C2C12 murine myoblasts (Figure 3.4A) and BHK-21 cells (Figure 3.4B). Wildtype CHIKV-D-Luc-SGR replicated to very high levels in both cell lines, with FLuc levels increasing ~ 1000 -fold between 4-24 h. In general the phenotypes of the panel of mutants were similar to those observed in RD, however two noticeable differences were detected. Firstly, R243A/K245A and V260/P261 replicated in a low level in C2C12 and BHK cells. Secondly, P247A/V248A was capable of replication to a high level in both (albeit nearly 10-fold lower than wildtype). Interestingly,

although FLuc levels for P247A/V248A were reduced, the concomitant RLuc levels were higher than wildtype, suggesting that although this mutant was competent in virus genome replication there might be a defect in transcription or translation of ORF2. These data suggested that P247 and V248 were required for CHIKV genome replication in liver-derived cells, whilst enhancing but not essential for replication in cells derived from muscle or kidney, implying some cell type specific interactions of nsP3. The zinc-coordinating cysteine mutant C262A/C264A were unable to replicate in either cell line, being indistinguishable from the GAA nsP4 control.

A C2C12



B BHK

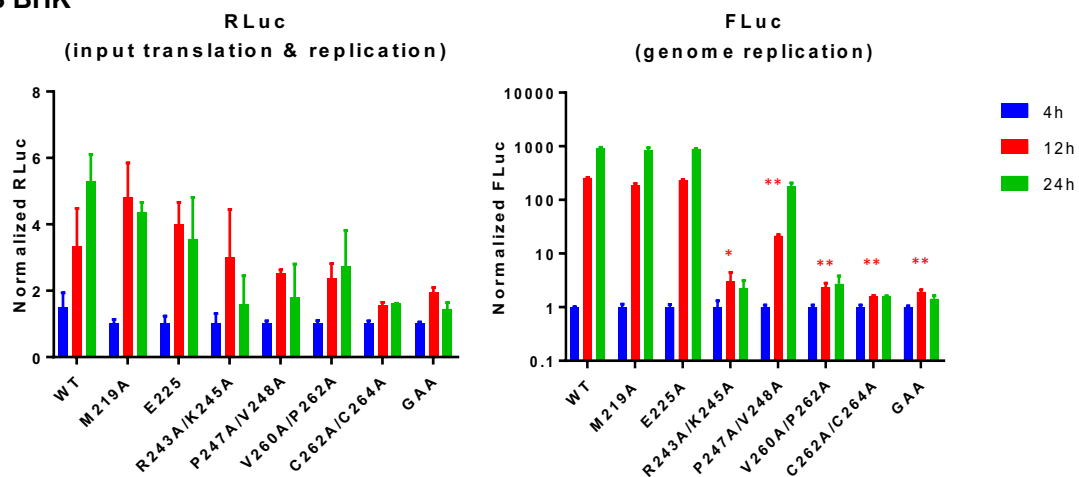


Figure 3.4. CHIKV AUD mutant replication in non-human mammalian cells.

The indicated cells were transfected with CHIKV-D-luc-SGR wildtype and mutant RNAs and harvested for both renilla and firefly luciferase assay at the indicated time points. Luciferase values of wildtype and each mutant were normalized to 4 h values. (GAA: inactive mutant of nsP4 polymerase). Significant differences denoted by * ($P < 0.05$), and ** ($P < 0.01$), compared to wildtype.

3.2.2.3 The role of AUD during CHIKV replication in mosquito cells

As an arbovirus transmitted by mosquitoes, CHIKV must replicate in both mammalian and mosquito cells. We therefore proceeded to evaluate the replicative capacity of the panel of mutants in cells derived from the *Ae. albopictus* mosquito. Two cell lines were used: U4.4 and C6/36. The major difference between these two cell lines is that C6/36 has a defect in the RNAi response due to a frameshift mutation in its Dcr2 gene (Morazzani et al., 2012). Consistent with this, although both mosquito cell lines were susceptible for CHIKV replication, C6/36 supported higher levels than U4.4 (up to 1000-fold increase at 48 h). As described below, remarkable differences were observed in the mutant phenotypes in these cells compared to the mammalian cells (Figure 3.2 CD and 3.5). The first difference was that M219A failed to replicate in U4.4 cells (Figure 3.2 C) but exhibited wildtype level of replication in C6/36 cells (Figure 3.5B), suggesting that M219 might be involved in interacting with, and inhibiting, the mosquito cell RNAi pathway. Secondly, R243A/K245A, which showed no replication in human cell lines and only slight replication in the C2C12 cells, was fully replication competent in both mosquito cell lines. Mutant P247A/V248A was partially replication competent in both cell lines, V260A/P261A and C262A/C264A showed little replication in C6/36 cells whereas as seen in mammalian cell lines neither V260A/P261A nor C262A/C264A replicated in U4.4 cells (Figure 3.2C).

C6/36

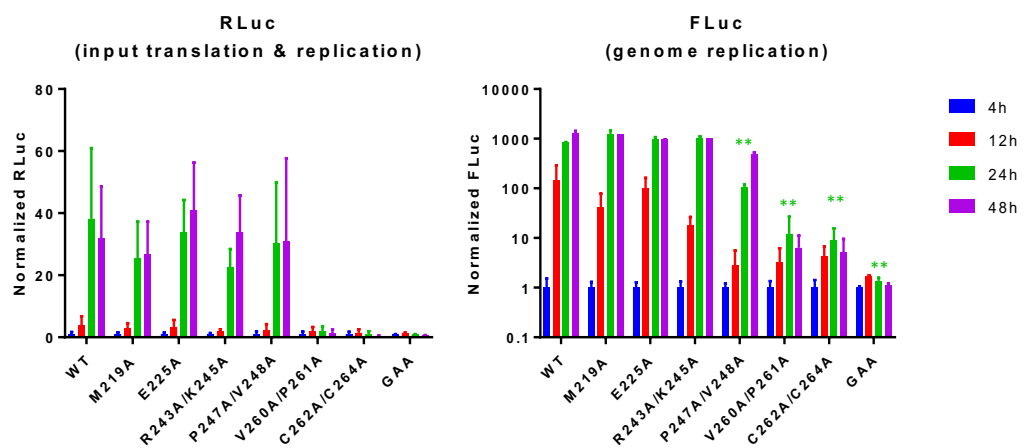


Figure 3.5. CHIKV AUD mutant replication in *Aedes albopictus* mosquito cells.

The C6/36 cells were transfected with CHIKV-D-luc-SGR wildtype and mutant RNAs and harvested for both renilla and firefly luciferase assay at the indicated time points. Luciferase values of wildtype and each mutant were normalized to 4 h values. (GAA: inactive mutant of nsP4 polymerase). Significant differences denoted by ** (P < 0.01), compared to wildtype

3.2.3 Sequence analysis of the CHIKV-D-Luc-SGR-AUD (R243A/K245A) RNA following replication in different cell types

The striking phenotypic difference between mammalian and mosquito cell lines for R243A/K245A led us to investigate this further. A simple explanation might be that the mutations had reverted in mosquito cell lines. To test this cytoplasmic RNA from C2C12, U4.4 and C6/36 cells was extracted at various time post transfection, and subjected them to RT-PCR and sequence analysis. In C2C12 at 48 h.p.t. no sign of reversion was observed (Figure 3.6) – the sequence remained the same as the input RNA. However, for both U4.4 at 48 h.p.t., and C6/36 samples the sequence traces revealed the presence of a mixed population of mutant and wildtype. Notably a sequential accumulation of revertants in the C6/36 samples was observed: At 24 h.p.t. a very low proportion of revertants at the first position in the two codons was seen, at 48 h.p.t. the proportion increased and at 72 h.p.t. the sequences were almost entirely wildtype. These data are consistent with a requirement for R243 and K245 for efficient CHIKV genome replication.

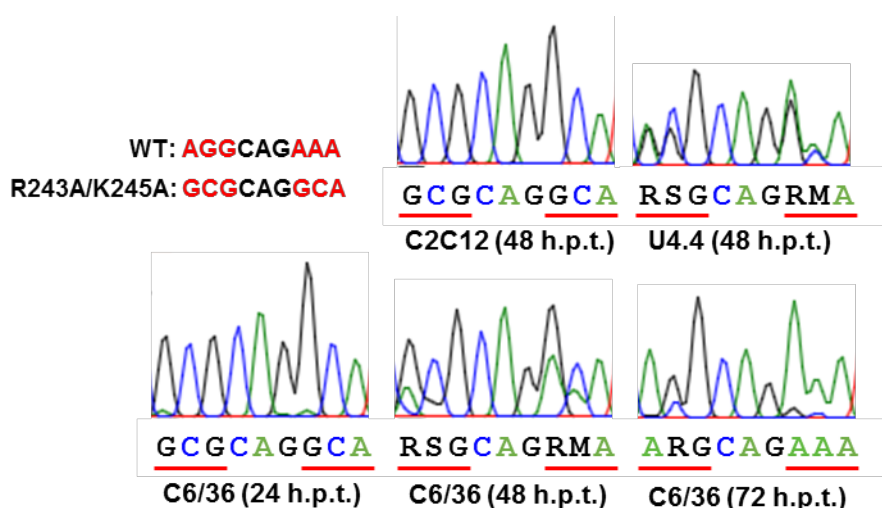


Figure 3.6. RT-PCR and sequencing analysis of CHIKV-D-luc-SGR-R243A/K245A.

RNA was harvested at the indicated times, amplified by RT-PCR and sequenced. The wildtype and mutated sequences are shown below the sequence traces for reference. Nucleotide ambiguity codes used: R (A/G), S (G/C) and M (A/C).

3.2.4 Lethal mutations do not interfere the expression and stability of nsP3/AUD

To investigate whether the defect of AUD mutants in RNA replication observed in the dual luciferase assay resulted from the loss or disruption of a specific function of nsP3, or from the degradation or instability of nsP3 or AUD protein, wildtype, M219A, E225A, R243A/K245A,

P247A/V248A, V260A/P261A and C262A/C264A nsP3 or AUD were separately cloned into pcDNA3.1 to allow their expression in mammalian cells. The plasmids were then transfected into different cells and cell lysates collected for WB to detect the expression of nsP3 or AUD. As shown in Figure 3.7, expression and stability of nsP3 or AUD were rarely affected by the mutations introduced into AUD.

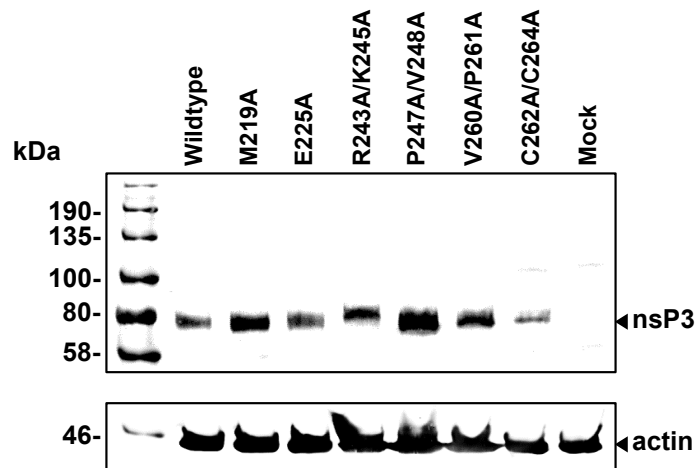


Figure 3.7. Expression and stability of nsP3.

Wildtype and mutant nsP3 were cloned into pcDNA3.1 and transfected into C2C12 cells for 48 hours before cell lysates collected with GLB. Expression and of nsP3 was detected by western blot.

3.3 Discussion

Of the four alphavirus non-structural proteins, nsP3 remains the least well understood (Gotte et al., 2018). The protein is composed of three domains, the N-terminal macrodomain has been proved to bind to ADP-ribose and possess ADP-ribosylhydrolase activity (Malet et al., 2009). Recent studies have suggested that this enzymatic activity plays a role in virus pathogenesis but the underlying mechanisms of it still remains elusive (McPherson et al., 2017). The C-terminal hypervariable domain shares low level of amino acid sequence identity with other alphaviruses and is intrinsically disordered. It has been demonstrated to interact with a range of cellular proteins, including components of stress granules (Kim et al., 2016), and is supposed to be involved in the assembly of virus genome replication complexes.

In contrast, virtually nothing is known about the function of the central AUD domain. AUD is a homologous sequence among different alphaviruses, suggesting that it plays a fundamental role in the virus lifecycle. The structural information of Sindbis virus AUD was determined in

the context of SINV nsP2-nsP3 precursor, including the C-terminal protease and methyltransferase-like domains of nsP2 and the macro and AUD domains of nsP3 (Shin et al., 2012). This analysis revealed that the AUD contained a unique zinc-binding fold with four cysteine residues coordinating a zinc molecule, which formed part of a putative RNA binding surface. Mutagenesis of two of these cysteines revealed an essential role of the zinc coordination site in virus replication. Our data agree with this observation, as the C262A/C264A mutant failed to replicate in any cell type tested.

Mutation of two residues adjacent to the zinc-binding cysteines, V260A/P261A, also completely abrogated CHIKV genome replication. Although adjacent in the primary amino acid sequence, these two residues are located on the distal surface of the AUD (Figure 3.1B), suggesting that they are not involved in the zinc coordination site, but may instead interact with key cellular factor(s) or play an alternative structural role.

In contrast, the other mutants generated in this chapter exhibited a number of distinct cell-type and species-specific phenotypes (summarised in Table 3.1). Mutation of two surface exposed basic residues (R243 and K245) abrogated replication in all mammalian cells but showed no effect on CHIKV replication in both mosquito cells. However, sequence analysis then revealed that these two mutations quickly reverted to wildtype in mosquito cells but not in C2C12 cells (Figure 3.6), explaining the different phenotypes shown by R243A/K245A and further implying the importance of R243 and K245 for CHIKV genome replication. The reason why only R243A/K245A, but not the other lethal mutations, was able to revert in mosquito cells was not clear. But it is sure that the R243A/V245A mutant is able to replicate in insect cells, even though just in a very low level, as this is a precondition for reversion. Therefore the reason why R243A/V245A mutant reversion occurred in insect cells but not mammalian cells might be that the activity of R243A/K245A is temperature sensitive and the mutant is tolerated better at 28 °C. However it is noteworthy that the reversion to the wildtype sequence took 72 h to become predominant in C6/36 cells, suggesting that perhaps the lack of cytopathology of CHIKV replication in mosquito cells could facilitate the replication of a minority species. Interestingly, the sequence trace at 24 h in C6/36 showed the presence of a minority species that would encode a Thr at 243 and 245, suggesting that the two basic residues were not absolutely required.

M219 was also of particular interest as mutation of this residue had no significant effect on genome replication in most cells tested in this chapter apart from U4.4 mosquito cells. As the key difference between U4.4 and C6/36 cells is that C6/36 have a defect in the RNAi response

because of a Dcr2 mutation (Morazzani et al., 2012), M219A phenotypes between U4.4 and C6/36 cells suggested a role of M219 in interaction with a component of the mosquito RNAi response to inhibit this key mosquito antiviral pathway. RNAi is believed to be the most significant innate antiviral immune response in mosquitoes (Sanders et al., 2005, Sanchez-Vargas et al., 2009, Campbell et al., 2008b, Myles et al., 2008, Cirimotich et al., 2009, Khoo et al., 2010), including three major types of small RNA molecules identified: small interfering RNA (siRNA), microRNA (miRNA) and PIWI-interacting RNA (piRNA) (Coffey et al., 2014). In Huh7 and Huh7.5 cells, M219A also showed a slight, and significant in Huh7.5 cells, lower replication capability compared to wildtype, which was not observed in muscle cells RD and C2C12. As Dicer is expressed at a lower level in skeletal muscle and heart than other tissues (Sago et al., 2004), it may be supposed that M219 was also associated with mammalian cells RNAi response although the significance of it in mammalian cells was not as vital as it was in mosquito cells, indicating a difference in Dicer-associated RNAi response between mammalian and mosquito cells. Moreover, Kalika et al demonstrated that the CHIKV AUD in nsP3 had RNAi suppressor activity although the functional motifs within AUD were not identified (Mathur et al., 2016), which to some extent, also supported the role of M219 in RNAi suppression.

P247A/V248A was also a mutant of interest as in the context of the subgenomic replicon it showed a variety of phenotypes from complete lack of replication in Huh7 and Huh7.5 cells (Figure 3.2 and 3.3), to a 10-fold reduction in other mammalian and mosquito cells (Fig 3.2 and 3.5). The defect of P247A/V248A replication capability in all the cells tested indicated a fundamental function of P247/V248 during CHIKV replication.

CHIKV-D-luc-SGR	Human			Rodent		Mosquito	
	Huh7	Huh7.5	RD	C2C12	BHK	U4.4	C6/36
Wildtype	■	■	■	■	■	■	■
M219A	■	■	■	■	■	■	■
E225A	■	■	■	■	■	■	■
R243A/K245A	■	■	■	■	■	■	■
P247A/V248A	■	■	■	■	■	■	■
V260A/P261A	■	■	■	■	■	■	■
C262A/C264A	■	■	■	■	■	■	■

Key: ■ Wildtype replication, ■ impaired replication, ■ no replication, ■ reversion

Table 1 AUD mutant replication phenotypes in different cell types.

On the other hand, the seven different cells used for dual luciferase assay in this study showed variable susceptibility to CHIKV genome replication. Huh7 and Huh7.5 cells are both human hepatoma cell lines, and the difference between them is Huh7.5 cells have a defect in innate immunity due to a mutation in one allele of the retinoic acid-inducible gene I (RIG-I) (Sumpter et al., 2005). CHIKV replicated to nearly 10-fold higher level in Huh7.5 cells compared to that in Huh7 cells. As Huh7.5 is known to be defective in RIG-I-associated innate immunity, which is different from Huh7 cell, this RIG-I associated innate immunity might be involved in the cellular antiviral response against CHIKV, although the data presented in this chapter showed that the AUD residues selected here were not involved in this interaction. Mammalian muscle cells, C2C12 and RD cells, were more susceptible for CHIKV replication than liver cells, which was consistent with the fact that muscle cells were the target cells for CHIKV pathogenicity. The high level of CHIKV replication in BHK-21 cells was also observed possibly because of its high efficiency for transient transfection. The two mosquito cells, U4.4 and C6/36 showed generally higher susceptibility than mammalian cells for CHIKV genome replication. *Aedes albopictus* mosquitoes are the vectors for CHIKV during virus transmission (Schuffenecker et al., 2006), which were susceptible for CHIKV replication but the infection was generally considered non-pathogenic (Coffey et al., 2014). Between these two cells, CHIKV replication in C6/36 cells were obviously higher than that in U4.4 cells, suggesting a role of RNAi response in mosquito antiviral reaction.

Chapter 4: nsP3 AUD is required for production of subgenomic RNA and structural proteins during CHIKV infection

4.1 Introduction

Use of the dual-luciferase reporter system demonstrated the effect of AUD on CHIKV genome RNA replication. In this chapter, I proceeded to introduce the panel of AUD mutations into infectious CHIKV (ICRES-CHIKV, derived from the ECSA strain) for detection of AUD function through CHIKV infection. As shown in the D-luci results, most of the CHIKV AUD mutants constructed in this study were able to replicate in C2C12 cells, and C2C12 cells are physiologically relevant, being muscle derived, further studies on CHIKV infection was performed in C2C12 cells.

A one-step growth curve provides valuable information on virus replication cycle in a specific cell system, and is a common experimental procedure for the study of virus replication. It describes the production of progeny virus over a period of time following infection under one-step conditions, where cells are infected simultaneously to prevent secondary cycles of infection. Samples of supernatant medium or cell lysates are collected at various times post infection for quantification of extracellular or intracellular virus, respectively. When virus titres are plotted as a function of time, the growth curve obtained shows different stages following virus infection, including adsorption and penetration, eclipse period, maturation and release. Therefore, the one-step growth curve detection was used in this chapter to study the effect of AUD on different stages of CHIKV infection.

During alphavirus replication, three kinds of RNAs are produced, including negative-strand genomic RNA, positive-strand genomic RNA and subgenomic RNA. The production of these three kinds of RNAs are highly regulated in different stages with early or late replication complex formed of viral non-structural proteins and host cellular proteins. Negative-strand RNA production reached a highest level at early stage of replication, and then rapidly decreases to undetectable level (Sawicki et al., 1981a). In contrast, the rate of viral positive-strand RNA synthesis increases at the early stage of replication, reaches a maximum level and stays at this rate until cells begin to deteriorate (Frolov and Schlesinger, 1994, Sawicki et al., 1981a, Sawicki et al., 1981b). The positive-strand RNA replicase complex regulates the synthesis of genomic and subgenomic RNA from the same negative-strand RNA template, and the two positive-strand RNAs were synthesized at a constant rate throughout virus replication cycle (Solignat et al., 2009). In this chapter, to analyse the synthesis of genomic and subgenomic RNA, [³H] was used to label nascent viral RNAs after cellular RNA synthesis was blocked by dactinomycin.

The three-dimensional structure of nsP2/3 fragment of Sindbis virus revealed a zinc coordination site within AUD, indicating a RNA-binding activity and gene regulation function of it (Shin et al., 2012, Berg, 1990). As the amino acid sequences consisting the zinc coordination site are conserved between Sindbis virus and CHIKV, it is supposed that this structure and its function is also applied in CHIKV AUD. To test CHIKV nsP3 binding activity to viral RNA *in vivo*, co-immunoprecipitation assay was performed with twin-strep tagged-nsP3 (TST-nsP3) CHIKV infectious virus, where CHIKV genomic RNA was quantified by qRT-PCR with pulled down and purified TST-nsP3 protein to detect if TST-nsP3 was able to bind viral RNA during virus replication in cells. Distribution of nsP3 in cells during virus replication may reflect its functions. Previous confocal immunofluorescence studies have revealed a process of nsP3 distribution during virus replication. Early after infection, nsP3 was observed on the plasma membrane as part of the virus replication complex on the cytoplasmic surface. Then for some alphaviruses such as SFV, nsP3 accumulated at spherules existing on the surface of the perinuclear cytopathic vacuoles (CPV) (Froshauer et al., 1988, Cristea et al., 2006, Kujala et al., 2001), which were originated from modified endosomes and lysosomes (Froshauer et al., 1988). During virus infection, while a part of nsP3 remained in the replication complexes with other viral proteins for virus genome replication, there was also a subpopulation of nsP3 existing free from the replication complexes, but in a formation of large cytoplasmic aggregates instead (Peranen et al., 1988). The proportion of nsP3 remained in the virus replication complexes or in the large cytoplasmic aggregates was different for different alphaviruses. In SFV infected cells, the majority of nsP3 was found to co-localize with dsRNA, but for CHIKV, much less nsP3 was shown in the co-localization with dsRNA while most of it remained in the large cytoplasmic aggregates. This chapter detected the sub-cellular localisation of nsP3, capsid protein and dsRNA to further explore the function of CHIKV nsP3, especially the importance of P247 and V248 residues within it.

4.2 Results

4.2.1 The effect of AUD mutations in infectious CHIKV production

In order to determine if the AUD played any role in other stages during virus infection, a subset of mutations that showed replication in all, or some of, the mammalian cells shown in D-luciferase reporter assay (M219A, E225A, R243A/K245A and P247A/V248A), were introduced into an infectious CHIKV construct (ICRES-CHIKV). The nsP4 GAA mutant was introduced into ICRES-CHIKV as negative control. *In vitro* transcribed virus RNAs (5'-capped) were electroporated into C2C12 cells, and the produced infectious viruses at different times post electroporation (8, 24

and 48 h.p.e.) were quantified by plaque assay of cell supernatants. C2C12 cells were chosen for further studies as our previous analysis had revealed that CHIKV showed high level of replication in these cells (Roberts et al., 2017), and they are physiologically relevant, being muscle derived.

As expected (Figure 4.1 A), wildtype CHIKV replicated well and produced a high titre of infectious virus in C2C12 cells following electroporation, while the negative control nsP4 GAA mutant failed to produce any infectious virus. M219A and E225A showed similar replication capability as wildtype, while P247A/V248A produced a significantly reduced amount of virus (approx. 10-fold reduced). Moreover, sequence analysis by RT-PCR of the produced infectious virus demonstrated that R243A/K245A quickly reverted to wildtype while M219A, E225A and P247A/V248A retained their mutations and showed no hint of reversion to wildtype. (Figure 4.1 B).

At the same time, during the course of plaque assays, the P247A/V248A mutant uniquely exhibited a much smaller plaque size than the wildtype (Figure 4.1 C).

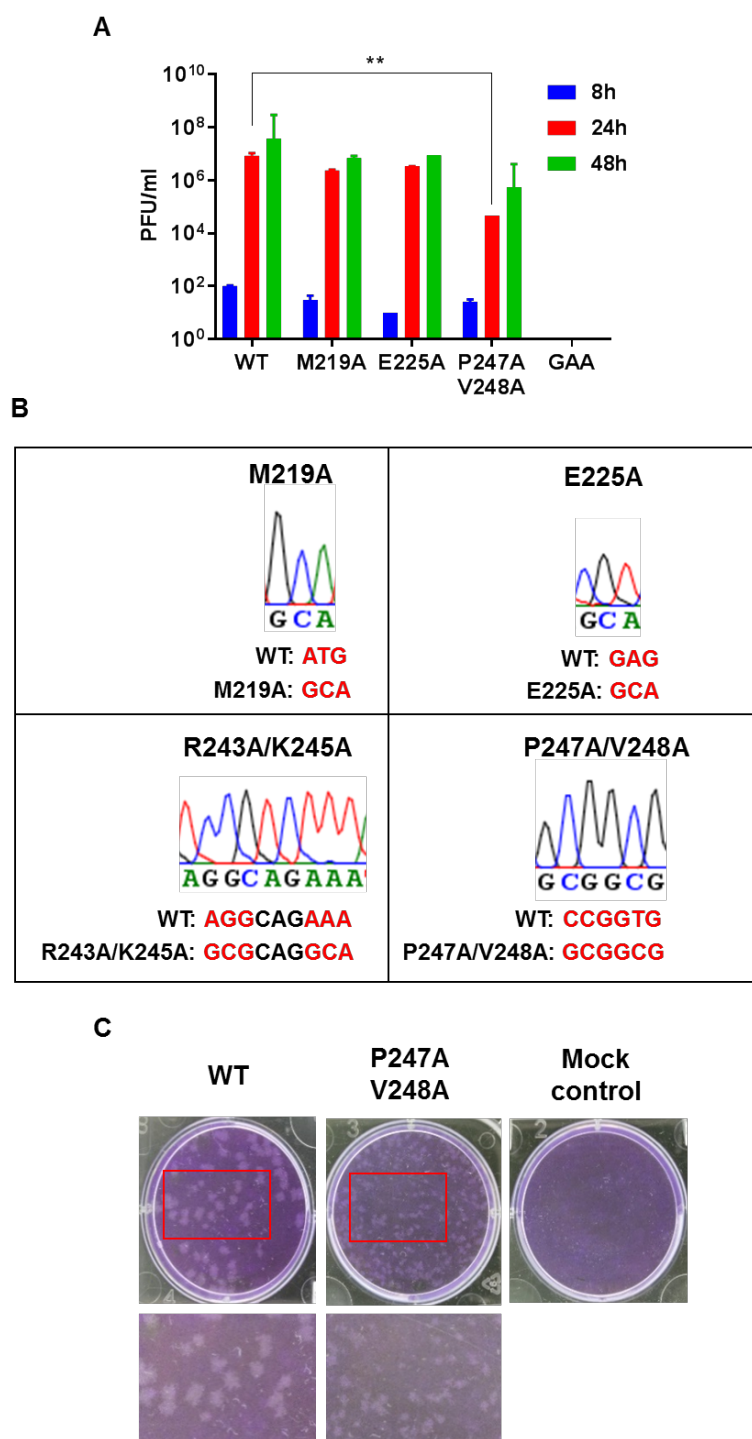


Figure 4.1 Phenotype of AUD mutations in the production of infectious virus.

A. ICRES-RNAs were electroporated into C2C12 cells and supernatants were collected at 48 h.p.e. Virus was titrated by plaque assay in BHK-21 cells. B. Sequencing analysis of virus passage P0. P0: supernatant virus stock obtained from C2C12 cells at 48 h.p.e. nsP3 coding sequence was amplified by RT-PCR and sequenced. The region spanning the indicated mutations is shown. Note that for E225A the sequence traces shown are from the negative strand, hence the colour of the trace does not match the colour code of the sequence below. All the mutants had not reverted. C. Plaques for wildtype and P247A/V248A were visualised illustrating the small plaque phenotype for this mutant.

4.2.2 One-step virus growth kinetics

The smaller plaques formed by P247A/V248A mutant implicated a defect in either virus production or spread, which was consistent with the reduced virus production post electroporation in C2C12 cells, although the high level of input RNA might, to some extent, recovered this defect. To verify this, a one-step growth assay was performed by infecting C2C12 cells at MOI=1 with either wildtype CHIKV or the 3 mutants (M291A, E225A and P247A/V248A). Cell supernatants were collected at various times post infection for quantification of genomic RNA by qRT-PCR (Figure 4.2A), and infectious virus by plaque assay (Figure 4.2B). Wildtype, M219A and E225A exhibited a rapid increase in both genomic RNA and infectious virus between 8-48 h.p.i., reaching very high titres (for wildtype: 3.4×10^{10} RNA copies/ml and 4.7×10^8 pfu/ml), followed by a sharp decrease of infectious virus due to the death of infected cells. However, the genomic RNA did not show a consistent decrease as infectious virus, probably because although infectious viruses were inactivated in vitro, their genomic RNAs did not get degraded immediately. At the same time, the one-step growth curve of P247A/V248A showed a significantly lower but similar trend of replication process. Levels of P247A/V248A accumulated very slowly, reaching a maximum of 4.6×10^6 RNA copies/ml and 2.8×10^5 pfu/ml at 48 h.p.i. After 48 h.p.i., the amount of genomic RNA and infectious viruses also decreased. However, different from what was observed for wildtype or the other two mutants, cells infected by P247A/V248A remained alive throughout the infection process, indicating that the decrease of P247A/V248A virus after 48 h.p.i. was due to a self-defect in virus replication. However, following analysis of direct comparison of the genomic RNA quantification with the infectivity revealed that the specific infectivity of all four viruses were indistinguishable (Figure 4.2C). Therefore in conclusion, although P247A/V248A exhibited a defect in production of virus particles, the virions produced were equally infectious as wildtype.

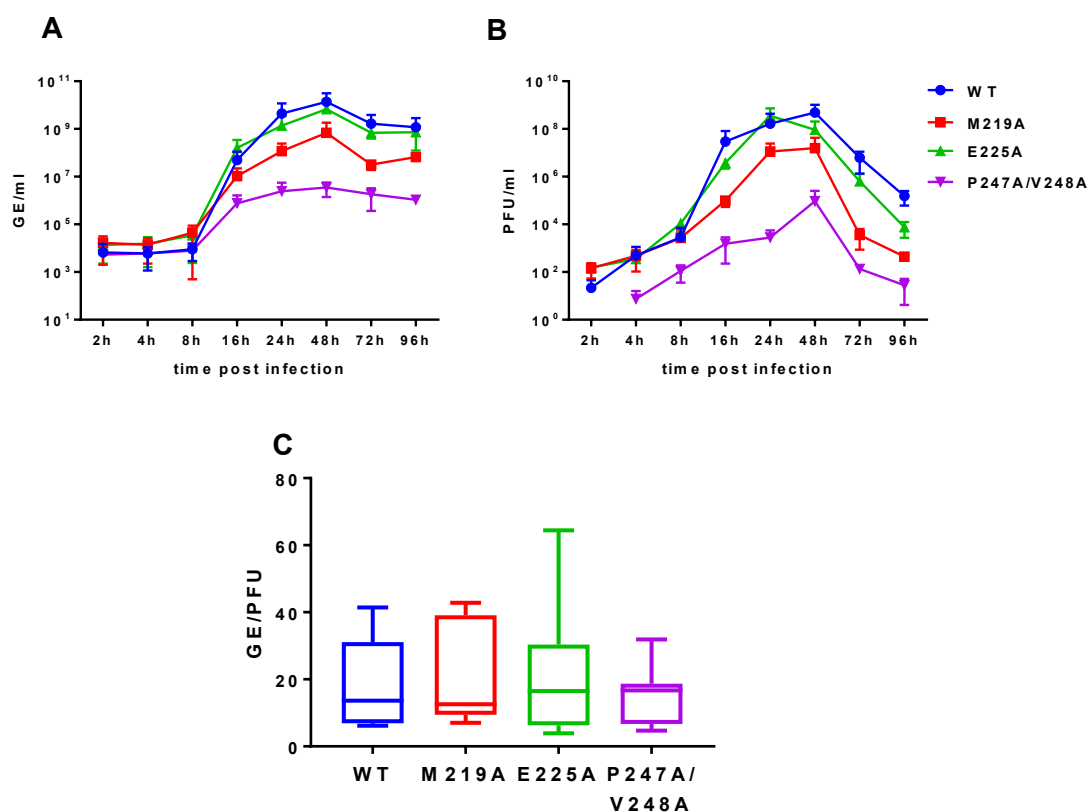


Figure 4.2 Multi-step growth kinetics of CHIKV.

C2C12 cells were infected with CHIKV (wildtype and mutants) at an MOI of 0.1. Supernatants were aliquot collected at the indicated times for genome RNA quantification (qRT-PCR) (A) and virus titration by plaque assay (B). The ratios of genome RNA:infectivity were determined from A and B at 16, 24 and 48 h.p.i. and presented graphically (C).

4.2.3 Role of AUD in CHIKV assembly and release

To explore whether the reduced virus production exhibited by P247A/V248A was because of its defect in virus assembly or release from infected cells, both the extracellular and intracellular samples were analysed of the infectious virus and genomic RNA within them. At first, the amount of viral genomic RNA (by qRT-PCR) and infectious virus (by plaque assay) were quantified with cells infected with wildtype or the 3 mutants (at an MOI of 1) at 24 h.p.i. This result (Figure 4.3A) showed that the levels of intracellular genomic RNA for wildtype, M291A and E225A were at similar levels whereas P247A/V248A exhibited a 1000-fold reduction, which was consistent with the D-luci replicon. The amount of intracellular infectious virus were comparable for wildtype, M219A and E225A, however, uniquely a dramatic 10⁷-fold reduction occurred for P247A/V248A compared to wildtype : from 2.4 x 10⁸ pfu/ml to 9.8 x 10¹ pfu/ml. The ratio of genomic RNA:infectivity (Figure 4.3B) clearly demonstrated this

difference, suggesting that besides the defect in genome replication, P247A/V248A had a more substantial phenotype in the production of infectious virus particles, possibly due to a defect in virus assembly. The magnitude difference between these two phenotypes suggests that the AUD plays multiple roles during CHIKV replication. In order to explore whether the P247A/V248A had a phenotype in virus release, we compared the amount of infectious virus in extracellular and intracellular samples by electroporation of C2C12 cells with wildtype or the 3 mutant virus RNAs (Figure 4.3C and D). This analysis showed that the ratio between extra- and intracellular virus titres was significantly higher for P247A/V248A compared to wildtype and the other two mutants, indicating that although P247A/V248A produced less infectious virus, the produced virus could be released from the infected cells more efficiently than wildtype and the other two mutants.

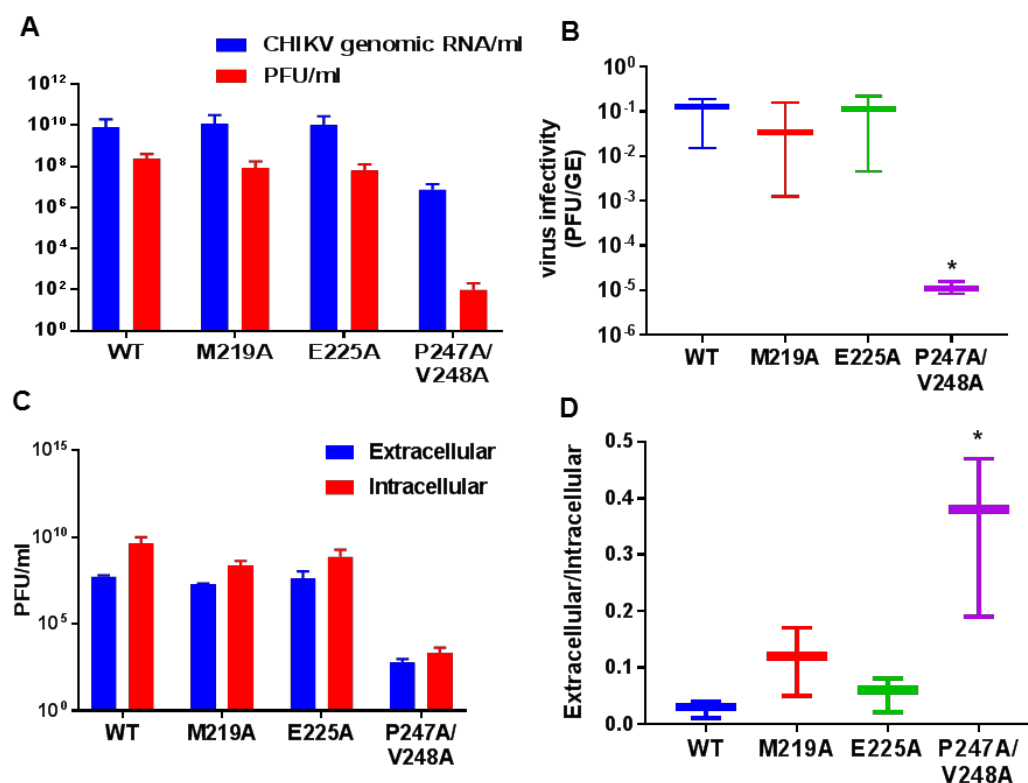


Figure 4.3 Phenotype of AUD mutations on virus entry, release and assembly.

A. C2C12 cells were infected with CHIKV at MOI of 1. At 24 h.p.i, cells were washed three times with PBS and resuspended in 1 ml fresh medium. Cell suspensions were freeze/thawed 3 times to obtain intracellular viruses. Genome RNA was quantified by qRT-PCR, and virus titrated by plaque assay. B. Graphical representation of the ratio of infectivity to genomic RNA. C. Intracellular and extracellular viruses were collected at 36 h.p.e from C2C12 cells electroporated with the indicated ICRES RNA, and titrated by plaque assay. D. Graphical representation of the ratio of extracellular to intracellular virus titres. Significant difference denoted by * ($P < 0.05$) compared to wildtype.

4.2.4 The P247A/V247A mutation selectively impairs subgenomic RNA synthesis

Infectious virus replication results in the last section demonstrated that besides an impairment in viral genome replication, the reduction of P247A/V248A mutant in infectious virus production resulted mainly from its defect in virus assembly, which might be due to a direct role of nsP3 in this process, or some defect in the production of the structural proteins. To further study it, the expression of both nsP3 and capsid protein was detected by western blot with viral RNA electroporated C2C12 cells. As shown in Figure 4.4A, P247A/V248A exhibited a modest reduction in nsP3 expression but a much greater reduction in the level of capsid expression. Analysis of the ratio between capsid and nsP3 expression determined from the western blot results showed that the corresponding capsid protein production of

P247A/V248A was approximately 10-fold lower than wildtype and the other two mutants (Figure 4.4A). During alphavirus replication, two kinds of positive-strand RNAs are produced using the same negative-strand RNA as template, the full-length genomic RNA (gRNA) used for translation of non-structural proteins (including nsP3), and the subgenomic RNA (sgRNA) for translation of structural proteins (capsid and other structural proteins). Therefore, the defect of P247A/V248A in nsP3 and capsid protein expression possibly resulted from the lack of gRNA and sgRNA. Regulation of the synthesis of gRNA or sgRNA is mediated by the viral replication complex composed of 4 non-structural proteins and some host cellular proteins, which initiates transcription from the 3' end of the negative-strand RNA or from the sub-genomic promoter. To test the synthesis of gRNA and sgRNA, C2C12 cells were electroporated and treated with actinomycin D (ActD) to block cellular RNA synthesis, prior to labelling with [³H]-uridine. Cellular RNA was then extracted and analysed by MOPS-formaldehyde gel electrophoresis and autoradiography. As shown in Figure 4.4B, for WT, M219A and E225A, 2 bands of radiolabelled RNAs corresponding to gRNA and sgRNA were detected. However, for P247A/V248A, the radioactive signal of sgRNA was in an almost undetectable low level, with the corresponding ratio of gRNA:sgRNA for P247A/V248A (25.3:1) significantly higher than that of WT (1.5:1). As controls, mock electroporated cells treated with ActD contained no [³H]-labelled RNA species, whereas in the absence of ActD the expected smear of [³H]-labelled RNAs with predominant bands corresponding to 18S and 28S ribosomal RNAs were observed (Figure 4.4B). To confirm these results, the harvested RNAs were also analysed by sucrose gradient centrifugation. Consistent with the electrophoretic analysis, wildtype, M219A and E225A showed two peaks corresponding to sgRNA and gRNA, whereas P247A/V248A exhibited a dramatically reduced sgRNA peak (Figure 4.4C).

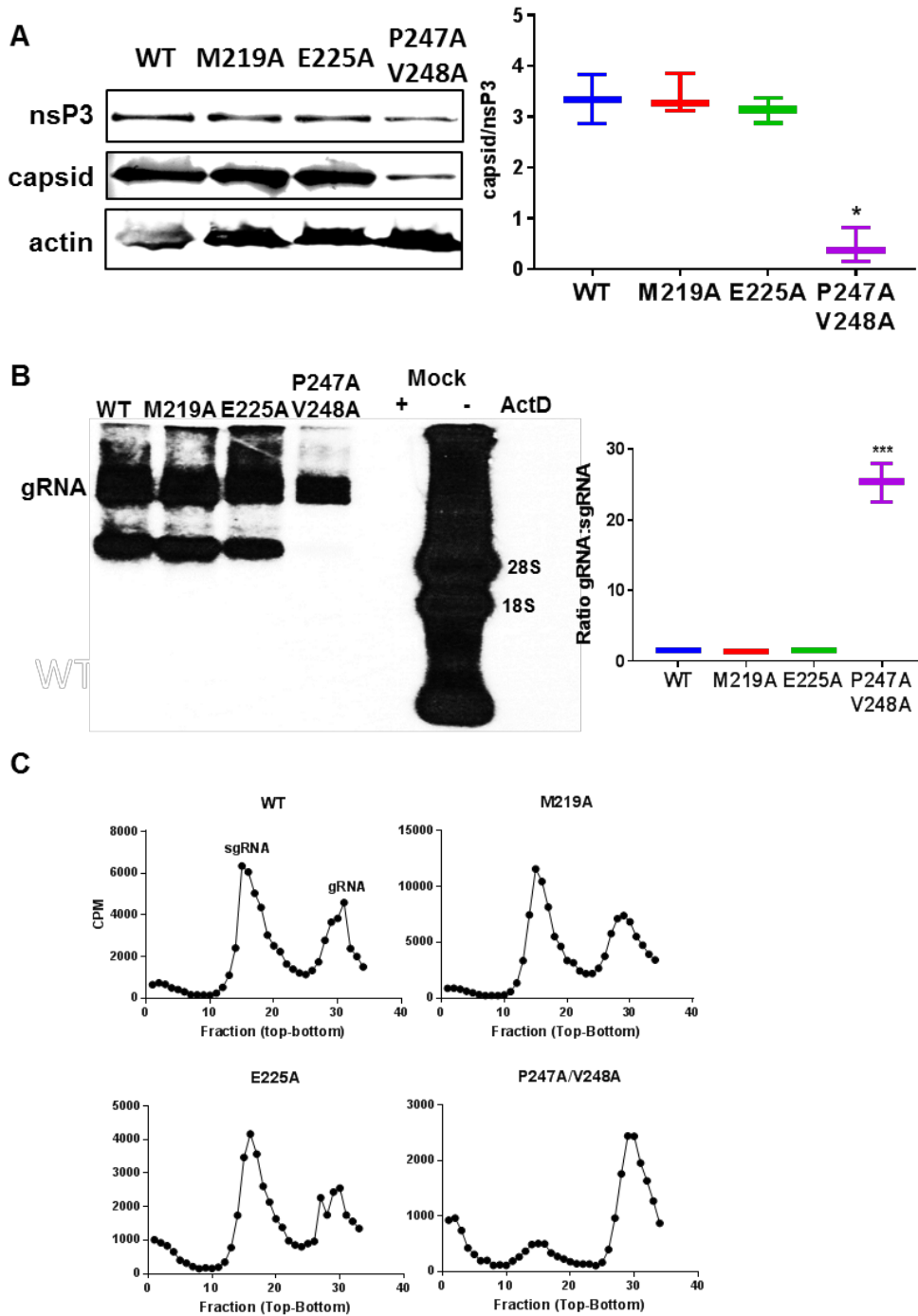


Figure 4.4 Effect of AUD mutations on CHIKV protein expression and RNA synthesis.

A. C2C12 cells were electroporated with ICRES-RNAs and cell lysates were collected at 36 h.p.e. Expression of nsP3 and capsid was analysed by western blot. Multiple western blots were quantified using the LiCor Odyssey Sa fluorescence imager and the graph on the right shows the ratio of capsid:nsP3 expression. B. C2C12 cells were electroporated with the indicated ICRES RNA, cellular RNA synthesis was inhibited by actinomycin D and nascent viral RNAs were labelled with [³H]-uridine. The graph on the right shows the ratio of gRNA to sgRNA. C. The same RNAs were separated by sucrose gradient and [³H]-labelled RNAs were detected by scintillation counting.

4.2.5 nsP3 RNA binding activity to CHIKV genome RNA

As nsP3 is predicted to have RNA binding activity, which is possibly important for CHIKV genome RNA replication, we next explored whether nsP3 was able to bind CHIKV genomic RNA during virus replication in cells. To do this, we exploited a previously generated derivative of the ICRES infectious clone in which a twin-strep tag (TST) was introduced in frame near the C-terminus of nsP3, allowing efficient affinity purification of nsP3 by streptactin chromatography. Similar experimental approach has been previously used in our lab to investigate protein-protein and protein-RNA interactions of the hepatitis C virus NS5A protein (Goonawardane et al., 2017, Ross-Thriepland and Harris, 2014, Yin et al., 2018). Before testing nsP3 RNA binding activity to CHIKV genomic RNA with the TST-CHIKV, the effect of the TST on CHIKV replication was determined and the results showed that the TST made no significant difference to either wildtype or P247A/V248A mutant replication. To test nsP3 RNA binding activity to CHIKV genomic RNA, wildtype or P247A/V248A mutant TST-nsP3 CHIKV RNAs were electroporated into C2C12 cells, from which nsP3 proteins were purified with streptactin beads and analysed by western blot for nsP3 (Figure 4.5A) and qRT-PCR to determine the amount of gRNA co-immunoprecipitated with nsP3 (Figure 4.5B). As shown in Figure 4.5C, P247A/V248A bound approximately 10-fold less gRNA compared to wildtype, indicating that nsP3 was able to bind CHIKV genomic RNA during virus replication and the P247A/V248A mutations impaired this binding activity. However, as P247A/V248A could not replicate well in C2C12 cells the input genomic RNA of P247A/V248A mutant was originally more than 10 times less than that of wildtype, which might also contributed to the reduction of the precipitated mutant viral RNA.

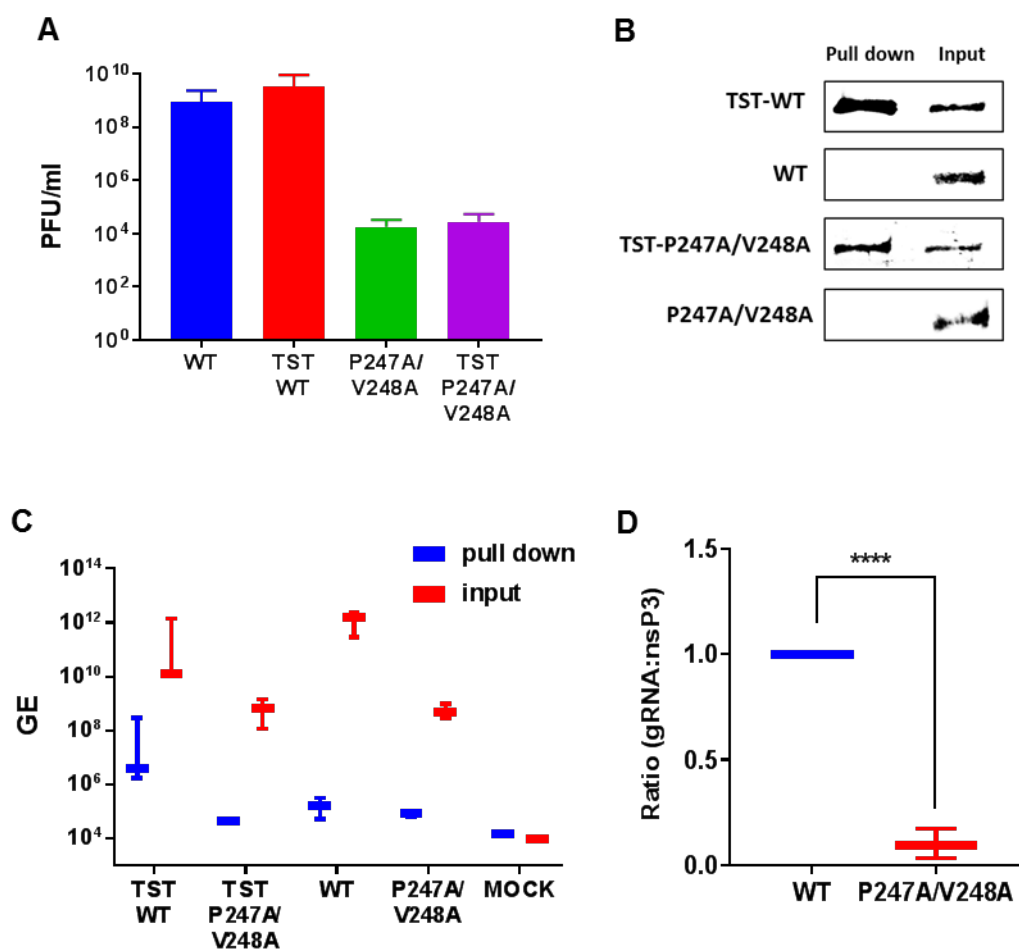


Figure 4.5 CHIKV genome RNA association with nsP3 during virus replication.

A. ICRES-WT, ICRES-TST-WT, ICRES-P247A/V248A, ICRES-TST-P247A/V248A RNAs were electroporated into C2C12 cells. Supernatant were collected at 48 h.p.e and titrated by plaque assay. BCD. C2C12 cells were electroporated with ICRES nsP3-TST or ICRES RNAs. Cell lysates were collected at 60 h.p.e., and nsP3-TST was precipitated with Streptactin-sepharose beads. Bound proteins were subjected to western blotting (B) and co-precipitated RNAs were extracted by TRIzol and quantified by qRT-PCR (C). The ratio of gRNA to nsP3 is depicted graphically (D).

4.2.6 Sub-cellular localisation of nsP3, capsid and dsRNA during CHIKV replication

The effect of P247A/V248A on the nsP3:gRNA interaction suggested that this mutation might also disrupt the subcellular localisation of nsP3 in relation to both replication complexes and sites of virion assembly. To test this we exploited another derivative of the ICRES infectious CHIKV clone in which ZsGreen was inserted into nsP3 at the same position as the TST tag (Remenyi et al., 2018, Pohjala et al., 2011). C2C12 cells were electroporated with ICRES-nsP3-ZsGreen-CHIKV RNAs (wildtype or P247A/V248A), and cells were analysed by confocal laser scanning microscopy (CLSM) with Airyscan for the distribution of nsP3, capsid (as a marker for virion assembly sites) and dsRNA (as a marker of genome replication) at different times post-electroporation. For wildtype at 4 h.p.e. (Fig 4.6), small clusters of nsP3, capsid and dsRNA appeared in the cytoplasm but there was little co-localisation. By 8 h.p.e., nsP3, capsid and dsRNA co-localised in larger clusters, these appeared to accumulate at the plasma membrane at 12 and 16 h.p.e., most of nsP3, capsid and dsRNA were co-localised on plasma membrane. By 24 h.p.e, it was clear that the infection cycle was complete as there was a reduction in levels of nsP3, capsid and dsRNA. Interestingly, capsid and dsRNA were still co-localised at the plasma membrane while most nsP3 was perinuclear. In contrast, P247A/V248A exhibited a very different distribution pattern of all three markers throughout the infection cycle (Fig 4.7). Consistent with the western blot data (Fig 4.5A) levels of capsid and dsRNA were lower than wildtype at all timepoints, but in addition the co-localisation of nsP3, capsid and dsRNA was markedly reduced and the three markers never accumulated at the plasma membrane as seen for wildtype. Consistent with the delay in virus release shown in Fig 4.2, it was clear that, unlike wildtype, the infection cycle was not complete by 24 h.p.e. as levels of nsP3 and capsid were highest at this timepoint.

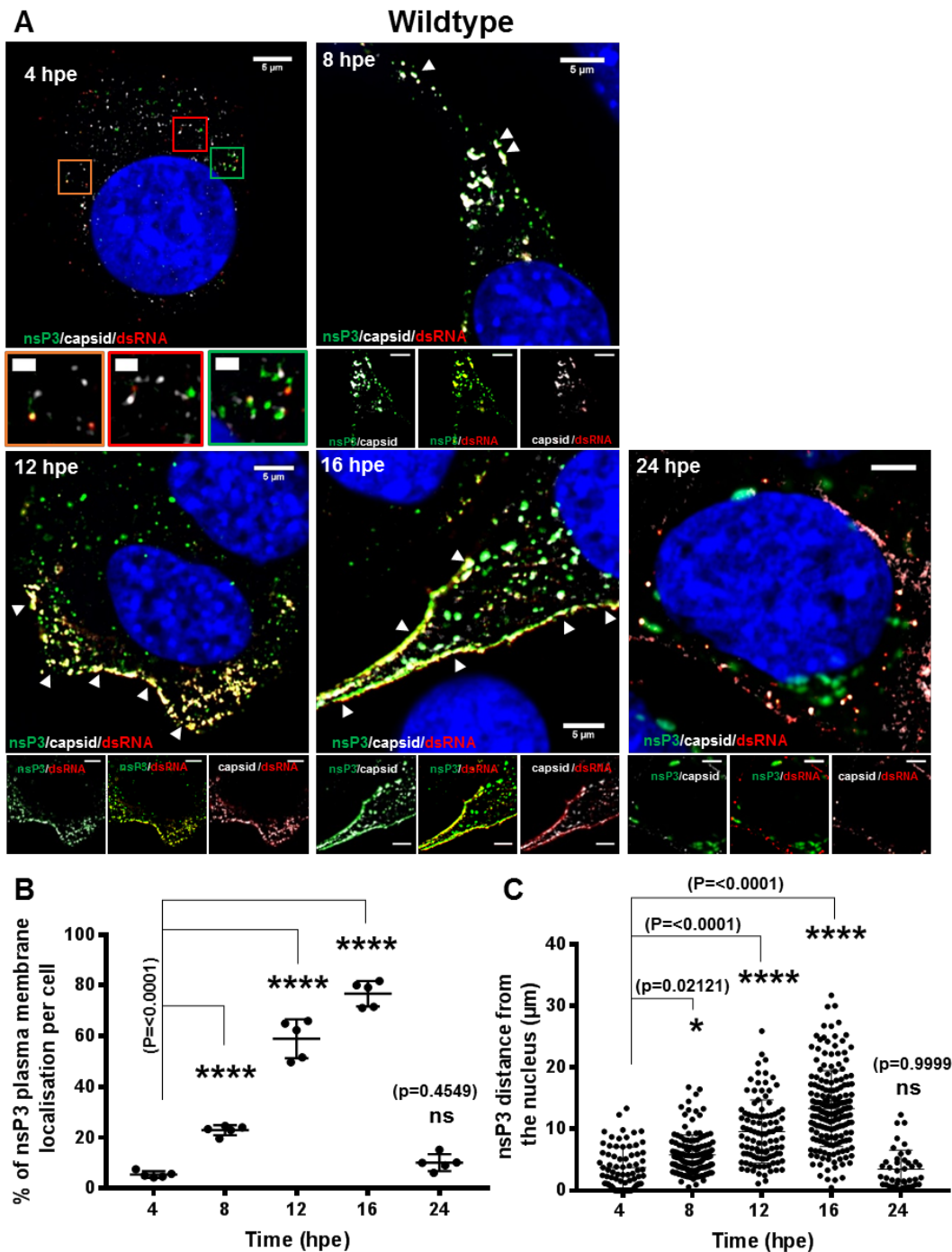


Figure 4.6 Fluorescence analysis of nsP3, capsid and dsRNA distribution during infection of C2C12 cells with wildtype CHIKV.

A. C2C12 cells were electroporated with ICRES-nsP3-ZsGreen-CHIKV RNA. Cells were fixed at the indicated time points post-infection and stained with antibodies to capsid protein (white) and dsRNA (red). Green: nsP3-ZsGreen fusion, blue: nuclear DAPI counterstain. The scale bars are 5 μm and 1 μm , respectively. B. Co-localisation of nsP3 with plasma membrane. C. Distance of nsP3 from the nucleus.

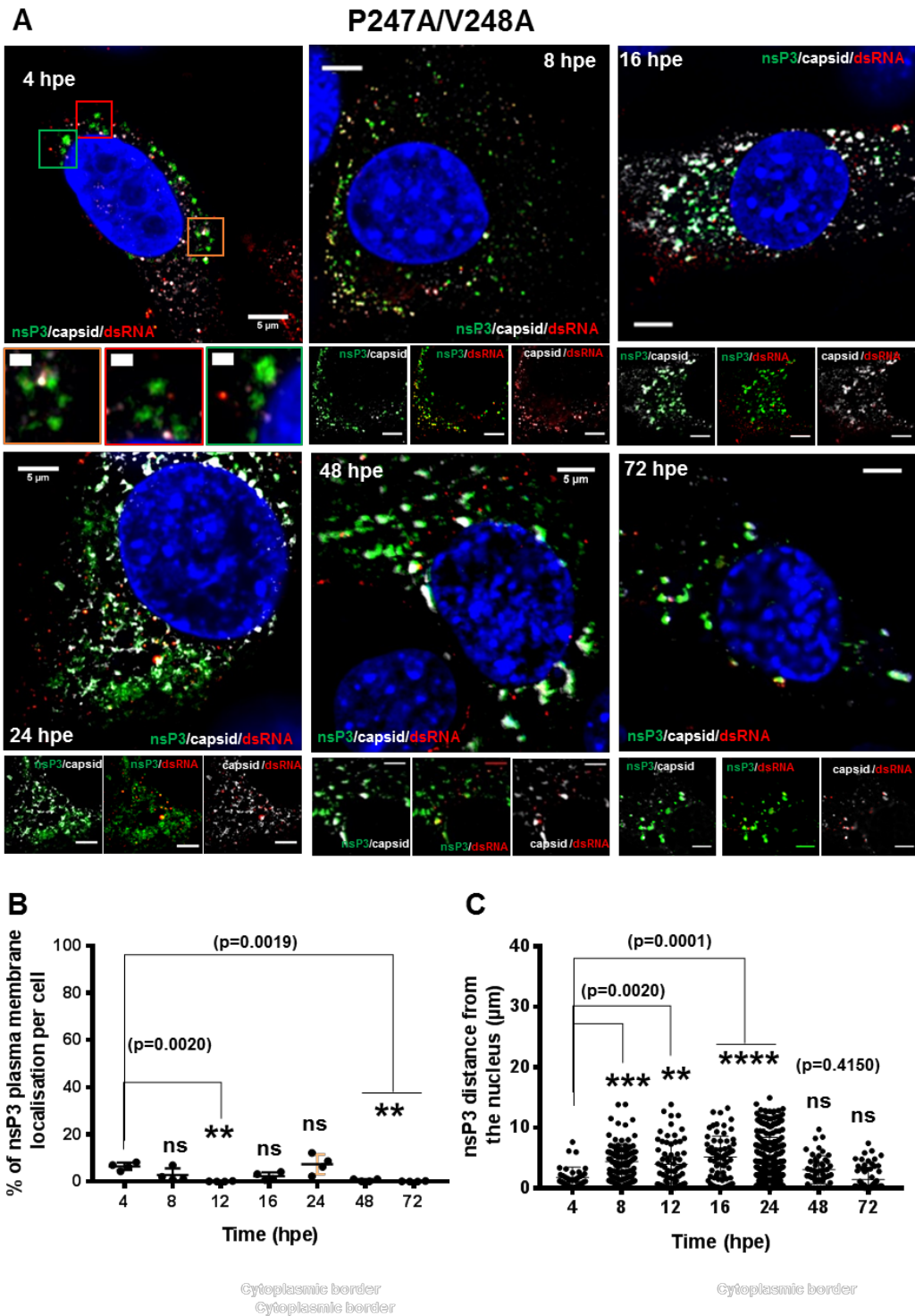


Figure 4.7 Fluorescence analysis of nsP3, capsid and dsRNA distribution during infection of C2C12 cells with P247A/V248A CHIKV.

A. C2C12 cells were electroporated with ICRES-nsP3-ZsGreen-CHIKV RNA. Cells were fixed at the indicated time points post-infection and stained with antibodies to capsid protein (white) and dsRNA (red). Green: nsP3-ZsGreen fusion, blue: nuclear DAPI counterstain. The scale bars are 5 μm and 1 μm , respectively. B. Co-localisation of nsP3 with plasma membrane. C. Distance of nsP3 from the nucleus.

4.3 Discussion

The introduction of AUD mutations into infectious virus confirmed the significance of AUD during CHIKV replication. After electroporation of ICRES-CHIKV RNAs, M219A and E225A did not show any phenotype on CHIKV replication compared to wildtype, but P247A/V248A displayed a defect in infectious CHIKV production which was consistent with replicon result performed with CHIKV-D-Luc-SGR. It was interesting to find that the plaques formed by P247A/V248A was obviously smaller than those of wildtype and the other two mutants. Together with the significantly reduced infectious virus production for P247A/V248A, an important role of P247/V248 residues within AUD was suggested for CHIKV replication. One-step growth kinetics of CHIKV wildtype and the 3 mutants were then analysed to validate the defect of P247A/V248A in virus replication. Moreover, the virus production defect of P247A/V248A shown by one-step growth kinetics was more severe than that shown by plaque assay of the electroporated cells, giving a hint that P247A/V248A might play some additional roles during other stages of CHIKV infection besides its effect on the intracellular virus genome RNA replication.

In order to explore if the AUD plays any roles in other stages during CHIKV infection, we first detected the specific infectivity of the virions produced by wildtype and each mutants with direct comparison of the genomic RNA quantification with the infectivity. The results indicated that although P247A/V248A was partially defective in virus particle production, its released virions were able to enter the cells and replicate, equally infectious as wildtype. Release of the infectious viruses were also detected by quantification and comparison of the extracellular and intracellular infectious virus particles. The results showed that although P247A/V248A produces less infectious virus, this can be released from the infected cells more efficiently than wildtype and the other two mutants, which might be because the P247A/V248A CHIKV infected cells were in a better condition for virus release as less virus were produced to cause cytotoxicity; or it might be just because for wildtype and other mutants, viruses were produced much more efficiently inside the cells than that for P247A/V248A mutant.

The most interesting result was that P247A/V248A exhibited a major defect in infectious virus particle assembly. This defect led to both a delay and a reduction in the release of infectious virus, consistent with the small plaque phenotype. A reduced level of both genome RNA copies and infectious virus particles were detected from the intracellular samples, moreover, the reduction in infectious virus particles was much more severe than that of genome RNA copies. This might resulted from two reasons: 1. nsP3 could be involved in virus packaging, and

P247A/V248A nsP3 failed to assemble virus particles in a right way therefore the intact P247A/V248A virus particles were partially infectious; 2. P247A/V248A virus was competent in genome RNA production but lacked structural proteins to form infectious virus particles. As in replicon data, it is noteworthy that in C2C12 cells the P247A/V248A replicon exhibited a 10-fold reduction in Fluc, but Rluc was higher than wildtype. This may be consistent with a defect in either transcription of the subgenomic mRNA or translation of ORF2, rather than a reduction in genome replication. Therefore it was supposed that the P247A/V248A mutant was possibly defective in structural proteins production.

To validate the hypothesis described above, expression of structural protein capsid protein and non-structural protein nsP3 were firstly detected from the virus-infected cells and confirmed that P247A/V248A had a partial defect in structural protein expression. Further study then revealed that the defect of P247A/V248A began at the stage of transcription of subgenomic RNA. Regulation of genomic RNA and subgenomic RNA synthesis is believed to be dependent on nsP4 as nsP4 binds to respective promoters with different motifs within it (Li and Stollar, 2004, Li and Stollar, 2007, Li et al., 2010). However, some mutational experiments suggested that nsP1, nsP2 and nsP3 were also involved in this process through interaction with nsP4 (Rupp et al., 2011, Fata et al., 2002, Pietila et al., 2017). The formation of CHIKV replicase for the synthesis of different kinds of viral RNAs has not been revealed yet, the results obtained in this chapter suggested a possible role of AUD, especially the P247/V248 residues, in the specific CHIKV subgenomic RNA synthetic replicase formation. The mechanism of the interaction between nsP3 and CHIKV genome RNA is not clear yet. As P247 and V248 are not positive-charged residues, it is predicted to bind genomic RNA with This function might be performed through interaction with nsP4 and other viral proteins, or recruitment of viral template RNAs or some host proteins for virus replication.

The immunoprecipitation assay suggested that nsP3 had RNA-binding activity to CHIKV genome RNA during virus replication in cells, P247A/V248A showed a significant defect in this binding activity, indicating that the RNA-binding activity to CHIKV genome RNA was critical for CHIKV genome replication, and AUD, especially P247/V248 residues, played an important role in it. However, on the other hand, the reduction of input viral RNA of P247A/V248A due to its impaired replication capability may also contribute to the lower level of immunoprecipitated mutant viral RNA. Further studies on this could be performed with a CMV promoter regulated viral RNA transcription when detecting the interaction between nsP3 and viral genome RNA. The mechanisms of how nsP3 binds CHIKV genome RNA is not clear. The interaction between

nsP3 and viral RNA can be direct or indirect through an nsP3-containing replication complex. Proline residue and aromatic residues can interact favourably with each other, due to both the hydrophobic effect and the interaction between the π aromatic face and the polarized C-H bonds, called a CH/ π interaction, and this aromatic-proline interaction has been observed in protein-RNA interaction, which might help to explain the importance of P247 in nsP3-viral RNA interaction. On the other hand, G3BP, which is involved in the replication complex of CHIKV, is a RNA-binding protein which might recruit viral RNA into the nsP3-containing replication complex. Therefore the P247A/V248A nsP3-immunoprecipitated viral RNA was reduced because of the obstruction in replication complex formation. However, which part of genome RNA was bound to nsP3/AUD and the exact roles of this protein-genome interaction within CHIKV replication were not determined and need further exploration.

Analysis of the distribution of nsP3, capsid and dsRNA during CHIKV replication by confocal microscopy revealed further insights into the P247A/V248A phenotype. High level co-localisation between nsP3 and dsRNA were observed for at all time points up to 24 h.p.e., consistent with the role of nsP3 in genome replication. At 12/16 h.p.e. both nsP3 and dsRNA also co-localised with capsid and were accumulated at the plasma membrane. In contrast, for P247A/V248A, at first the co-localisation between nsP3 and dsRNA was shown in a significantly reduced level, moreover a loss of nsP3 accumulation on the plasma membrane was observed at later time points post electroporation. These observations suggested a role of nsP3 (and the AUD in particular) during the processes of genome replication and virus assembly to facilitate production of infectious virus particles at the plasma membrane. This is consistent with the early evidence for a juxtaposition of sites of genome replication, viral protein translation and nucleocapsid assembly in the case of Sindbis virus (Froshauer, 1988). The mechanisms of the reduction of the dsRNA-co-localized nsP3 for P247A/V248A compared to that of wildtype observed in the immunofluorescence figures might be that the P247A/V248A nsP3 was less efficient in recruitment of the template viral RNAs to form the replicase complexes, which was consistent with our RNA-binding data of nsP3 and virus genome RNA shown in Figure 4.5. The loss of the accumulation of P247A/V248A mutant nsP3 on plasma membrane might be because that the nsP3 has a role in the trafficking of nucleocapsids from these sites (CPVs) to the plasma membrane but the P247A/V248A mutations shut off this function as even at later stage of CHIKV infection when both nsP3 and capsid protein were expressed in high levels, accumulation of co-localized nsP3/capsid proteins could not be detected on plasma membrane for P247A/V248A mutant. In this study, nsP3 showed at least four forms of existence, dsRNA-co-localized nsP3, capsid protein-co-localized nsP3, dsRNA/capsid protein-co-localized nsP3

and individual nsP3 clusters. These four forms of nsP3 indicated the different functions of nsP3 in the development of CHIKV infection. Different from previous studies, which showed that for most CHIKV nsP3 existed in the formation of large aggregates (Gotte et al., 2018), although different forms of nsP3 were detected, most of it was shown to co-localize with dsRNA. The difference may be because of the different cells for research, and nsP3 shows different phenotypes in various cells.

Chapter 5: Biochemical analysis of AUD

After functional analysis of nsP3, especially AUD, during virus replication in the context of infectious virus, a variety of biochemical characters of AUD were analysed in this chapter, including RNA-binding activity (session 5.1), RNAi suppression activity (session 5.2), self-multimerization character (session 5.3), and nsP3 interactions with host proteins (session 5.4).

5.1 AUD RNA binding activity

5.1.1 Introduction

The central AUD of nsP3 is a homologous sequence across alphavirus, with undefined but important roles during virus replication. Some mutagenesis research revealed that the AUD was involved in the early event during virus replication, probably the formation of early replication complex for negative-strand RNA synthesis (LaStarza et al., 1994b, Wang et al., 1994). Based on the crystal structure of the nsP2/nsP3 fragment of Sindbis virus, a zinc coordination site was found within AUD, and mutations of any of the four cysteine residues absolutely blocked virus replication, indicating that the zinc coordination site, as well as each individual cysteine residue, was essential for virus replication. Besides this, the amino acids located around the zinc coordination site were proposed to have RNA-binding activity (Shin et al., 2012). Host or viral proteins RNA-binding activity to genome RNA is believed to be important for the replicase complexes formation during CHIKV genome replication. The 3' UTR of CHIKV consists of 498-723 nt of the 3' end of genome, including a 50-200 nt poly (A) tail. It is involved in the initiation of negative-strand RNA synthesis (Rupp et al., 2015). And the 19-20 nt 3' CSE located before poly (A) tail within alphavirus 3' UTR is highly conserved in sequence across the genus and has been proved to be critical for RNA synthesis (Kuhn et al., 1990). The 5' end of virus genome, or its complementary sequences in the 3' end of the negative-strand RNA, includes two conserved CSE: one in the 60 nt 5'UTR and the other one is a 51 nt CSE located in nsP1 coding region (Kuhn et al., 1990). The 5' UTR has a conserved stem-loop structure which has been proved to be important for RNA synthesis (Nickens and Hardy, 2008), and its complement is also predicted to be structured and functions in genome RNA synthesis (Niesters and Strauss, 1990, Frolov et al., 2001). This structure stability and the access of polymerase to the promoter within this structure is believed to be significant for the initiation and regulation of genome RNA synthesis (Shirako and Strauss, 1998). The 5' UTR was also shown to be essential for negative-strand RNA synthesis initiating at the 3' end of the genome, probably because of a circularization structure formed by templated RNAs (Frolov et al., 2001). A third UTR, named subgenomic RNA (sgRNA) promoter, is located in the junction region

between the non-structural and structural proteins ORFs (Rupp et al., 2015). The full and optimal promoter was mapped to -98 to +14 from the transcription start site (Wielgosz et al., 2001), while the essential part was from -19 to +5 (Levis et al., 1990). Our data in the previous chapters showed that a panel of AUD mutants (M219A, R243A/K245A, P247A/V248A, V260A/P261A, C262A/C264A) were defective in CHIKV genome replication with uncertain reasons, and the AUD played an important role in subgenomic RNA synthesis, where nsP3 RNA binding activity to viral genomic RNA was probably involved. Therefore, it was of interest to detect the RNA-binding activity of AUD, which might give a hint of the mechanisms why impaired or abrogated replication capability was caused by these AUD mutants.

Fluorescent polarisation anisotropy assay was used to test the interaction between AUD and short RNAs. Fluorescence polarization is a powerful tool for studying molecular interactions by monitoring changes in the apparent size of fluorescently-labeled or inherently fluorescent molecules, often referred to as the tracer or ligand (Checovich et al., 1995, Heyduk et al., 1996, Jameson and Sawyer, 1995, Nasir and Jolley, 1999). The theory of Fluorescent Polarization, firstly described by Perrin in 1926, is based on the observation that when a small fluorescent molecule is excited with plane-polarized light, the emitted light is largely depolarized because molecules tumble rapidly in solution during its fluorescence lifetime (the time between excitation and emission). However, if the tracer is bound by a larger molecule its effective molecular volume is increased. The tracer's rotation is slowed so that the emitted light is in the same plane as the excitation energy. The bound and free states of the tracer each have an intrinsic polarization value: a high value for the bound state and a low value for the free state. The measured polarization is a weighted average of the two values, thus providing a direct measure of the fraction of tracer bound to receptor. An increase in molecular volume due to receptor-ligand (Bolger et al., 1998), DNA-protein (Lundblad et al., 1996, Ozers et al., 1997), or peptide-protein binding (Wu et al., 1997) or a decrease in molecular volume due to dissociation or enzymatic degradation (Bolger and Checovich, 1994, Bolger and Thompson, 1994) can be followed by Fluorescent Polarization.

To verify the RNA-binding activity of AUD to CHIKV genome RNA, an *in vitro* RNA filter binding assay was performed. Filter binding assay is one of the oldest and simplest methods to detect RNA-protein interactions, measuring affinities between them. The mixture of protein and RNA are applied to pass through a nitrocellulose filter, which is negative charged and therefore immobilizing the positive charged protein while releasing the free negative charged RNA. But if the protein is able to bind the RNA, then the RNA will be retained on the filter as well. The

RNAs used in this assay is labelled with [³²P] and the amount of RNA stuck to the nitrocellulose membrane is quantified by measuring the amount of radioactivity on the filter using a scintillation counter.

5.1.2 Results

5.1.2.1 Purification of AUD

5.1.2.1.1 Cloning of AUD into pET-28a-SUMO expression vector

The whole AUD of nsP3 was amplified from CHIKV-D-Luc-SGR and cloned into pET28aSUMO vector. The recombinant construct is referred to as pET-28aSUMO-AUD and results in the expression of His-SUMO tagged AUD fusion protein (His-SUMO-AUD).

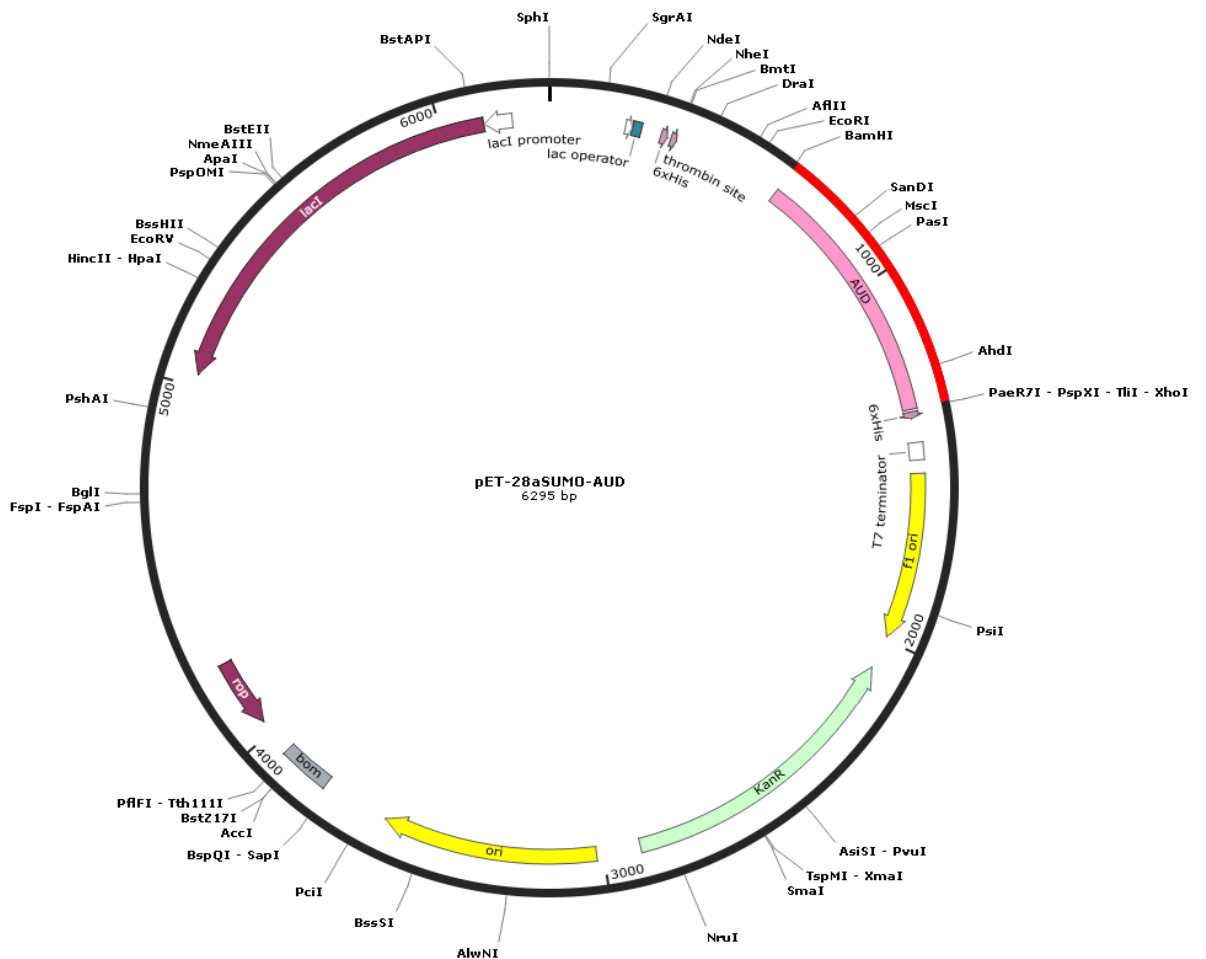


Figure 5.1 Diagram of pET-28aSUMO-AUD.

AUD is cloned into pET-28aSUMO vector with BamHI and XhoI restriction sites.

5.1.2.1.2 Optimization of expression of AUD

His-SUMO-AUD was expressed in Rosetta2 cells induced by different concentrations of IPTG (0.1 mM, 0.5 mM and 1 mM) at different temperatures (18 °C, 27 °C and 37 °C) for 5 hours to overnight. Cells were then harvested by centrifugation and resuspended with lysis buffer. Then the resuspended cells were sonicated before being clarified by centrifugation at 15,000 rpm for 1 hour at 4 °C. Supernatant and cell lysates pellet were both collected for analysis in SDS-PAGE gel. As shown in Figure 5.2, the best condition chosen for expression of His-SUMO-AUD was 0.5 mM IPTG induction at 18 °C for 5 hours. The predicted molecular mass of His-SUMO-AUD is 40 kDa.

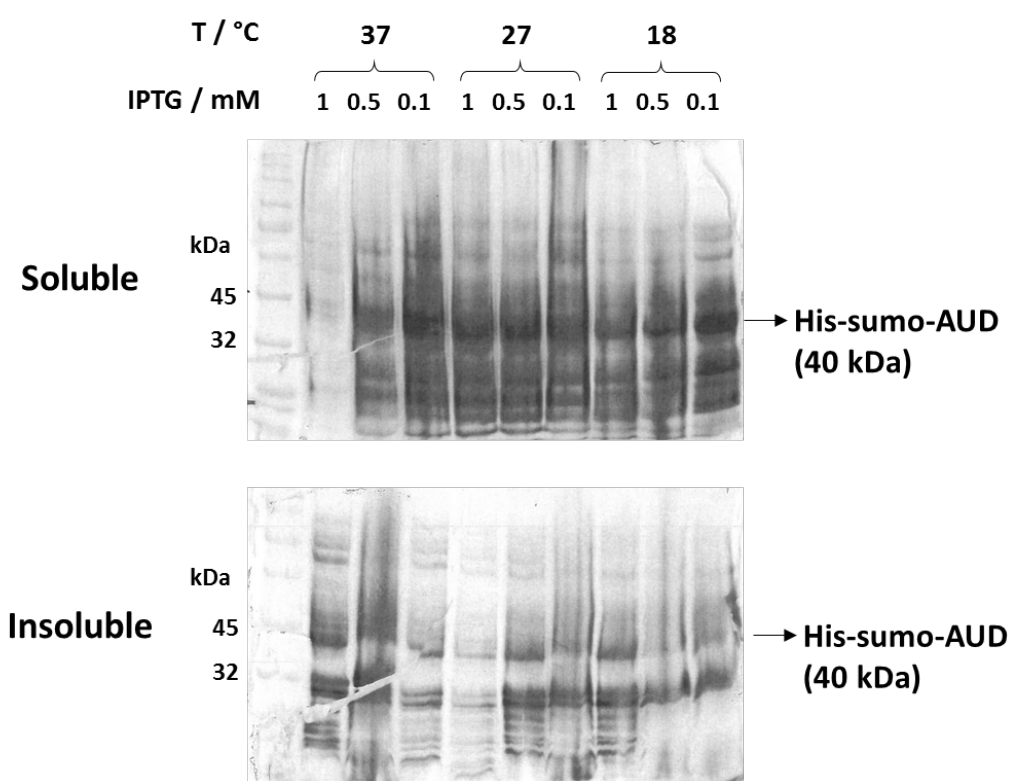


Figure 5.2 Optimization of AUD expression in pET-28aSUMO-AUD.

Different concentrations of IPTG (1 mM, 0.5 mM and 0.1 mM) were used for induction of the expression of His-SUMO-AUD (40 kDa) at 18 °C, 27 °C or 37 °C for 6 hours. Bacterial cell lysates were harvested by centrifugation and lysed in lysis buffer for sonication. Both supernatant (soluble proteins) and inclusion body pellet (insoluble proteins) after centrifugation were analysed by SDS-PAGE and Coomassie Brilliant Blue staining.

5.1.2.1.3 Purification of AUD

HisTrap™ HP was used for His-SUMO-AUD purification with the supernatant obtained after sonication of the resuspended bacterial cells. HisTrap™ HP is a prepacked, ready-to-use

column for the preparative purification of His-tagged recombinant proteins by immobilized metal affinity chromatography (IMAC). Pre-equilibration of the column was performed with wash buffer before clarified and filtered cell lysates supernatants containing His-SUMO-AUD protein were loaded into it. Then the His-SUMO-AUD bound to the Ni⁺ resin and was collected in the columns while at the same time the unbound proteins just went through the column. Then the column was washed for 3 times with 5 x column volumes of wash buffer. Finally, the Ni⁺ bound His-SUMO-AUD in the column was eluted using 5 x column volume elution buffer (Figure 5.3). The eluted fractions of His-SUMO-AUD were then dialysed at 4 °C overnight, and at the same time, His tagged SUMO protease was added into the eluted fractions to cleave the His-SUMO tag from the AUD. For the next step, the dialysed mixture of His-SUMO tag, His tagged SUMO protease and AUD was loaded into the HisTrap™ HP column for a second round when His-SUMO tag and His tagged SUMO protease were bound to the Ni⁺ on the column while AUD passed through the column and was collected for further analysis. The column was then washed with wash buffer with 5 x column volume wash buffer and the flowthrough of it was also collected as purified AUD protein. Then the bound His-SUMO tag and His tagged SUMO protease in the column were eluted with elution buffer and collected for analysis in SDS-PAGE gel. As shown in Figure 5.3, an approximately 26 kDa protein (the same molecular weight as predicted for AUD) was observed in the Coomassie blue stained SDS-PAGE gel after the whole purification process.

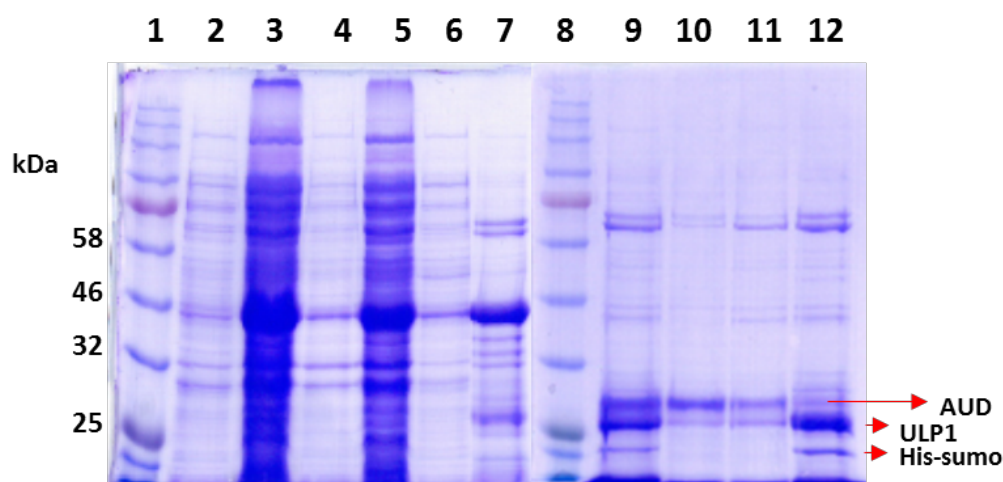


Figure 5.3 Purification of AUD.

1. Ladder. 2. Uninduced sample. 3. Soluble sample post IPTG induction. 4. Insoluble sample post IPTG induction. 5. Flowthrough fraction post his-sumo-AUD purification. 6. Wash fraction post his-sumo-AUD purification. 7. Eluted his-sumo-AUD. 8. Ladder. 9. Samples post dialysis and sumo protease cleavage. 10. Purified AUD (flowthrough fraction). 11. Purified AUD (wash fraction). 12. Eluted his-sumo tag and sumo protease (ULP1).

5.1.2.1.4 Characterization of AUD by mass spectrometry

To confirm the identity of the purified protein obtained in the last step, the purified 26 kDa protein was sent to the Mass spectrometry office in University of Leeds for protein ID analysis. The purified protein was loaded and run in SDS-PAGE gel and after Coomassie blue staining, the predicted band was cut out for further analysis. As shown in Figure 5.4., although the protein ID analysis failed to cover 100% of the protein peptides, it was enough to show that the purified protein corresponded to the amino acid sequence of AUD. Therefore, the purified AUD was confirmed as AUD and used for further studies.

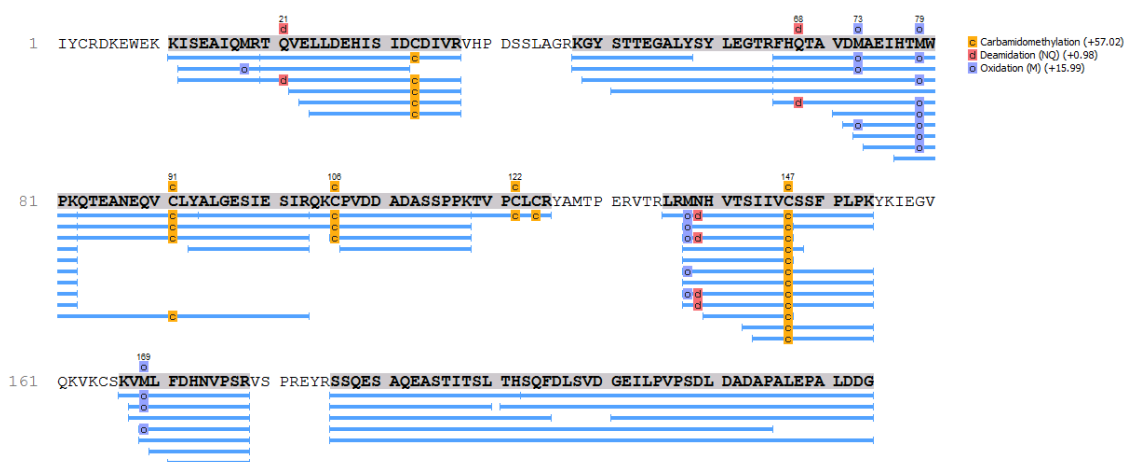


Figure 5.4 Identification of AUD protein.

Protein peptides digested by trypsin were analysed by mass spectrometry and then compared with the known expressed protein sequence and protein database. The sequence at the top is the AUD amino acid sequence. A series of peptides below in blue are the digested AUD fragments for mass spectrometry.

5.1.2.2 Purification of E.coli expressed AUD mutants

The whole fragments of each AUD mutant (M219A, E225A, R243A/K245A, P247A/V248A, V260A/V261A, C262A/C264A) flanked with *Bam*HI and *Xho*I was amplified from the corresponding CHIKV-D-Luc-SGR and cloned into pET28a-SUMO vector to generate pET28a-SUMO-AUD mutants expression plasmids, as described in session 5.2.1.1. Following the same expression and purification process as wildtype AUD protein, each AUD mutant protein were analysed in SDS-PAGE gel by Coomassie blue staining and shown in Figure 5.5.

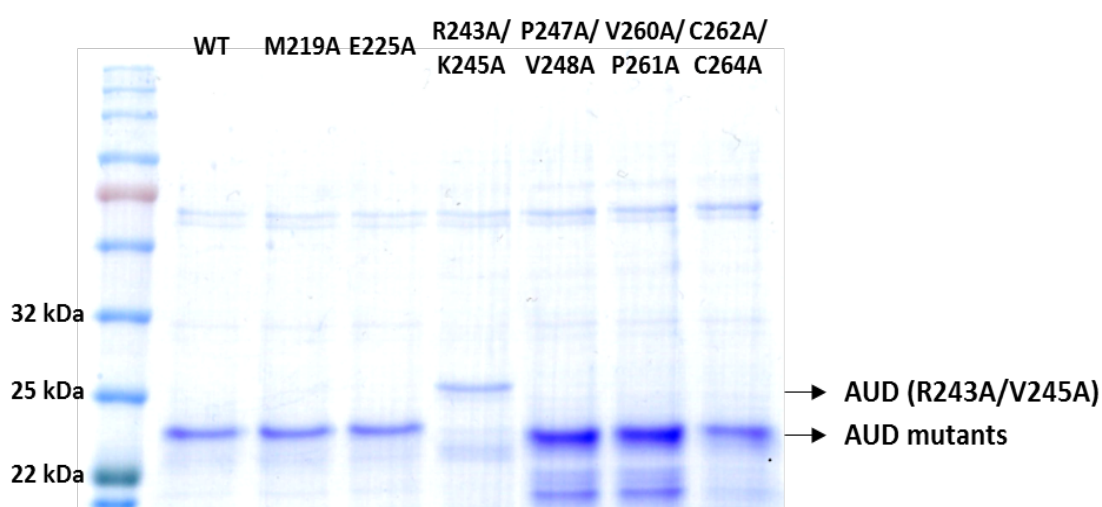


Figure 5.5 Expression of wildtype AUD and its mutants.

Purification of AUD with corresponding mutations analysed by SDS-PAGE and Coomassie blue staining. Most of the mutants were of the predicted correct size in SDS-PAGE gel while R243A/K245A mutant appeared larger than wildtype and other mutants.

5.1.2.3 Mass spectrometry analysis of AUD-R243A/K245A mutant.

As the R243A/K245A mutant AUD protein appeared larger than wildtype and other mutant AUDs in SDS-PAGE (Figure 5.5), to confirm that it was the correct protein, mass spectrometry analysis was performed to detect both its protein identity and its molecular mass. The purified untagged AUD was used for protein ID analysis, and the result showed that although not every amino acids of AUD was identified through the assay, it was clearly the AUD protein containing the R243A/K245A mutations (Figure 5.6A). As untagged AUD protein was easily degraded during protein molecular mass analysis (data not shown), the His-SUMO-AUD-R243A/K245A was used for this analysis. The result showed that a peak for a 39.45-kDa protein (corresponding to the predicted molecular mass of His-SUMO-AUD-R243A/K245A (39.63 kDa)) was detected, further confirming that the purified protein was exactly the expected AUD-R243A/K245A.

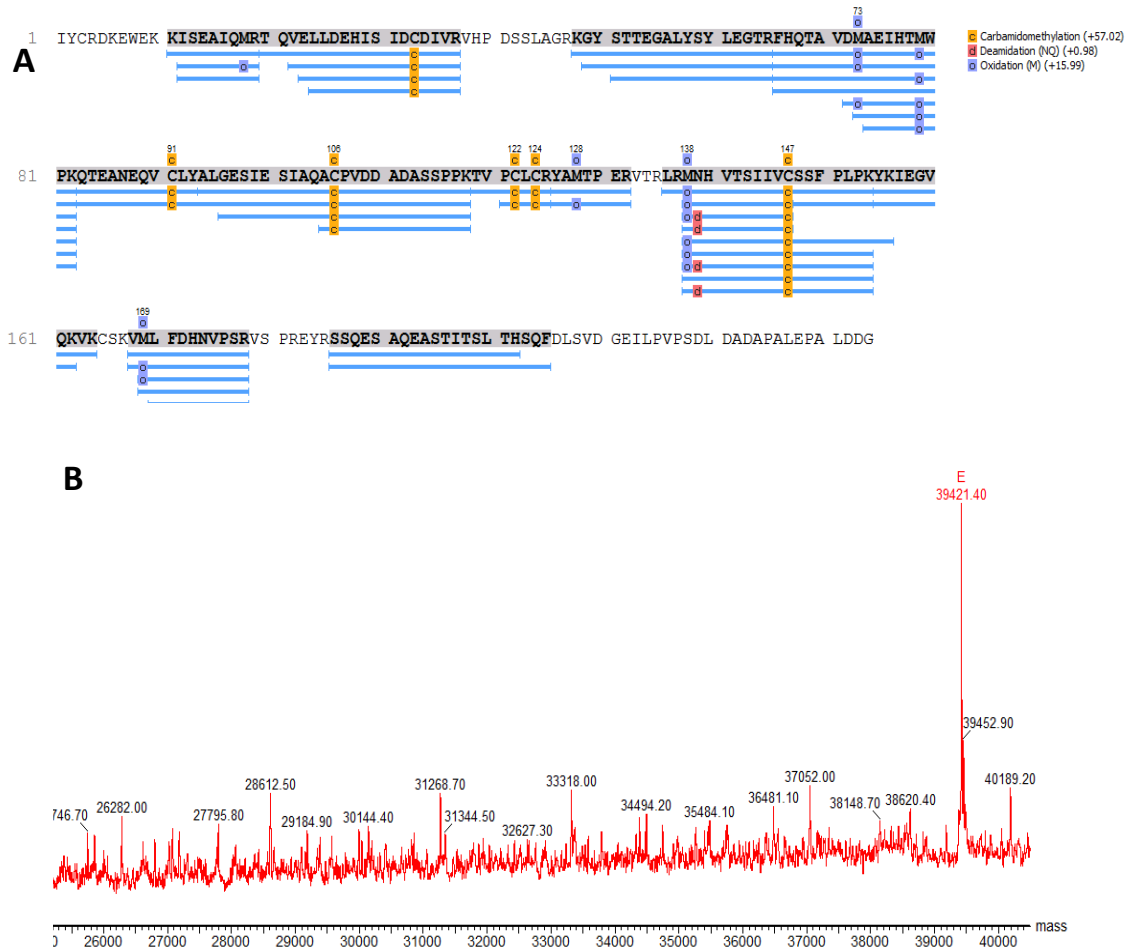


Figure 5.6 Mass spectrometry analysis of AUD-R243A/K245A and His-SUMO-AUD-R243A/K245A.

A. Protein peptides digested by trypsin were analysed by mass spectrometry and then compared with the known expressed protein sequence and protein database. The sequence at the top is the AUD amino acid sequence. A series of peptides below in blue are the digested AUD fragments for mass spectrometry. B. Protein mass analysis of His-SUMO-AUD-R243A/K245A.

5.1.2.4 Circular Dichroism assay of AUD

Far-UV CD spectroscopy was performed to detect the secondary structure of AUD and its mutants (M219A, E225A, R243A/K245A, P247A/V248A, V260A/P261A, C262A/C264A). The results showed that wildtype AUD and the mutants all comprised predominantly α -helix with no significant differences in the overall structure as a result of the mutations (Figure 5.7).

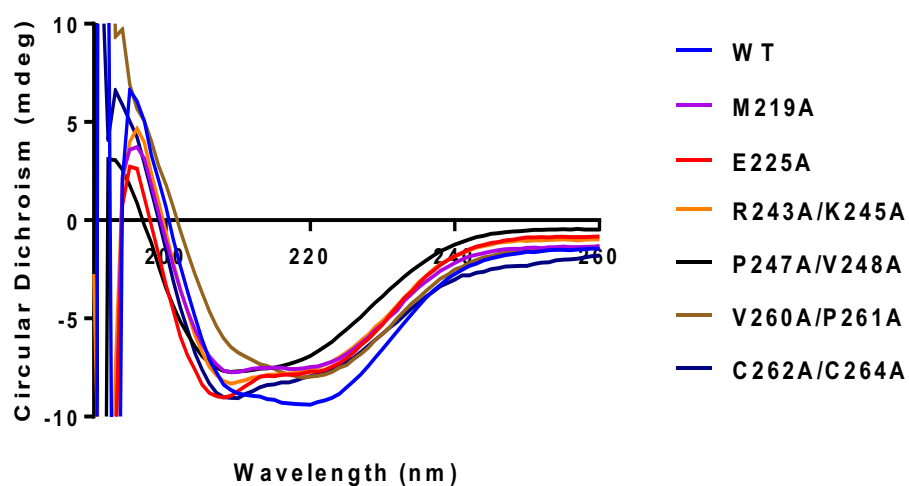


Figure 5.7 Circular Dichroism results of AUDs.

Far-UV CD spectroscopy was performed on an APP Chirascan CD spectropolarimeter to obtain the secondary structure of AUDs. Spectra (190-260) were recorded using 200 μ l protein solution (at a concentration of 0.2 mg/ml) in a 1 mm path-length cuvette. Protein CD spectra deconvolution was analysed by DichroWeb.

5.1.2.5 Fluorescent polarisation anisotropy assay with AUD and short RNAs

Like other macromolecules, RNA is dynamic. The process of folding into a structured RNA involves dynamic rearrangement of RNA helices. As the movements of individual helices are often on the nanosecond timescale, FPA is a natural choice for studying RNA dynamics; FPA measures the rate of depolarization of a fluorophore during its lifetime, which is often in the low nanosecond regime. To perform the FPA, the RNA used should be specifically probed with 6-methylisoxanthopterin (6-MI), 1,3-diaza-2-oxophenothiazine (tC) or 1,3-diaza-2-oxophenoxazine (tCo) as a tracer of the RNA. In this project, purified AUD was used to test the interaction between AUD and some specific short RNAs (A13mer, A8, U13, C13, C8 and G8 and random RNAs) probed with 6-MI by PFA. As shown in Figure 5.8, no interactions between AUD and any of the tested RNAs could be detected, indicating that AUD had no RNA-binding activity to these short RNAs.

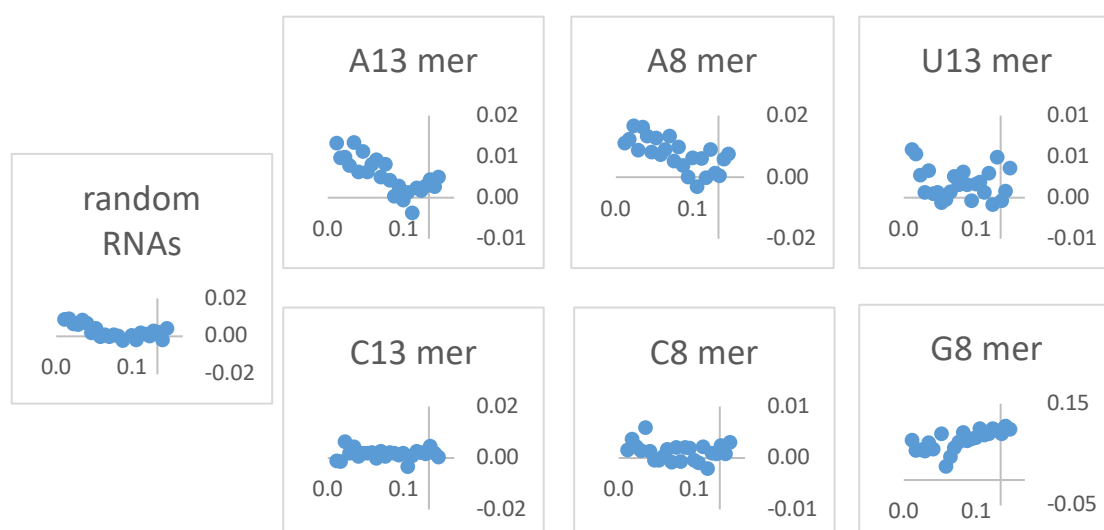


Figure 5.8 AUD binding activity to short RNAs.

Fluorescent polarisation anisotropy was performed to detect the RNA binding activity of AUD to short RNAs. 15 μ l RNA binding buffer (50 mM Tris pH=7, 300 mM NaCl) was added into each well of the 384-well black optiplate (Perkin Elmer). 30 μ l protein solution was added into the first well of the row followed by dilution of the proteins along the row, taking 40 μ l from the previous well to the next one. 20 μ l of 20 mM RNA was then added into each well, mixed and incubated for 30 min at RT. Polarisation was measured using an EnVision multilabel Plate Reader (Perkin Elmer) that contains an excitation filter at 480 nm and S and P channel emission filters at 530 nm.

5.1.2.6 RNA-filter binding assay with AUD and viral RNA fragments

As previous result has shown that nsP3 was capable of binding virus genome RNA during virus replication, and the P247A/V248A mutations within AUD, which impaired virus replication significantly reduced this RNA binding activity (Figure 4.5), it was speculated that AUD was able to bind genome RNA and this binding activity was important for CHIKV replication. As the genome 3' UTR is involved in the initiation of negative-strand RNA, it was interesting to detect the RNA-binding activity of wildtype AUD and its mutants to it. To do this, a cDNA corresponding to the 3' UTR of genome RNA was amplified and cloned into pcDNA3.1 vector. Then the pcDNA3.1-3' UTR plasmid was linearized and used as template for in vitro transcription of ³²P labelled 3' UTR, which was used in the RNA-filter binding assay to detect the RNA binding activity of wildtype AUD and its mutants. The mixture of serially diluted proteins were mixed with ³²P labelled 3' UTR transcripts for 30 min before passing through first a nitrocellulose membrane then a Hybond-nylon membrane such that the nitrocellulose membrane bound protein-RNA complex and Hybond-Nylon membrane bound free RNA. Then the membranes were exposed to a film for quantification of radioactivity and fitting was performed using GraphPad Prism 5 software (GraphPad Software). As shown in Figure 5.9, wildtype and all AUD mutants, with the exception of R243A/K245A, were able to bind the CHIKV 3'UTR RNA. The radioactive signal weakened with the decrease of AUD protein added into each well. Somewhat surprisingly the two mutants of residues that either bind to zinc (C262A/C264A), or are adjacent to the zinc-binding site (V260A/P261A), both of which were unable to replicate in any cells were of competent RNA-binding activity. It is concluded that AUD residues R243 and K245 are involved in the binding of the domain to the CHIKV 3'UTR RNA, and that this activity is essential for CHIKV replication. Interestingly, the P247A/V248A mutant also showed a significantly lower RNA binding activity, which was consistent with its impaired replication capability in the replicon assay.

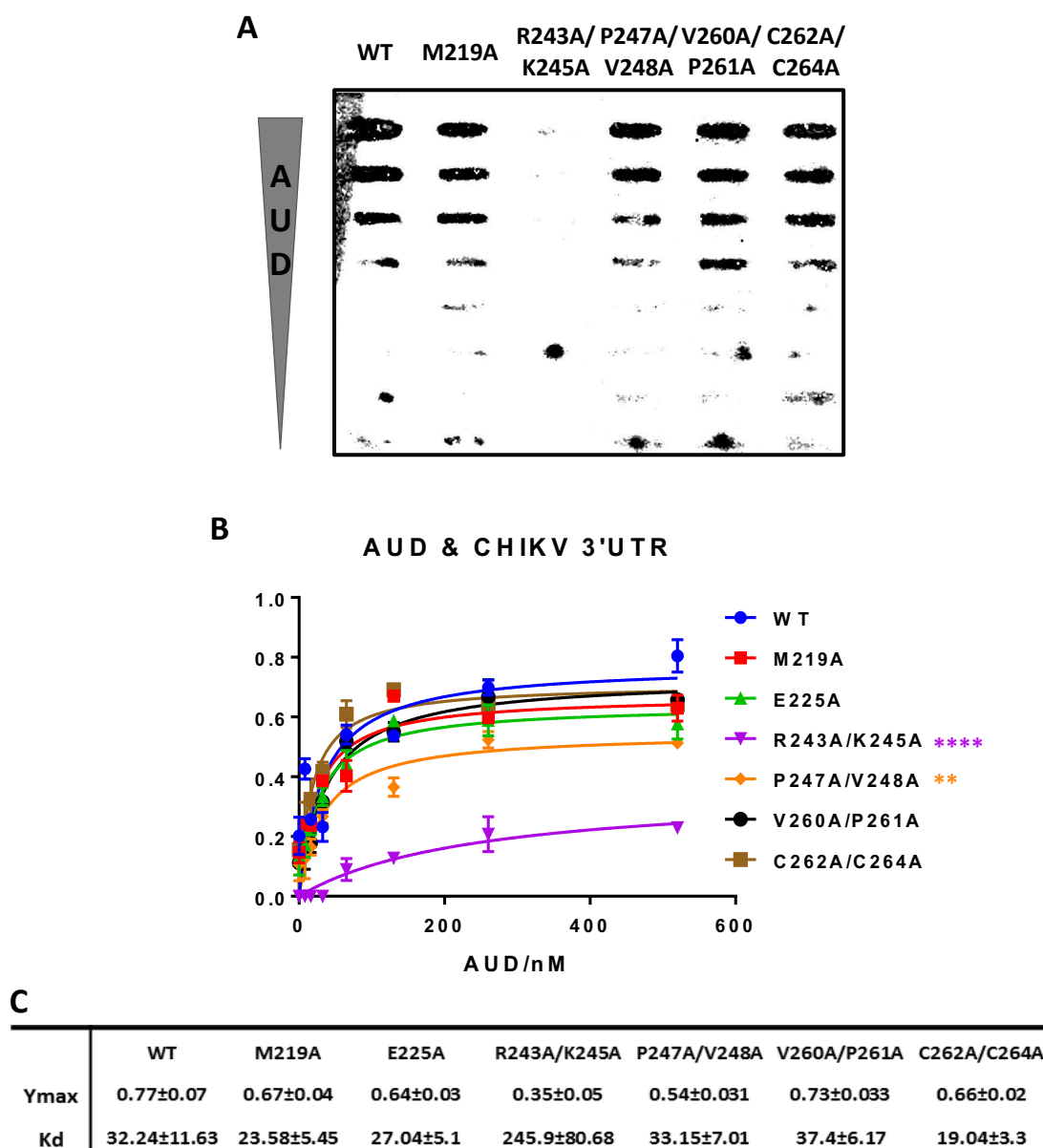


Figure 5.9 AUD RNA-binding activity to CHIKV 3'UTR RNA.

Nitrocellulose membrane obtained post filter binding analysis of the interaction between AUDs and the CHIKV 3'UTR RNA. The indicated proteins were incubated with radiolabelled RNA (1 nM) before application to a slot blot apparatus, filtering through nitrocellulose (protein-RNA complex) and Hybond-N (free RNA) membranes, and visualization by phosphoimaging. From top to bottom, the proteins were applied to the slots at concentrations of 2500, 1250, 625, 312.5, 156.25, 78.125, 39.0625 and 0 nM. B. The percentage of RNA bound to the nitrocellulose membrane and the binding affinity were quantified and plotted as a function of the AUD concentration. The data was fitted to a hyperbolic equation. C. Endpoint (% of total RNA bound) and Kd values derived from the graphs in B.

At the same time, Hepatitis C virus (HCV) 3' UTR and foot and mouth disease virus (FMDV) aptamer RNA were used as controls. For HCV 3' UTR, it was surprised to find that the AUD had similar RNA-binding activity to it as to CHIKV 3' UTR (Figure 5.10), indicating that the RNA-binding activity of AUD to CHIKV 3' UTR was not specific.

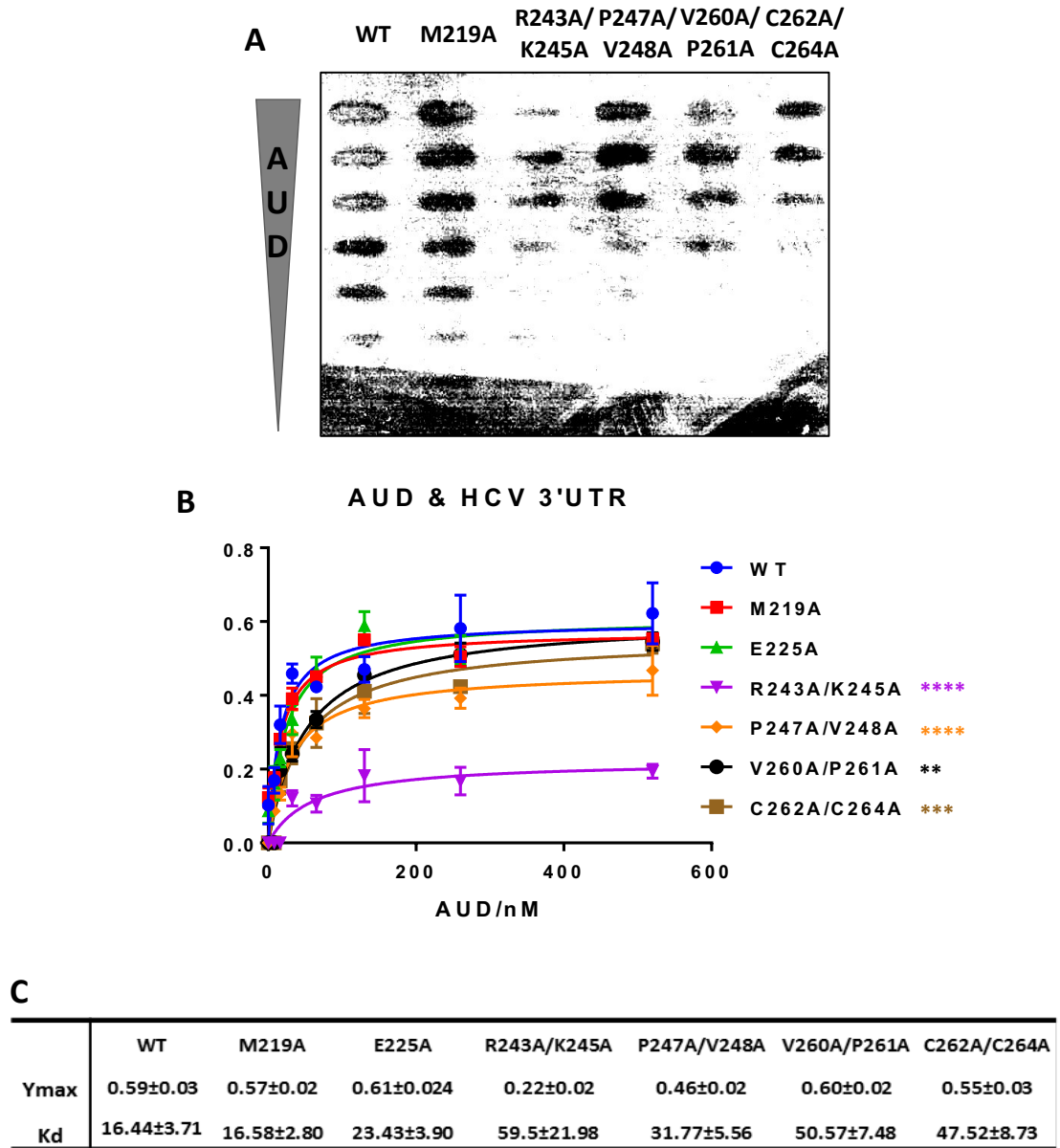


Figure 5.10 AUD RNA-binding activity to HCV 3'UTR RNA.

A. Nitrocellulose membrane obtained post filter binding analysis of the interaction between AUDs and the CHIKV 3'UTR RNA. The indicated proteins were incubated with radiolabelled RNA (1 nM) before application to a slot blot apparatus, filtering through nitrocellulose (protein-RNA complex) and Hybond-N (free RNA) membranes, and visualization by phosphoimaging. From top to bottom, the proteins were applied to the slots at concentrations of 2500, 1250, 625, 312.5, 156.25, 78.125, 39.0625 and 0 nM. B. The percentage of RNA bound to the nitrocellulose membrane and the binding affinity were quantified and plotted as a function of the AUD concentration. The data was fitted to a hyperbolic equation. C. Endpoint (% of total RNA bound) and Kd values derived from the graphs in B.

Then the RNA-filter binding assay was repeated with the AUD and FMDV aptamer RNA, the results clearly showed that no signal of AUD-FMDV aptamer RNA complex could be detected on the nitrocellulose membrane while on the Hybond nylon membrane, strong radioactive signal of free RNA were detected. This result demonstrated that there was no interaction between AUD and FMDV aptamer RNA (Figure 5.11).

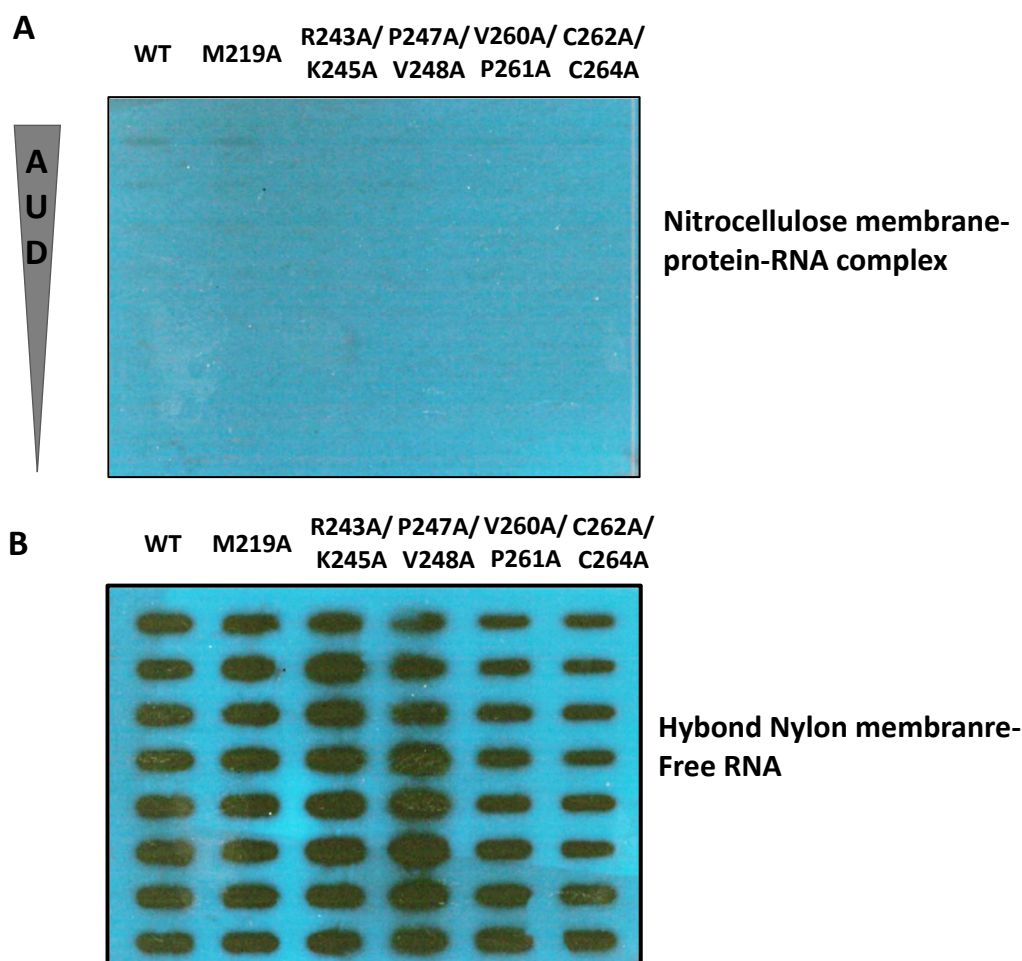


Figure 5.11. RNA-filter binding assay with AUD and FMDV aptamer RNA.

A. Nitrocellulose membrane bound with AUD-FMDV aptamer RNA complex post RNA-filter binding assay. B. Hybond nylon membrane bound with free FMDV aptamer RNA.

As CHIKV 3' UTR and HCV 3' UTR are both long specific structured RNAs while FMDV aptamer RNA is much shorter, based on all the RNA-filter binding results obtained in this session, it was suspected that the AUD was capable of binding the RNAs of longer length or with some specific but unknown structures.

P247A/V248A mutant CHIKV has been shown to be defective in the synthesis of subgenomic RNA during virus replication previously in this study. As the negative strand subgenomic RNA promoter (sg-5' prom(-)) is involved in the initiation of subgenomic RNA synthesis, we then detected the interaction between wildtype AUD and its P247A/V248A mutant and ³²P labelled sg-5' prom(-) RNA (Figure 5.13A). At the same time, the 3' end of the genomic negative strand RNA (5' RNA(-)) (Figure 5.12A) was also produced to detect its interaction with AUD, as 5' RNA(-) is involved in the initiation of positive strand RNA synthesis. As shown in Figure 5.12, both wildtype and P247A/V248A AUD were able to bind 5' RNA(-) (Fig 5.12B), however P247A/V248A exhibited a significant reduction in both K_d values and maximal binding levels (endpoints) compared to wildtype. As 3' UTR and 5' RNA(-) are involved in the initiation of negative and positive strand genome RNA synthesis, respectively; impaired binding of the P247A/V248A mutant AUD may explain the observed defect in CHIKV genome replication (Fig 4.1 and 4.2). For binding to the sg-5' prom(-) RNA (Fig 5.12C), P247A/V248A AUD showed a different phenotype with a higher endpoint but a higher K_d than wildtype. K_d and endpoint values are listed in Fig 5.12D. This result suggested that the P247A/V248A defect in subgenomic RNA synthesis may be in part explained by a reduction in the ability to specifically bind the subgenomic RNA promoter.

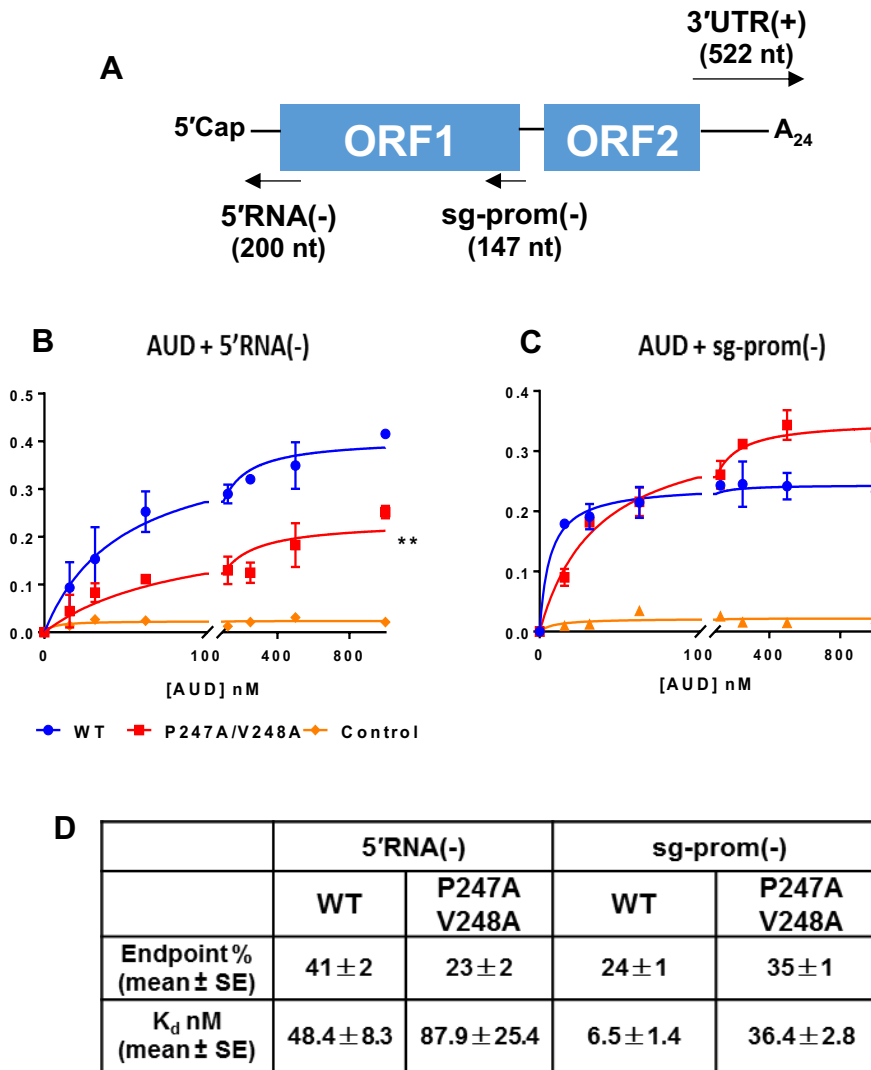


Figure 5.12 AUD RNA binding activity to CHIKV 5' RNA(-) and sg-5' prom(-).

A. Schematic of the CHIKV genome showing the location of the various RNAs used in subsequent filter binding analysis. B and C. Filter binding analysis of the interaction between AUD and the indicated RNA species. Purified AUD at the indicated concentrations was incubated with radiolabelled RNA (1 nM) before application to a slot blot apparatus, filtering through nitrocellulose (protein-RNA complex) and Hybond-N (free RNA) membranes, and visualization by phosphoimaging. The percentage of RNA bound to the nitrocellulose membrane was quantified and plotted as a function of the AUD concentration. The data was fitted to a hyperbolic equation. D. Endpoint (% of total RNA bound) and K_d values derived from the graphs in (B and C).

5.1.3 Discussion

The central AUD domain has been shown to be essential for CHIKV replication but its precise roles within this process were unknown. Some mutagenesis research revealed that the AUD was involved in the early event during virus replication, probably the formation of early replication complex for negative-strand RNA synthesis (LaStarza et al., 1994b, Wang et al., 1994). A zinc coordination site, which is always involved in RNA-binding proteins, was revealed in the AUD within a crystal structure of Sindbis virus nsP23 (Shin et al., 2012). Previously in this project, mutant P247A/V248A CHIKV was proved to be partially defective in virus replication because of its defect in subgenomic RNA/structural proteins production, and the immuno co-precipitation assay demonstrated that nsP3-P247A/V248A had a reduced RNA-binding activity to CHIKV genome RNA compared to wildtype nsP3. Therefore, the RNA-binding activity of AUD to short RNAs and different elements of genome RNA was detected in this chapter (Table 2). Fluorescent polarisation anisotropy assay showed no interaction between AUD and short RNAs, but the RNA-filter binding assay proved a binding activity of AUD to different fragments of CHIKV genomic RNA as well as HCV 3' UTR RNA, suggesting that the interaction between AUD to RNA was not unique but still based on some specific RNA structures.

RNA	length	character
CHIKV 3'UTR	522 nt	Structured
CHIKV 5'RNA(-)	200 nt	Structured
CHIKV sg-Prom(-)	147 nt	Structured
HCV 3'UTR	236 nt	Structured
FMDV aptamer RNA	76 nt	Structured
Short RNAs (Fluorescent polarisation anisotropy assay)	8-13 nt	Unstructured

Table 2 RNAs used in the detection of protein-RNA interaction

The first major conclusion from this section is that AUD has binding activity to all the three important untranslated elements of the virus genome: 3' UTR, 5' UTR(-) and sg-Prom(-). In the RNA filter binding assay with AUDs and CHIKV 3' UTR RNA, wildtype AUD and most of its mutants, except for R243A/K245A, showed binding activity to CHIKV 3' UTR. Previous result in this project showed that CHIKV R243A/K245A mutant was defective in virus genome replication, while genome 3' UTR is involved in the initiation of negative-strand RNA synthesis

(Rupp et al., 2015), together with the RNA binding result, it was predicted that the RNA binding activity of AUD to genome 3' UTR was necessary for CHIKV replication, probably because of its involvement in negative-strand RNA synthesis. P247A/V248A AUD showed a significantly reduced binding activity to CHIKV 3' UTR RNA, consistent with its impaired replication capability, also indicating the importance of the interaction between AUD and CHIKV 3' UTR for CHIKV replication. Surprisingly, the mutations made in or around the zinc coordination site (V260A/P261A and C262A/C264A) did not interfere the binding activity of AUD to 3' UTR, while these two CHIKV mutants failed to replicate in any cells tested in this project, it was believed that the zinc coordination site must have some other vital functions but not involved in the interaction with 3' UTR.

The RNA filter binding assay with AUD and HCV 3' UTR showed a similar result to that between AUD and CHIKV 3' UTR, indicating that the RNA binding activity of AUD was not specific. However, when detecting the interaction between AUD and FMDV aptamer RNA, no binding activity of AUD was observed to FMDV aptamer RNA. And the FPA assay also showed no interaction between AUD and the short RNAs. As CHIKV 3' UTR and HCV 3' UTR were both long and highly structured (Chen et al., 2013, Anjum et al., 2013) while FMDV aptamer RNA and the small RNAs were much shorter, it was believed that the RNA binding activity of AUD was specific to some structured RNA, but the precise interaction elements still needs further study.

As the P247A/V248A CHIKV mutant has been shown to have defect in subgenomic RNA synthesis, and the RNA binding activity of AUD was not specific to 3' UTR sequence, it was interesting to detect the RNA binding activity of AUD to sg-Prom (-) and to test if the P247A/V248A mutations affected this binding activity. Here, different from the interaction between AUD and CHIKV 3' UTR, P247A/V248A AUD showed reduction in the affinity to subgenomic RNA promoter, might be in part explained the P247A/V248A defect in subgenomic RNA synthesis. Although sg-Prom functions in a dsRNA molecule during virus replication in cells, it is believed that the single-stranded sg-Prom (-) RNA used in this experiment is adequate to detect the interaction between AUD and sg-Prom. At the same time, the binding activity of wildtype AUD and the P247A/V248A mutant to CHIKV 5' UTR (-) was detected with 200 nt CHIKV 5' RNA(-) (part of CHIKV 5' UTR(-)) and the result was similar to that to CHIKV 3' UTR, indicating that P247A/V248A CHIKV might also be partially defective in positive strand RNA synthesis, where 5' UTR (-) was involved (Shirako and Strauss, 1998, Nickens and Hardy, 2008) (Niesters and Strauss, 1990, Frolov et al., 2001).

One further implication of the independent RNA binding activity of AUD to these three important genome RNA elements is the potential function of AUD to mediate genome circularization. The CHIKV 5' UTR was shown to be essential for negative strand RNA synthesis initiating at the 3' end of genome, indicating a circularization structure formed by template RNA for RNA replication (Frolov et al., 2001). The defect of CHIKV P247A/V248A mutant in virus replication and the different phenotypes of AUD P247A/V248A mutant to the 3' UTR, 5' RNA(-) and subgenomic RNA promoter compared to wildtype AUD, raise a possibility that the binding of AUD to these three CHIKV genome RNA elements may alter genome RNA structure and change the interaction pathway between virus genome RNA and RNA polymerase nsP4, further drive the necessary switch from the utilization of genome RNA for negative, positive or subgenomic RNA synthesis.

On the other hand, when tracking the distribution of nsP3, capsid protein and dsRNA of wildtype CHIKV and P247A/V248A mutant previously in this project, it was observed that for wildtype CHIKV, in the later stage of infection, nsP3 and capsid co-localized cluster accumulated on plasma membrane, indicating a role of nsP3 to traffic genome RNA or nucleocapsid to virus assembly site. However, in P247A/V248A mutant CHIKV infected cells, even when nsP3 and capsid protein were expressed to a high level, co-localized nsP3/capsid protein were not observed on plasma membrane. Taken the reduced RNA binding activity of P247A/V248A AUD together with previous results, it was suggested that the RNA binding activity of AUD to CHIKV genome RNA might play a role in the regulation of virus assembly through transport of genome RNA to sites of assembly. Similarly to what observed here for CHIKV, the HCV NS5A protein was also proved to bind both 5' UTR and 3' UTR of HCV genome RNA, and this RNA binding activity of NS5A was also believed to function in both genome RNA replication and virus assembly (Foster et al., 2010, Huang et al., 2005).

In conclusion, the binding activity of AUD to viral genome RNA implicates that nsP3 is involved in multiple processes during CHIKV life cycle, including both positive strand genome RNA, negative strand mediates viral RNA and subgenomic RNA synthesis, and virus assembly. In this regard, the interaction between nsP3 and CHIKV genomic RNA could be a valid target for antiviral intervention although more detailed molecular mechanism within this process needs further study.

5.2 RNAi suppression activity

5.2.1 Introduction

RNAi is generally an antiviral mechanism for various organisms such as fungi, plants, nematodes and arthropods (Ding, 2010, Voinnet et al., 1999, Billmyre et al., 2013, Blair, 2011). After infection of the pathogens, the virus produced double stranded RNA (dsRNA) lead to the formation of RNA interference silencing complex (RISC) for recruitment of dsRNA and siRNA and finally accomplish the cleavage of virus RNAs (Flynt et al., 2009, Ghildiyal and Zamore, 2009, van Rij et al., 2006). The RISC consists of several components, of which ribonuclease III Dicer and Argonaute protein (AGO) are the most important. Dicer functions to produce small RNA from dsRNA, and the produced small RNA are then transferred to AGO for final cleavage. However, it has been shown that Dicer was not necessary for some specific RNAi pathways where short RNA transcripts were produced by the RNA-dependent RNA polymerase (RdRP) and directly sent to AGO for cleavage (Ketting, 2011). A Piwi RNAi pathway has also been found to function specifically in mosquito cells (Guzzardo et al., 2013). In response to the RNAi response of the hosts, many viruses have developed their own mechanisms to counteract the host RNAi pathways with viral proteins or sequence elements (Ding and Voinnet, 2007), for example some viral suppressors of RNAi bind long dsRNA to protect them from Dicer (van Rij et al., 2006, Merai et al., 2006) or short RNAs (Aliyari et al., 2008), while others act through a combination of different mechanisms (Qi et al., 2011, Singh et al., 2009). A recent study showed that some viruses could encode host specific RNAi suppressors because of the co-evolution of virus and its host, indicating that viruses develop different surviving mechanisms in different hosts (van Mierlo et al., 2014). As arbovirus, CHIKV is transmitted through *Aedes* species mosquitoes, and displays differential replication pattern in the two kinds of hosts. CHIKV persists in a low level in mosquitoes, taking it as a maintenance host, however in vertebrate hosts, CHIKV replicates in a high efficiency and gets very high titre (Vasilakis et al., 2009). It was once speculated that arbovirus does not possess RNAi suppressor activity (Umbach and Cullen, 2009), but recently flavivirus Dengue virus NS4B protein was shown to play an important role in the modulation of host RNAi pathway to favor virus replication (Kakumani et al., 2013), and Mathur et al. revealed a RNA interference (RNAi) suppression activity of CHIKV nsP2 and nsP3 in Sf21 RNAi sensor cell line, where for nsP3 macrodomain played a predominant role while AUD was also involved in it (Mathur et al., 2016). In the current study, based on the D-luciferase assay performed within CHIKV-D-Luc-SGR, in general wildtype and most mutant CHIKV showed a higher replication level in C6/36 cells than in U4.4 cells, and the AUD mutant M219A showed no replication in U4.4 but a wildtype replication

capability in C6/36 cells. U4.4 and C6/36 cells are both *Aedes albopictus* derived mosquito cells, but C6/36 was deficient in RNAi response because of a mutation in its Dcr2 gene (Morazzani et al., 2012). This result indicated that RNAi was associated with CHIKV replication, and M219 residue might be involved in and prevent some mosquito specific antiviral RNAi response. At the same time, to compare the D-luc activity of CHIKV between muscle cells and other mammalian cells, muscle cells were more susceptible for CHIKV replication. As it has been shown that muscle cells, such as C2C12 cells, produce less Dicer proteins than other tissues (Sago et al., 2004), it is predicted that besides in mosquito cells, CHIKV replication was also suppressed by RNAi in mammalian cells.

5.2.2 Results

5.2.2.1 nsP3/AUD RNAi suppression activity

5.2.2.1.1 Co-transfection of nsP3/AUD and GFP/siGFP in cells

To detect the RNAi suppression activity of nsP3/AUD, a plasmid containing both GFP and a GFP siRNA sequence was firstly constructed (Figure 5.13). pMKO.1-GFP plasmid was purchased from Addgene (plasmid No. 10676). GFP siRNA sequence (AAGCAGATCCTGAAGAACACCTCAAGAGAGGTGTTCTTCAGGATCTGCTT) were cloned into pMKO.1-GFP plasmid and the resulting plasmid was named as pMKO.1-GFP-shGFP. At the same time, nsP3 and AUD were also cloned into pcDNA3.1 plasmid to get pcDNA3.1-nsP3 or AUD. Then to detect the RNAi suppression activity of nsP3/AUD, pcDNA3.1-nsP3 or AUD was co-transfected into C2C12 cells with pMKO.1-GFP or pMKO.1-GFP-shGFP. Cells were collected by trypsin and used for flow cytometry analysis to quantify the GFP signal. pcDNA3.1 vector was used as negative control and pcDNA3.1-DENV-NS4B was used as positive control (Kakumani et al., 2013). As the percentage of GFP reversion shown in Figure 5.14, when co-transfected CHIKV nsP3, the GFP signal expressed in pMKO.1-GFP-siGFP was significantly reverted. AUD also showed a slight but not significant RNAi suppression activity.

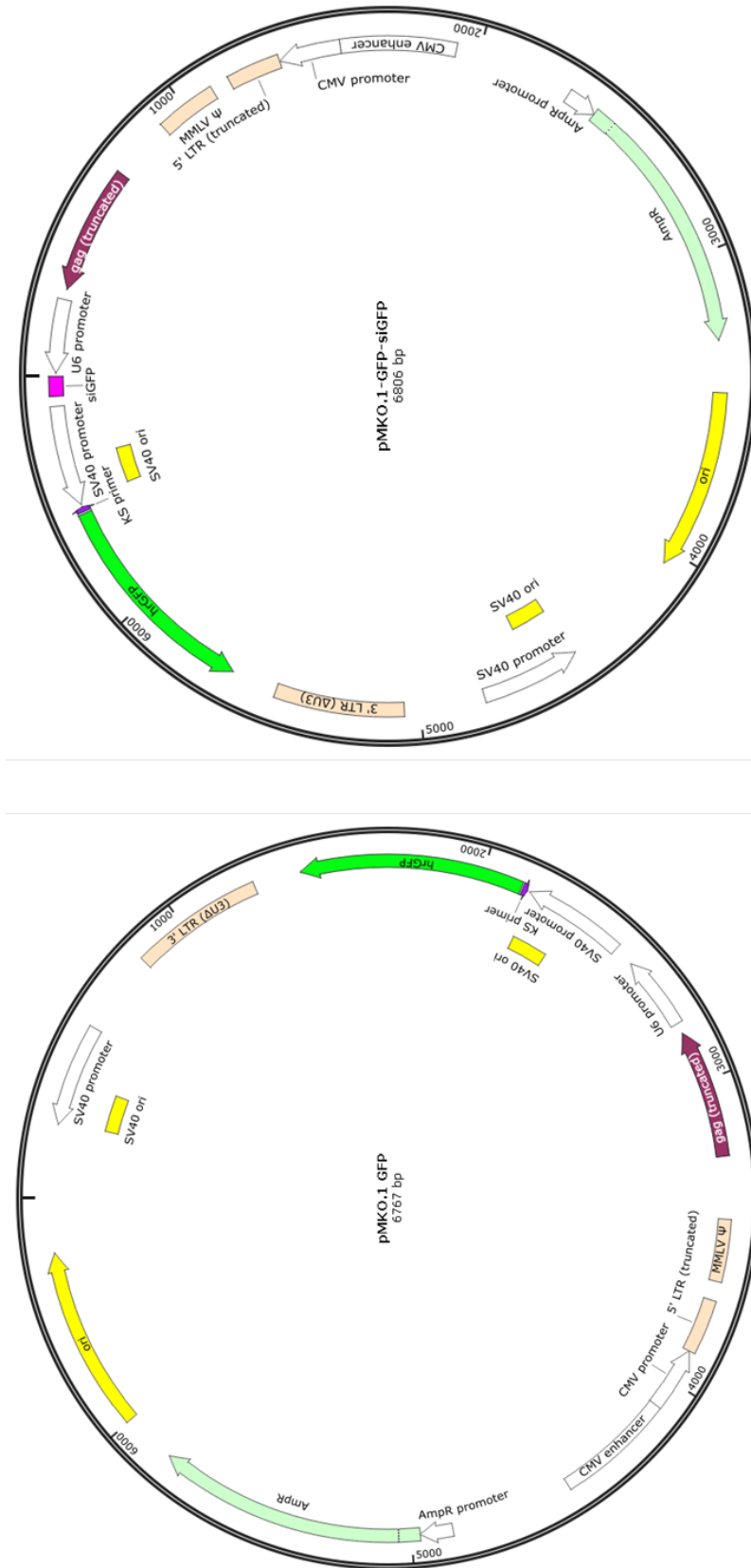


Figure 5.13 Diagram of pMKO.1-GFP and pMKO.1-GFP-siGFP.

GFP-siRNA (siGFP) was inserted into the pMKO.1-GFP with AgeI and EcoRI restriction sites.

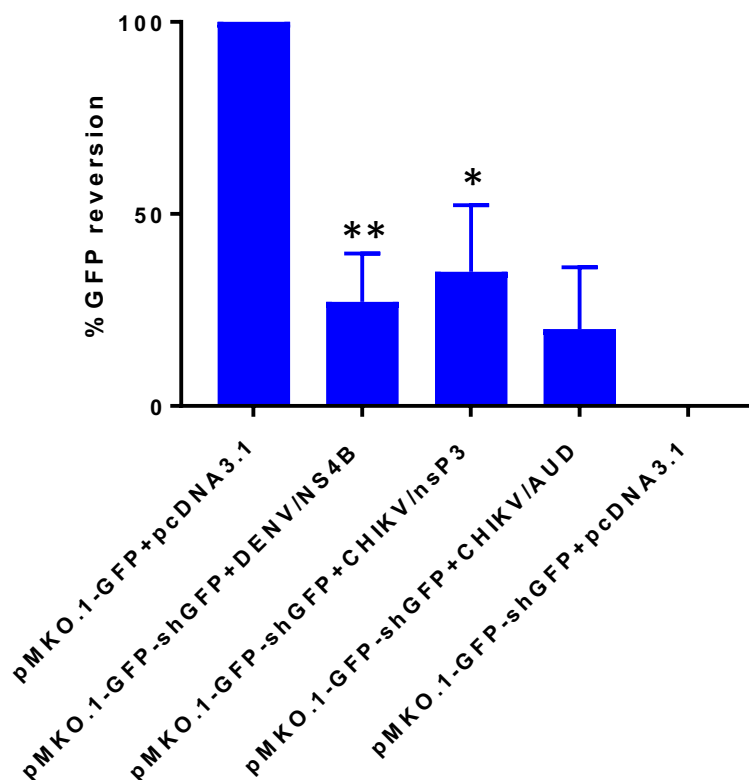


Figure 5.14 GFP reversion assay of CHIKV nsP3/AUD in C2C12 cells.

Dengue virus NS4B was used as positive controls. The GFP signal of pMKO.1-GFP co-transfection with pcDNA3.1 was normalized to 100%, and the GFP signal of pMKO.1-GFP-siGFP co-transfection with pcDNA3.1 was normalized to 0. The y-axis shows % GFP reversion (Mean \pm SD). Statistical significance was analysed using student's t-test using empty vector as control. The * symbol indicates a statistically significant difference in terms of the P value ($P < 0.05$), and ** indicates $P < 0.01$.

5.2.2.1.2 Construction of GFP/siGFP stable expressed cell line

In order to further study the mechanism of nsP3/AUD RNAi suppression activity, I tried to make a cell line stably expressed GFP or GFP-shGFP. To do this, GFP gene or GFP-shGFP sequence were cloned into pcDNA3.1 as pcDNA3.1 contains the neomycin gene that could be selected by G418. pcDNA3.1-GFP and pcDNA3.1-GFP-shGFP were then transfected into C2C12 cells, respectively; and G418 was added into cell culture for selection of the successfully transfected cells. Then the cells were split every 48 hours at 1:10 with G418 (500 ng/ml). However, after one month, a lot of cells survived G418 but only a few of them expressed GFP fluorescence in the pcDNA3.1-GFP transfected cells, while in pcDNA3.1-GFP-siGFP transfected one, cells survived with almost no GFP expression. Therefore the cells were thought not

suitable for further utilisation. Then I tried to use Huh7 cells and HEK293 cells to repeat the construction of the stable cell line, but the results were similar to that of C2C12 cells.

5.2.2.2 Interaction between nsP3/AUD and Dicer protein

5.2.2.2.1 Purification of *E.coli* expressed GST-tagged AUD

Dicer is one of the most important functional proteins in the RNAi pathway (Jaronczyk et al., 2005). As previous result has shown that AUD has RNAi suppression activity, it was interesting to detect if AUD could bind to Dicer protein to suppress the RNAi pathway. GST pull down assay was conducted to detect the interaction between AUD and Dicer. To set up the experiment, the GST tagged AUD was expressed and purified. The whole AUD fragment flanked with *Bam*HI and *Xho*I was amplified from CHIKV-D-Luc-SGR plasmid and cloned into pGEX6P-2 vector after digestion with the corresponding two restriction enzymes to generate recombinant pGEX6P-2-AUD to express GST tagged AUD. The GST tagged AUD was produced in Rosetta2 strain of *E.coli* with 1 mM IPTG induction at 18 °C for 5 hours. Then the expressed GST tagged AUD was purified with glutathione sepharose 4B resin as described in session 2.6.1. The purified protein was analysed in SDS-PAGE gel with Coomassie blue staining (Figure 5.15).

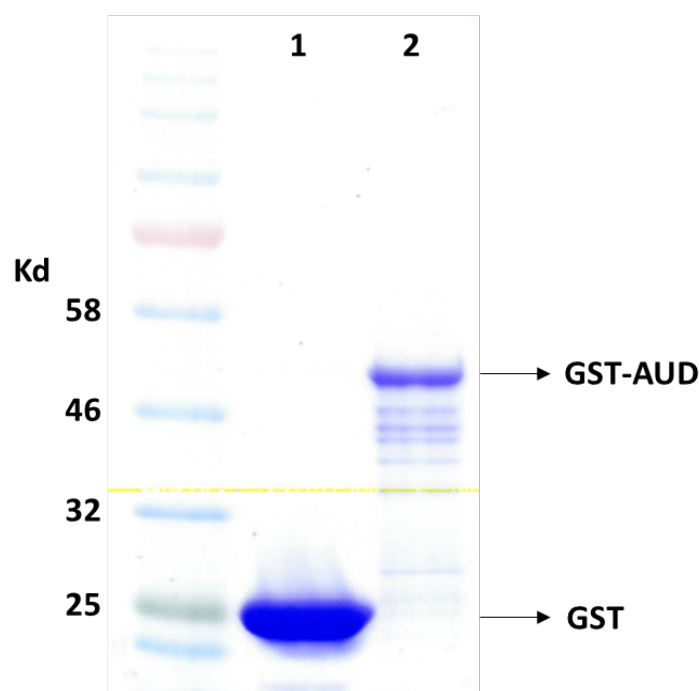


Figure 5.15 Expression of GST-AUD.

1. Expression of GST protein in pGEX6P-2. 2. Expression of GST-AUD in pGEX6P-2-AUD.

5.2.2.2.2 GST pull down assay

To detect the interaction between AUD and Dicer protein, a GST pull down assay was performed. To do this, a Dicer expression plasmid pDESTmycDICER (Dicer 1, ribonuclease type III, *H. sapiens*) purchased from Addgene was used. pDESTmycDICER was transfected into HEK293T cells by lipofectamine 2000. Cells were collected at 72 h.p.t. and lysed with GLB on ice for 30 min before centrifugation at $15,000 \times g$ for 15 min to collect the supernatant. Purified GST tagged AUD was added into glutathione sepharose 4B resin and left on rotator for overnight incubation at 4 °C. Then the resin was washed with 50 mM Tris, pH=7 and GLB buffer before mixed with the cell lysates supernatant for 3 hours incubation at 4 °C. Finally the GST tagged AUD was eluted from the resin after 3 times wash of the resin and was collected for western blot analysis of the pull down results for AUD and Dicer. As the western blot result shown in Figure 5.17, Dicer protein was detected in cell lysates, and was not unspecific bound to the resin. Both GST and GST tagged AUD protein could be pulled down by the resin, however, no Dicer protein was pulled down by GST tagged AUD, indicating that there was no direct interaction between AUD and Dicer protein. On the other hand, based on the western blot result, it seemed that not much Dicer protein was expressed in the transfected cells, therefore even if there was interaction between AUD and Dicer protein, this interaction was difficult to be detected with a lack of Dicer protein expression. Moreover, the GST tagged AUD used in this experiment was expressed in *E.coli*, which might result in the loss of some protein structures or decorations which could be important for the interaction between AUD and Dicer protein.

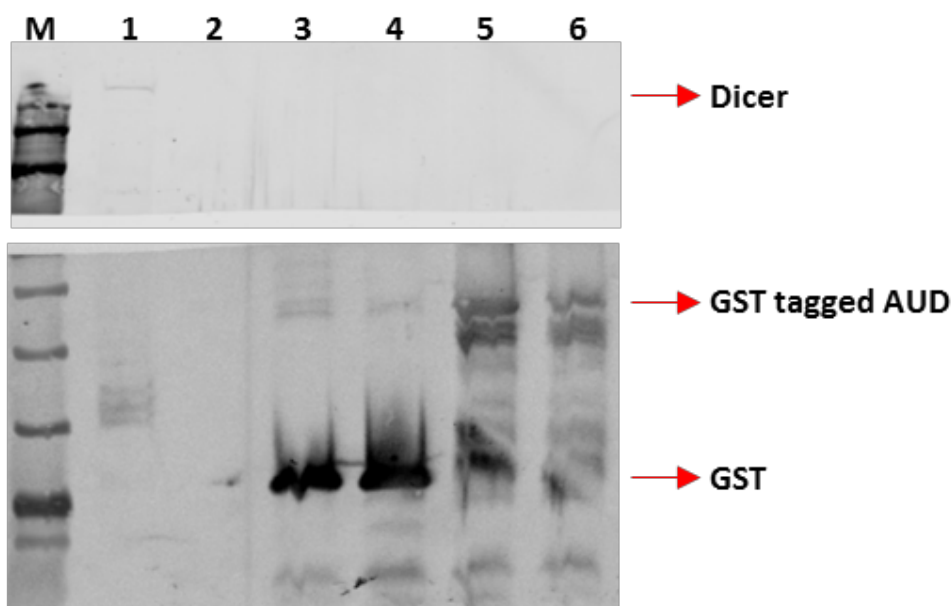


Figure 5.16 GST tagged AUD failed to pull down Dicer protein.

E.coli expressed GST tagged AUD and cell lysates of Dicer transfected 293T cells were used for GST pull down assay. Precipitated proteins were analysed by western blot using anti-Dicer and anti-GST antibody. 1. Cell lysates. 2. Cell lysates + resin. 3. GST + resin. 4. GST + cell lysates + resin. 5. GST tagged AUD + resin. 6. GST tagged AUD + cell lysates + resin.

5.2.2.2.3 GFP-trap assay

Results of the GST pull down assay showed that the *E.coli* expressed GST tagged AUD did not show any interaction with Dicer protein, to further confirm it, a GFP-trap assay with both cell expressed AUD and Dicer protein was performed. To do this, at first, the whole sequence of nsP3 or AUD was amplified from the ICRES-CHIKV plasmid and cloned into pEGFP-N1-GFP plasmid to get pEGFP-N1-GFP-nsP3/AUD. pDESTmycDICER and pEGFP-N1-GFP-nsP3/AUD were co-transfected into HEK293T cells for 72 hours before the transfected cells were collected and lysed with GLB for 30 min on ice. Then the cell lysates were centrifuged at $15,000 \times g$ for 15 min and the supernatant was collected and added into GFP-trap beads for incubation at 4°C overnight with rotation. After incubation, the GFP-trap beads were washed for 5 times followed by the elution and collection of the precipitated proteins for western blot analysis. In Figure 5.17, in cell lysates, Dicer protein, nsP3 and AUD could all be detected in the corresponding transfected cells. In the GFP-trap pull down samples, GFP tagged nsP3 and AUD were pulled down by GFP-trap beads, however, no Dicer protein was pulled down by either nsP3 or AUD, indicating no interaction between GFP tagged nsP3/AUD and Dicer protein. In the cell lysates samples, the western blot result showed that not much Dicer was expressed in

the cells, especially when it was co-transfected with GFP tagged nsP3 or AUD. Therefore, the same as the result in GST pull down assay, although no interaction between nsP3/AUD and Dicer protein was detected by western blot analysis post GFP-trap assay, it might be because that the low expression level of Dicer protein obstructed the detection of the possible protein-protein interactions.

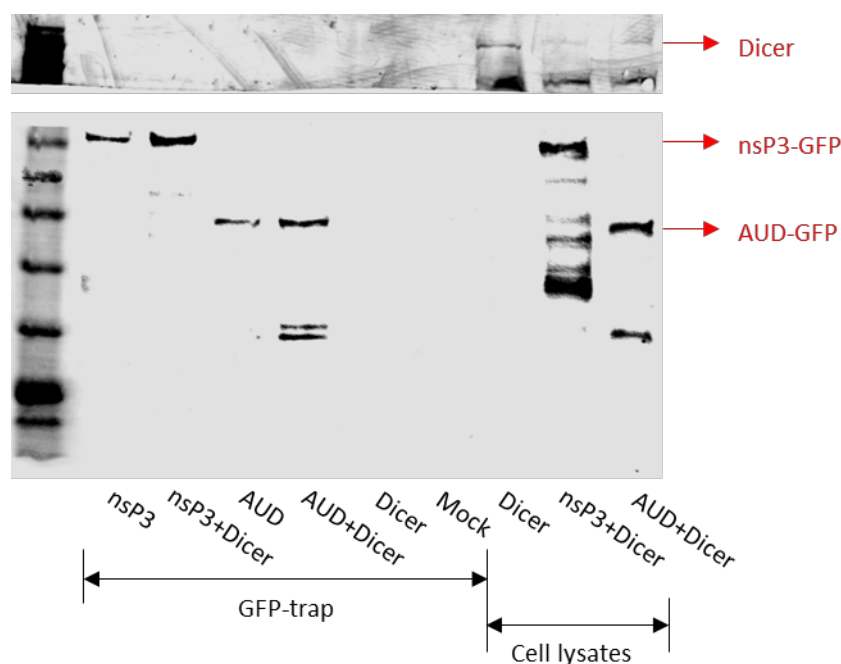


Figure 5.17 GFP tagged nsP3 or AUD failed to pull down Dicer protein.

GFP tagged nsP3/AUD were co-transfected into HEK293T cells with myc tagged Dicer protein. The cell lysates were incubated in GFP-trap beads at 4 °C overnight with rotation for precipitation of GFP tagged nsP3/AUD. Precipitated proteins were detected by western blot using anti-nsP3 and anti-Dicer antibody.

5.2.3 Discussion

As an arbovirus, CHIKV is maintained in both mosquito and vertebrate hosts. The infection of CHIKV in mosquitoes is persistent and asymptomatic, but in vertebrate hosts, it is both acute and self-limiting (Strauss and Strauss, 1994). The infectivity of virus in both mosquito vectors and vertebrate hosts depends on not only the replication capability of the virus itself, but also its ability to counteract the antiviral defence of the hosts. Mosquitoes utilise a variety of pathway to resist virus infection such as TOLL pathway, JAK STAT pathway and RNAi pathway (Lemaitre and Hoffmann, 2007). RNAi is a predominant antiviral defence mechanism in invertebrates and plants (Ding, 2010, Voinnet et al., 1999, Billmyre et al., 2013, Blair, 2011), and viruses have developed different strategies to evade this host immune system antiviral

response. For example, some viruses protect themselves from the recognition of RISC through adaptive mutations in or near the target sequences of RNAi pathway (Haasnoot et al., 2007); others would use their viral proteins as RNAi suppressors to inhibit the function of Dicer or other important proteins within RNAi pathway, thus blocking the host RNAi response (van Rij et al., 2006, Haasnoot et al., 2007, Li and Ding, 2006). Arboviruses were once speculated to have no RNAi suppressors until the NS4B protein of Dengue virus was proved to possess the RNAi suppression activity (Kakumani et al., 2013); and then nsP2 and nsP3 proteins of CHIKV were also reported to play an RNAi suppression role in both insect sf21 cells and mammalian HEK293T cells (Mathur et al., 2016). The GFP reversion experiment in this project demonstrated the same, but to some extent, weaker RNAi suppression function of nsP3/AUD in C2C12 cells as well. The mechanism that nsP3 suppressed host RNAi antiviral pathway was absolutely unknown until now. Both macrodomain and AUD in nsP3 were reported to have RNA-binding activity (Malet et al., 2009, Shin et al., 2012), and this project also proved the nsP3/AUD RNA binding activity to CHIKV genome RNA, therefore it is speculated that the interaction between nsP3 and RNAs might be a way that nsP3 protected genome RNA from Dicer-induced RNAi antiviral pathway. On the other hand, nsP3 could also bind Dicer protein or other functional proteins within RNAi pathway to interfere Dicer targeting on specific genome RNA sequences or the formation of RISC. However, in this study, we performed both a GST pull down assay to detect the in vitro interaction between *E.coli* expressed AUD and cell expressed Dicer protein, and a GFP-trap assay to detect the interaction between nsP3/AUD and Dicer protein in cells, neither of them showed a possible interaction between these two proteins. I also tried to perform immunofluorescence with the Dicer and nsP3/AUD co-transfected cells to detect if Dicer and nsP3/AUD was co-localized in this study, however, either because that the expression of Dicer in the transfected cells was in a low level or the dicer protein antibody was not suitable for IF analysis, no signal of Dicer could be detected (data not shown). For further study, it is believed that a dicer knockout cell line should be constructed and used to detect the effect of dicer on CHIKV replication and the possible interactions between dicer and different viral proteins.

5.3 nsP3/AUD formation/distribution in cells

5.3.1 Introduction

Fros et al. found that nsP3 was expressed in a formation of foci in cells, but when AUD, fused with GFP, was individually expressed in the cells, it formed in filaments instead of foci. And as no colocalization between AUD and cell cytoskeleton could be detected, it was supposed that

the AUD exhibited intrinsic multimerization capacity (Fros et al., 2012). Despite these, the significance and functional roles of the multimerization of AUD during virus infection are absolutely not known. In this section, the distribution and formation of each mutant AUDs individually expressed in different cells were analysed to detect if the multimerization of AUD was associated with CHIKV replication capability.

5.3.2 Results

5.3.2.1 Formation and localisation of wildtype AUD and its mutants in C2C12 cells

The GFP-fused AUD has been shown to exist in the formation of fibres when expressed in vero cells (reference AUD fibres). This AUD formed fibre in the cells did not co-localized with cytoskeleton protein tubulin, and therefore the fibre formation was believed to result from the intrinsic multimerization character of the AUD. However, the significance of this multimerization property of AUD for CHIKV replication was unknown, therefore in this project, we explored if the panel of mutations introduced into AUD affected its multimerization character and if the multimerization character was associated with CHIKV replication capability. To start the experiment, the whole sequence of AUD and its mutants (M219A, E225A, R243A/K245A, P247A/V248A, V260A/P261A, C262A/C264A) flanked with EcoRI and BamHI were amplified from the CHIKV-D-Luc-SGR and its AUD mutants, and then cloned into pEGFP-N1 vector to get AUD expression plasmid pEGFP-N1-AUD. The resulting plasmids were then transfected into C2C12 cells for 48 hours before cells were fixed with 4% PFA. The fixed cells were then permeabilized with ice-cold methanol and blocked with 2% BSA before incubated with DAPI stain at RT for 5 min and finally analysed by confocal microscope. As shown in Figure 5.18, wildtype AUD and its M219A and E225A mutants were expressed in the formation of fibres; AUD-R243A/K245A showed a different phenotype of the formation of dots; and AUD-P247A/V248A, V260A/P261A and C262A/C264A expressed in C2C12 cells were dispersed distributed in both nucleus and cytoplasm. Interestingly, the previous results in this project showed that M219A, E225A CHIKV viruses were competent in virus replication in C2C12 cells, the same as wildtype; P247A/V248A was partially defective in virus replication in C2C12 cells, and the replication of R243A/K245A, V260A/P261A and C62A/C264A mutants in C2C12 cells were absolutely abrogated. Therefore, the formation of wildtype AUD and its mutants in C2C12 cells shown here indicated that the multimerization character of AUD was important for CHIKV replication, although the role of it during virus replication needs further exploration.

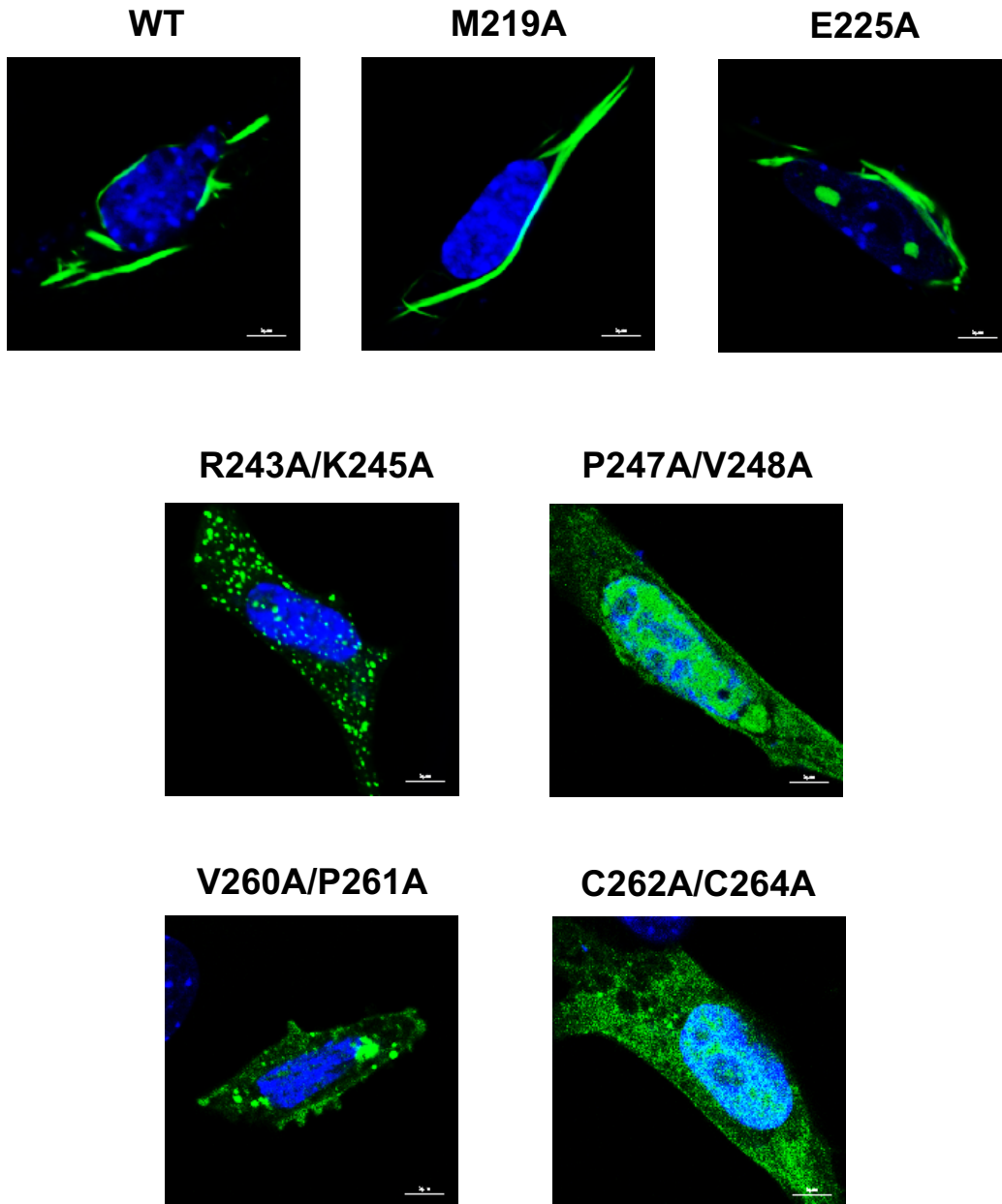


Figure 5.18 GFP tagged wildtype AUD and mutant distribution in C2C12 cells.

pEGFP-N1-AUDs were transfected in C2C12 cells and AUD distribution were detected by confocal microscopy at 48 h.p.t. AUD was detected by GFP fluorescence. WT, M219A and E225A AUDs showed fibre formation. AUD-R243A/K245A showed formation of dots. P247A/V248A, V260A/P261A and C262A/C264A AUDs were dispersed distributed in C2C12 cells.

5.3.2.2 Distribution of wildtype nsP3 and AUD mutants in C2C12 cells

It was shown from the last section that the mutations introduced into AUD altered its multimerization character and distribution in cells, as during CHIKV replication, AUD functions within the whole nsP3, we then detected the nsP3 and its AUD mutants distribution in C2C12 cells. The whole sequence of nsP3 and its AUD mutants flanked with EcoRI and BamHI were amplified from wildtype or corresponding mutants ICRES-CHIKV plasmids and cloned into pEGFP-N1 vector after digestion with EcoRI and BamHI restriction enzymes. The resulting plasmids were transfected into C2C12 cells and cells were collected and fixed with 4% PFA at 48 h.p.t. As G3BP has been proved to be an important interaction protein with nsP3 and involved in CHIKV replication complex (Fros et al., 2012), G3BP was also labelled with primary G3BP antibody and Alexa Fluor-594 secondary antibody for confocal microscope analysis. The results (Figure 5.19) showed that WT, M219A and E225A nsP3 showed co-localization with G3BP in the formation of clusters in C2C12 cells. R243A/K245A and P247A/V248A nsP3 were also co-localized with G3BP but the co-localized dots were smaller than those of wildtype nsP3. No G3BP was detected in nsP3-V260A/P261A or -C262A/C264A transfected cells, and nsP3-V260A/P261A expressed in C2C12 formed as small dots while nsP3-C262A/C264A was dispersed distributed in C2C12 cells. It was interesting to see no G3BP could be detected in V260A/P261A and C262A/C264A nsP3 expressed cells because interaction between G3BP and the hypervariable region within nsP3 was revealed in previous studies (Foy et al., 2013, Frolov et al., 2017, Panas et al., 2014) and the expression of nsP3 was able to trigger G3BP production in cells (Fros et al., 2012). C262 and C264 residues are constituent part of the zinc coordination site within AUD, V260 and P261 are located around the zinc coordination part, therefore it was predicted that the zinc coordination site played a role in the interaction between nsP3 and G3BP. For R243A/K245A and P247A/V248A nsP3 transfected cells, although G3BP could still be detected and co-localized with nsP3, the co-localized dots were smaller than those with wildtype nsP3, indicating a loss of other proteins or interaction factors within nsP3-containing complex.

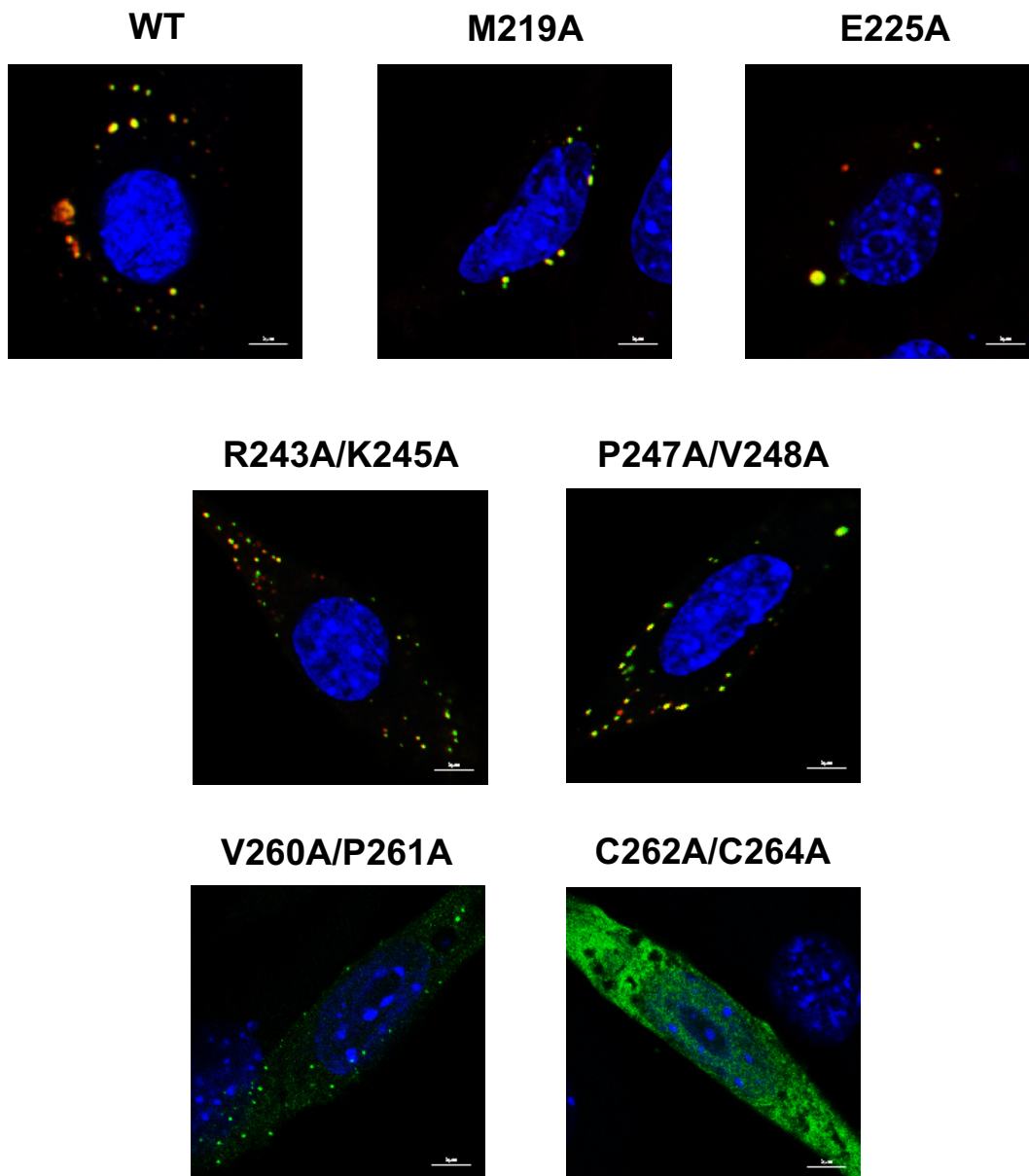


Figure 5.19 Distribution of wildtype nsP3 and its AUD mutants with G3BP in C2C12 cells.

A panel of pEGFP-N1-nsP3 plasmids were transfected in C2C12 cells and nsP3 distribution were detected by GFP fluorescence while G3BP was detected by primary G3BP antibody and Fluorescent 594 secondary antibody through confocal microscopy at 48 h.p.t. nsP3: Green; G3BP: red.

5.3.3 Discussion

The filaments formation of AUD when individually expressed in cells was first revealed by Jelke et al (Fros et al., 2012). As the AUD filaments resembled the cytoskeleton, they detected the distribution of both AUD and tubulin but found no co-localization between them. Therefore it was suspected that the multimerization was an intrinsic character of the conserved AUD. In this project, we explored the effect of a panel of mutations on AUD filament formation, and the relationship between AUD multimerization character and CHIKV replication capability. The result was of great interest: the AUD mutations which impaired CHIKV replication also disrupted the AUD filament formation, while those who did not affect CHIKV replication retained the AUD multimerization character, indicating that the filament formation of AUD was associated with CHIKV replication capability. At the same time, we found that the mutations not only altered AUD formation, but also affected the corresponding nsP3 formation. R243A/K245A and P247A/V248A nsP3 dots formed in cells were obviously smaller than the clusters formed by wildtype nsP3, indicating a loss of some interaction proteins in the nsP3-containing complex. Therefore based on the previous supposition, it might be because that the loss of AUD multimerization property affected the accumulation of the corresponding nsP3 proteins; or there is also a possibility that AUD filament formation is due to its interaction with some unknown host factors, and when then interaction was destroyed, the interacting host factors no longer existed in nsP3-containing complex, thus the nsP3 mutants-containing complex became smaller. On the other hand, it was reported that in Rift Valley fever virus-infected C6/36 cells, the non-structural proteins formed fibres in the cell nucleus, however in U4.4 cells, where virus could not replicate well because of cell RNAi response, no fibre structure of non-structural proteins could be detected. They believed that the formation of the fibres depended on the production of the non-structural proteins. However here in our study, from IF images, no significant difference of the expression between wildtype AUD or its mutants in each cells was observed.

In conclusion, although the mechanism of the filament formation of AUD was not clear, it was believed that this phenotype of AUD formation in cells was associated with CHIKV replication. And in the next session of this chapter, proteomics analysis of the possible host interaction proteins with nsP3 would be listed and gave more information about this.

5.4 Proteomic analysis of nsP3 binding partner

5.4.1 Introduction

It is well accepted that the functions of nsP3 during the alphavirus life cycle are dependent on its interactions with other viral proteins and cellular proteins. Previous studies have revealed that for alphaviruses, besides other viral proteins and viral genomic RNAs, nsP3 is able to bind to many host proteins and factors, most of which are bound to the protein motifs within macrodomain and hypervariable region. For example, the macrodomain mediates nsP3 interaction with both monomeric and poly adenosine diphosphate ribese (ADP ribose) (Karras et al., 2005, Malet et al., 2009, Park and Griffin, 2009, Foy et al., 2013); the hypervariable region mediated nsP3 interactions with G3BP (Frolova et al., 2006, Gorchakov et al., 2008), Fragile-X-related (FXR) proteins (Tamanini et al., 2000, Tamanini et al., 1999, Anderson and Kedersha, 2008) and amphiphysins (Foy et al., 2013). Interaction between nsP3 and PARP-1 is thought to be important in stabilizing the virus replicase complex or for the recruitment of other host factors (Park and Griffin, 2009); involvement of amphiphysins in nsP3-containing repliation complex is important for invagination of lysosomal membranes to house the virus replication complex (Lark et al., 2017). There are also many proteins interacting with nsP3 with not yet clear roles during virus replication, such as Y-box-binding protein 1 (YBX1) (Gorchakov et al., 2008), heat shock proteins (Gorchakov et al., 2008), PI3K-Akt-mTOR (Panas et al., 2015), DDX1/DDX3 (Amaya et al., 2016) and IKK β (Amaya et al., 2016).

In the current chapter, in order to better understand the protein-protein interaction between nsP3 and cellular proteins for CHIKV, and to detect if the replication defect of CHIKV P247A/V248A mutant is due to its loss of interactions with some cellular proteins, proteomic analysis with twin-strep tagged nsP3 CHIKV was performed.

The introduction of the isotope-coded affinity tag (ICAT) was one of the milestones to isotopic chemical labelling for relative quantification of peptides/proteins with mass spectrometry (MS). Tandem Mass Tagging (TMT) is a quantitative proteomic approach, which allows the comparison of protein levels in up to 10 different samples in a single experiment. With this approach, it is possible to identify and quantitate thousands of proteins in a single experiment. Samples for TMT analysis are labelled, fractionated and analysed by Nano-LC MS. Protein quantitation is based on the median values of multiple peptides identified from the same protein, resulting in highly accurate protein quantitation between samples. Measuring protein changes between mutants with significantly different phenotypes and wildtype is one of the important tasks of proteomics.

The molecular mechanism underpinning the phenotype of the AUD mutants can be explained by the roles of AUD in regulating interactions between nsP3 and cellular proteins. To address this, affinity purification of Twin-Strep-tagged nsP3 was performed followed by TMT quantitative proteomics analysis to compare the interactome of wild type AUD and its mutant after pull down assays from virus transfected cells by nano-LC mass spectrometry and quantitative proteomic analysis. The abundance ratio of the peptide for each samples were taken as the parameters for comparing with untagged WT (negative control) and Twin-Strep-tagged WT (positive control).

5.4.2 Results

5.4.2.1 Purification of Twin-strep-tagged (TST) nsP3 from virus transfected cells

nsP3 is known to be involved in a variety of interactions or pathways with host proteins. The previous results in this project have revealed that the P247A/V248A mutations within nsP3 impaired CHIKV replication due to its defect in subgenomic RNA synthesis, further studies proved that the P247A/V248A mutations reduced nsP3 RNA binding activity to CHIKV genomic RNA, we then explored in this chapter if the nsP3-P247A/V248A mutant also lost any interactions with some certain host proteins compared to wildtype nsP3. To do this, the P247A/V248A mutations were firstly introduced into an ICRES-CHIKV-TST-nsP3 virus construct, in which the TST was inserted into the nsP3 hypervariable region and had been proved to not affect virus replication in our lab, by quickchange site-directed mutagenesis. Wildtype ICRES-CHIKV-TST-nsP3 and its P247A/V248A mutant, as well as no tagged ICRES-CHIKV were transfected into Huh7 cells using lipofectamine 2000. Purification of TST-nsP3 was performed using strep tag resins (Strep-Tactin® Sepharose®) with GLB-lysed cell lysates harvested at 72 h.p.t. After four times washes, protein bound resins were analysed by western blot using anti-nsP3 antibody and stored at -80 °C for further analysis. As shown in Figure 5.20, after transfection with 1 µg wildtype ICRES-CHIKV-TST-nsP3 RNA, the corresponding TST-nsP3 was abundantly produced and pulled down by strep tag resins. However, for P247A/V248A mutant, transfection of 1 µg RNA could not produce enough nsP3 due to the defect of P247A/V248A mutant replication; whereas when transfected with 4 µg RNA, the expression of nsP3 was sufficient to be tested and for the pull down assay. As expected, no tagged wildtype control showed enough nsP3 expression in cell lysates but could not be pulled down.

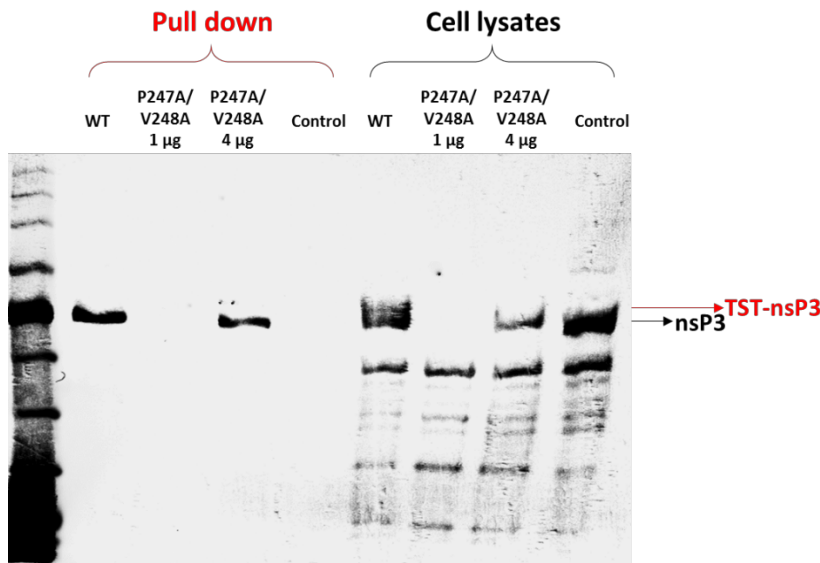


Figure 5.20 Purification of Twin-Strep-Tagged nsP3 (TST-nsP3).

TST tagged CHIKV (wildtype and P247A/V248A mutant) and untagged CHIKV (wildtype) RNAs were transfected into Huh7 cells. Cells were lysed at 48 h.p.t with GLB and incubated with Strep Tag purification resins. After 5 times wash with wash buffer, resins were analysed by western blot with nsP3 antibody.

5.4.2.2 Proteomics analysis of nsP3 binding partners

To identify cellular candidates potentially involved in the P247A/V248A phenotype, bound fractions following purification from cytoplasmic lysates of TST-nsP3-WT and TST-nsP3-P247A/V248A, together with no tagged nsP3 (3 replicates of each samples), were analysed by mass spectrometry. A great number of known nsP3 interacting proteins were identified by this approach. These proteins had at least two high confidence peptide matches per protein ($p < 0.05$). After comparisons of abundance of interacting partners between wildtype and mutant, as well as no tagged negative control (Figure 5.21), interaction networks that nsP3-P247A/V248A mutant potentially involved in was determined.

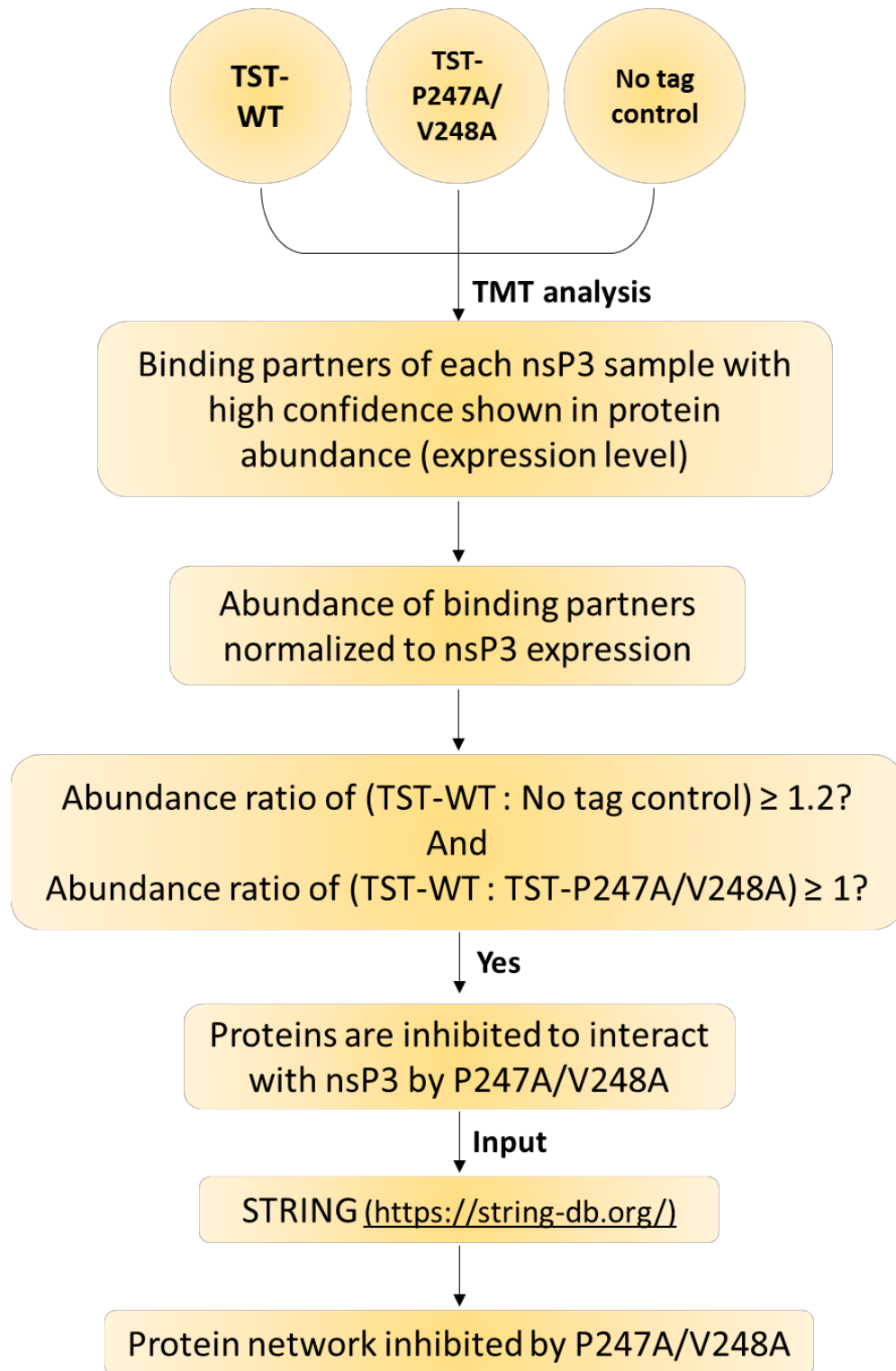


Figure 5.21 Flow chart of comparative analysis of nsP3-binding proteins involved in nsP3-P247A/V248A.

After analysis by STRING, a group of proteins functioning as mitochondrial carriers were identified to be correlated with P247A/V248A mutant (Figure 5.23).

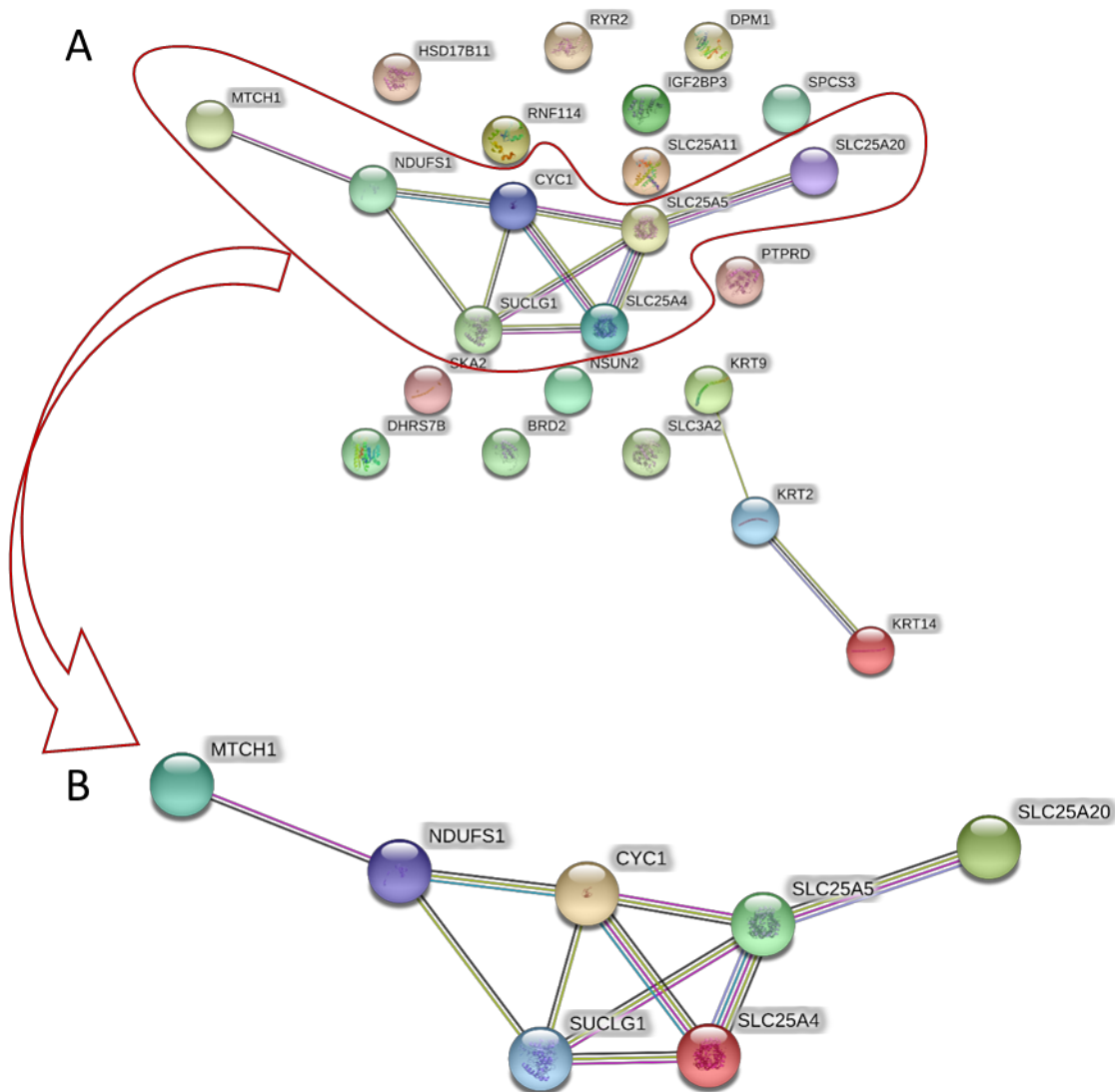


Figure 5.22 nsP3 interacting protein network inhibited by P247A/V248A.

A. Network illustration of the interactions analysed via STRING (<https://string-db.org/>) by input the proteins, of which TST-WT: No tag control ≥ 1.2 and TST-WT: TST-P247A/V248A ≥ 1 . B. Proteins involved in the mitochondrial network.

Quantification analysis revealed 23 different proteins potentially interacting with wildtype nsP3 but not with P247A/V248A nsP3 (Figure 5.22A). Among them, 7 proteins were grouped in a mitochondrial-associated network (Figure 5.22B), including mitochondrial carrier 1 (MTCH1), NADH dehydrogenase (ubiquinone) Fe-S protein 1 (NDUFS1), cytochrome c-1 (CYC1), solute carrier family 25 (mitochondrial carrier; adenine nucleotide translocator), member 5 (SLC25A5), solute carrier family 25 (carnitine/acylcarnitine translocase), member 20 (SLC25A20), solute

carrier family 25 (mitochondrial carrier; adenine nucleotide translocatoer), member 4 (SLC25A4), succinate-CoA ligase, alpha subunit (SUCLG1). The importance and functions of these mitochondria associated proteins for CHIKV replication have never been reported before.

5.4.3 Discussion

Previous data in this project showed that the P247A/V248A mutant formed smaller plaques in BHK cells during plaque assay, consistant with its impaired replication capability but also indicating a defect of it in cytotoxicity. Some mitochondrial carrier proteins are thought to be correlated with cell apoptosis, for example, mitochondrial carrier homolog 1 (MTCH1), an outer mitochondrial membrane protein, is believed to be an apoptosis gene (Iplik et al., 2018). Apoptosis is a mode of programmed cell death necessary for development of multicellular organisms as well as for tissue homeostasis in developing and adult animals (Danial and Korsmeyer, 2004). Among the cellular pathways leading to apoptosis, the extrinsic one is initiated in response to extrinsic signal and mediated by death receptors at the plasma membrane , while the intrinsic one initiated within the cell and the mitochondria have a primary role in the final decision step (Kroemer and Reed, 2000). Based on the results obtained in this session, it was supposed that the attenuated cytotoxicity of P247A/V248A CHIKV mutant was potentially due to its defect in interaction with some mitochondrial proteins, besides its impaired replication capability.

Chapter 6: Conclusion and future perspectives

As a member of the alphavirus genus, the genome of CHIKV is a single positive-stranded RNA including two ORFs, the first of which encodes four non-structural proteins (nsP1-4), and the second one encodes five structural proteins (capsid protein, E1, E2, E3 and 6k). The four non-structural proteins are important for the regulation of CHIKV replication. Among them, the function of nsP3 is the least understood. It consists of three domains, the macrodomain, the AUD and the hypervariable region. The macrodomain has been shown to possess ADP-ribose and RNA binding activity, and the hypervariable region is involved in multiple virus-host protein interactions. However, the AUD, as a homologous sequence among alphaviruses, is essential for CHIKV replication with absolutely unknown functions. In this project, a mutagenic strategy was initially performed in the context of CHIKV-D-Luc-SGR. Using as a guide the structure of the SINV AUD and an alignment of the AUD amino acid sequences of different alphaviruses, conserved solvent-accessible residues were identified and mutated. By dual-luciferase reporter assay, the effect of the AUD mutations on both input translation and genome RNA replication of the replicon were revealed. The mutants showed a series of species- and cell type-specific phenotypes. Mutations of the two cysteines involved in, or two residues adjacent to the zinc coordination site completely abrogated CHIKV replication in any cell type tested, indicating an essential role of the zinc coordination site during virus replication. Zinc coordination site is always associated with RNA-binding activity, however, as demonstrated in this project, this zinc coordination site within AUD was not involved in the AUD binding activity to CHIKV genome 3'UTR. At the same time, mutations of R243A/K245A abrogated AUD RNA-binding activity to CHIKV genome RNA, and this CHIKV mutant showed no replication in all the mammalian cells and quick reversion in mosquito cells, indicating that the AUD RNA-binding activity to CHIKV genome RNA played an important role during virus replication. M219A showed an interesting phenotype as in the two mosquito cells tested, M219A showed a wildtype level replication in C6/36 cells but no replication in U4.4 cells. C6/36 and U4.4 are both *Aedes. Albopictus* derived mosquito cells, and the main difference between them is that the C6/36 cells are RNAi defective due to a shift mutation in its Dcr2 gene. Therefore, the residue M219 is possibly associated with, and inhibited a mosquito-specific RNAi response to CHIKV infection. P247A/V248A showed a consistent impaired replication level in all the cells tested, indicating a fundamental function of P247/V248 residues during virus replication. Then the mutants showing replication in all / most cells (M219A, E225A, R243A/K245A, P247A/V248A) were further analysed in the context of infectious virus. The R243A/K245A mutant showed quick reversion after virus electroporation and therefore could not be further analysed. In infectious virus, the replication defect of P247A/V248A was

consistent with the subgenomic replicon data. Exploration in other processes during virus infection demonstrated that the P247A/V248A mutations led to a defect in subgenomic RNA synthesis during virus replication, resulting in the lack of structural proteins, which was shown as a defect in virus assembly. Then RNA-binding activity analysis revealed that nsP3 binding activity to CHIKV genome RNA was important for CHIKV replication and P247A/V248A nsP3 showed reduced affinity to CHIKV subgenomic promoter which was possibly associated with its defect in subgenomic RNA synthesis. In conclusion, the nsP3 P247/V248 residues played significant roles in subgenomic RNA synthesis via binding CHIKV subgenomic promoter. It will be interesting to further explore the role of P247/V248 residues in the interaction with CHIKV genome RNA and the direct consequence of this interaction in order to study the precise process of CHIKV genome replication. The revealed significance of P247/V248A also gives a new opportunity for drug development against CHIKV replication.

Other biochemical characteristics of nsP3 were also analysed in this project. RNAi suppression activity was revealed in nsP3, whereas AUD showed a slight but not significant effect. Co-immunoprecipitation assay showed no interaction between nsP3/AUD and Dicer protein, therefore the RNAi suppression activity of nsP3 was not because of a direct inhibition of dicer protein function but associated with other steps through RNAi response. At the same time, CHIKV-D-Luc-SGR M219A mutant showed a phenotype that it could not replicate in U4.4 cells but showed a wildtype replication in C6/36 cells. U4.4 and C6/36 are both *Aedes albopictus* derived mosquito cell lines, the difference between them was that the C6/36 cells were defective in Dcr2-induced RNAi because of a deletion in its Dcr 2 gene leading to the expression of a non-functional Dcr2 protein (Morazzani et al., 2012). This result indicated a role of nsP3 M219 residue in resistance against mosquito cells RNAi antiviral response to virus infection. At the same time, the M219A mutant did not show any significant defect in the mammalian cells detected, therefore it was believed that the involvement of M219 in RNAi was specific to some mosquito-unique RNAi pathway. Three major RNAi pathways have been revealed in mosquitoes: small interfering RNA (siRNA), micro RNA (miRNA) and Piwi-interacting RNA (piRNA) pathways (Blair and Olson, 2014). As the piRNA pathway existing in C6/36 cells did not affect CHIKV M219A mutant genome replication, and the exogenous-siRNA (exo-siRNA) pathway performs the predominant antiviral innate immune response to virus infection in mosquitoes (Blair, 2011), it was more likely that the nsP3 M219 residue was involved in the exo-siRNA antiviral pathway of mosquito cells. During the exo-siRNA response in mosquitoes, dsRNA is firstly recognized by Dcr2 protein to initiate the process (Blair, 2011, Campbell et al., 2008a). Dcr2 protein in mosquitoes is different from the corresponding Dicer

protein in mammalian cells. It is a big protein with a N-terminal DExD/H helicase domain, in the middle there is a second helicase domain, a dsRNA-binding domain and a PAZ domain responsible for recognition of dsRNA ends, and in the C-terminus are two RNase III domains (Campbell et al., 2008a). Dcr2 protein cleaves dsRNA, which derived from both viral genome and negative strand RNA in arbovirus infected cells, into 19-22 bp siRNA duplexes, and then with the help of dsRNA-binding protein R2D2, the Dcr2-siRNA complex is loaded into the Ago2-containing RISC for degradation of the “passenger” strand RNA. Then the “guide” strand RNA binds to its complementary sequence on viral mRNA to form a perfectly base-paired duplex, which is the acting site for Ago2 to cleave target viral RNA (Matranga et al., 2005). The mammalian cells also possess a Dicer-initiated siRNA pathway, but as the Dicer protein in mammalian cells and mosquito cells were not the same, interactions between Dicer protein and viral proteins in mosquito and mammalian cells could be different. Therefore, even though no interaction between mammalian Dicer and CHIKV nsP3/AUD was observed in this project, there is still a possibility that nsP3/AUD binds to mosquito Dcr2 protein to interfere mosquito siRNA antiviral pathway. Further studies on this part is now in progress in our lab.

Distribution and formation of individually expressed nsP3 or AUD was also analyzed in this project. It is interesting to find that the formation of each mutant nsP3/AUD was, to some extent, consistent with their phenotypes. The fibre formation of wildtype AUD was believed to result from a self-multimerization character. The mutations which led to no or impaired virus replication (R243A/K245A, P247A/V248A, V260A/P261A and C262A/C264A) also disrupted of the fibre formation, indicating that this multimerization character was important for a functional nsP3. For the formation of nsP3, C262A/C264A mutant showed an absolutely different phenotype compared to the dots formed by wildtype, while R243A/K245A, P247A/V248A and V260A/P261A mutants showed a formation of smaller dots, indicating that those mutations introduced into nsP3 interrupted the interactions between nsP3 and some cellular proteins. However, proteomic analysis to explore possible interaction partners of nsP3 did not give a clear insight. More data are needed here to study the role nsP3/AUD during CHIKV replication.

In conclusion of this project, the AUD within nsP3 is a multi-functional domain, playing essential roles for CHIKV replication. This project, for the first time, revealed the function of AUD and more importantly, the data here validate the AUD as a novel target for antiviral agents and provide opportunities for rational design of an attenuated virus vaccine.

References

References

- ADEBAJO, A. O. 1996. Rheumatic manifestations of tropical diseases. *Curr Opin Rheumatol*, 8, 85-9.
- AHN, A., KLIMJACK, M. R., CHATTERJEE, P. K. & KIELIAN, M. 1999. An epitope of the Semliki Forest virus fusion protein exposed during virus-membrane fusion. *J Virol*, 73, 10029-39.
- AHOLA, T. & KAARIAINEN, L. 1995. Reaction in alphavirus mRNA capping: formation of a covalent complex of nonstructural protein nsP1 with 7-methyl-GMP. *Proc Natl Acad Sci U S A*, 92, 507-11.
- AHOLA, T., KUJALA, P., TUUTTILA, M., BLOM, T., LAAKKONEN, P., HINKKANEN, A. & AUVINEN, P. 2000. Effects of palmitoylation of replicase protein nsP1 on alphavirus infection. *J Virol*, 74, 6725-33.
- AKHRYMUK, I., FROLOV, I. & FROLOVA, E. I. 2016. Both RIG-I and MDA5 detect alphavirus replication in concentration-dependent mode. *Virology*, 487, 230-41.
- ALIYARI, R., WU, Q., LI, H. W., WANG, X. H., LI, F., GREEN, L. D., HAN, C. S., LI, W. X. & DING, S. W. 2008. Mechanism of induction and suppression of antiviral immunity directed by virus-derived small RNAs in *Drosophila*. *Cell Host Microbe*, 4, 387-97.
- AMAYA, M., BROOKS-FAULCONER, T., LARK, T., KECK, F., BAILEY, C., RAMAN, V. & NARAYANAN, A. 2016. Venezuelan equine encephalitis virus non-structural protein 3 (nsP3) interacts with RNA helicases DDX1 and DDX3 in infected cells. *Antiviral Res*, 131, 49-60.
- ANDERSON, P. & KEDERSHA, N. 2008. Stress granules: the Tao of RNA triage. *Trends Biochem Sci*, 33, 141-50.
- ANJUM, S., ALI, S., AHMAD, T., AFZAL, M. S., WAHEED, Y., SHAFI, T., ASHRAF, M. & ANDLEEB, S. 2013. Sequence and structural analysis of 3' untranslated region of hepatitis C virus, genotype 3a, from pakistani isolates. *Hepat Mon*, 13, e8390.
- ATKINS, G. J. & SHEAHAN, B. J. 2016. Molecular determinants of alphavirus neuropathogenesis in mice. *J Gen Virol*, 97, 1283-96.
- BARRAL, P. M., SARKAR, D., SU, Z. Z., BARBER, G. N., DESALLE, R., RACANIELLO, V. R. & FISHER, P. B. 2009. Functions of the cytoplasmic RNA sensors RIG-I and MDA-5: key regulators of innate immunity. *Pharmacol Ther*, 124, 219-34.
- BEESON, S., FUNKHOUSER, E., KOTEA, N., SPIELMAN, A. & ROBICH, R. M. 2008. Chikungunya fever, Mauritius, 2006. *Emerg Infect Dis*, 14, 337-8.
- BERBEN-BLOEMHEUVEL, G., KASPERAITIS, M. A., VAN HEUGTEN, H., THOMAS, A. A., VAN STEEG, H. & VOORMA, H. O. 1992. Interaction of initiation factors with the cap structure of chimaeric mRNA containing the 5'-untranslated regions of Semliki Forest virus RNA is related to translational efficiency. *Eur J Biochem*, 208, 581-7.
- BERG, J. M. 1990. Zinc fingers and other metal-binding domains. Elements for interactions between macromolecules. *J Biol Chem*, 265, 6513-6.
- BERNARD, E., SOLIGNAT, M., GAY, B., CHAZAL, N., HIGGS, S., DEVAUX, C. & BRIANT, L. 2010. Endocytosis of chikungunya virus into mammalian cells: role of clathrin and early endosomal compartments. *PLoS One*, 5, e11479.
- BILLMYRE, R. B., CALO, S., FERETZAKI, M., WANG, X. & HEITMAN, J. 2013. RNAi function, diversity, and loss in the fungal kingdom. *Chromosome Res*, 21, 561-72.
- BLAIR, C. D. 2011. Mosquito RNAi is the major innate immune pathway controlling arbovirus infection and transmission. *Future Microbiol*, 6, 265-77.
- BLAIR, C. D. & OLSON, K. E. 2014. Mosquito immune responses to arbovirus infections. *Curr Opin Insect Sci*, 3, 22-29.
- BOLGER, R. & CHECOVICH, W. 1994. A new protease activity assay using fluorescence polarization. *Biotechniques*, 17, 585-9.
- BOLGER, R. & THOMPSON, D. 1994. A quantitative RNase assay using fluorescence polarization. *Am Biotechnol Lab*, 12, 113, 116.

- BOLGER, R., WIESE, T. E., ERVIN, K., NESTICH, S. & CHECOVICH, W. 1998. Rapid screening of environmental chemicals for estrogen receptor binding capacity. *Environ Health Perspect*, 106, 551-7.
- BORGHNERINI, G., POUBEAU, P., STAIKOWSKY, F., LORY, M., LE MOULLEC, N., BECQUART, J. P., WENGLING, C., MICHAULT, A. & PAGANIN, F. 2007. Outbreak of chikungunya on Reunion Island: early clinical and laboratory features in 157 adult patients. *Clin Infect Dis*, 44, 1401-7.
- BRANDLER, S., RUFFIE, C., COMBREDT, C., BRAULT, J. B., NAJBURG, V., PREVOST, M. C., HABEL, A., TAUBER, E., DESPRES, P. & TANGY, F. 2013. A recombinant measles vaccine expressing chikungunya virus-like particles is strongly immunogenic and protects mice from lethal challenge with chikungunya virus. *Vaccine*, 31, 3718-25.
- BROWN, R. S., WAN, J. J. & KIELIAN, M. 2018. The Alphavirus Exit Pathway: What We Know and What We Wish We Knew. *Viruses*, 10.
- BURT, F. J., CHEN, W., MINER, J. J., LENSCHOW, D. J., MERITS, A., SCHNETTLER, E., KOHL, A., RUDD, P. A., TAYLOR, A., HERRERO, L. J., ZAID, A., NG, L. F. P. & MAHALINGAM, S. 2017. Chikungunya virus: an update on the biology and pathogenesis of this emerging pathogen. *Lancet Infect Dis*, 17, e107-e117.
- CAMPBELL, C. L., BLACK, W. C. T., HESS, A. M. & FOY, B. D. 2008a. Comparative genomics of small RNA regulatory pathway components in vector mosquitoes. *BMC Genomics*, 9, 425.
- CAMPBELL, C. L., KEENE, K. M., BRACKNEY, D. E., OLSON, K. E., BLAIR, C. D., WILUSZ, J. & FOY, B. D. 2008b. *Aedes aegypti* uses RNA interference in defense against Sindbis virus infection. *BMC Microbiol*, 8, 47.
- CASTELLO, A., SANZ, M. A., MOLINA, S. & CARRASCO, L. 2006. Translation of Sindbis virus 26S mRNA does not require intact eukariotic initiation factor 4G. *J Mol Biol*, 355, 942-56.
- CHANG, L. J., DOWD, K. A., MENDOZA, F. H., SAUNDERS, J. G., SITAR, S., PLUMMER, S. H., YAMSHCHIKOV, G., SARWAR, U. N., HU, Z., ENAMA, M. E., BAILER, R. T., KOUP, R. A., SCHWARTZ, R. M., AKAHATA, W., NABEL, G. J., MASCOLA, J. R., PIERSON, T. C., GRAHAM, B. S., LEDGERWOOD, J. E. & TEAM, V. R. C. S. 2014. Safety and tolerability of chikungunya virus-like particle vaccine in healthy adults: a phase 1 dose-escalation trial. *Lancet*, 384, 2046-52.
- CHECOVICH, W. J., BOLGER, R. E. & BURKE, T. 1995. Fluorescence polarization--a new tool for cell and molecular biology. *Nature*, 375, 254-6.
- CHEN, C. I., CLARK, D. C., PESAVENTO, P., LERCHE, N. W., LUCIW, P. A., REISEN, W. K. & BRAULT, A. C. 2010. Comparative pathogenesis of epidemic and enzootic Chikungunya viruses in a pregnant Rhesus macaque model. *Am J Trop Med Hyg*, 83, 1249-58.
- CHEN, R., WANG, E., TSETSARKIN, K. A. & WEAVER, S. C. 2013. Chikungunya virus 3' untranslated region: adaptation to mosquitoes and a population bottleneck as major evolutionary forces. *PLoS Pathog*, 9, e1003591.
- CHENG, R. H., KUHN, R. J., OLSON, N. H., ROSSMANN, M. G., CHOI, H. K., SMITH, T. J. & BAKER, T. S. 1995. Nucleocapsid and glycoprotein organization in an enveloped virus. *Cell*, 80, 621-30.
- CHIU, Y. H., MACMILLAN, J. B. & CHEN, Z. J. 2009. RNA polymerase III detects cytosolic DNA and induces type I interferons through the RIG-I pathway. *Cell*, 138, 576-91.
- CHOW, A., HER, Z., ONG, E. K., CHEN, J. M., DIMATATAC, F., KWEK, D. J., BARKHAM, T., YANG, H., RENIA, L., LEO, Y. S. & NG, L. F. 2011. Persistent arthralgia induced by Chikungunya virus infection is associated with interleukin-6 and granulocyte macrophage colony-stimulating factor. *J Infect Dis*, 203, 149-57.
- CIRIMOTICH, C. M., SCOTT, J. C., PHILLIPS, A. T., GEISS, B. J. & OLSON, K. E. 2009. Suppression of RNA interference increases alphavirus replication and virus-associated mortality in *Aedes aegypti* mosquitoes. *BMC Microbiol*, 9, 49.

- COFFEY, L. L., FAILLOUX, A. B. & WEAVER, S. C. 2014. Chikungunya virus-vector interactions. *Viruses*, 6, 4628-63.
- COOMBS, K. M. & BROWN, D. T. 1989. Form-determining functions in Sindbis virus nucleocapsids: nucleosomelike organization of the nucleocapsid. *J Virol*, 63, 883-91.
- COUDERC, T., CHRETIEN, F., SCHILTE, C., DISSON, O., BRIGITTE, M., GUIVEL-BENHASSINE, F., TOURET, Y., BARAU, G., CAYET, N., SCHUFFENECKER, I., DESPRES, P., ARENZANA-SEISDEDOS, F., MICHAULT, A., ALBERT, M. L. & LECUIT, M. 2008. A mouse model for Chikungunya: young age and inefficient type-I interferon signaling are risk factors for severe disease. *PLoS Pathog*, 4, e29.
- CRISTEA, I. M., CARROLL, J. W., ROUT, M. P., RICE, C. M., CHAIT, B. T. & MACDONALD, M. R. 2006. Tracking and elucidating alphavirus-host protein interactions. *J Biol Chem*, 281, 30269-78.
- DANIAL, N. N. & KORSMEYER, S. J. 2004. Cell death: critical control points. *Cell*, 116, 205-19.
- DAVIS, N. L., WILLIS, L. V., SMITH, J. F. & JOHNSTON, R. E. 1989. In vitro synthesis of infectious venezuelan equine encephalitis virus RNA from a cDNA clone: analysis of a viable deletion mutant. *Virology*, 171, 189-204.
- DE GROOT, R. J., HARDY, W. R., SHIRAKO, Y. & STRAUSS, J. H. 1990. Cleavage-site preferences of Sindbis virus polyproteins containing the non-structural proteinase. Evidence for temporal regulation of polyprotein processing in vivo. *EMBO J*, 9, 2631-8.
- DE, I., FATA-HARTLEY, C., SAWICKI, S. G. & SAWICKI, D. L. 2003. Functional analysis of nsP3 phosphoprotein mutants of Sindbis virus. *J Virol*, 77, 13106-16.
- DE RANITZ, C. M., MYERS, R. M., VARKEY, M. J., ISAAC, Z. H. & CAREY, D. E. 1965. Clinical impressions of chikungunya in Vellore gained from study of adult patients. *Indian J Med Res*, 53, 756-63.
- DE WET, J. R., WOOD, K. V., HELINSKI, D. R. & DELUCA, M. 1985. Cloning of firefly luciferase cDNA and the expression of active luciferase in Escherichia coli. *Proc Natl Acad Sci U S A*, 82, 7870-3.
- DELISLE, E., ROUSSEAU, C., BROCHE, B., LEPARC-GOFFART, I., L'AMBERT, G., COCHET, A., PRAT, C., FOULONGNE, V., FERRE, J. B., CATELINOIS, O., FLUSIN, O., TCHERNOG, E., MOUSSION, I. E., WIEGANDT, A., SEPTFONS, A., MENDY, A., MOYANO, M. B., LAPORTE, L., MAUREL, J., JOURDAIN, F., REYNES, J., PATY, M. C. & GOLLIOT, F. 2015. Chikungunya outbreak in Montpellier, France, September to October 2014. *Euro Surveill*, 20.
- DELLER, J. J., JR. & RUSSELL, P. K. 1967. An analysis of fevers of unknown origin in American soldiers in Vietnam. *Ann Intern Med*, 66, 1129-43.
- DELLER, J. J., JR. & RUSSELL, P. K. 1968. Chikungunya disease. *Am J Trop Med Hyg*, 17, 107-11.
- DIALLO, M., THONNON, J., TRAORE-LAMIZANA, M. & FONTENILLE, D. 1999. Vectors of Chikungunya virus in Senegal: current data and transmission cycles. *Am J Trop Med Hyg*, 60, 281-6.
- DICKSON, A. M., ANDERSON, J. R., BARNHART, M. D., SOKOLOSKI, K. J., OKO, L., OPYRCHAL, M., GALANIS, E., WILUSZ, C. J., MORRISON, T. E. & WILUSZ, J. 2012. Dephosphorylation of HuR protein during alphavirus infection is associated with HuR relocalization to the cytoplasm. *J Biol Chem*, 287, 36229-38.
- DING, S. W. 2010. RNA-based antiviral immunity. *Nat Rev Immunol*, 10, 632-44.
- DING, S. W. & VOINNET, O. 2007. Antiviral immunity directed by small RNAs. *Cell*, 130, 413-26.
- DOMINGO, E. & HOLLAND, J. J. 1997. RNA virus mutations and fitness for survival. *Annu Rev Microbiol*, 51, 151-78.
- DOXSEY, S. J., BRODSKY, F. M., BLANK, G. S. & HELENIUS, A. 1987. Inhibition of endocytosis by anti-clathrin antibodies. *Cell*, 50, 453-63.
- DRAKE, J. W. 1993. Rates of spontaneous mutation among RNA viruses. *Proc Natl Acad Sci U S A*, 90, 4171-5.

- DRAKE, J. W. & HOLLAND, J. J. 1999. Mutation rates among RNA viruses. *Proc Natl Acad Sci U S A*, 96, 13910-3.
- DUPUIS-MAGUIRAGA, L., NORET, M., BRUN, S., LE GRAND, R., GRAS, G. & ROQUES, P. 2012. Chikungunya disease: infection-associated markers from the acute to the chronic phase of arbovirus-induced arthralgia. *PLoS Negl Trop Dis*, 6, e1446.
- ECKEL, L., KRIEG, S., BUTEPAGE, M., LEHMANN, A., GROSS, A., LIPPOK, B., GRIMM, A. R., KUMMERER, B. M., ROSSETTI, G., LUSCHER, B. & VERHEUGD, P. 2017. The conserved macrodomains of the non-structural proteins of Chikungunya virus and other pathogenic positive strand RNA viruses function as mono-ADP-ribosylhydrolases. *Sci Rep*, 7, 41746.
- FATA, C. L., SAWICKI, S. G. & SAWICKI, D. L. 2002. Modification of Asn374 of nsP1 suppresses a Sindbis virus nsP4 minus-strand polymerase mutant. *J Virol*, 76, 8641-9.
- FEHR, A. R., JANKEVICIUS, G., AHEL, I. & PERLMAN, S. 2018. Viral Macrodomains: Unique Mediators of Viral Replication and Pathogenesis. *Trends Microbiol*, 26, 598-610.
- FIRTH, A. E., CHUNG, B. Y., FLEETON, M. N. & ATKINS, J. F. 2008. Discovery of frameshifting in Alphavirus 6K resolves a 20-year enigma. *Virol J*, 5, 108.
- FIRTH, A. E., WILLS, N. M., GESTELAND, R. F. & ATKINS, J. F. 2011. Stimulation of stop codon readthrough: frequent presence of an extended 3' RNA structural element. *Nucleic Acids Res*, 39, 6679-91.
- FLYNT, A., LIU, N., MARTIN, R. & LAI, E. C. 2009. Dicing of viral replication intermediates during silencing of latent Drosophila viruses. *Proc Natl Acad Sci U S A*, 106, 5270-5.
- FORRESTER, N. L., PALACIOS, G., TESH, R. B., SAVJI, N., GUZMAN, H., SHERMAN, M., WEAVER, S. C. & LIPKIN, W. I. 2012. Genome-scale phylogeny of the alphavirus genus suggests a marine origin. *J Virol*, 86, 2729-38.
- FOSTER, T. L., BELYAEVA, T., STONEHOUSE, N. J., PEARSON, A. R. & HARRIS, M. 2010. All three domains of the hepatitis C virus nonstructural NS5A protein contribute to RNA binding. *J Virol*, 84, 9267-77.
- FOY, N. J., AKHRYMUK, M., AKHRYMUK, I., ATASHEVA, S., BOPDA-WAFFO, A., FROLOV, I. & FROLOVA, E. I. 2013. Hypervariable domains of nsP3 proteins of New World and Old World alphaviruses mediate formation of distinct, virus-specific protein complexes. *J Virol*, 87, 1997-2010.
- FROLOV, I., HARDY, R. & RICE, C. M. 2001. Cis-acting RNA elements at the 5' end of Sindbis virus genome RNA regulate minus- and plus-strand RNA synthesis. *RNA*, 7, 1638-51.
- FROLOV, I., KIM, D. Y., AKHRYMUK, M., MOBLEY, J. A. & FROLOVA, E. I. 2017. Hypervariable Domain of Eastern Equine Encephalitis Virus nsP3 Redundantly Utilizes Multiple Cellular Proteins for Replication Complex Assembly. *J Virol*, 91.
- FROLOV, I. & SCHLESINGER, S. 1994. Comparison of the effects of Sindbis virus and Sindbis virus replicons on host cell protein synthesis and cytopathogenicity in BHK cells. *J Virol*, 68, 1721-7.
- FROLOVA, E., GORCHAKOV, R., GARMASHOVA, N., ATASHEVA, S., VERGARA, L. A. & FROLOV, I. 2006. Formation of nsP3-specific protein complexes during Sindbis virus replication. *J Virol*, 80, 4122-34.
- FROS, J. J., DOMERADZKA, N. E., BAGGEN, J., GEERTSEMA, C., FLIPSE, J., VLAK, J. M. & PIJLMAN, G. P. 2012. Chikungunya virus nsP3 blocks stress granule assembly by recruitment of G3BP into cytoplasmic foci. *J Virol*, 86, 10873-9.
- FROS, J. J. & PIJLMAN, G. P. 2016. Alphavirus Infection: Host Cell Shut-Off and Inhibition of Antiviral Responses. *Viruses*, 8.
- FROSHAUER, S. 1988. Alphavirus RNA replicase is located on the cytoplasmic surface of endosomes and lysosomes. *The Journal of Cell Biology*, 107, 2075-2086.
- FROSHAUER, S., KARTENBECK, J. & HELENIUS, A. 1988. Alphavirus RNA replicase is located on the cytoplasmic surface of endosomes and lysosomes. *J Cell Biol*, 107, 2075-86.

- GAEDIGK-NITSCHKO, K. & SCHLESINGER, M. J. 1990. The Sindbis virus 6K protein can be detected in virions and is acylated with fatty acids. *Virology*, 175, 274-81.
- GALBRAITH, S. E., SHEAHAN, B. J. & ATKINS, G. J. 2006. Deletions in the hypervariable domain of the nsP3 gene attenuate Semliki Forest virus virulence. *J Gen Virol*, 87, 937-47.
- GARDNER, C. L., BURKE, C. W., HIGGS, S. T., KLIMSTRA, W. B. & RYMAN, K. D. 2012. Interferon-alpha/beta deficiency greatly exacerbates arthritogenic disease in mice infected with wild-type chikungunya virus but not with the cell culture-adapted live-attenuated 181/25 vaccine candidate. *Virology*, 425, 103-12.
- GARDNER, J., ANRAKU, I., LE, T. T., LARCHER, T., MAJOR, L., ROQUES, P., SCHRODER, W. A., HIGGS, S. & SUHRBIER, A. 2010. Chikungunya virus arthritis in adult wild-type mice. *J Virol*, 84, 8021-32.
- GARNEAU, N. L., SOKOLOSKI, K. J., OPYRCHAL, M., NEFF, C. P., WILUSZ, C. J. & WILUSZ, J. 2008. The 3' untranslated region of sindbis virus represses deadenylation of viral transcripts in mosquito and Mammalian cells. *J Virol*, 82, 880-92.
- GAROFF, H., HUYLEBROECK, D., ROBINSON, A., TILLMAN, U. & LILJESTROM, P. 1990. The signal sequence of the p62 protein of Semliki Forest virus is involved in initiation but not in completing chain translocation. *J Cell Biol*, 111, 867-76.
- GHILDIYAL, M. & ZAMORE, P. D. 2009. Small silencing RNAs: an expanding universe. *Nat Rev Genet*, 10, 94-108.
- GHOSH, A., DESAI, A., RAVI, V., NARAYANAPPA, G. & TYAGI, B. K. 2017. Chikungunya Virus Interacts with Heat Shock Cognate 70 Protein to Facilitate Its Entry into Mosquito Cell Line. *Intervirology*, 60, 247-262.
- GIBBONS, D. L., AHN, A., CHATTERJEE, P. K. & KIELIAN, M. 2000. Formation and characterization of the trimeric form of the fusion protein of Semliki Forest Virus. *J Virol*, 74, 7772-80.
- GIBBONS, D. L., ERK, I., REILLY, B., NAVAZA, J., KIELIAN, M., REY, F. A. & LEPAULT, J. 2003. Visualization of the target-membrane-inserted fusion protein of Semliki Forest virus by combined electron microscopy and crystallography. *Cell*, 114, 573-83.
- GOONAWARDANE, N., GEBHARDT, A., BARTLETT, C., PICHLMAIR, A. & HARRIS, M. 2017. Phosphorylation of Serine 225 in Hepatitis C Virus NS5A Regulates Protein-Protein Interactions. *J Virol*, 91.
- GORCHAKOV, R., GARMASHOVA, N., FROLOVA, E. & FROLOV, I. 2008. Different types of nsP3-containing protein complexes in Sindbis virus-infected cells. *J Virol*, 82, 10088-101.
- GOTTE, B., LIU, L. & MCINERNEY, G. M. 2018. The Enigmatic Alphavirus Non-Structural Protein 3 (nsP3) Revealing Its Secrets at Last. *Viruses*, 10.
- GUZZARDO, P. M., MUERDTER, F. & HANNON, G. J. 2013. The piRNA pathway in flies: highlights and future directions. *Curr Opin Genet Dev*, 23, 44-52.
- HAASNOOT, J., WESTERHOUT, E. M. & BERKHOUT, B. 2007. RNA interference against viruses: strike and counterstrike. *Nat Biotechnol*, 25, 1435-43.
- HAESE, N. N., BROECKEL, R. M., HAWMAN, D. W., HEISE, M. T., MORRISON, T. E. & STREBLOW, D. N. 2016. Animal Models of Chikungunya Virus Infection and Disease. *J Infect Dis*, 214, S482-S487.
- HAHN, Y. S., STRAUSS, E. G. & STRAUSS, J. H. 1989. Mapping of RNA- temperature-sensitive mutants of Sindbis virus: assignment of complementation groups A, B, and G to nonstructural proteins. *J Virol*, 63, 3142-50.
- HALLENGARD, D., KAKOULIDOU, M., LULLA, A., KUMMERER, B. M., JOHANSSON, D. X., MUTSO, M., LULLA, V., FAZAKERLEY, J. K., ROQUES, P., LE GRAND, R., MERITS, A. & LILJESTROM, P. 2014. Novel attenuated Chikungunya vaccine candidates elicit protective immunity in C57BL/6 mice. *J Virol*, 88, 2858-66.

- HALSTEAD, S. B., NIMMANNITYA, S. & MARGIOTTA, M. R. 1969a. Dengue d chikungunya virus infection in man in Thailand, 1962-1964. II. Observations on disease in outpatients. *Am J Trop Med Hyg*, 18, 972-83.
- HALSTEAD, S. B., UDOMSAKDI, S., SINGHARAJ, P. & NISALAK, A. 1969b. Dengue chikungunya virus infection in man in Thailand, 1962-1964. 3. Clinical, epidemiologic, and virologic observations on disease in non-indigenous white persons. *Am J Trop Med Hyg*, 18, 984-96.
- HAMMAR, L., MARKARIAN, S., HAAG, L., LANKINEN, H., SALMI, A. & CHENG, R. H. 2003. Prefusion rearrangements resulting in fusion Peptide exposure in Semliki forest virus. *J Biol Chem*, 278, 7189-98.
- HARDY, R. W. & RICE, C. M. 2005. Requirements at the 3' end of the sindbis virus genome for efficient synthesis of minus-strand RNA. *J Virol*, 79, 4630-9.
- HAWMAN, D. W., STOERMER, K. A., MONTGOMERY, S. A., PAL, P., OKO, L., DIAMOND, M. S. & MORRISON, T. E. 2013. Chronic joint disease caused by persistent Chikungunya virus infection is controlled by the adaptive immune response. *J Virol*, 87, 13878-88.
- HEIDNER, H. W., MCKNIGHT, K. L., DAVIS, N. L. & JOHNSTON, R. E. 1994. Lethality of PE2 incorporation into Sindbis virus can be suppressed by second-site mutations in E3 and E2. *J Virol*, 68, 2683-92.
- HELENIUS, A. 1984. Semliki Forest virus penetration from endosomes: a morphological study. *Biol Cell*, 51, 181-5.
- HELENIUS, A., KARTENBECK, J., SIMONS, K. & FRIES, E. 1980. On the entry of Semliki forest virus into BHK-21 cells. *J Cell Biol*, 84, 404-20.
- HER, Z., MALLERET, B., CHAN, M., ONG, E. K., WONG, S. C., KWEK, D. J., TOLOU, H., LIN, R. T., TAMBYAH, P. A., RENIA, L. & NG, L. F. 2010. Active infection of human blood monocytes by Chikungunya virus triggers an innate immune response. *J Immunol*, 184, 5903-13.
- HEYDUK, T., MA, Y., TANG, H. & EBRIGHT, R. H. 1996. Fluorescence anisotropy: rapid, quantitative assay for protein-DNA and protein-protein interaction. *Methods Enzymol*, 274, 492-503.
- HIGGS, S. 2006. The 2005-2006 Chikungunya epidemic in the Indian Ocean. *Vector Borne Zoonotic Dis*, 6, 115-6.
- HOARAU, J. J., JAFFAR BANDJEE, M. C., KREJBICH TROTOT, P., DAS, T., LI-PAT-YUEN, G., DASSA, B., DENIZOT, M., GUICHARD, E., RIBERA, A., HENNI, T., TALLET, F., MOITON, M. P., GAUZERE, B. A., BRUNIQUET, S., JAFFAR BANDJEE, Z., MORBIDELLI, P., MARTIGNY, G., JOLIVET, M., GAY, F., GRANDADAM, M., TOLOU, H., VIEILLARD, V., DEBRE, P., AUTRAN, B. & GASQUE, P. 2010. Persistent chronic inflammation and infection by Chikungunya arthritogenic alphavirus in spite of a robust host immune response. *J Immunol*, 184, 5914-27.
- HOCHEDÉZ, P., CANESTRI, A., GUIHOT, A., BRICHLER, S., BRICAIRE, F. & CAUMES, E. 2008. Management of travelers with fever and exanthema, notably dengue and chikungunya infections. *Am J Trop Med Hyg*, 78, 710-3.
- HOLLAND, J., SPINDLER, K., HORODYSKI, F., GRABAU, E., NICHOL, S. & VANDEPOL, S. 1982. Rapid evolution of RNA genomes. *Science*, 215, 1577-85.
- HSIEH, P. & ROBBINS, P. W. 1984. Regulation of asparagine-linked oligosaccharide processing. Oligosaccharide processing in *Aedes albopictus* mosquito cells. *J Biol Chem*, 259, 2375-82.
- HUANG, L., HWANG, J., SHARMA, S. D., HARGITTAI, M. R., CHEN, Y., ARNOLD, J. J., RANEY, K. D. & CAMERON, C. E. 2005. Hepatitis C virus nonstructural protein 5A (NS5A) is an RNA-binding protein. *J Biol Chem*, 280, 36417-28.

- HYDE, J. L., CHEN, R., TROBAUGH, D. W., DIAMOND, M. S., WEAVER, S. C., KLIMSTRA, W. B. & WILUSZ, J. 2015. The 5' and 3' ends of alphavirus RNAs--Non-coding is not non-functional. *Virus Res*, 206, 99-107.
- INAMADAR, A. C., PALIT, A., SAMPAGAVI, V. V., RAGHUNATH, S. & DESHMUKH, N. S. 2008. Cutaneous manifestations of chikungunya fever: observations made during a recent outbreak in south India. *Int J Dermatol*, 47, 154-9.
- INOUE, H., NOJIMA, H. & OKAYAMA, H. 1990. High efficiency transformation of *Escherichia coli* with plasmids. *Gene*, 96, 23-8.
- IPLIK, E. S., ERTUGRUL, B., CANDAN, G., PAMUK, S., AYDEMIR, L., CELIK, M., ULUSAN, M., ERGEN, A. & CAKMAKOGLU, B. 2018. ROS related enzyme levels and its association to molecular signaling pathway in the development of head and neck cancer. *Cell Mol Biol (Noisy-le-grand)*, 64, 24-29.
- JAMESON, D. M. & SAWYER, W. H. 1995. Fluorescence anisotropy applied to biomolecular interactions. *Methods Enzymol*, 246, 283-300.
- JARONCZYK, K., CARMICHAEL, J. B. & HOBMAN, T. C. 2005. Exploring the functions of RNA interference pathway proteins: some functions are more RISCy than others? *Biochem J*, 387, 561-71.
- JOSE, J., SNYDER, J. E. & KUHN, R. J. 2009. A structural and functional perspective of alphavirus replication and assembly. *Future Microbiol*, 4, 837-56.
- KAARIAINEN, L. & AHOLA, T. 2002. Functions of alphavirus nonstructural proteins in RNA replication. *Prog Nucleic Acid Res Mol Biol*, 71, 187-222.
- KAKUMANI, P. K., PONIA, S. S., S, R. K., SOOD, V., CHINNAPPAN, M., BANERJEA, A. C., MEDIGESHI, G. R., MALHOTRA, P., MUKHERJEE, S. K. & BHATNAGAR, R. K. 2013. Role of RNA interference (RNAi) in dengue virus replication and identification of NS4B as an RNAi suppressor. *J Virol*, 87, 8870-83.
- KALLIO, K., HELLSTROM, K., JOKITALO, E. & AHOLA, T. 2016. RNA Replication and Membrane Modification Require the Same Functions of Alphavirus Nonstructural Proteins. *J Virol*, 90, 1687-92.
- KARO-ASTOVER, L., SAROVA, O., MERITS, A. & ZUSINAITE, E. 2010. The infection of mammalian and insect cells with SFV bearing nsP1 palmitoylation mutations. *Virus Res*, 153, 277-87.
- KARRAS, G. I., KUSTATSCHER, G., BUHECHA, H. R., ALLEN, M. D., PUGIEUX, C., SAIT, F., BYCROFT, M. & LADURNER, A. G. 2005. The macro domain is an ADP-ribose binding module. *EMBO J*, 24, 1911-20.
- KERANEN, S. & KAARIAINEN, L. 1979. Functional defects of RNA-negative temperature-sensitive mutants of Sindbis and Semliki Forest viruses. *J Virol*, 32, 19-29.
- KETTING, R. F. 2011. The many faces of RNAi. *Dev Cell*, 20, 148-61.
- KHOO, C. C., PIPER, J., SANCHEZ-VARGAS, I., OLSON, K. E. & FRANZ, A. W. 2010. The RNA interference pathway affects midgut infection- and escape barriers for Sindbis virus in *Aedes aegypti*. *BMC Microbiol*, 10, 130.
- KIM, D. Y., FIRTH, A. E., ATASHEVA, S., FROLOVA, E. I. & FROLOV, I. 2011. Conservation of a packaging signal and the viral genome RNA packaging mechanism in alphavirus evolution. *J Virol*, 85, 8022-36.
- KIM, D. Y., REYNAUD, J. M., RASALOUSKAYA, A., AKHRYMUK, I., MOBLEY, J. A., FROLOV, I. & FROLOVA, E. I. 2016. New World and Old World Alphaviruses Have Evolved to Exploit Different Components of Stress Granules, FXR and G3BP Proteins, for Assembly of Viral Replication Complexes. *PLoS Pathog*, 12, e1005810.
- KLIMSTRA, W. B., RYMAN, K. D., BERNARD, K. A., NGUYEN, K. B., BIRON, C. A. & JOHNSTON, R. E. 1999. Infection of neonatal mice with sindbis virus results in a systemic inflammatory response syndrome. *J Virol*, 73, 10387-98.

- KNIGHT, R. L., SCHULTZ, K. L., KENT, R. J., VENKATESAN, M. & GRIFFIN, D. E. 2009. Role of N-linked glycosylation for sindbis virus infection and replication in vertebrate and invertebrate systems. *J Virol*, 83, 5640-7.
- KOBILER, D., RICE, C. M., BRODIE, C., SHAHAR, A., DUBUISSON, J., HALEVY, M. & LUSTIG, S. 1999. A single nucleotide change in the 5' noncoding region of Sindbis virus confers neurovirulence in rats. *J Virol*, 73, 10440-6.
- KOLOKOLTSOV, A. A., FLEMING, E. H. & DAVEY, R. A. 2006. Venezuelan equine encephalitis virus entry mechanism requires late endosome formation and resists cell membrane cholesterol depletion. *Virology*, 347, 333-42.
- KOONIN, E. V., GORBALENYA, A. E., PURDY, M. A., ROZANOV, M. N., REYES, G. R. & BRADLEY, D. W. 1992. Computer-assisted assignment of functional domains in the nonstructural polyprotein of hepatitis E virus: delineation of an additional group of positive-strand RNA plant and animal viruses. *Proc Natl Acad Sci U S A*, 89, 8259-63.
- KROEMER, G. & REED, J. C. 2000. Mitochondrial control of cell death. *Nat Med*, 6, 513-9.
- KUHN, R. J., GRIFFIN, D. E., ZHANG, H., NIESTERS, H. G. & STRAUSS, J. H. 1992. Attenuation of Sindbis virus neurovirulence by using defined mutations in nontranslated regions of the genome RNA. *J Virol*, 66, 7121-7.
- KUHN, R. J., HONG, Z. & STRAUSS, J. H. 1990. Mutagenesis of the 3' nontranslated region of Sindbis virus RNA. *J Virol*, 64, 1465-76.
- KUJALA, P., IKAHEIMONEN, A., EHSANI, N., VIHINEN, H., AUVINEN, P. & KAARIANEN, L. 2001. Biogenesis of the Semliki Forest virus RNA replication complex. *J Virol*, 75, 3873-84.
- KULASEGARAN-SHYLINI, R., ATASHEVA, S., GORENSTEIN, D. G. & FROLOV, I. 2009. Structural and functional elements of the promoter encoded by the 5' untranslated region of the Venezuelan equine encephalitis virus genome. *J Virol*, 83, 8327-39.
- LABADIE, K., LARCHER, T., JOUBERT, C., MANNIOUI, A., DELACHE, B., BROCHARD, P., GUIGAND, L., DUBREIL, L., LEBON, P., VERRIER, B., DE LAMBALLERIE, X., SUHRBIER, A., CHEREL, Y., LE GRAND, R. & ROQUES, P. 2010. Chikungunya disease in nonhuman primates involves long-term viral persistence in macrophages. *J Clin Invest*, 120, 894-906.
- LAMPIO, A., KILPELAINEN, I., PESONEN, S., KARHI, K., AUVINEN, P., SOMERHARJU, P. & KAARIANEN, L. 2000. Membrane binding mechanism of an RNA virus-capping enzyme. *J Biol Chem*, 275, 37853-9.
- LANCIOTTI, R. S., KOSOY, O. L., LAVEN, J. J., PANELLA, A. J., VELEZ, J. O., LAMBERT, A. J. & CAMPBELL, G. L. 2007. Chikungunya virus in US travelers returning from India, 2006. *Emerg Infect Dis*, 13, 764-7.
- LARK, T., KECK, F. & NARAYANAN, A. 2017. Interactions of Alphavirus nsP3 Protein with Host Proteins. *Front Microbiol*, 8, 2652.
- LASTARZA, M. W., GRAKOU, A. & RICE, C. M. 1994a. Deletion and duplication mutations in the C-terminal nonconserved region of Sindbis virus nsP3: effects on phosphorylation and on virus replication in vertebrate and invertebrate cells. *Virology*, 202, 224-32.
- LASTARZA, M. W., LEMM, J. A. & RICE, C. M. 1994b. Genetic analysis of the nsP3 region of Sindbis virus: evidence for roles in minus-strand and subgenomic RNA synthesis. *J Virol*, 68, 5781-91.
- LAURENT, P., LE ROUX, K., GRIVARD, P., BERTIL, G., NAZE, F., PICARD, M., STAIKOWSKY, F., BARAU, G., SCHUFFENECKER, I. & MICHAULT, A. 2007. Development of a sensitive real-time reverse transcriptase PCR assay with an internal control to detect and quantify chikungunya virus. *Clin Chem*, 53, 1408-14.
- LEMAITRE, B. & HOFFMANN, J. 2007. The host defense of *Drosophila melanogaster*. *Annu Rev Immunol*, 25, 697-743.
- LEMAY, J. F., LEMIEUX, C., ST-ANDRE, O. & BACHAND, F. 2010. Crossing the borders: poly(A)-binding proteins working on both sides of the fence. *RNA Biol*, 7, 291-5.

- LEMM, J. A. & RICE, C. M. 1993. Roles of nonstructural polyproteins and cleavage products in regulating Sindbis virus RNA replication and transcription. *J Virol*, 67, 1916-26.
- LESCAR, J., ROUSSEL, A., WIEN, M. W., NAVAZA, J., FULLER, S. D., WENGLER, G., WENGLER, G. & REY, F. A. 2001. The Fusion glycoprotein shell of Semliki Forest virus: an icosahedral assembly primed for fusogenic activation at endosomal pH. *Cell*, 105, 137-48.
- LEVIS, R., SCHLESINGER, S. & HUANG, H. V. 1990. Promoter for Sindbis virus RNA-dependent subgenomic RNA transcription. *J Virol*, 64, 1726-33.
- LEVITT, N. H., RAMSBURG, H. H., HASTY, S. E., REPIK, P. M., COLE, F. E., JR. & LUPTON, H. W. 1986. Development of an attenuated strain of chikungunya virus for use in vaccine production. *Vaccine*, 4, 157-62.
- LI, F. & DING, S. W. 2006. Virus counterdefense: diverse strategies for evading the RNA-silencing immunity. *Annu Rev Microbiol*, 60, 503-31.
- LI, G. & RICE, C. M. 1993. The signal for translational readthrough of a UGA codon in Sindbis virus RNA involves a single cytidine residue immediately downstream of the termination codon. *J Virol*, 67, 5062-7.
- LI, M. L. & STOLLAR, V. 2004. Identification of the amino acid sequence in Sindbis virus nsP4 that binds to the promoter for the synthesis of the subgenomic RNA. *Proc Natl Acad Sci U S A*, 101, 9429-34.
- LI, M. L. & STOLLAR, V. 2007. Distinct sites on the Sindbis virus RNA-dependent RNA polymerase for binding to the promoters for the synthesis of genomic and subgenomic RNA. *J Virol*, 81, 4371-3.
- LI, M. L., WANG, H. & STOLLAR, V. 2010. In vitro synthesis of Sindbis virus genomic and subgenomic RNAs: influence of nsP4 mutations and nucleoside triphosphate concentrations. *J Virol*, 84, 2732-9.
- LI, Y. G., SIRIPANYAPHINYO, U., TUMKOSIT, U., NORANATE, N., A, A. N., TAO, R., KUROSU, T., IKUTA, K., TAKEDA, N. & ANANTAPREECHA, S. 2013. Chikungunya virus induces a more moderate cytopathic effect in mosquito cells than in mammalian cells. *Intervirology*, 56, 6-12.
- LIGON, B. L. 2006. Reemergence of an unusual disease: the chikungunya epidemic. *Semin Pediatr Infect Dis*, 17, 99-104.
- LITZBA, N., SCHUFFENECKER, I., ZELLER, H., DROSTEN, C., EMMERICH, P., CHARREL, R., KREHER, P. & NIEDRIG, M. 2008. Evaluation of the first commercial chikungunya virus indirect immunofluorescence test. *J Virol Methods*, 149, 175-9.
- LIU, L. N., LEE, H., HERNANDEZ, R. & BROWN, D. T. 1996. Mutations in the endo domain of Sindbis virus glycoprotein E2 block phosphorylation, reorientation of the endo domain, and nucleocapsid binding. *Virology*, 222, 236-46.
- LIU, N. & BROWN, D. T. 1993. Phosphorylation and dephosphorylation events play critical roles in Sindbis virus maturation. *Virology*, 196, 703-11.
- LO PRESTI, A., CICCOCCHI, M., CELLA, E., LAI, A., SIMONETTI, F. R., GALLI, M., ZEHENDER, G. & REZZA, G. 2012. Origin, evolution, and phylogeography of recent epidemic CHIKV strains. *Infect Genet Evol*, 12, 392-8.
- LO PRESTI, A., LAI, A., CELLA, E., ZEHENDER, G. & CICCOCCHI, M. 2014. Chikungunya virus, epidemiology, clinics and phylogenesis: A review. *Asian Pacific Journal of Tropical Medicine*, 7, 925-932.
- LOEWY, A., SMYTH, J., VON BONSDORFF, C. H., LILJESTROM, P. & SCHLESINGER, M. J. 1995. The 6-kilodalton membrane protein of Semliki Forest virus is involved in the budding process. *J Virol*, 69, 469-75.
- LOGUE, C. H., SHEAHAN, B. J. & ATKINS, G. J. 2008. The 5' untranslated region as a pathogenicity determinant of Semliki Forest virus in mice. *Virus Genes*, 36, 313-21.
- LOPEZ, S., YAO, J. S., KUHN, R. J., STRAUSS, E. G. & STRAUSS, J. H. 1994. Nucleocapsid-glycoprotein interactions required for assembly of alphaviruses. *J Virol*, 68, 1316-23.

- LU, Y. E. & KIELIAN, M. 2000. Semliki forest virus budding: assay, mechanisms, and cholesterol requirement. *J Virol*, 74, 7708-19.
- LUDWIG, G. V., KONDIG, J. P. & SMITH, J. F. 1996. A putative receptor for Venezuelan equine encephalitis virus from mosquito cells. *J Virol*, 70, 5592-9.
- LULLA, A., LULLA, V. & MERITS, A. 2012. Macromolecular assembly-driven processing of the 2/3 cleavage site in the alphavirus replicase polyprotein. *J Virol*, 86, 553-65.
- LULLA, V., SAWICKI, D. L., SAWICKI, S. G., LULLA, A., MERITS, A. & AHOLA, T. 2008. Molecular defects caused by temperature-sensitive mutations in Semliki Forest virus nsP1. *J Virol*, 82, 9236-44.
- LUNDBLAD, J. R., LAURANCE, M. & GOODMAN, R. H. 1996. Fluorescence polarization analysis of protein-DNA and protein-protein interactions. *Mol Endocrinol*, 10, 607-12.
- LUSA, S., GAROFF, H. & LILJESTROM, P. 1991. Fate of the 6K membrane protein of Semliki Forest virus during virus assembly. *Virology*, 185, 843-6.
- LUSTIG, S., JACKSON, A. C., HAHN, C. S., GRIFFIN, D. E., STRAUSS, E. G. & STRAUSS, J. H. 1988. Molecular basis of Sindbis virus neurovirulence in mice. *J Virol*, 62, 2329-36.
- LYKOURAS, M. V., TSIKA, A. C., LICHIERE, J., PAPAGEORGIOU, N., COUTARD, B., BENTROP, D. & SPYROULIAS, G. A. 2018. NMR study of non-structural proteins-part III: (1)H, (13)C, (15)N backbone and side-chain resonance assignment of macro domain from Chikungunya virus (CHIKV). *Biomol NMR Assign*, 12, 31-35.
- MAHA, M. S., SUSILARINI, N. K., HARIASTUTI, N. I. & SUBANGKIT 2015. Chikungunya virus mutation, Indonesia, 2011. *Emerg Infect Dis*, 21, 379-81.
- MAHAUAD-FERNANDEZ, W. D., JONES, P. H. & OKEOMA, C. M. 2014. Critical role for bone marrow stromal antigen 2 in acute Chikungunya virus infection. *J Gen Virol*, 95, 2450-61.
- MALET, H., COUTARD, B., JAMAL, S., DUTARTRE, H., PAPAGEORGIOU, N., NEUVONEN, M., AHOLA, T., FORRESTER, N., GOULD, E. A., LAFITTE, D., FERRON, F., LESCAR, J., GORBALENYA, A. E., DE LAMBALLERIE, X. & CANARD, B. 2009. The crystal structures of Chikungunya and Venezuelan equine encephalitis virus nsP3 macro domains define a conserved adenosine binding pocket. *J Virol*, 83, 6534-45.
- MANIMUNDA, S. P., VIJAYACHARI, P., UPPOOR, R., SUGUNAN, A. P., SINGH, S. S., RAI, S. K., SUDEEP, A. B., MURUGANANDAM, N., CHAITANYA, I. K. & GURUPRASAD, D. R. 2010. Clinical progression of chikungunya fever during acute and chronic arthritic stages and the changes in joint morphology as revealed by imaging. *Trans R Soc Trop Med Hyg*, 104, 392-9.
- MARSH, M., BOLZAU, E. & HELENIUS, A. 1983. Penetration of Semliki Forest virus from acidic prelysosomal vacuoles. *Cell*, 32, 931-40.
- MARTIN, J. L. & MCMILLAN, F. M. 2002. SAM (dependent) I AM: the S-adenosylmethionine-dependent methyltransferase fold. *Curr Opin Struct Biol*, 12, 783-93.
- MARTINEZ, M. G., SNAPP, E. L., PERUMAL, G. S., MACALUSO, F. P. & KIELIAN, M. 2014. Imaging the alphavirus exit pathway. *J Virol*, 88, 6922-33.
- MATHUR, K., ANAND, A., DUBEY, S. K., SANAN-MISHRA, N., BHATNAGAR, R. K. & SUNIL, S. 2016. Analysis of chikungunya virus proteins reveals that non-structural proteins nsP2 and nsP3 exhibit RNA interference (RNAi) suppressor activity. *Sci Rep*, 6, 38065.
- MATRANGA, C., TOMARI, Y., SHIN, C., BARTEL, D. P. & ZAMORE, P. D. 2005. Passenger-strand cleavage facilitates assembly of siRNA into Ago2-containing RNAi enzyme complexes. *Cell*, 123, 607-20.
- MAVALANKAR, D., SHASTRI, P., BANDYOPADHYAY, T., PARMAR, J. & RAMANI, K. V. 2008. Increased mortality rate associated with chikungunya epidemic, Ahmedabad, India. *Emerg Infect Dis*, 14, 412-5.
- MCGILL, P. E. 1995. Viral infections: alpha-viral arthropathy. *Baillieres Clin Rheumatol*, 9, 145-50.

- MCPHERSON, R. L., ABRAHAM, R., SREEKUMAR, E., ONG, S. E., CHENG, S. J., BAXTER, V. K., KISTEMAKER, H. A., FILIPPOV, D. V., GRIFFIN, D. E. & LEUNG, A. K. 2017. ADP-ribosylhydrolase activity of Chikungunya virus macrodomain is critical for virus replication and virulence. *Proc Natl Acad Sci U S A*, 114, 1666-1671.
- MEISSNER, J. D., HUANG, C. Y., PFEFFER, M. & KINNEY, R. M. 1999. Sequencing of prototype viruses in the Venezuelan equine encephalitis antigenic complex. *Virus Res*, 64, 43-59.
- MERAI, Z., KERENYI, Z., KERTESZ, S., MAGNA, M., LAKATOS, L. & SILHAVY, D. 2006. Double-stranded RNA binding may be a general plant RNA viral strategy to suppress RNA silencing. *J Virol*, 80, 5747-56.
- MESHAM, C. D., AGBACK, P., SHILIAEV, N., URAKOVA, N., MOBLEY, J. A., AGBACK, T., FROLOVA, E. I. & FROLOV, I. 2018. Multiple Host Factors Interact with the Hypervariable Domain of Chikungunya Virus nsP3 and Determine Viral Replication in Cell-Specific Mode. *J Virol*, 92.
- MESSAOUDI, I., VOMASKE, J., TOTONCHY, T., KREKLYWICH, C. N., HABERTHUR, K., SPRINGGAY, L., BRIEN, J. D., DIAMOND, M. S., DEFILIPPIS, V. R. & STREBLOW, D. N. 2013. Chikungunya virus infection results in higher and persistent viral replication in aged rhesus macaques due to defects in anti-viral immunity. *PLoS Negl Trop Dis*, 7, e2343.
- MORAZZANI, E. M., WILEY, M. R., MURREDDU, M. G., ADELMAN, Z. N. & MYLES, K. M. 2012. Production of virus-derived ping-pong-dependent piRNA-like small RNAs in the mosquito soma. *PLoS Pathog*, 8, e1002470.
- MORRISON, T. E., OKO, L., MONTGOMERY, S. A., WHITMORE, A. C., LOTSTEIN, A. R., GUNN, B. M., ELMORE, S. A. & HEISE, M. T. 2011. A mouse model of chikungunya virus-induced musculoskeletal inflammatory disease: evidence of arthritis, tenosynovitis, myositis, and persistence. *Am J Pathol*, 178, 32-40.
- MUKHOPADHYAY, S., ZHANG, W., GABLER, S., CHIPMAN, P. R., STRAUSS, E. G., STRAUSS, J. H., BAKER, T. S., KUHN, R. J. & ROSSMANN, M. G. 2006. Mapping the structure and function of the E1 and E2 glycoproteins in alphaviruses. *Structure*, 14, 63-73.
- MUTHUMANI, K., LANKARAMAN, K. M., LADDY, D. J., SUNDARAM, S. G., CHUNG, C. W., SAKO, E., WU, L., KHAN, A., SARDESAI, N., KIM, J. J., VIJAYACHARI, P. & WEINER, D. B. 2008. Immunogenicity of novel consensus-based DNA vaccines against Chikungunya virus. *Vaccine*, 26, 5128-34.
- MYERS, R. M. & CAREY, D. E. 1967. Concurrent isolation from patient of two arboviruses, Chikungunya and dengue type 2. *Science*, 157, 1307-8.
- MYLES, K. M., WILEY, M. R., MORAZZANI, E. M. & ADELMAN, Z. N. 2008. Alphavirus-derived small RNAs modulate pathogenesis in disease vector mosquitoes. *Proc Natl Acad Sci U S A*, 105, 19938-43.
- NASIR, M. S. & JOLLEY, M. E. 1999. Fluorescence polarization: an analytical tool for immunoassay and drug discovery. *Comb Chem High Throughput Screen*, 2, 177-90.
- NEUVONEN, M., KAZLAUSKAS, A., MARTIKAINEN, M., HINKKANEN, A., AHOLA, T. & SAKSELA, K. 2011. SH3 domain-mediated recruitment of host cell amphiphysins by alphavirus nsP3 promotes viral RNA replication. *PLoS Pathog*, 7, e1002383.
- NICKENS, D. G. & HARDY, R. W. 2008. Structural and functional analyses of stem-loop 1 of the Sindbis virus genome. *Virology*, 370, 158-72.
- NIESTERS, H. G. & STRAUSS, J. H. 1990. Defined mutations in the 5' nontranslated sequence of Sindbis virus RNA. *J Virol*, 64, 4162-8.
- NIMMANNITYA, S., HALSTEAD, S. B., COHEN, S. N. & MARGIOTTA, M. R. 1969. Dengue and chikungunya virus infection in man in Thailand, 1962-1964. I. Observations on hospitalized patients with hemorrhagic fever. *Am J Trop Med Hyg*, 18, 954-71.
- O'REILLY, E. K. & KAO, C. C. 1998. Analysis of RNA-dependent RNA polymerase structure and function as guided by known polymerase structures and computer predictions of secondary structure. *Virology*, 252, 287-303.

- OBERSTE, M. S., PARKER, M. D. & SMITH, J. F. 1996. Complete sequence of Venezuelan equine encephalitis virus subtype IE reveals conserved and hypervariable domains within the C terminus of nsP3. *Virology*, 219, 314-20.
- OZERS, M. S., HILL, J. J., ERVIN, K., WOOD, J. R., NARDULLI, A. M., ROYER, C. A. & GORSKI, J. 1997. Equilibrium binding of estrogen receptor with DNA using fluorescence anisotropy. *J Biol Chem*, 272, 30405-11.
- PAL, P., DOWD, K. A., BRIEN, J. D., EDELING, M. A., GORLATOV, S., JOHNSON, S., LEE, I., AKAHATA, W., NABEL, G. J., RICHTER, M. K., SMIT, J. M., FREMONT, D. H., PIERSON, T. C., HEISE, M. T. & DIAMOND, M. S. 2013. Development of a highly protective combination monoclonal antibody therapy against Chikungunya virus. *PLoS Pathog*, 9, e1003312.
- PANAS, M. D., AHOLA, T. & MCINERNEY, G. M. 2014. The C-terminal repeat domains of nsP3 from the Old World alphaviruses bind directly to G3BP. *J Virol*, 88, 5888-93.
- PANAS, M. D., SCHULTE, T., THAA, B., SANDALOVA, T., KEDERSHA, N., ACHOUR, A. & MCINERNEY, G. M. 2015. Viral and cellular proteins containing FGDF motifs bind G3BP to block stress granule formation. *PLoS Pathog*, 11, e1004659.
- PANNING, M., GRYWNA, K., VAN ESBROECK, M., EMMERICH, P. & DROSTEN, C. 2008. Chikungunya fever in travelers returning to Europe from the Indian Ocean region, 2006. *Emerg Infect Dis*, 14, 416-22.
- PARDIGON, N., LENCHES, E. & STRAUSS, J. H. 1993. Multiple binding sites for cellular proteins in the 3' end of Sindbis alphavirus minus-sense RNA. *J Virol*, 67, 5003-11.
- PARDIGON, N. & STRAUSS, J. H. 1992. Cellular proteins bind to the 3' end of Sindbis virus minus-strand RNA. *J Virol*, 66, 1007-15.
- PARK, E. & GRIFFIN, D. E. 2009. Interaction of Sindbis virus non-structural protein 3 with poly(ADP-ribose) polymerase 1 in neuronal cells. *J Gen Virol*, 90, 2073-80.
- PARROTT, M. M., SITARSKI, S. A., ARNOLD, R. J., PICTON, L. K., HILL, R. B. & MUKHOPADHYAY, S. 2009. Role of conserved cysteines in the alphavirus E3 protein. *J Virol*, 83, 2584-91.
- PERERA, R., OWEN, K. E., TELLINGHUISEN, T. L., GORBALENYA, A. E. & KUHN, R. J. 2001. Alphavirus nucleocapsid protein contains a putative coiled coil alpha-helix important for core assembly. *J Virol*, 75, 1-10.
- PFEFFER, M., KINNEY, R. M. & KAADEN, O. R. 1998. The alphavirus 3'-nontranslated region: size heterogeneity and arrangement of repeated sequence elements. *Virology*, 240, 100-8.
- PIERRO, A., LANDINI, M. P., GAIBANI, P., ROSSINI, G., VOCALE, C., FINARELLI, A. C., CAGARELLI, R., SAMBRI, V. & VARANI, S. 2014. A model of laboratory surveillance for neuro-arbovirology applied during 2012 in the Emilia-Romagna region, Italy. *Clin Microbiol Infect*, 20, 672-7.
- PIETILA, M. K., HELLSTROM, K. & AHOLA, T. 2017. Alphavirus polymerase and RNA replication. *Virus Res*, 234, 44-57.
- PLANTE, K., WANG, E., PARTIDOS, C. D., WEGER, J., GORCHAKOV, R., TSETSARKIN, K., BORLAND, E. M., POWERS, A. M., SEYMOUR, R., STINCHCOMB, D. T., OSORIO, J. E., FROLOV, I. & WEAVER, S. C. 2011. Novel chikungunya vaccine candidate with an IRES-based attenuation and host range alteration mechanism. *PLoS Pathog*, 7, e1002142.
- PLETNEV, S. V., ZHANG, W., MUKHOPADHYAY, S., FISHER, B. R., HERNANDEZ, R., BROWN, D. T., BAKER, T. S., ROSSMANN, M. G. & KUHN, R. J. 2001. Locations of carbohydrate sites on alphavirus glycoproteins show that E1 forms an icosahedral scaffold. *Cell*, 105, 127-136.
- POHJALA, L., UTT, A., VARJAK, M., LULLA, A., MERITS, A., AHOLA, T. & TAMMELA, P. 2011. Inhibitors of alphavirus entry and replication identified with a stable Chikungunya replicon cell line and virus-based assays. *PLoS One*, 6, e28923.
- POO, Y. S., RUDD, P. A., GARDNER, J., WILSON, J. A., LARCHER, T., COLLE, M. A., LE, T. T., NAKAYA, H. I., WARRILOW, D., ALLCOCK, R., BIELEFELDT-OHMANN, H., SCHRODER, W. A., KHROMYKH, A. A., LOPEZ, J. A. & SUHRBIER, A. 2014. Multiple immune factors are

- involved in controlling acute and chronic chikungunya virus infection. *PLoS Negl Trop Dis*, 8, e3354.
- POWERS, A. M., BRAULT, A. C., SHIRAKO, Y., STRAUSS, E. G., KANG, W., STRAUSS, J. H. & WEAVER, S. C. 2001. Evolutionary relationships and systematics of the alphaviruses. *J Virol*, 75, 10118-31.
- QI, N., CAI, D., QIU, Y., XIE, J., WANG, Z., SI, J., ZHANG, J., ZHOU, X. & HU, Y. 2011. RNA binding by a novel helical fold of b2 protein from wuhan nodavirus mediates the suppression of RNA interference and promotes b2 dimerization. *J Virol*, 85, 9543-54.
- QUEYRIAUX, B., SIMON, F., GRANDADAM, M., MICHEL, R., TOLOU, H. & BOUTIN, J. P. 2008. Clinical burden of chikungunya virus infection. *Lancet Infect Dis*, 8, 2-3.
- RACK, J. G., PERINA, D. & AHREL, I. 2016. Macrod domains: Structure, Function, Evolution, and Catalytic Activities. *Annu Rev Biochem*, 85, 431-54.
- RAJU, R. & HUANG, H. V. 1991. Analysis of Sindbis virus promoter recognition in vivo, using novel vectors with two subgenomic mRNA promoters. *J Virol*, 65, 2501-10.
- RAMSAUER, K., SCHWAMEIS, M., FIRBAS, C., MULLNER, M., PUTNAK, R. J., THOMAS, S. J., DESPRES, P., TAUBER, E., JILMA, B. & TANGY, F. 2015. Immunogenicity, safety, and tolerability of a recombinant measles-virus-based chikungunya vaccine: a randomised, double-blind, placebo-controlled, active-comparator, first-in-man trial. *Lancet Infect Dis*, 15, 519-27.
- RAMSEY, J. & MUKHOPADHYAY, S. 2017. Disentangling the Frames, the State of Research on the Alphavirus 6K and TF Proteins. *Viruses*, 9.
- RATSITORAHINA, M., HARISOA, J., RATOVONJATO, J., BIACABE, S., REYNES, J. M., ZELLER, H., RAOELINA, Y., TALARMIN, A., RICHARD, V. & LOUIS SOARES, J. 2008. Outbreak of dengue and Chikungunya fevers, Toamasina, Madagascar, 2006. *Emerg Infect Dis*, 14, 1135-7.
- REISINGER, E. C., TSCHISMAROV, R., BEUBLER, E., WIEDERMANN, U., FIRBAS, C., LOEBERMANN, M., PFEIFFER, A., MUELLNER, M., TAUBER, E. & RAMSAUER, K. 2019. Immunogenicity, safety, and tolerability of the measles-vectored chikungunya virus vaccine MV-CHIK: a double-blind, randomised, placebo-controlled and active-controlled phase 2 trial. *Lancet*, 392, 2718-2727.
- REMEYI, R., GAO, Y., HUGHES, R. E., CURD, A., ZOTHNER, C., PECKHAM, M., MERITS, A. & HARRIS, M. 2018. Persistent Replication of a Chikungunya Virus Replicon in Human Cells is Associated with Presence of Stable Cytoplasmic Granules Containing Non-structural Protein 3. *J Virol*.
- REMEYI, R., ROBERTS, G. C., ZOTHNER, C., MERITS, A. & HARRIS, M. 2017. SNAP-tagged Chikungunya Virus Replicons Improve Visualisation of Non-Structural Protein 3 by Fluorescence Microscopy. *Sci Rep*, 7, 5682.
- RENAULT, P., BALLEYDIER, E., D'ORTENZIO, E., BAVILLE, M. & FILLEUL, L. 2012. Epidemiology of Chikungunya infection on Reunion Island, Mayotte, and neighboring countries. *Med Mal Infect*, 42, 93-101.
- RENAULT, P., SOLET, J. L., SISSOKO, D., BALLEYDIER, E., LARRIEU, S., FILLEUL, L., LASSALLE, C., THIRIA, J., RACHOU, E., DE VALK, H., ILEF, D., LEDRANS, M., QUATRESOUS, I., QUENEL, P. & PIERRE, V. 2007. A major epidemic of chikungunya virus infection on Reunion Island, France, 2005-2006. *Am J Trop Med Hyg*, 77, 727-31.
- REYES-SANDOVAL, A. 2019. 51 years in of Chikungunya clinical vaccine development: A historical perspective. *Hum Vaccin Immunother*.
- RIKKONEN, M., PERANEN, J. & KAARIAINEN, L. 1994. ATPase and GTPase activities associated with Semliki Forest virus nonstructural protein nsP2. *J Virol*, 68, 5804-10.
- ROBERTS, G. C., ZOTHNER, C., REMEYI, R., MERITS, A., STONEHOUSE, N. J. & HARRIS, M. 2017. Evaluation of a range of mammalian and mosquito cell lines for use in Chikungunya virus research. *Sci Rep*, 7, 14641.

- ROBIN, S., RAMFUL, D., ZETTOR, J., BENHAMOU, L., JAFFAR-BANDJEE, M. C., RIVIERE, J. P., MARICHY, J., EZZEDINE, K. & ALESSANDRI, J. L. 2010. Severe bullous skin lesions associated with Chikungunya virus infection in small infants. *Eur J Pediatr*, 169, 67-72.
- ROBINSON, M. C. 1955. An epidemic of virus disease in Southern Province, Tanganyika Territory, in 1952-53. I. Clinical features. *Trans R Soc Trop Med Hyg*, 49, 28-32.
- ROSS-THRIEPLAND, D. & HARRIS, M. 2014. Insights into the complexity and functionality of hepatitis C virus NS5A phosphorylation. *J Virol*, 88, 1421-32.
- ROZANOV, M. N., KOONIN, E. V. & GORBALENYA, A. E. 1992. Conservation of the putative methyltransferase domain: a hallmark of the 'Sindbis-like' supergroup of positive-strand RNA viruses. *J Gen Virol*, 73 (Pt 8), 2129-34.
- RUBACH, J. K., WASIK, B. R., RUPP, J. C., KUHN, R. J., HARDY, R. W. & SMITH, J. L. 2009. Characterization of purified Sindbis virus nsP4 RNA-dependent RNA polymerase activity in vitro. *Virology*, 384, 201-8.
- RUDD, P. A., WILSON, J., GARDNER, J., LARCHER, T., BABARIT, C., LE, T. T., ANRAKU, I., KUMAGAI, Y., LOO, Y. M., GALE, M., JR., AKIRA, S., KHROMYKH, A. A. & SUHRBIER, A. 2012. Interferon response factors 3 and 7 protect against Chikungunya virus hemorrhagic fever and shock. *J Virol*, 86, 9888-98.
- RUPP, J. C., JUNDT, N. & HARDY, R. W. 2011. Requirement for the amino-terminal domain of sindbis virus nsP4 during virus infection. *J Virol*, 85, 3449-60.
- RUPP, J. C., SOKOLOSKI, K. J., GEBHART, N. N. & HARDY, R. W. 2015. Alphavirus RNA synthesis and non-structural protein functions. *J Gen Virol*, 96, 2483-500.
- RUSSO, A. T., WHITE, M. A. & WATOWICH, S. J. 2006. The crystal structure of the Venezuelan equine encephalitis alphavirus nsP2 protease. *Structure*, 14, 1449-58.
- SAGO, N., OMI, K., TAMURA, Y., KUNUGI, H., TOYO-OKA, T., TOKUNAGA, K. & HOHJOH, H. 2004. RNAi induction and activation in mammalian muscle cells where Dicer and eIF2C translation initiation factors are barely expressed. *Biochem Biophys Res Commun*, 319, 50-7.
- SALMINEN, A., WAHLBERG, J. M., LOBIGS, M., LILJESTROM, P. & GAROFF, H. 1992. Membrane fusion process of Semliki Forest virus. II: Cleavage-dependent reorganization of the spike protein complex controls virus entry. *J Cell Biol*, 116, 349-57.
- SALONEN, A., VASILJEVA, L., MERITS, A., MAGDEN, J., JOKITALO, E. & KAARIAINEN, L. 2003. Properly folded nonstructural polyprotein directs the semliki forest virus replication complex to the endosomal compartment. *J Virol*, 77, 1691-702.
- SANCHEZ-VARGAS, I., SCOTT, J. C., POOLE-SMITH, B. K., FRANZ, A. W., BARBOSA-SOLOMIEU, V., WILUSZ, J., OLSON, K. E. & BLAIR, C. D. 2009. Dengue virus type 2 infections of *Aedes aegypti* are modulated by the mosquito's RNA interference pathway. *PLoS Pathog*, 5, e1000299.
- SANDERS, H. R., FOY, B. D., EVANS, A. M., ROSS, L. S., BEATY, B. J., OLSON, K. E. & GILL, S. S. 2005. Sindbis virus induces transport processes and alters expression of innate immunity pathway genes in the midgut of the disease vector, *Aedes aegypti*. *Insect Biochem Mol Biol*, 35, 1293-307.
- SAWICKI, D. L., SAWICKI, S. G., KERANEN, S. & KAARIAINEN, L. 1981a. Specific Sindbis virus-coded function for minus-strand RNA synthesis. *J Virol*, 39, 348-58.
- SAWICKI, S. G., SAWICKI, D. L., KAARIAINEN, L. & KERANEN, S. 1981b. A Sindbis virus mutant temperature-sensitive in the regulation of minus-strand RNA synthesis. *Virology*, 115, 161-72.
- SAXTON-SHAW, K. D., LEDERMANN, J. P., BORLAND, E. M., STOVALL, J. L., MOSSEL, E. C., SINGH, A. J., WILUSZ, J. & POWERS, A. M. 2013. O'nyong nyong virus molecular determinants of unique vector specificity reside in non-structural protein 3. *PLoS Negl Trop Dis*, 7, e1931.

- SCHILTE, C., BUCKWALTER, M. R., LAIRD, M. E., DIAMOND, M. S., SCHWARTZ, O. & ALBERT, M. L. 2012. Cutting edge: independent roles for IRF-3 and IRF-7 in hematopoietic and nonhematopoietic cells during host response to Chikungunya infection. *J Immunol*, 188, 2967-71.
- SCHILTE, C., STAIKOWSKY, F., COUDERC, T., MADEC, Y., CARPENTIER, F., KASSAB, S., ALBERT, M. L., LECUIT, M. & MICHAULT, A. 2013. Chikungunya virus-associated long-term arthralgia: a 36-month prospective longitudinal study. *PLoS Negl Trop Dis*, 7, e2137.
- SCHLUCKEBIER, G., O'GARA, M., SAENGER, W. & CHENG, X. 1995. Universal catalytic domain structure of AdoMet-dependent methyltransferases. *J Mol Biol*, 247, 16-20.
- SCHUFFENECKER, I., ITEMAN, I., MICHAULT, A., MURRI, S., FRANGEUL, L., VANEY, M. C., LAVENIR, R., PARDIGON, N., REYNES, J. M., PETTINELLI, F., BISCORNET, L., DIANCOURT, L., MICHEL, S., DUQUERROY, S., GUIGON, G., FRENKIEL, M. P., BREHIN, A. C., CUBITO, N., DESPRES, P., KUNST, F., REY, F. A., ZELLER, H. & BRISSSE, S. 2006. Genome microevolution of chikungunya viruses causing the Indian Ocean outbreak. *PLoS Med*, 3, e263.
- SCHULTE, T., LIU, L., PANAS, M. D., THAA, B., DICKSON, N., GOTTE, B., ACHOUR, A. & MCINERNEY, G. M. 2016. Combined structural, biochemical and cellular evidence demonstrates that both FGDF motifs in alphavirus nsP3 are required for efficient replication. *Open Biol*, 6.
- SCHWARTZ, O. & ALBERT, M. L. 2010. Biology and pathogenesis of chikungunya virus. *Nat Rev Microbiol*, 8, 491-500.
- SEFTON, B. M. 1977. Immediate glycosylation of Sindbis virus membrane proteins. *Cell*, 10, 659-68.
- SHAH, K. V., GIBBS, C. J., JR. & BANERJEE, G. 1964. Virological Investigation of the Epidemic of Haemorrhagic Fever in Calcutta: Isolation of Three Strains of Chikungunya Virus. *Indian J Med Res*, 52, 676-83.
- SHIN, G., YOST, S. A., MILLER, M. T., ELROD, E. J., GRAKOU, A. & MARCOTRIGIANO, J. 2012. Structural and functional insights into alphavirus polyprotein processing and pathogenesis. *Proc Natl Acad Sci U S A*, 109, 16534-9.
- SHIRAKO, Y., STRAUSS, E. G. & STRAUSS, J. H. 2000. Suppressor mutations that allow sindbis virus RNA polymerase to function with nonaromatic amino acids at the N-terminus: evidence for interaction between nsP1 and nsP4 in minus-strand RNA synthesis. *Virology*, 276, 148-60.
- SHIRAKO, Y., STRAUSS, E. G. & STRAUSS, J. H. 2003. Modification of the 5' terminus of Sindbis virus genomic RNA allows nsP4 RNA polymerases with nonaromatic amino acids at the N terminus to function in RNA replication. *J Virol*, 77, 2301-9.
- SHIRAKO, Y. & STRAUSS, J. H. 1990. Cleavage between nsP1 and nsP2 initiates the processing pathway of Sindbis virus nonstructural polyprotein P123. *Virology*, 177, 54-64.
- SHIRAKO, Y. & STRAUSS, J. H. 1994. Regulation of Sindbis virus RNA replication: uncleaved P123 and nsP4 function in minus-strand RNA synthesis, whereas cleaved products from P123 are required for efficient plus-strand RNA synthesis. *J Virol*, 68, 1874-85.
- SHIRAKO, Y. & STRAUSS, J. H. 1998. Requirement for an aromatic amino acid or histidine at the N terminus of Sindbis virus RNA polymerase. *J Virol*, 72, 2310-5.
- SIMMONS, D. T. & STRAUSS, J. H. 1972a. Replication of Sindbis virus. I. Relative size and genetic content of 26 s and 49 s RNA. *J Mol Biol*, 71, 599-613.
- SIMMONS, D. T. & STRAUSS, J. H. 1972b. Replication of Sindbis virus. II. Multiple forms of double-stranded RNA isolated from infected cells. *J Mol Biol*, 71, 615-31.
- SIMON, F., PAROLA, P., GRANDADAM, M., FOURCADE, S., OLIVER, M., BROUQUI, P., HANCE, P., KRAEMER, P., ALI MOHAMED, A., DE LAMBALLERIE, X., CHARREL, R. & TOLOU, H. 2007. Chikungunya infection: an emerging rheumatism among travelers returned from Indian Ocean islands. Report of 47 cases. *Medicine (Baltimore)*, 86, 123-37.

- SINGH, G., POPLI, S., HARI, Y., MALHOTRA, P., MUKHERJEE, S. & BHATNAGAR, R. K. 2009. Suppression of RNA silencing by Flock house virus B2 protein is mediated through its interaction with the PAZ domain of Dicer. *FASEB J*, 23, 1845-57.
- SINGH, I. & HELENIUS, A. 1992. Role of ribosomes in Semliki Forest virus nucleocapsid uncoating. *J Virol*, 66, 7049-58.
- SISSOKO, D., MALVY, D., EZZEDINE, K., RENAULT, P., MOSCETTI, F., LEDRANS, M. & PIERRE, V. 2009. Post-epidemic Chikungunya disease on Reunion Island: course of rheumatic manifestations and associated factors over a 15-month period. *PLoS Negl Trop Dis*, 3, e389.
- SISSOKO, D., MOENDANDZE, A., MALVY, D., GIRY, C., EZZEDINE, K., SOLET, J. L. & PIERRE, V. 2008. Seroprevalence and risk factors of chikungunya virus infection in Mayotte, Indian Ocean, 2005-2006: a population-based survey. *PLoS One*, 3, e3066.
- SMITH, A. L. & TIGNOR, G. H. 1980. Host cell receptors for two strains of Sindbis virus. *Arch Virol*, 66, 11-26.
- SOKOLOSKI, K. J., DICKSON, A. M., CHASKEY, E. L., GARNEAU, N. L., WILUSZ, C. J. & WILUSZ, J. 2010. Sindbis virus usurps the cellular HuR protein to stabilize its transcripts and promote productive infections in mammalian and mosquito cells. *Cell Host Microbe*, 8, 196-207.
- SOKOLOSKI, K. J., HAIST, K. C., MORRISON, T. E., MUKHOPADHYAY, S. & HARDY, R. W. 2015. Noncapped Alphavirus Genomic RNAs and Their Role during Infection. *J Virol*, 89, 6080-92.
- SOLIGNAT, M., GAY, B., HIGGS, S., BRIANT, L. & DEVAUX, C. 2009. Replication cycle of chikungunya: a re-emerging arbovirus. *Virology*, 393, 183-97.
- SOURISSEAU, M., SCHILTE, C., CASARTELLI, N., TROUILLET, C., GUIVEL-BENHASSINE, F., RUDNICKA, D., SOL-FOULON, N., LE ROUX, K., PREVOST, M. C., FSIHI, H., FRENKIEL, M. P., BLANCHET, F., AFONSO, P. V., CECCALDI, P. E., OZDEN, S., GESSAIN, A., SCHUFFENECKER, I., VERHASSELT, B., ZAMBORLINI, A., SAIB, A., REY, F. A., ARENZANA-SEISDEDOS, F., DESPRES, P., MICHAULT, A., ALBERT, M. L. & SCHWARTZ, O. 2007. Characterization of reemerging chikungunya virus. *PLoS Pathog*, 3, e89.
- SUUUL, P., BALISTRERI, G., KAARIANEN, L. & AHOLA, T. 2010. Phosphatidylinositol 3-kinase-, actin-, and microtubule-dependent transport of Semliki Forest Virus replication complexes from the plasma membrane to modified lysosomes. *J Virol*, 84, 7543-57.
- SUUUL, P., SALONEN, A., MERITS, A., JOKITALO, E., KAARIANEN, L. & AHOLA, T. 2007. Role of the amphipathic peptide of Semliki forest virus replicase protein nsP1 in membrane association and virus replication. *J Virol*, 81, 872-83.
- STAPLES, J. E., BREIMAN, R. F. & POWERS, A. M. 2009. Chikungunya fever: an epidemiological review of a re-emerging infectious disease. *Clin Infect Dis*, 49, 942-8.
- STRAUSS, E. G., DE GROOT, R. J., LEVINSON, R. & STRAUSS, J. H. 1992. Identification of the active site residues in the nsP2 proteinase of Sindbis virus. *Virology*, 191, 932-40.
- STRAUSS, E. G., LEVINSON, R., RICE, C. M., DALRYMPLE, J. & STRAUSS, J. H. 1988. Nonstructural proteins nsP3 and nsP4 of Ross River and O'Nyong-nyong viruses: sequence and comparison with those of other alphaviruses. *Virology*, 164, 265-74.
- STRAUSS, E. G., RICE, C. M. & STRAUSS, J. H. 1983. Sequence coding for the alphavirus nonstructural proteins is interrupted by an opal termination codon. *Proc Natl Acad Sci U S A*, 80, 5271-5.
- STRAUSS, E. G., RICE, C. M. & STRAUSS, J. H. 1984. Complete nucleotide sequence of the genomic RNA of Sindbis virus. *Virology*, 133, 92-110.
- STRAUSS, J. H. & STRAUSS, E. G. 1994. The alphaviruses: gene expression, replication, and evolution. *Microbiol Rev*, 58, 491-562.
- SUHRBIER, A., JAFFAR-BANDJEE, M. C. & GASQUE, P. 2012. Arthritogenic alphaviruses--an overview. *Nat Rev Rheumatol*, 8, 420-9.

- SUMPTER, R., JR., LOO, Y. M., FOY, E., LI, K., YONEYAMA, M., FUJITA, T., LEMON, S. M. & GALE, M., JR. 2005. Regulating intracellular antiviral defense and permissiveness to hepatitis C virus RNA replication through a cellular RNA helicase, RIG-I. *J Virol*, 79, 2689-2699.
- SUOMALAINEN, M., LILJESTROM, P. & GAROFF, H. 1992. Spike protein-nucleocapsid interactions drive the budding of alphaviruses. *J Virol*, 66, 4737-47.
- SUOPANKI, J., SAWICKI, D. L., SAWICKI, S. G. & KAARIAINEN, L. 1998. Regulation of alphavirus 26S mRNA transcription by replicase component nsP2. *J Gen Virol*, 79 (Pt 2), 309-19.
- SUTHAR, M. S., SHABMAN, R., MADRIC, K., LAMBETH, C. & HEISE, M. T. 2005. Identification of adult mouse neurovirulence determinants of the Sindbis virus strain AR86. *J Virol*, 79, 4219-28.
- TALARMIN, F., STAIKOWSKY, F., SCHOENLAUB, P., RISBOURG, A., NICOLAS, X., ZAGNOLI, A. & BOYER, P. 2007. [Skin and mucosal manifestations of chikungunya virus infection in adults in Reunion Island]. *Med Trop (Mars)*, 67, 167-73.
- TAMANINI, F., BONTEKOE, C., BAKKER, C. E., VAN UNEN, L., ANAR, B., WILLEMSSEN, R., YOSHIDA, M., GALJAARD, H., OOSTRA, B. A. & HOOGEVEEN, A. T. 1999. Different targets for the fragile X-related proteins revealed by their distinct nuclear localizations. *Hum Mol Genet*, 8, 863-9.
- TAMANINI, F., KIRKPATRICK, L. L., SCHONKEREN, J., VAN UNEN, L., BONTEKOE, C., BAKKER, C., NELSON, D. L., GALJAARD, H., OOSTRA, B. A. & HOOGEVEEN, A. T. 2000. The fragile X-related proteins FXR1P and FXR2P contain a functional nucleolar-targeting signal equivalent to the HIV-1 regulatory proteins. *Hum Mol Genet*, 9, 1487-93.
- TAUBITZ, W., CRAMER, J. P., KAPAUN, A., PFEFFER, M., DROSTEN, C., DOBLER, G., BURCHARD, G. D. & LOSCHER, T. 2007. Chikungunya fever in travelers: clinical presentation and course. *Clin Infect Dis*, 45, e1-4.
- TELLINGHUISEN, T. L. & KUHN, R. J. 2000. Nucleic acid-dependent cross-linking of the nucleocapsid protein of Sindbis virus. *J Virol*, 74, 4302-9.
- TOMAR, S., HARDY, R. W., SMITH, J. L. & KUHN, R. J. 2006. Catalytic core of alphavirus nonstructural protein nsP4 possesses terminal adenylyltransferase activity. *J Virol*, 80, 9962-9.
- TROBAUGH, D. W., GARDNER, C. L., SUN, C., HADDOW, A. D., WANG, E., CHAPNIK, E., MILDNER, A., WEAVER, S. C., RYMAN, K. D. & KLIMSTRA, W. B. 2014. RNA viruses can hijack vertebrate microRNAs to suppress innate immunity. *Nature*, 506, 245-8.
- TUCKER, P. C. & GRIFFIN, D. E. 1991. Mechanism of altered Sindbis virus neurovirulence associated with a single-amino-acid change in the E2 Glycoprotein. *J Virol*, 65, 1551-7.
- TUITTILA, M. & HINKKANEN, A. E. 2003. Amino acid mutations in the replicase protein nsP3 of Semliki Forest virus cumulatively affect neurovirulence. *J Gen Virol*, 84, 1525-33.
- TUITTILA, M. T., SANTAGATI, M. G., ROYTITA, M., MAATTA, J. A. & HINKKANEN, A. E. 2000. Replicase complex genes of Semliki Forest virus confer lethal neurovirulence. *J Virol*, 74, 4579-89.
- UMBACH, J. L. & CULLEN, B. R. 2009. The role of RNAi and microRNAs in animal virus replication and antiviral immunity. *Genes Dev*, 23, 1151-64.
- VAN DER HEIJDEN, M. W. & BOL, J. F. 2002. Composition of alphavirus-like replication complexes: involvement of virus and host encoded proteins. *Arch Virol*, 147, 875-98.
- VAN MIERLO, J. T., OVERHEUL, G. J., OBADIA, B., VAN CLEEF, K. W., WEBSTER, C. L., SALEH, M. C., OBBARD, D. J. & VAN RIJ, R. P. 2014. Novel Drosophila viruses encode host-specific suppressors of RNAi. *PLoS Pathog*, 10, e1004256.
- VAN RIJ, R. P., SALEH, M. C., BERRY, B., FOO, C., HOUK, A., ANTONIEWSKI, C. & ANDINO, R. 2006. The RNA silencing endonuclease Argonaute 2 mediates specific antiviral immunity in *Drosophila melanogaster*. *Genes Dev*, 20, 2985-95.
- VANLANDINGHAM, D. L., HONG, C., KLINGLER, K., TSETSARKIN, K., MCELROY, K. L., POWERS, A. M., LEHANE, M. J. & HIGGS, S. 2005. Differential infectivities of o'nyong-nyong and

- chikungunya virus isolates in *Anopheles gambiae* and *Aedes aegypti* mosquitoes. *Am J Trop Med Hyg*, 72, 616-21.
- VARJAK, M., ZUSINAITE, E. & MERITS, A. 2010. Novel functions of the alphavirus nonstructural protein nsP3 C-terminal region. *J Virol*, 84, 2352-64.
- VASILAKIS, N., DEARDORFF, E. R., KENNEY, J. L., ROSSI, S. L., HANLEY, K. A. & WEAVER, S. C. 2009. Mosquitoes put the brake on arbovirus evolution: experimental evolution reveals slower mutation accumulation in mosquito than vertebrate cells. *PLoS Pathog*, 5, e1000467.
- VASILJEVA, L., MERITS, A., AUVINEN, P. & KAARIAINEN, L. 2000. Identification of a novel function of the alphavirus capping apparatus. RNA 5'-triphosphatase activity of Nsp2. *J Biol Chem*, 275, 17281-7.
- VASILJEVA, L., MERITS, A., GOLUBTSOV, A., SIZEMSKAJA, V., KAARIAINEN, L. & AHOLA, T. 2003. Regulation of the sequential processing of Semliki Forest virus replicase polyprotein. *J Biol Chem*, 278, 41636-45.
- VIHINEN, H., AHOLA, T., TUUTTILA, M., MERITS, A. & KAARIAINEN, L. 2001. Elimination of phosphorylation sites of Semliki Forest virus replicase protein nsP3. *J Biol Chem*, 276, 5745-52.
- VIHINEN, H. & SAARINEN, J. 2000. Phosphorylation site analysis of Semliki forest virus nonstructural protein 3. *J Biol Chem*, 275, 27775-83.
- VOINNET, O., PINTO, Y. M. & BAULCOMBE, D. C. 1999. Suppression of gene silencing: a general strategy used by diverse DNA and RNA viruses of plants. *Proc Natl Acad Sci U S A*, 96, 14147-52.
- VOLK, S. M., CHEN, R., TSETSARKIN, K. A., ADAMS, A. P., GARCIA, T. I., SALL, A. A., NASAR, F., SCHUH, A. J., HOLMES, E. C., HIGGS, S., MAHARAJ, P. D., BRAULT, A. C. & WEAVER, S. C. 2010. Genome-scale phylogenetic analyses of chikungunya virus reveal independent emergences of recent epidemics and various evolutionary rates. *J Virol*, 84, 6497-504.
- VOSS, J. E., VANEY, M. C., DUQUERROY, S., VONRHEIN, C., GIRARD-BLANC, C., CRUBLET, E., THOMPSON, A., BRICOGNE, G. & REY, F. A. 2010. Glycoprotein organization of Chikungunya virus particles revealed by X-ray crystallography. *Nature*, 468, 709-12.
- WAHID, B., ALI, A., RAFIQUE, S. & IDREES, M. 2017. Global expansion of chikungunya virus: mapping the 64-year history. *Int J Infect Dis*, 58, 69-76.
- WAHLBERG, J. M., BRON, R., WILSCHUT, J. & GAROFF, H. 1992. Membrane fusion of Semliki Forest virus involves homotrimers of the fusion protein. *J Virol*, 66, 7309-18.
- WAITE, M. R., LUBIN, M., JONES, K. J. & BOSE, H. R. 1974. Phosphorylated proteins of Sindbis virus. *J Virol*, 13, 244-6.
- WANG, K. S., KUHN, R. J., STRAUSS, E. G., OU, S. & STRAUSS, J. H. 1992. High-affinity laminin receptor is a receptor for Sindbis virus in mammalian cells. *J Virol*, 66, 4992-5001.
- WANG, Y. F., SAWICKI, S. G. & SAWICKI, D. L. 1991. Sindbis virus nsP1 functions in negative-strand RNA synthesis. *J Virol*, 65, 985-8.
- WANG, Y. F., SAWICKI, S. G. & SAWICKI, D. L. 1994. Alphavirus nsP3 functions to form replication complexes transcribing negative-strand RNA. *J Virol*, 68, 6466-75.
- WENGLER, G., KOSCHINSKI, A., WENGLER, G. & DREYER, F. 2003. Entry of alphaviruses at the plasma membrane converts the viral surface proteins into an ion-permeable pore that can be detected by electrophysiological analyses of whole-cell membrane currents. *J Gen Virol*, 84, 173-81.
- WERNEKE, S. W., SCHILTE, C., ROHATGI, A., MONTE, K. J., MICHAULT, A., ARENZANA-SEISDEDOS, F., VANLANDINGHAM, D. L., HIGGS, S., FONTANET, A., ALBERT, M. L. & LENSCHOW, D. J. 2011. ISG15 is critical in the control of Chikungunya virus infection independent of Ube1L mediated conjugation. *PLoS Pathog*, 7, e1002322.

- WHITE, L. J., WANG, J. G., DAVIS, N. L. & JOHNSTON, R. E. 2001. Role of alpha/beta interferon in Venezuelan equine encephalitis virus pathogenesis: effect of an attenuating mutation in the 5' untranslated region. *J Virol*, 75, 3706-18.
- WIELGOSZ, M. M., RAJU, R. & HUANG, H. V. 2001. Sequence requirements for Sindbis virus subgenomic mRNA promoter function in cultured cells. *J Virol*, 75, 3509-19.
- WINTACHAI, P., WIKAN, N., KUADKITKAN, A., JAIMIPUK, T., UBOL, S., PULMANAUSAHAKUL, R., AUEWARAKUL, P., KASINRERK, W., WENG, W. Y., PANYASRIVANIT, M., PAEMANEE, A., KITTISENACHAI, S., ROYTRAKUL, S. & SMITH, D. R. 2012. Identification of prohibitin as a Chikungunya virus receptor protein. *J Med Virol*, 84, 1757-70.
- WOOD, K. V., DE WET, J. R., DEWJI, N. & DELUCA, M. 1984. Synthesis of active firefly luciferase by in vitro translation of RNA obtained from adult lanterns. *Biochem Biophys Res Commun*, 124, 592-6.
- WU, P., BRASSEUR, M. & SCHINDLER, U. 1997. A high-throughput STAT binding assay using fluorescence polarization. *Anal Biochem*, 249, 29-36.
- WU, S. R., HAAG, L., SJOBERG, M., GAROFF, H. & HAMMAR, L. 2008. The dynamic envelope of a fusion class II virus. E3 domain of glycoprotein E2 precursor in Semliki Forest virus provides a unique contact with the fusion protein E1. *J Biol Chem*, 283, 26452-60.
- YACTAYO, S., STAPLES, J. E., MILLOT, V., CIBRELUS, L. & RAMON-PARDO, P. 2016. Epidemiology of Chikungunya in the Americas. *J Infect Dis*, 214, S441-S445.
- YIN, C., GOONAWARDANE, N., STEWART, H. & HARRIS, M. 2018. A role for domain I of the hepatitis C virus NS5A protein in virus assembly. *PLoS Pathog*, 14, e1006834.
- ZHANG, R., KIM, A. S., FOX, J. M., NAIR, S., BASORE, K., KLIMSTRA, W. B., RIMKUNAS, R., FONG, R. H., LIN, H., PODDAR, S., CROWE, J. E., JR., DORANZ, B. J., FREMONT, D. H. & DIAMOND, M. S. 2018. Mxra8 is a receptor for multiple arthritogenic alphaviruses. *Nature*, 557, 570-574.
- ZHANG, W., MUKHOPADHYAY, S., PLETNEV, S. V., BAKER, T. S., KUHN, R. J. & ROSSMANN, M. G. 2002. Placement of the structural proteins in Sindbis virus. *J Virol*, 76, 11645-58.
- ZUSINAITE, E., TINTS, K., KIIVER, K., SPUUL, P., KARO-ASTOVER, L., MERITS, A. & SARAND, I. 2007. Mutations at the palmitoylation site of non-structural protein nsP1 of Semliki Forest virus attenuate virus replication and cause accumulation of compensatory mutations. *J Gen Virol*, 88, 1977-85.

Appendix

Appendix Figure 9.1 Alignment of full AUD amino acid sequences among different alphaviruses.

The image shows a sequence alignment of full AUD amino acid sequences for various alphaviruses. The sequences are listed on the left, with their corresponding amino acid sequences on the right. The sequences are highly conserved, with only minor differences observed between different strains. The alignment is shown in a standard format, with the amino acid sequences aligned vertically. The sequences are: SINV-HRE16, SINV-XJ-160, Ockelbo, MNV-56650, CHIKV-3462, CHIKV-99659, CHIKV-1nDRE-4CHIK, CHIKV-1nDRE-S1CHIK, CHIKV-PE1160-H803609, CHIKV-TR206/H804187, CHIKV-H129, CHIKV-5THM601, CHIKV-5THM602, CHIKV-BH13745/H804709, CHIKV-60115, CHIKV-R91064, CHIKV-HV/08/065, CHIKV-HV/08/068, CHIKV-Com5, CHIKV-T10-06-6uJ, CHIKV-5UK0P09, CHIKV-H0603310_KH11_B7B, CHIKV-LR2006_OPY1, RVV, SFV-A7, SFV-L10, VEEV-TC83, FMV-CM4-146, EEEV-PE6, HighLands-3-virus-B-230, MEEV, SINV-HRE16, SINV-XJ-160, Ockelbo, MNV-56650, CHIKV-3462, CHIKV-99659, CHIKV-1nDRE-4CHIK, CHIKV-1nDRE-S1CHIK, CHIKV-PE1160-H803609, CHIKV-TR206/H804187, CHIKV-H129, CHIKV-5THM601, CHIKV-5THM602, CHIKV-BH13745/H804709, CHIKV-60115, CHIKV-R91064, CHIKV-HV/08/065, CHIKV-HV/08/068, CHIKV-Com5, CHIKV-T10-06-6uJ, CHIKV-5UK0P09, CHIKV-H0603310_KH11_B7B, CHIKV-LR2006_OPY1, RVV, SFV-A7, SFV-L10, VEEV-TC83, FMV-CM4-146, EEEV-PE6, HighLands-3-virus-B-230, MEEV, SINV-HRE16, SINV-XJ-160, Ockelbo, MNV-56650, CHIKV-3462, CHIKV-99659, CHIKV-1nDRE-4CHIK, CHIKV-1nDRE-S1CHIK, CHIKV-PE1160-H803609, CHIKV-TR206/H804187, CHIKV-H129, CHIKV-5THM601, CHIKV-5THM602, CHIKV-BH13745/H804709, CHIKV-60115, CHIKV-R91064, CHIKV-HV/08/065, CHIKV-HV/08/068, CHIKV-Com5, CHIKV-T10-06-6uJ, CHIKV-5UK0P09, CHIKV-H0603310_KH11_B7B, CHIKV-LR2006_OPY1, RVV, SFV-A7, SFV-L10, VEEV-TC83, FMV-CM4-146, EEEV-PE6, HighLands-3-virus-B-230, MEEV.

Appendix Figure 9.1 Alignment of full AUD amino acid sequences among different alphaviruses.

Replicons	
Mutants	Backbones
WT	pcDNA3.1 (+), CHIKV-D-Luc-SGR, ICRES, ICRES-nsP3-TST, ICRES-nsP3-ZsGreen
GAA	CHIKV-D-Luc-SGR, ICRES
M219A	pcDNA3.1 (+), CHIKV-D-Luc-SGR, ICRES
E225A	pcDNA3.1 (+), CHIKV-D-Luc-SGR, ICRES
R243A/K245A	pcDNA3.1 (+), CHIKV-D-Luc-SGR, ICRES
P247A/V248A	pcDNA3.1 (+), CHIKV-D-Luc-SGR, ICRES, ICRES-nsP3-TST, ICRES-nsP3-ZsGreen
D249A	pcDNA3.1 (+), CHIKV-D-Luc-SGR
V260A/P261A	pcDNA3.1 (+), CHIKV-D-Luc-SGR
C262A/C264A	pcDNA3.1 (+), CHIKV-D-Luc-SGR
Y324A	pcDNA3.1 (+), CHIKV-D-Luc-SGR
Atru-1-12	CHIKV-D-Luc-SGR
Constructs	
Plasmids for transcription of 3'UTR, 5'UTR, subgenomic promoter	pcDNA3.1-3'UTR, pcDNA3.1-5'UTR, pcDNA3.1-sgProm ⁺
Plasmids for AUD/nsP3 expression	pET28a-SUMO-AUD, pGEX6P-2-AUD, pcDNA3.1-AUD, pcDNA3.1-nsP3, pEGFP-N1-AUD, pEGFP-N1-nsP3
Plasmids for RNAi suppression detection	pMKO.1-GFP, pMKO.1-GFP-siGFP
Plasmids for expression of Dicer	pDESTmycDicer

Appendix Table 9.1 List of constructs generated and used throughout this study.

Appendix

Mutants		Site-directed mutagenesis (Quickchange or Q5)
M219A	Forward	GAGATACATACTGCATGGCCAAAGCAA
	Reverse	TTGCTTTGGCCATGCAGTATGTATCTC
E225A	Forward	CCAAAGCAAACAGCAGCCAATGAGCAA
	Reverse	TTGCTCATTGGCTGCTGTTTGGCTTTGG
R243A	Forward	ATTGAATCGATCGCACAGAAATGCCCG
	Reverse	CGGGCATTCTGTGCGATCGATTCAAT
K245A	Forward	AGTATTGAATCGATCAGGCAGGCATGC
	Reverse	GCATGCCTGCCTGATCGATTCAATACT
R243A/K245A	Forward	GAATCGATCGCGCAGGCATGCCCGGTG
	Reverse	CACCGGCATGCCTGCGCGATCGATTTC
P247A	Forward	AGGCAGAAATGCGCCGTGGATGATGCA
	Reverse	TGCATCATCCACGGCGCATTCTGCCT
V248A	Forward	CAGAAATGCCCGGGGATGATGCAGAC
	Reverse	GTCTGCATCATCCGCCGGCATTCTG
P247A/V248A	Forward	CAGAAATGCGCGGGGATGATGCAGAC
	Reverse	GTCTGCATCATCCGCCGGCATTCTG
D249A	Forward	CAGAAATGCCCGGGTGGCTGATGCAGAC
	Reverse	GTCTGCATCAGCCACCGGGCATTCTG
V260A/P261A	Forward	CCAAAATGCCCGGTGCCTTTGCCGT
	Reverse	ACGGCAAAGGCACGCGGCAGTTTTGGG
C262A/C264A	Forward	ACTGTCCCGGCCCTTGCACGTTACGCT
	Reverse	AGCGTAACGTGCAAGGGCCGGGACAGT
Y324A	Forward	CGCGTAAGTCCAAGGGAAGCTAGATCT
	Reverse	AGATCTAGCTTCCCTTGGACTTACGCG
GAA	Forward	TTCATCGGCGCCGCAACATAATACATGGA
	Reverse	GGCCGCGCACGCGGATTTTGTC
PCR primers		
Atrun-1	Forward	GCAATCCACGCTGTTGGACCAAACCT
	Reverse	CGCTTGACTATGCGTCAGTGACG
	Reverse-2	TTATTCGAAGTCATGCCACCACTAGTTGTGGATGGCAGCGTGTGTGTCGCTTGACTATGCGTCAGTGA CG
Atrun-2	Forward	GCAATCCACGCTGTTGGACCAAACCT
	Reverse	CGCTAGCATTACCTTAGAGCATT
	Reverse-2	TTATTCGAAGTCATGCCACCACTAGTTGTGGATGGCAGCGTGTGTGTCGCTAGCATTACCTTAGAGCA TT
Atrun-3	Forward	GCAATCCACGCTGTTGGACCAAACCT
	Reverse	CGCAAGCCGGGTGACGCGTTCTG
	Reverse-2	TTATTCGAAGTCATGCCACCACTAGTTGTGGATGGCAGCGTGTGTGTCGCAAGCCGGGTGACGCGTTC TG
Atrun-4	Forward	GCAATCCACGCTGTTGGACCAAACCT
	Reverse	CGCGATCGATTCAATACTTTCCC
	Reverse-2	TTATTCGAAGTCATGCCACCACTAGTTGTGGATGGCAGCGTGTGTGTCGCGATCGATTCAATACTTTCC C
Atrun-5	Forward	GCAATCCACGCTGTTGGACCAAACCT
	Reverse	CGCCTGATGAAAACGGGTCCCTT
	Reverse-2	TTATTCGAAGTCATGCCACCACTAGTTGTGGATGGCAGCGTGTGTGTCGCTGATGAAAACGGGTCCC TT
Atrun-6	Forward	GCAATCCACGCTGTTGGACCAAACCT
	Reverse	CGCATCGCAGTCTATGGAGATGT
	Reverse-2	TTATTCGAAGTCATGCCACCACTAGTTGTGGATGGCAGCGTGTGTGTCGATCGCAGTCTATGGAGAT GT
Atrun-7	Forward	CGACGGATGCAGACGTGGTCTTCGACCTAAGCGTTGATGG
Atrun-7	Reverse	GTCTTCGAAGTCATGCCACCACTAG
Atrun-8	Forward	CGACGGATGCAGACGTGGTCTTCGACCAACGTGCCATC
	Reverse	GTCTTCGAAGTCATGCCACCACTAG
Atrun-9	Forward	CGACGGATGCAGACGTGGTCCGCATGAACCACGTCAACAAG
	Reverse	GTCTTCGAAGTCATGCCACCACTAG
Atrun-10	Forward	CGACGGATGCAGACGTGGTCAGGCAGAAATGCCCGTGGGA
	Reverse	GTCTTCGAAGTCATGCCACCACTAG
Atrun-11	Forward	CGACGGATGCAGACGTGGTCACGGCTGTGGATATGGCGGA
	Reverse	GTCTTCGAAGTCATGCCACCACTAG
Atrun-12	Forward	GTCATTGTTCCGCTGCACCCTGA
	Forward-2	CGACGGATGCAGACGTGGTCATTGTTCCGCTGCACCCTGA
	Reverse	GTCTTCGAAGTCATGCCACCACTAG

Appendix

AUD fragment in pcDNA3.1 for quickchange mutagenesis	Forward	GCAAAGCTTGGGACCCGTTTTTCATCAGAC
	Reverse	GCATCTAGATTCGAAGTCATGCCACCACT
Sequencing for AUD reversion	Forward	AATTGGCAGCTGCCTATCGA
Sequencing for CHIKV whole genome	CF1	AAT TGG CAG CTG CCT ATC GA
	CF3	GCAGACGGATTCTGATGTG
	CF5	TACACCATATTGCGATGCAC
	CF7	CAACTATTAAGGAGTGGGAG
	CF9	GCAGCCTTCGTAGGACAGGT
	CF11	TGCTATTTGACCACAACGTG
	CF13	ACGTCCGATTGTCCAATCCC
	CF15	AAACATCACCATGCCAGCC
	CS1	ATCGATAACGCGGACCTGGC
	CS3	ACCGCAGCACGGTAAAGAGC
	CS5	TAATGAGCGTCGGTGCCAC
	CS7	GCAAGAAAGGCAAGTGTGCG
	CHR2	GCCCACTTACTGAAGGCTTG
	CHR4	TGCCAGATCCCGGTACTCCG
	CHR6	GCCCCTGTCTAGATCCACC
	CHR8	TCCCGTCCCCTTCAAGACTC
	CHR10	CAGGTACGGTGTCTATTACC
	CHR12	GCTGCTGCCAGTACATTCTG
	CHR14	TTAGCGGGTCTGCCACTCTG
	CSR1	GCTCCTCCTAAGACTATGGC
CSR3	GTGACCGCGGCATGACATTG	
CSR5	CGGTGAAGACCTTACAGCTG	
CSR7	CCTCCCGTGATCTTCTGCAC	
CSR8	CATCTCCTACGTCCCTGTGG	
qRT-PCR-nsP3	Forward	GCGCGTAAGTCCAAGGGAAT
	Reverse	AGCATCCAGTCTGACGGG
qRT-PCR-actin	Forward	GGCATGGGTGCAAGGAT T
	Reverse	GGGGTGTGAAGGTCTCAA
pcDNA3.1-nsP3	Forward	CAAGGATCCATGGCACCGTGTACCGGGTAAA
	Reverse	CGAGAATTCTTACCCACCTGCCCTGTCTAGTC
pcDNA3.1-AUD	Forward	CAAGGATCCATGATCTACTGCCGCGACAAAGA
	Reverse	CGAGAATTCTTACCCGTCGTCTAGTGCTGGTT
pEGFP-N1-nsP3	Forward	CAAGAATTCACCATGGCACCGTGTACCGGGTAAA
	Reverse	CAAGGATCCATCCCACCTGCCCTGTCTAGTC
pEGFP-N1-AUD	Forward	CAAGAATTCACCATGATCTACTGCCGCGACAAAGA
	Reverse	CAAGGATCCATCCCCTGTCTAGTGCTGGTT
pET-28a-SUMO-AUD	Forward	GCAGGATCCATGATCTACTGCCGCGACAAAGA
	Reverse	TAGCTCGAGTTACCCGTCGTCTAGTGCTGGTT
pGEX6P-2-AUD	Forward	GCAGGATCCATGATCTACTGCCGCGACAAAGA
	Reverse	TAGCTCGAGTTACCCGTCGTCTAGTGCTGGTT
CHIKV-3'UTR	Forward	GAAGGATCCCTTGACAATTAAGTATGAAG
	Reverse	GCCGATATCTTTTTTTTTTTTTTTTTTTTT
CHIKV-5'UTR	Forward	CATGAATTCATGGCTGCGTGAGACACACG
	Reverse	GCCGGTACCCTTAGCATTAGCATGGTCA
CHIKV-sg Prom	Forward	GTAGAATTCATGGCCACCTTTGCAAGCT
	Reverse	GGCGGATCTGTAGCTGATTAGTGTITAG
DENV NS4B	Forward	TAAGGATCCATGGCAGCAGCGGGCATCATGAA
	Reverse	GCCGAATCTTACCTTCTCGTGTITGTGT

Appendix Table 9.2 List of oligonucleotide primers used in this project.

‘Forward’ and ‘Reverse’ indicate forward primer and reverse primer, respectively.

Appendix

Accession	Description	Abundance Ratio: (TST-WT) / WT	Abundance Ratio: (TST-PV) / WT	Abundance Ratio: (TST-WT) / (TST-PV)
Q9H307	Pinin	100	100	0.064
Q53G35	Phosphoglycerate mutase (Fragment)	100	100	0.042
Q3ZBS7	Uncharacterized protein	100	100	0.089
M0QYS1	60S ribosomal protein L13a (Fragment)	100	100	0.089
Q68DE3	Basic helix-loop-helix domain-containing protein USF3	100	100	0.018
A0A024RDE5	Ras-GTPase activating protein SH3 domain-binding protein 2, isoform CRA_a	10.171	14.304	0.711
Q59EK7	CSODF038Y005 variant (Fragment)	3.444	34.751	0.099
P35527	Keratin, type I cytoskeletal 9	3.331	1.639	2.033
V9HWE9	Epididymis secretory protein Li 22	3.286	100	0.032
A0A024R0E2	Cold shock domain containing E1, RNA-binding, isoform CRA_a	3.028	18.168	0.167
Q6IT96	Histone deacetylase	2.379	13.479	0.177
B1AHD1	NHP2-like protein 1	2.119	5.84	0.363
P39023	60S ribosomal protein L3	2.106	20.682	0.102
Q15181	Inorganic pyrophosphatase	2.006	25.278	0.079

Appendix

A0A087WUZ3	Spectrin beta chain	1.969	14.245	0.138
Q9BRJ6	Uncharacterized protein C7orf50	1.93	15.179	0.127
O60264	SWI/SNF-related matrix-associated actin-dependent regulator of chromatin subfamily A member 5	1.869	17.39	0.107
Q9Y5B9	FACT complex subunit SPT16	1.828	6.932	0.264
P46063	ATP-dependent DNA helicase Q1	1.789	3.578	0.5
B2R6J3	cDNA, FLJ92974	1.76	8.063	0.218
Q8N1N0	C-type lectin domain family 4 member F	1.752	1.98	0.885
Q9NR30	Nucleolar RNA helicase 2	1.741	33.353	0.052
P07737	Profilin-1	1.732	77.868	0.022
B3KMC9	cDNA FLJ10711 fis, clone NT2RP3000917, highly similar to 5'-3' exoribonuclease 2 (EC 3.1.11.-)	1.728	12.888	0.134
F8WAR4	MICOS complex subunit	1.65	5.136	0.321
P42766	60S ribosomal protein L35	1.648	14.056	0.117
E5KSX8	Mitochondrial transcription factor A	1.646	9.934	0.166
A0A1B0GVD3	Protein lin-28 homolog B	1.63	17.777	0.092
A0A0S2Z4Z9	Non-POU domain containing octamer-binding isoform 1 (Fragment)	1.622	20.696	0.078
A0A024QZK8	Heterogeneous nuclear ribonucleoprotein H3 (2H9), isoform CRA_a	1.62	6.715	0.241

Appendix

P05387	60S acidic ribosomal protein P2	1.619	13.634	0.119
B4DJ38	cDNA FLJ56092, highly similar to Pentatricopeptide repeat protein 1	1.594	1.549	1.029
Q9UBS4	DnaJ homolog subfamily B member 11	1.582	2.397	0.66
P50402	Emerin	1.579	2.162	0.731
Q6NTF9	Rhomboid domain-containing protein 2	1.579	1.464	1.079
P02533	Keratin, type I cytoskeletal 14	1.577	0.767	2.055
Q12906	Interleukin enhancer-binding factor 3	1.558	41.368	0.038
P49756	RNA-binding protein 25	1.554	17.294	0.09
Q59GX2	Solute carrier family 2 (Facilitated glucose transporter), member 1 variant (Fragment)	1.549	1.458	1.063
A0A024R8W0	DEAD (Asp-Glu-Ala-Asp) box polypeptide 48, isoform CRA_a	1.533	1.599	0.959
P46459	Vesicle-fusing ATPase	1.529	2.657	0.575
P10620	Microsomal glutathione S-transferase 1	1.527	2.953	0.517
J3KQ32	Obg-like ATPase 1	1.527	28.359	0.054
Q59EL4	PRPF4 protein variant (Fragment)	1.52	7.544	0.201
A0A024RBF6	HCG26523, isoform CRA_a	1.505	18.888	0.08
M0R0R2	40S ribosomal protein S5	1.504	4.624	0.325
A0A0A0MRM9	Nucleolar and coiled-body phosphoprotein 1 (Fragment)	1.504	7.511	0.2

Appendix

Q9Y2W1	Thyroid hormone receptor-associated protein 3	1.497	2.883	0.519
Q15436	Protein transport protein Sec23A	1.493	2.94	0.508
A0A126LB20	Rep	1.47	0.989	1.487
J3KPF3	4F2 cell-surface antigen heavy chain	1.469	1.251	1.174
V9HWC7	Epididymis secretory sperm binding protein Li 128m	1.452	12.968	0.112
E9PNW5	Uncharacterized protein C4orf50	1.45	0.915	1.584
O43776	Asparagine--tRNA ligase, cytoplasmic	1.447	17.8	0.081
A0A024R5Z7	Annexin	1.439	1.813	0.794
Q8TCJ2	Dolichyl-diphosphooligosaccharide--protein glycosyltransferase subunit STT3B	1.436	3.003	0.478
Q04828	Aldo-keto reductase family 1 member C1	1.433	18.161	0.079
Q96CS3	FAS-associated factor 2	1.432	2.602	0.55
Q5VV89	Microsomal glutathione S-transferase 3	1.432	1.502	0.954
Q5QJE6	Deoxynucleotidyltransferase terminal-interacting protein 2	1.431	7.266	0.197
P00387	NADH-cytochrome b5 reductase 3	1.429	9.387	0.152
A0A1W2PP11	Uncharacterized protein	1.421	1.069	1.33
P35908	Keratin, type II cytoskeletal 2 epidermal	1.414	0.704	2.008

Appendix

P27824	Calnexin	1.413	6.865	0.206
P09110	3-ketoacyl-CoA thiolase, peroxisomal	1.407	6.063	0.232
P14625	Endoplasmin	1.406	6.269	0.224
Q4LE48	STAG1 variant protein (Fragment)	1.405	4.466	0.315
A6NCS6	Uncharacterized protein C2orf72	1.395	2.011	0.694
Q9Y277	Voltage-dependent anion- selective channel protein 3	1.384	1.827	0.757
B4DPD5	Ubiquitin thioesterase	1.382	14.03	0.098
Q9Y3U8	60S ribosomal protein L36	1.381	20.436	0.068
P49458	Signal recognition particle 9 kDa protein	1.373	5.949	0.231
Q5T4U5	Acyl-Coenzyme A dehydrogenase, C-4 to C-12 straight chain, isoform CRA_a	1.37	2.765	0.496
H0Y4R2	NADPH--cytochrome P450 reductase (Fragment)	1.369	7.747	0.177
O00425	Insulin-like growth factor 2 mRNA-binding protein 3	1.367	1.841	0.743
Q8IW90	MTCH1 protein (Fragment)	1.366	1.187	1.151
P61513	60S ribosomal protein L37a	1.36	5.469	0.249
A0A024R8D2	Solute carrier family 27 (Fatty acid transporter), member 4, isoform CRA_a	1.351	1.22	1.107
A8K1K8	Chromosome 18 open reading frame 55, isoform CRA_b	1.351	1.74	0.777
Q9Y3I0	tRNA-splicing ligase RtcB	1.349	11.186	0.121

Appendix

	homolog			
P35659	Protein DEK	1.344	4.187	0.321
Q549C5	HCG2010808, isoform CRA_a	1.343	1.245	1.079
H0Y368	Dolichol-phosphate mannosyltransferase subunit 1 (Fragment)	1.338	1.395	0.959
P83731	60S ribosomal protein L24	1.336	12.162	0.11
D3DP46	SPCS3-Signal peptidase complex subunit 3 homolog (S. cerevisiae), isoform CRA_a	1.334	1.055	1.264
B4DR52	Histone H2B	1.333	63.708	0.021
Q16777	Histone H2A type 2-C	1.33	36.97	0.036
Q5BKZ1	DBIRD complex subunit ZNF326	1.329	5.385	0.247
A0A024RBH2	Cytoskeleton-associated protein 4, isoform CRA_c	1.327	8.398	0.158
O95831	Apoptosis-inducing factor 1, mitochondrial	1.326	1.98	0.67
O95373	Importin-7	1.315	1.042	1.262
V9HW31	ATP synthase subunit beta	1.307	2.744	0.476
Q9Y5M8	Signal recognition particle receptor subunit beta	1.306	2.686	0.486
B7Z7X3	cDNA FLJ51770, highly similar to Microsomal triglyceride transfer protein large subunit	1.305	6.273	0.208
A0A024R8Z9	Aspartyl-tRNA synthetase 2 (Mitochondrial), isoform CRA_b	1.305	4.083	0.32
Q9BPU6	Dihydropyrimidinase-related protein 5	1.303	16.015	0.081

Appendix

H0Y2W2	ATPase family AAA domain-containing protein 3A (Fragment)	1.3	2.237	0.581
P23468	Receptor-type tyrosine-protein phosphatase delta	1.3	0.906	1.436
J3QQ67	60S ribosomal protein L18 (Fragment)	1.299	19.19	0.068
P15907	Beta-galactoside alpha-2,6-sialyltransferase 1	1.288	2.963	0.435
P04843	Dolichyl-diphosphooligosaccharide--protein glycosyltransferase subunit 1	1.287	2.468	0.522
O00159	Unconventional myosin-Ic	1.287	1.929	0.667
A0A0S2Z492	DNA helicase	1.282	6.762	0.19
P53597	SUCLG1-Succinate--CoA ligase [ADP/GDP-forming] subunit alpha, mitochondrial	1.279	1.03	1.241
A0A024RBE7	Thymopoietin, isoform CRA_c	1.277	4.611	0.277
A0A0S2Z471	Creatine kinase brain isoform 2 (Fragment)	1.277	2.567	0.497
B7Z6Z4	Myosin light polypeptide 6	1.276	3.74	0.341
P49411	Elongation factor Tu, mitochondrial	1.274	1.897	0.672
A0A024R415	Paroxysmal nonkinesigenic dyskinesia, isoform CRA_a	1.269	1.218	1.042
P46060	Ran GTPase-activating protein 1	1.269	2.188	0.58
A0A087WZN1	Isocitrate dehydrogenase [NAD] subunit, mitochondrial	1.268	1.721	0.737

Appendix

B4E0L0	cDNA FLJ54030, highly similar to Polymerase delta-interacting protein 3	1.267	3.093	0.41
O94905	Erlin-2	1.263	2.669	0.473
Q08J23	tRNA (cytosine(34)-C(5))- methyltransferase	1.263	1.317	0.959
Q96PK6	RNA-binding protein 14	1.262	2.615	0.483
A0A024QZN9	Voltage-dependent anion channel 2, isoform CRA_a	1.261	2.788	0.452
A0A140VKA6	Testis secretory sperm-binding protein Li 233m	1.261	44.718	0.028
Q8NBS9	Thioredoxin domain-containing protein 5	1.259	2.464	0.511
Q9NP08	Homeobox protein HMX1	1.258	0.896	1.404
Q8NBQ5	HSD17B11-Estradiol 17-beta- dehydrogenase 11	1.257	1.185	1.061
Q9Y508	RNF114-E3 ubiquitin-protein ligase	1.257	0.744	1.689
Q16891	MICOS complex subunit MIC60	1.255	3.148	0.399
A0A0S2Z4J1	Hydroxysteroid (17-beta) dehydrogenase 4, isoform CRA_b (Fragment)	1.255	19.328	0.065
Q15424	Scaffold attachment factor B1	1.255	25.453	0.049
Q02978	Mitochondrial 2- oxoglutarate/malate carrier protein	1.254	0.836	1.5
Q6NVC0	SLC25A5 protein (Fragment)	1.251	0.924	1.353
B7Z8Z6	DNA helicase	1.251	58.568	0.021

Appendix

A0A024RD03	Mitochondrial ribosomal protein S10, isoform CRA_a	1.25	2.818	0.444
A8MXP9	Matrin-3	1.248	4.386	0.285
P15559	NAD(P)H dehydrogenase [quinone] 1	1.248	15.715	0.079
B4DP48	cDNA FLJ61147	1.248	1.24	1.007
Q92736	RYR2-Ryanodine receptor 2	1.247	1.053	1.184
B2RCH7	cDNA, FLJ96082, highly similar to Homo sapiens cervical cancer 1 protooncogene (HCCR1), mRNA	1.246	1.195	1.042
V9HWB8	Pyruvate kinase	1.241	4.952	0.25
O43772	SLC25A20-Mitochondrial carnitine/acylcarnitine carrier protein	1.241	0.93	1.334
Q8WVK7	SKA2-Spindle and kinetochore-associated protein 2	1.24	0.741	1.674
P38646	Stress-70 protein, mitochondrial	1.238	1.74	0.711
B2RBD5	Tubulin beta chain	1.236	1.147	1.078
P08574	CYC1-Cytochrome c1, heme protein, mitochondrial	1.236	1.034	1.196
A0A0G2JK44	BRD2-Bromodomain-containing protein 2	1.236	0.69	1.792
A0A0D9SF53	ATP-dependent RNA helicase DDX3X	1.234	5.238	0.236
P09874	Poly [ADP-ribose] polymerase 1	1.232	13.51	0.091
J3QK89	Calcium homeostasis endoplasmic reticulum protein	1.232	4.547	0.271
P51648	Fatty aldehyde dehydrogenase	1.231	3.798	0.324

Appendix

B4DL07	cDNA FLJ53353, highly similar to ATP-binding cassette sub-family D member 3	1.229	1.306	0.941
Q6IQ30	Polyadenylate-binding protein	1.229	5.583	0.22
Q9UEY8	Gamma-adducin	1.229	6.687	0.184
A0A1B0W1E4	Cytochrome c oxidase subunit 2 (Fragment)	1.228	1.298	0.946
Q59EI9	ADP,ATP carrier protein, liver isoform T2 variant (Fragment)	1.226	0.949	1.293
O60701	UDP-glucose 6-dehydrogenase	1.222	5.463	0.224
Q59FF0	EBNA-2 co-activator variant (Fragment)	1.218	7.34	0.166
Q8WWC4	m-AAA protease-interacting protein 1, mitochondrial	1.216	1.213	1.003
A0A140TA86	MICOS complex subunit MIC13	1.214	1.465	0.829
A0A0S2Z3H3	SLC25A4-Solute carrier family 25 member 4 isoform 1 (Fragment)	1.213	0.84	1.443
O00116	Alkyldihydroxyacetonephosphate synthase, peroxisomal	1.212	3.998	0.303
B2RMV2	CYTSA protein	1.211	0.822	1.474
P28331	NDUFS1-NADH-ubiquinone oxidoreductase 75 kDa subunit, mitochondrial	1.21	1.066	1.135
O75964	ATP synthase subunit g, mitochondrial	1.208	1.216	0.994
A0A024RBB7	Nucleosome assembly protein 1- like 1, isoform CRA_a	1.205	3.921	0.307
Q6IAN0	Dehydrogenase/reductase SDR	1.204	1.314	0.917

	family member 7B			
B3KM97	cDNA FLJ10554 fis, clone NT2RP2002385, highly similar to Synaptic glycoprotein SC2	1.204	1.103	1.092
B2R8R5	cDNA, FLJ94025, highly similar to Homo sapiens tripartite motif- containing 28 (TRIM28), mRNA O	1.202	6.125	0.196
A0A024R608	Ribosomal protein, large, P1, isoform CRA_a	1.202	9.786	0.123
Q13427	Peptidyl-prolyl cis-trans isomerase G	1.2	17.847	0.067

Appendix Table 9.3 Host proteins identified by proteomic analysis.

Host proteins listed here are Twin-Strep-tagged nsP3 samples from wildtype and P247A/V248A with more than 1.2-fold enrichment compared with untagged wildtype resins. Abundance ratio (TST-WT / WT) is the ratio protein abundance for the wildtype TST-nsP3 pull down to the untagged wildtype negative control. Abundance ratio (TST-PV / WT) is the ratio protein abundance for the P247A/V248A TST-nsP3 pull down to the wildtype nsP3 positive control. Abundance ratio (TST-WT / TST-PV) is the ratio protein abundance for the wildtype TST-nsP3 to P247A/V248A TST-nsP3. 3 replicates of each TST-WT, TST-PV and WT samples are analysed and the averaged values are shown. Proteins involved in the nsP3 interacting protein network inhibited by P247A/V248 (as shown in Figure 5.22B) are labelled in red.